ersity "Politehnica" of Timisoara
Timisoara, Romania

University of Applied Sciences Gelsenkirchen
Gelsenkirchen, Germany

PhD Thesis

estigations Regarding the Properties Improvement of Injection Moulded Polypropylene Composites Containing VGCNFs

PhD Student: Eng. Valentin Daniel CHIRILA

Supervisors:

Prof. Dr.-Eng. Tudor ICLANZAN

Prof. Dr.-Eng. Waltraut BRANDL

2006

Contents

List of Figures

List of Tables

List of Abbreviations and Acronyms

ACM – advanced composite materials;

AM – advanced materials;

C – carbon;

CCVD – catalytic chemical vapour deposition;

CF – carbon fibres;

Co – cobalt;

CVD – chemical vapour deposition;

DC – direct current;

DEAC– diethylaluminium chloride;

EDX – energy dispersive X-ray spectrometry;

EMI – electromagnetic interference;

e.g. – for example;

Fe – iron;

Hf – hafnium;

HRTEM – high resolution transmission electron microscopy;

IUPAC – International Union of Pure and Applied Chemistry;

M – metal;

MAO – methylaluminoxane;

MFC – mass flow controller;

MW – microwave frequency;

Ni – nickel;

N_2 – nitrogen;

OM – optical microscope;

O_2 – oxygen;

PAHs – Polycyclic aromatic hydrocarbons;

PAN – polyacrylonitrile;

PMC – polymer matrix composite;

PP – polypropylene;

Pt – platinum;

RF – radio frequency;

RFI – radio frequency interference;

SEM – scanning electron microscopy;

Si – silicon;

TEM – transmission electron microscopy;

TGA – thermogravimetric analysis;

VGCFs – vapour grown carbon fibres;

VGCNFs – vapour grown carbon nanofibres;

WCA – water contact angle;

XPS – X-ray photoelectron spectrometry;

XRD – X – ray diffraction;

Zr – zirconium.

List of Symbols

C – Celsius;

ccm – cubic centimetre;

cm – centimetre;

D – diameter;

F – force;

g – gram;

GHz – giga hertz;

GPa – giga Pascal;

G_p – graphitisation degree;

h – hour;

I – current;

J – -Joule;

k – Kelvin;

kg – kilogram;

kJ – kilo Joule;

kV – kilovolt;

kW – kilowatt;

l – length;

m – metre;

MHz – megahertz;

min – minute;

ml – millilitre;

mm – millimetre;

mN – milli Newton;

MPa – mega Pascal;

nm – nanometre;

Pa – Pascal;

r – radius;

R – electrical resistance;

S – second;

sccm – standard cubic centimetre;

T_B – burning temperature;

T_g – glass transition temperature;

T_m – melting temperature;

v – volume;

V – volt;

W – watt;

wt.% - weight percent;

θ – contact angle;

θ_a – advancing angle;

θ_r – receding angle;

σ – tensile strength;

σ_r – radial gripping stress;

τ_I – interfacial shear stress;

ρ – electrical resistivity;

μ – friction coefficient;

μm – micrometer;

Ω – ohm;

° – grade.

CHAPTER I

INTRODUCTION

1.1 Background and Motivation

Advanced materials have received much attention because of their great scientific significance and promising potential applications in engineering components. In the last years, a new generation of sophisticated materials promises to reshape our world and solve some of the planet's most pressing problems. These materials save lives (artificial hearts, biofluidic chips, bullet-proof vests), conserve energy (lightweight cars) and expand human horizons (aircraft, spacecraft, computers through the Word Wide Web). The advanced materials should satisfy more than one property, to be light and in the same time strong, to have a good thermal stability and electrical conductivity, like reinforced polymeric materials.

Polymer composites can cover a broad range of material combinations. As matrix, polymeric composites can be placed into thermoplastic or thermoset category. Thermoplastics are able to be repeatedly heated and cooled and are characterized by two-dimensional polymeric chains. By heating they become softened or liquefied, and on cooling returning to a solid. During each controlled heating and cooling cycle these materials suffer a small loss in physical properties, because the heating process breaks down the material's molecular bonds. However, very important is that the thermoplastics can be recycled. Thermosets category, or thermosetting polymers, have three-dimensional polymeric chains and very essentially is that they support only one heating cycle. Once thermosets have reacted and cooled, they cannot be remelted or reformed. Thermosets are a one-time reaction polymer systems, therefore are unrecyclable.

As reinforcement materials a wide variety of materials can be used, such as minerals, glass beads, fibres, talc, cellulose and rags. Glass and carbon fibres are by far the most common types and are produced by a number of manufacturers worldwide. In the last years, carbon fibres became the most important researched fibres worldwide. They combine excellent mechanical, electrical and thermal properties with light weight. Carbon fibres have the following attributes:

- available in many grades and forms with wide – ranging properties;
- high modulus, especially pitch based fibres and carbon nano-tubes (single- and multi-walled);
- good strength, especially PAN based fibres and carbon nano-tubes;

- low density;
- excellent thermal stability in the absence of oxygen;
- low thermal expansion coefficient;
- excellent creep resistance;
- good chemical resistance;
- good electrical conductivity;
- biocompatibility.

Today, the commercial carbon fibres can be classified on the manufacture precursors:

- cellulosic precursor: rayon – based carbon fibres;
- acrylic precursor: polyacrylonitrile – based carbon fibres;
- pitch precursor: petroleum or coal tar pitch;
- other precursors, like coal, polyvinylchloride, aromatic hydrocarbons.

The precursor materials have direct influence on the morphology and structure of the fibres and indirect on the physical properties. A new class of carbon fibres which are manufactured from hydrocarbon precursors are *vapour grown carbon fibres*.

Vapour grown carbon fibre (VGCFs) are a special class of carbon fibres which are distinctively different from other types of carbon fibres in the method of production, their unique physical characteristics and the prospect of low cost fabrication. Those fibres could grow on a substrate having diameters about 10 – 30 μm and length up to more centimetres, or in floating bed reactor having usually a diameter about 100 nm and the length more than 1μm. Therefore, these fibres are situated in the domain of nano-scale and they can be easily called vapour grown carbon nano-fibres. Research on VGCNF has been fuelled by the perspective potential, not only for the marked improvement in the physical properties of the composites, but also for the production of graphitic reinforcements in a wide range of forms at low costs.

The composite materials can be defined as a macroscopic combination of two or more distinct materials, having a recognizable interface between them. The physical properties of the composite depend not only on the properties of constituent materials but also on the interface between them. When a load is applied to the carbon fibre composite, the stress is transferred from one carbon filament to another via the matrix material. If a weak fibre-polymer bond is present, then it will result in poor mechanical properties of the composite, such as low interlaminar shear strength, which is attributed to a lack of bonding between the polymer

matrix and fibre filaments. The quality of this connection determines many properties, including strength and toughness. The interfacial interactions at fibre-polymer interface in composites characterise the adhesion phenomena. A good adhesion has a positive influence on the composite properties, such as compressive strength and interlaminar shear strength between the fibre and the matrix. Generally, this problem can be overcome by some form of surface treatment of the fibres.

Treatments can be applied using oxidative and non-oxidative methods. The oxidative treatments can be subdivided into gas-phase oxidations at lower or at higher temperatures, liquid phase oxidations (chemically or electrochemically), and plasma.

Plasma surface treatment is a dry reaction process and can have the following effects on a carbon fibres surface:

- cleans the outside, creating a hydrophilic surface for enhanced bonding;
- remove the surface layer by a micro-etching process;
- penetrates the top few molecular layers (100 about 10 nm) and modifies the surface, creating a new surface chemistry, enabling improved interfacial adhesion in composites.

The functional groups created on the carbon fibres surface depend on the gases used to create plasma, thus:

- air plasma – on the fibres have been detected —COOH and —OH groups;
- O_2 plasma – on the fibres have been detected —OH, ═O, —C═O, —COOH, —COOX, —CO_3, quinone and lactone groups;
- NH_3 and N_2 plasma – on the fibres have been detected aliphatic, aromatic amines (—CNH_2) and some imines (—C═NH).

These functional groups are able to produce strong chemical bonds at the interface between carbon fibres and polymeric chains.

Carbon fibres reinforced materials can have various applications. Depending on the type of carbon fibres and the polymeric matrices, they can be used in the following fields: aerospace (defence aircraft, civil aircraft, helicopters, etc.), space, rocket motor cases, marine applications, oil exploration, automobile and racing car applications, bikes, railways, textile applications, turbine blades, chemical and nuclear applications, medical and prosthetic applications, dental, sports and leisure goods, musical instruments, etc.

Vapour grown carbon (nano-)fibres reinforced polymeric composites have industrial applications, like silicon wafer production, batteries and fuel cells, disk drive components; automotive applications as improving the electrical conductivity and mechanical properties, like fuel systems, bumpers and fenders, interior parts, tires, mirror housing; aerospace, aircraft braking systems, thermal management, EMI/RFI shielding, etc.

1.2 Purpose

The goal of this PhD thesis is to explore the production of new materials that contain the new type of vapour grown carbon nano-fibres (VGCNF), and conventional thermoplastic polymer matrices, like polypropylene (PP). The vapour grown carbon nano-fibres are incorporated in polypropylene matrix through extrusion and injection moulding process. The role of VGCNFs in polymer matrix is to improve the mechanical, electrical and thermal properties of the final composite. In order to obtain composites with improved physical properties, the VGCNF must be uniform dispersed in the polymeric matrix to form a conductive network. Further more, to enhance the mechanical properties of the composite, it is very important to optimise the fibres / matrix adhesion.

The VGCNFs / PP adhesion can be improved through surface treatment of the fibres or fibres polymerisation. Plasma chemical treatment is in detail discussed in this work. The effects of plasma gas (oxygen, and ammonia) onto the functionalisation degree of VGCNFs, as well as the plasma parameters are discussed. For industrial applications of such surface treatment it is very important to reduce the treatment time and to increase the quantity of fibres used in one charge of treatment. These problems have direct influence onto the treatment costs and finally on the products.

One of the aims of this work is to optimise the plasma treatment process in order to functionalise the surface of vapour grown carbon fibres. It is very important to find an optimum between the most important plasma parameters such as plasma treatment time and plasma power in order to obtain a high functionalisation degree of the VGCNF surface without burning (destroying) the fibres. Another important goal is to assure a homogeneous plasma treatment of the fibres. These treatments are carried out in a plasma reactor equipped with two generators (radio frequency and microwave generator) and a rotary barrel.

The effect of plasma treatment onto the VGCNFs was measured using an electronic balance. The contact angle in at least two liquids (n-hexane and water) was measured. The surface energy of the fibres was also calculated. The amount of acidic functional groups was quantified by titration measurements.

The morphology and structure of the VGCNFs in "as grown" status and plasma treated were characterised by scanning electron microscopy and transmission electron microscopy. The graphitisation degree of the vapour grown carbon nano-fibres was measured by X – rays diffraction technique. The thermal stability was characterised using a thermogravimetrical balance and the specific electrical resistivity was measured using a DC – circuit.

Different weight percent of VGCNFs in thermoplastics resin (polypropylene) were mixed manually before extrusion in order to obtain the composite in pellets shape and for the production of the samples for further mechanical and physical tests, the injection moulding process was used. The dispersion and orientation of the VGCNFs in PP matrix was investigated by SEM. The samples were analysed also in cross section in order to observe the adhesion between fibres and matrix. The modification of the mechanical properties of the composite containing untreated and oxygen plasma treated fibres were determined by tensile and impact resistance tests.

The thermal conductivity of the polypropylene and VGCNFs composite was investigated by thermoanalytical analysis as a function of temperature. The influence of the extrusion and injection moulding process on the electrical resistivity of the composite were examined.

CHAPTER II

ADVANCED COMPOSITE MATERIALS

2.1 Introduction

Advanced Materials (AM) are materials that are either designed or processed using new methods or modified concepts that led to paradigm shifts in understanding, and have vast potential for application in nice areas. Metallic glasses, quasicrystals, nanostructured materials, fullerenes and carbon nanotubes, carbon nanofibres, biomimetic materials, functionally graded materials and smart materials, structural and complex intermetallics all find their special place in the development of advanced materials [1].

Advanced composite materials (ACM) can be best characterised as materials that are governed primarily by the properties of the reinforcing materials which have high strength and high stiffness characteristics and occupy a high volume fraction of the composite [2].

This chapter presents a literature review with three topics to get a better understanding of the background of the present research. It contains a review of composite materials, matrix and reinforcement materials, especially grow process and physical properties of the VGCNFs.

2.2 Composite Materials

Actually exists a variety of definitions for composite materials. Composite materials can be defined simple as materials made from several elements. Another definition is that, the composite materials are engineering materials made from a matrix phase and a reinforcement phase, with the overall quality and efficiency of the material being primarily determined by the efficiency of the load transfer mechanisms at the interface level, see Figure 2.1 [3]. The matrix (matrix phase) is the continuous phase of the composite that holds the reinforcement in place. In a composite, the matrix is required to fulfill the following functions:

- to bind together the reinforcement fibres and to protect their surface from handling damage;
- to disperse the fibres and maintain the desired fibre orientation and spacing;
- to transfer stresses to the fibres by adhesion and/or friction across the fibre-matrix interface when the composite is under load, and thus to avoid any catastrophic propagation of cracks and subsequent failure of the composites;
- to be chemically and thermally compatible with the reinforcing materials;

- to be compatible with the manufacturing methods which are available to fabricate the desired composite components.

Reinforcement materials are added to the matrix in order to increase the physical or mechanical properties of the final composite. To improve the mechanical properties of the composite, the reinforcement materials required to have the following criteria:

- a high aspect ratio (length/diameter) that allows a very large fraction of the applied load to be transferred from the matrix to the fibre across the interface;
- a high degree of flexibility, which allows a variety of manufacturing techniques.

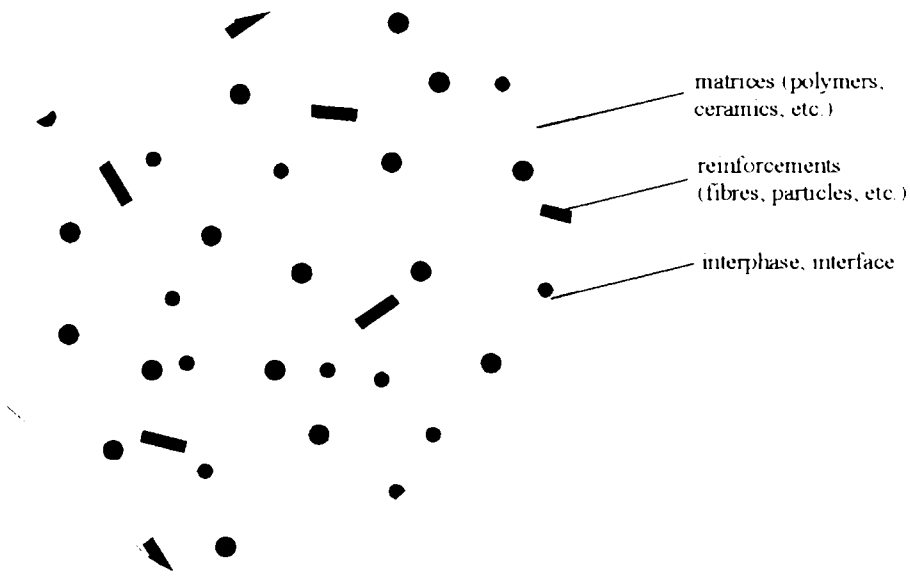

Figure 2.1 A schematic presentation of the composites structure.

Composite materials can be classified in terms of reinforcement materials (Figure 2.2) and in terms of matrix materials (Figure 2.3).

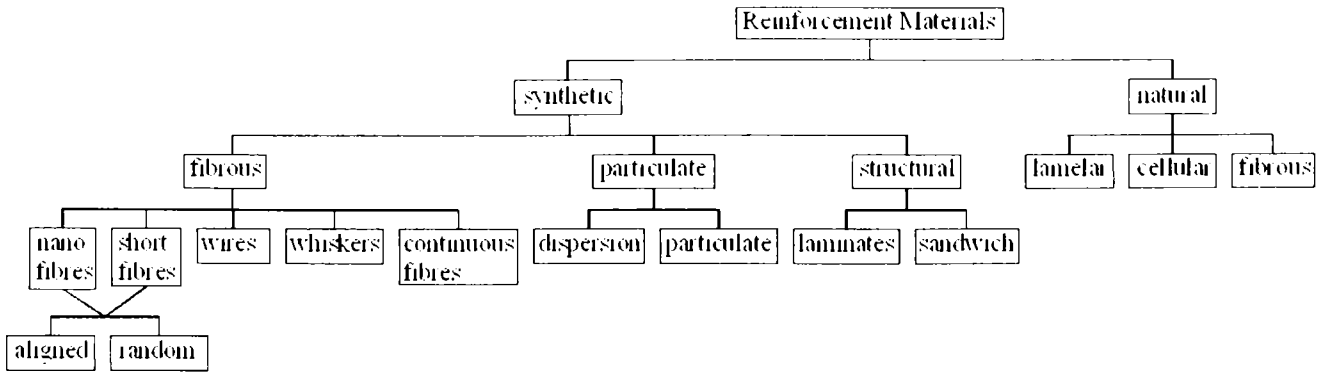

Figure 2.2 Composite materials classification tree - reinforcement base.

It can be observed that exists a variety of composite materials, but in the last years the nanoscale filled polymer composites have been more researched. The nanoscale filled

polymer composites can be defined as composites which have the filler in the nanometre range (less than 100 nm), in at least one dimension [4]. The nano-filler can be three-dimensional (Figure 2.4a) or bi-dimensional (Figure 2.4b) [5, 6].

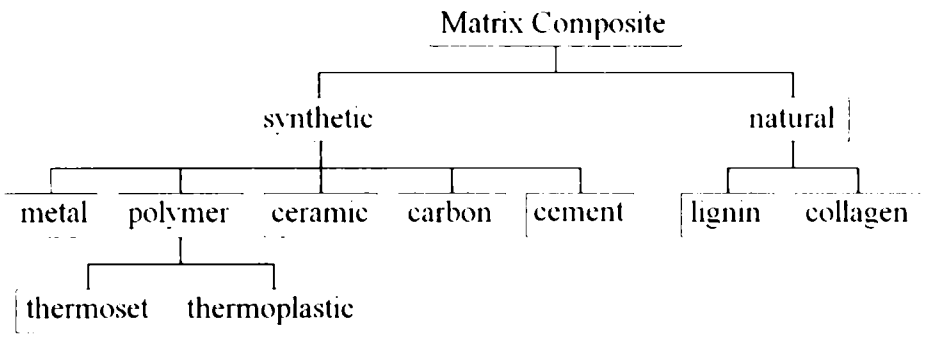

Figure 2.3 Composite materials classification tree - matrix base.

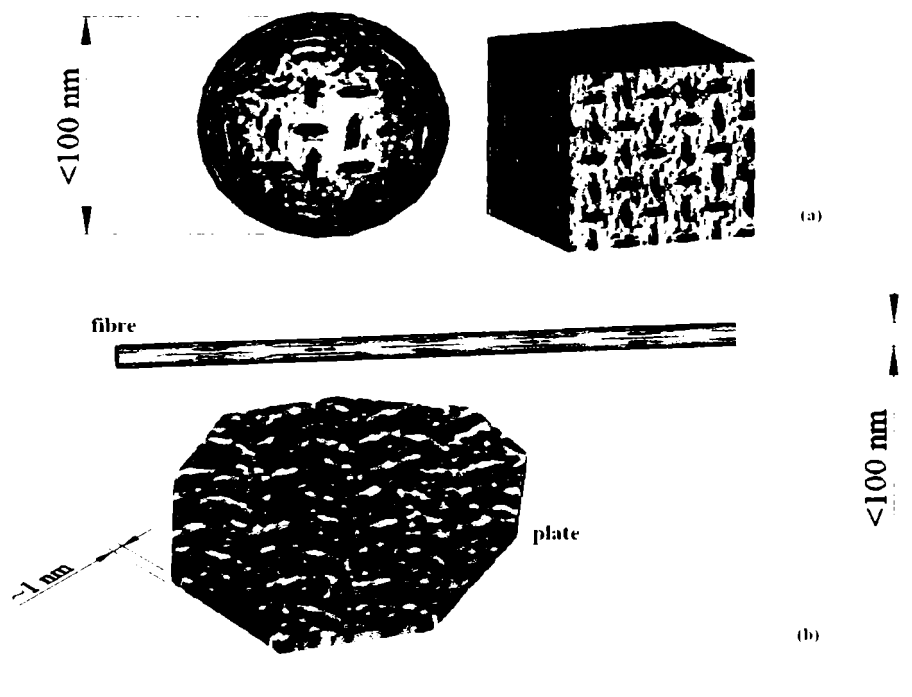

Figure 2.4 Schematic representation of nanoscale fillers: (a) three-dimensional; (b) bi-dimensional [5].

Nano-fillers, like carbon black and fumed silica, have been used for more than one century [7-11]. In the last years, nano-filled polymer composites have been more researched for several reasons:

- unprecedented combinations of properties have been observed in some polymer composites [12-16];
- significant development in the chemical processing of nanoparticles and in the in-situ processing of nanocomposites has led to unprecedented control over the morphology

of such composites. Therefore, if its now the chemistry of the nanoparticles can be created, than exists an ability to control the interface between the filler and the matrix [17-21];

- the discovery of carbon nanotubes in the early 1990s by Iijima [22] make that the nanoscale filled polymers to be more researched and developed.

2.3 Polymer Matrix Materials

The polymer matrix is the continuous phase of the composite and provides uniform load distribution to the fibre and protects the surface of the composite against abrasion or environmental corrosion (see Figure 2.1).

The high performance matrix resin should posses a modulus of at least 3GPa for optimum strength and sufficient shear modulus to prevent buckling of fibre under compression load [2]. A variety of thermosetting and thermoplastic resin have been utilised as matrix resin [23-31]. Thermoplastics are those polymers that solidify as they are cooled, no longer allowing the long molecules to move freely. When heated, these materials regain the ability to flow, as the molecules are able to slide past each other. Thermoplastic polymers are divided into two classes (Figure 2.5) [32]:

- amorphous polymers;
- semi-crystalline polymers.

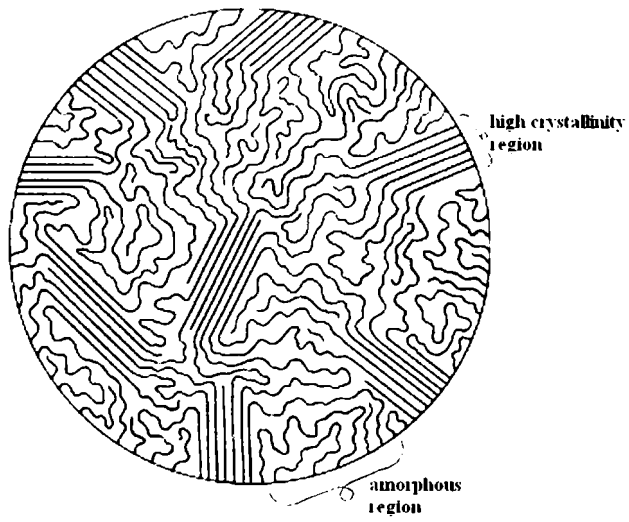

Figure 2.5 A schematic presentation of the amorphous and high crystalline region of the thermoplastic polymers.

Amorphous thermoplastics are those with molecules that remain in disorder during cooling, leading to a material with a fairly random molecular structure. The characteristic size of the largest ordered regions is of the order of a carbon-carbon bond. This dimension is much smaller than the wavelength of visible light and so generally makes amorphous thermoplastics transparent. Amorphous polymers are glassy solids at low temperatures, since molecular motion is severely restricted. The temperature at which a polymer softens is known as the glass transition temperature, T_g. Over this temperature, T_g, the solid amorphous polymer changes to the rubber state and, with further increase in temperature, to a viscous liquid, as shown in Figure 2.6.

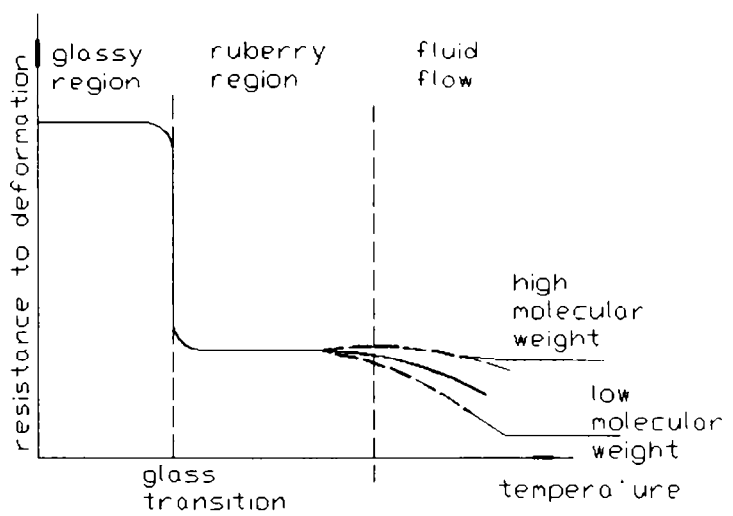

Figure 2.6 Amorphous thermoplastics – glass transition temperature.

Semi-crystalline thermoplastics solidify with a certain order in their molecular structure. Hence, as they are cooled, they harden when the molecules begin to arrange in a regular order below what is usually referred to as the melting temperature, T_m, Figure 2.7. The molecules in semi-crystalline polymers that are not transformed into ordered regions remain as small amorphous regions. These amorphous regions within the semi-crystalline domains solidify at the glass transition temperature. Most semi-crystalline polymers have a glass transition temperature under zero degree, hence, behaving at room temperature as rubbery or leathery materials [33].

The major reasons for the increased use of thermoplastic matrix composites in recent years are:

- their excellent property retention at elevated temperatures;
- highly recyclable;

- cost savings can be achieved from improved processing and handling compared to highly cross-linked epoxies, e.g. adaptability of thermoplastics to high rate processing, reduced scrap rate because of deformability, simple storage, easy handling of materials and indefinite shelf life without refrigeration;
- mechanical enhancement is more easily achieved than in epoxies, e.g. fracture toughness and moisture resistance.

Unfortunately, thermoplastics have several drawbacks as well:

- poor creep resistance;
- environmentally, not as stable as thermosets (amorphous only);
- relatively costly raw materials;
- required processing temperatures much higher than thermosets;
- wetting of the fibres not as easy as with thermosets.

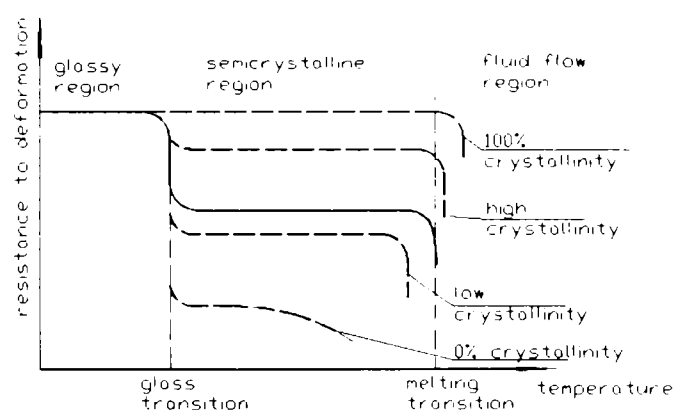

Figure 2.7 Semi-crystalline thermoplastics – melting temperature.

Thermosetting polymers solidify by being chemically cured. Here, the long macromolecules cross-link with each other, during cure, resulting in a network of molecules that cannot slide past each other. The formation of these networks causes the material to lose the ability to flow even after re-heating. The high density of cross-linking between the molecules makes thermosetting material stiff and brittle. Thermosets also exhibit a glass transition temperature, which is sometimes near or above thermal degradation temperatures.

The configuration of the polymer molecules has a great influence on the properties of the final polymer matrix [34]. The preferential spatial positions of the atoms in a molecule are described by the polarity flexibility and regularity of the macromolecule. During polymerisation it is possible to place the X groups (methyl groups, CH_3, in the case of PP) on the carbon-carbon backbone in different directions. The order in which they are arranged is called activity. The polymers with side groups that are placed in a random matter are called atactic. The polymers whose side groups are all on the same side are called isotactic, and

those molecules with regularly alternating side groups are called syndiotactic. In Figure 2.8 are shows three different tacticity cases for polypropylene.

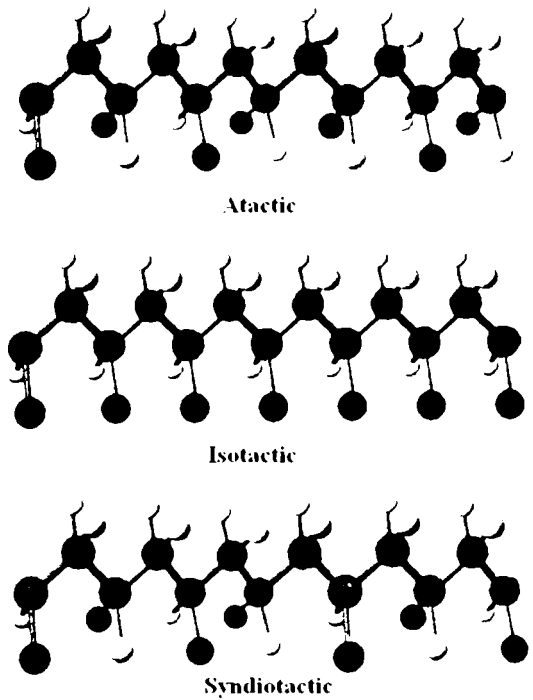

Figure 2.8 A schematic presentation of different polypropylene structures.

2.4 Polypropylene

Polypropylene (PP) is an economical material that offers a combination of outstanding physical, chemical, mechanical, thermal and electrical properties not found in any other thermoplastic [35]. PP is a thermoplastic polymer, used in a wide variety of applications, including automotive components [36], food packaging [37], textiles [38], laboratory equipment [39], and polymer banknotes [40].

PP can be made from the monomer propylene (C_3H_6) by Ziegler-Natta polymerization [41]. A Ziegler-Natta catalyst can be defined as a transition metal compound bearing a metal carbon bond able to carry out a repeated insertion of olefin units. Usually, the catalyst consists of two components: a transition metal salt (most frequently a halide) and a main-group metal alkyl (activator) which serves the purpose of generating the active metal-carbon bond. The molecular formula of the polypropylene is as follow:

$$\left(-CH_2 - \underset{\displaystyle CH_3}{\underset{|}{CH}} - \right)_n$$

The first highly isotactic PP (80 – 90%) was discovered in 1954 by Giulio Natta using $TiCl_4$ as catalyst and AlR_3 as cocatalyst ($AlEt_3$) [42]. The development of more efficient and more sophisticated catalysts is still in research today. The catalysts can be classified as follows:

- heterogeneous catalysts, like $TiCl_3/AlEt_2Cl$ (AA–$TiCl_3$ + DEAC);
- homogeneous catalysts.

The last important step began in 1980 with the discovery of the homogeneous stereospecific catalysts [43], like stereorigid metallocenes of transition metals, such as Zr and Hf, when combined with methylaluminoxane (MAO), were able to provide highly stereoregular isotactic or syndiotactic PPs in extremely high yields. Metallocene-based polymers, ranging from crystalline to elastomeric materials, have been available commercially since about 1991. The discovery of metallocenes aroused an enormous interest because it appears to open the way to materials with unprecedented properties. Metallocenes are the only catalysts which are able to control over the molecular weight and the microstructure (tacticity, regioregularity, comonomer distribution) of polyolefins over a very wide range, making possible the synthesis of improved and new polyolefin materials [44].

Polypropylene homopolymer is a semi-crystalline polymer. The crystallizability of the PP chain is an important factor governing the resultant morphology. The degree of crystallinity of PP homopolymer is controlled primarily by the tacticity of the chain. Figure 2.8 illustrates a simplistic view of stereoregularity in PP homopolymer. In addition to stereoregularity, there are many other determinants of PP morphology. Figure 2.9 shows that the polymer morphology provides a critical bridge among polymer structure, polymer processing and end-use properties [45]. Understanding the effects of these structural and processing variables on PP morphology is important, because it is the morphology which provides the most direct link with polymer properties.

From the Figure 2.9, it can be observed that, the fabrication processes of the polymer have an essential part on the finally PP properties. PP can be fabricated by a wide variety of processes. The most used processes for fabrications of polypropylene are extrusion and injection moulding technique. E. P. Moore, Jr. described the effect of the extrusion and injection moulding techniques on the polypropylene fabrication [46]. The Table 2.1 summarizes typical properties of the moulded PP [47].

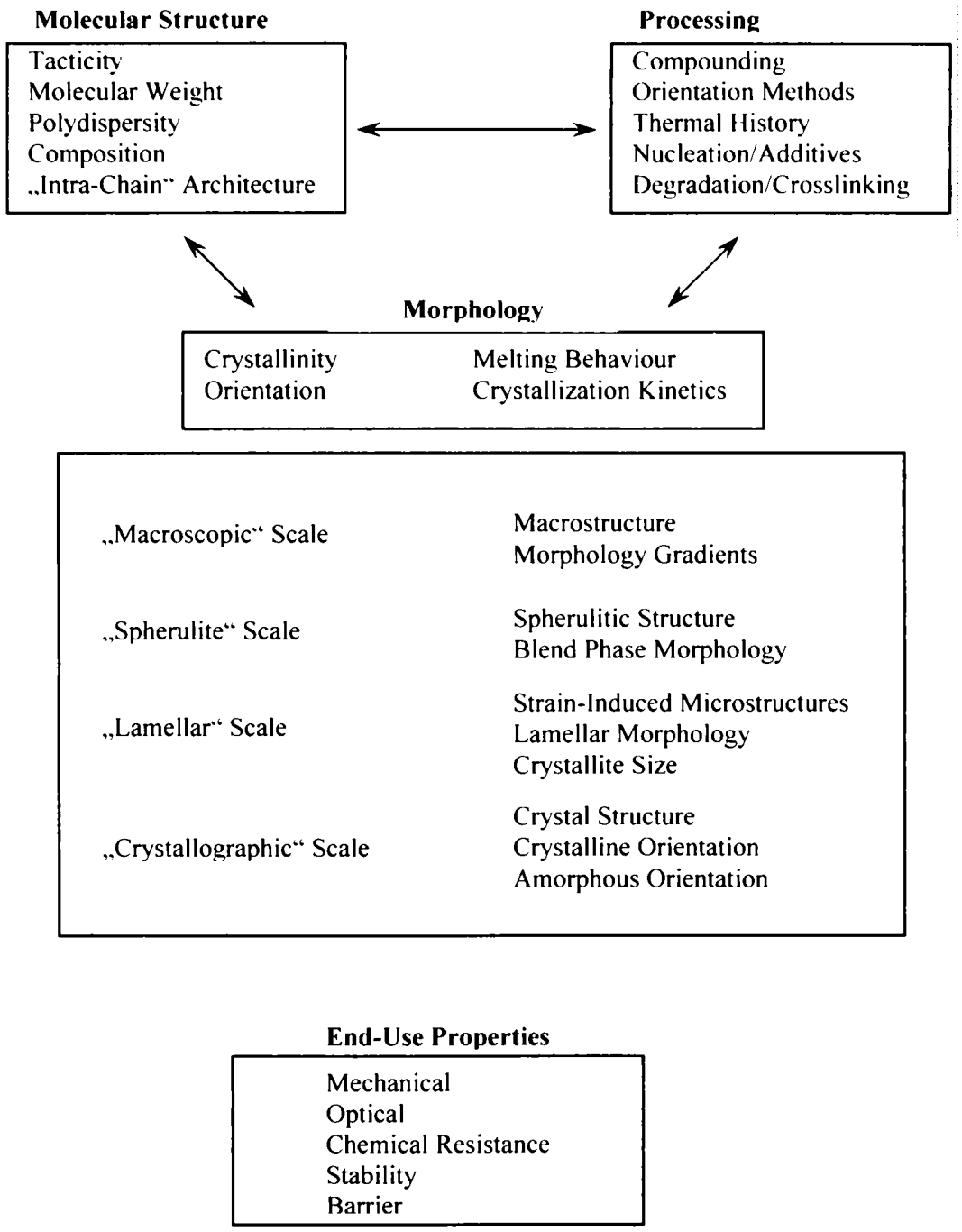

Figure 2.9 Relationships among polymer structure, processing, morphology, and end-use properties [45].

Table 2.1 Properties of the moulded PP [47].

Property	Values	Units
Density	0.9 – 1.25	g/cm^3
Water Absorption (24h)	0.01 – 0.2	%
Glass transition temperature	-20 – -10	°C
Melting temperature	173	°C
Amorphous density at 25°C	0.85	g/cm^3
Crystalline density at 25°C	0.95	g/cm^3
Molecular weight of repeat unit	42.08	g/mol
Hardness, Rockwell R	70 – 113	
Tensile Strength, Ultimate	19.7 – 80	MPa
Tensile Strength, Yield	12 – 43	MPa
Elongation at break	3 – 887	%
Tensile modulus	0.5 – 7.6	GPa
Charpy Impact, unnotched	1.4 – NB	J/cm^2
Charpy Impact, notched	0.2 – 9.5	J/cm^2
Electrical resistivity	$1\times10^{14} - 1\times10^{17}$	ohm-cm
Heat Capacity	2	J/g°C
Thermal Conductivity	0.1 – 0.13	W/m-K

2.5 *Nanoscale Materials Used as Reinforcement in Polymer Composites*

Nanoscale materials are generally considered to be a number of atoms or molecules bonded together with at least a dimension less of 100 nm. The spectrum of nanomaterials ranges from inorganic or organic, crystalline or amorphous particles, which can be found as single particles, aggregates, powder or dispersed in matrix, over colloids, suspension and emulsion, nanolayers and nanofilms, up to class of fullerenes and their derivates. Generally there are different approaches for classification of nanomaterials, some of which are summarised in Table 2.2 [48].

Table 2.2 Classification of nanomaterials with regard to different parameters [48].

Classification	Examples
Dimension	
3 dimensions < 100nm	Particles, quantum dots, hollow spheres, etc.
2 dimensions < 100nm	Tubes, fibres, wires, platelets, etc.
1 dimension < 100nm	Films, coatings, multilayer, etc.
Phase composition	
Single-phase solids	Crystalline, amorphous particles and layers, etc.
Multi-phase solids	Matrix composites, coated particles, etc.
Multi-phase systems	Colloids, aerogels, ferrofluids, etc.
Manufacturing process	
Gas phase reaction	Flame synthesis, condensation, CVD, etc.
Liquid phase reaction	Sol-gel, precipitation, hydrothermal processing, etc.
Mechanical procedures	Ball milling, plastic deformation, etc.

The main classes of nanoscale structure can be summarised as follows:

- nanoparticles, like metal oxide nanopowders, such as iron oxide (Fe_3O_4, Fe_2O_3); ceramic nanopowder like titania (TiO_2), alumina (Al_2O_3) zirconium oxide (ZrO), or nanoparticulate substances like compound semiconductors (cadmium telluride, CdTe, gallium arsenide, GaAs) and alloys (like Ni base alloy);
- linear nanostructure such as nanowires, nanotubes or nanorods can be generated from different material classes (metals, semiconductors, or carbon). Carbon nanotube is one of the most promising linear nanostructures, which can occur in a variety of structure (single- or multi- wall, fullerenes, or nanofibres);
- quantum dots of semiconductors, metals and metal oxides have been at the forefront of research for the last five years due to their novel electronic, optical, magnetic and catalytic properties.

2.6 Carbon Fibres

Carbon can exists in allotropic form in two common categories diamond and graphite. Carbon fibres (CF) can exists also as fibres or filaments. The carbon fibres are not a new material. The first use evidence of carbon fibres is since more than one century old. Thomas Alva Edison (1880, USA) patented the use of carbon fibres as filament material for incandescent

electric lamp [49]. The carbon filaments were developed by Edison by dissolving cellulosic materials like natural cellulose or cotton in a solvent (such as $ZnCl_2$) to give a dope which could be extruded, which would regenerate the cellulose in the form of thread or filaments. The filament material was carbonized in the absence of air at high temperature in a gas furnace.

In the early of 1950s the carbon fibres with well-aligned carbon hexagons were extensive researched in UK, USA and Japan. These filaments are in most cases derived from organic precursors (polyacrylonitrile precursor – PAN) by extrusion into polymeric fibres, followed by heat treatment (stabilization) and subsequent carbonization (heat treatment above ~1000°C) and the further heat treatment up to ~3000°C in an inert atmosphere (graphitization). These carbon fibres are called "ex-polymer fibres" and became commercially available in the early 1960s [50]. More recently (1970s), a new type of fibres has appeared, based on pitch. These mesophase pitch-based carbon fibres attain their alignment through a liquid-crystal-like state (mesophase). The resulting spun fibres have high elastic module (~500-800GPa) after carbonization and graphitization [51]. Another kind of filaments has been developed recently, produced by decomposing of hydrocarbons on a heated substrate in the presence of transition metal catalysts (catalytic chemical vapour deposition (CCVD) carbon filaments) [52]. These filaments are not continuous like ex-polymer fibres, but their lengths can reach several hundred millimetres.

2.6.1 Vapour Grown Carbon Fibres

Vapour grown carbon fibres (VGCFs) represent another variety of reinforcement with significant commercial potential. Early technology for producing VGCFs dates back over a century when filaments were grown from a CH_4/H_2 mixture pyrolysed in an iron retort for possible use as a material for electric lamp [53]. The effective evidence and research of VGCFs was possible after the electron microscope was built in 1986 by Ernst Ruska [54]. Endo [55], Tibbetts [56], Gadelle [57], Baker and Harris [58] researched intensive the growth of vapour deposited carbon fibres. The first commercial VGCFs was produced by Nikkoso in 1991 and called Grasker [53].

VGCFs are produced from the gas phase by decomposing a hydrocarbon gas (CH_4, C_6H_6, C_2H_2) on a heated substrate (around 1000°C; SiO_2, C, Si) in the presence of a transition metal (Fe, Ni, Co) [59]. The simple way how filaments are formed by a catalytic particle is showed in Figure 2.10.

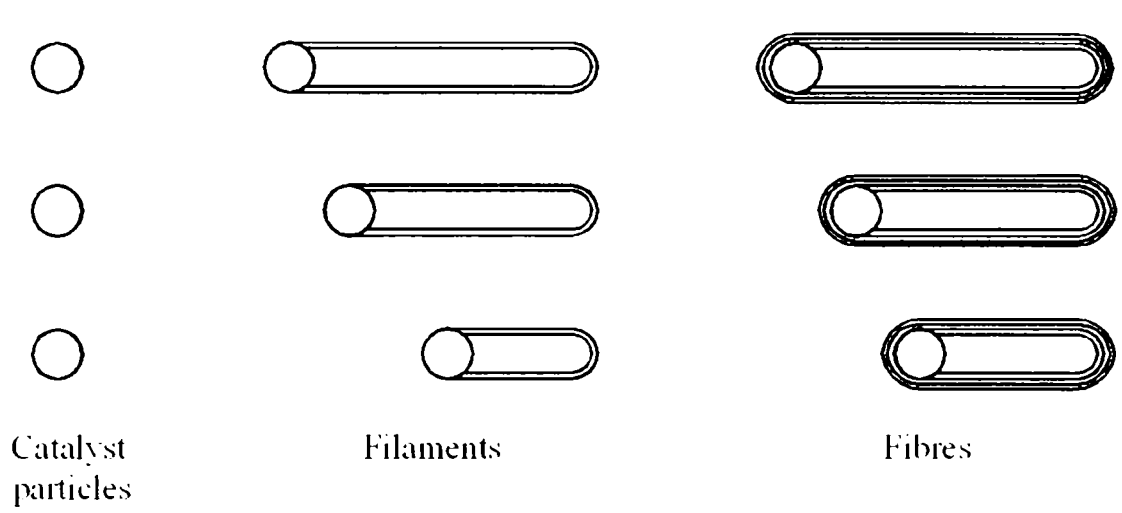

Figure 2.10 Schematic representation of growth mechanism of VGCF in the presence of catalyst particles [53].

Because a transition is employed, these filaments are sometimes referred in literature as catalytic chemical vapour deposited (CCVD) carbon filaments. Some authors, like Dresselhaus and co. [60] use this term of CCVD filament in their book, but is not a generally accepted term. The International Union of Pure and Applied Chemistry (IUPAC) have accepted the general term for this fibre as VGCF.

2.6.2 Preparation and Growth Process of VGCFs

Tibbetts developed a batch process for producing VGCFs using the apparatus presented in Figure 2.11 depositing the filaments on a series of nested of semi-cylindrical mullite tubes with the following chemical composition: Al_2O_3 (58.6%), SiO_2 (36.8%), Fe_2O_3 (0.9%), TiO_2 (0.9%), CaO/MgO (0.8%), Na_2O/K_2O (1.32%), Balance (0.68%) [61]. These tubes contained within a mullite muffle, passing a hydrocarbon/hydrogen mixture over the mullite substrate, maintained at around 1000°C, on which iron-containing particles, acting as a catalyst, had been deposited. It was found beneficial to obtain a build-up in the equipment of reactive hydrocarbons (C_2H_x), formed in the process, to promote a faster rate of formation, since methane itself tends to be un-reactive and has poor solubility in the iron particles. The filaments could growth up to several centimetres in length, with diameters of 7-10 μm. At temperatures around 1000°C they were relatively straight, whereas at lower temperatures, they tend to vary and could be twisted, or helical. Helium, as inert gas, helps to prevent convection and adjusting the gas stream carbon content to 15% v/v CH_4 in H_2, with a gas

residence time of about 20s will promote fibre lengthening at about 1000°C and filaments will lengthen to several centimetres in about 10 min. At higher methane concentrations (≈30% CH_4 in H_2) and temperatures above 1050°C the formation of carbon on the surface will be promoted increasing the thickness of the fibre (Figure 2.12a). Thinner fibres tend to produce a crenulated surface due to differential concentration of the layers during cooling (Figure 2.12b) [53].

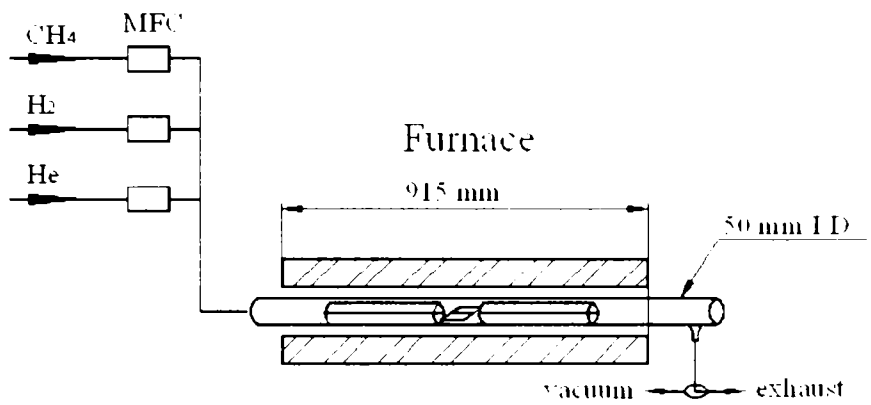

Figure 2.11 An apparatus for growing VGCFs at atmospheric pressure.

Figure 2.12 (a) Cross section view of a VGCF which has been exposed during growing to a maximum temperature of 1130°C; (b) SEM of a thinner fibre showing crenulations due to hoop stress [56].

For the mass production, Koyama and Endo introduced a continuous process [62], where ultrafine catalytic particles (5 – 25 nm diameter) were incorporated in the feedstock and fed into a reaction chamber (Figure 2.13a) or produced directly in the reactor by decomposition of an organometallic at 1100°C, which decomposes into a suspension of ultrafine catalyst particles that are transported by the flow of hydrocarbons and hydrogen gas into the furnace area (Figure 2.13b). The diameter of the fibres depends on the catalyst – hydrocarbon feed ratio. Once the catalyst particle becomes covered with carbon, oxygen or any form of

impurity, the fibres lengthening reaction will stop and fibre thickening takes place. Therefore, in order to ensure long filaments, all constituents must be of a high purity. The diameters of the fibres produced in the continuous process are uniform and they are not as long as fibres produced by the batch process.

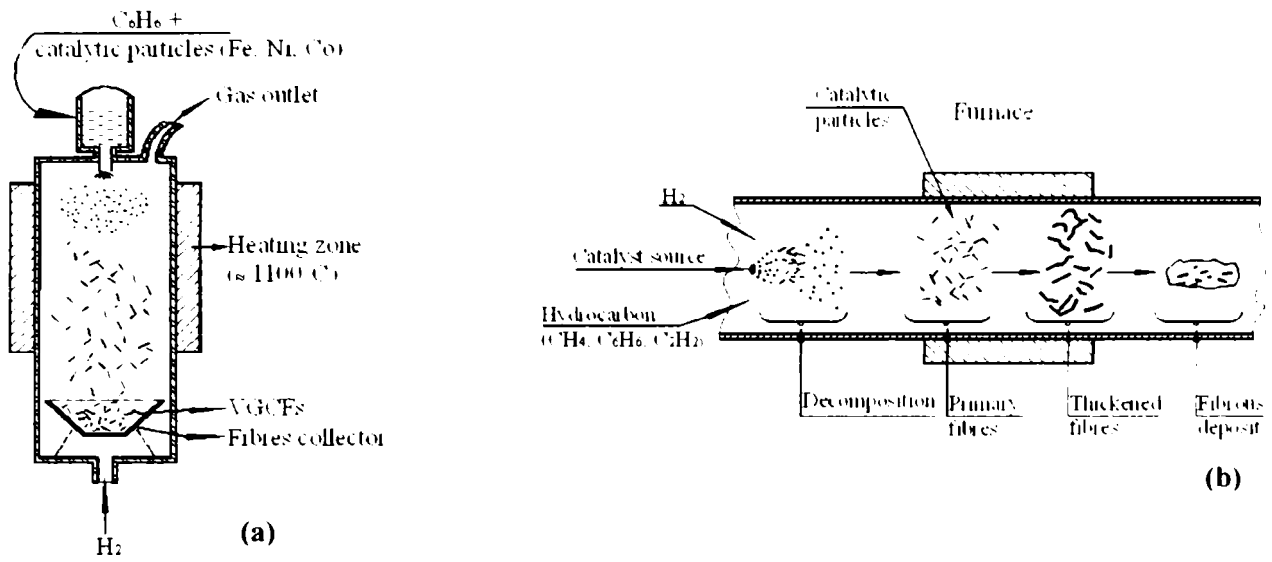

Figure 2.13 Floating catalytic particle methods for three-dimensional growth of fibres in a reaction chamber: (a) direct introduction of catalytic particles using benzene feedstock; (b) catalyst introduction by source such as ferrocene (the ferrocene decomposes into a suspension of ultrafine catalyst particles which are transported by the flow of hydrocarbons and hydrogen gas into the furnace area) [62].

Catalyst particles can be dispersed on the substrate as follow (Figure 2.14) [63]:

- Figure 2.14a – fine iron catalyst (diameter less than 10nm) in an alcoholic suspension are sprayed onto a substrate and dried by evaporation;
- Figure 2.14b – a solution of an inorganic salt is sprayed onto a metalic substrate and thermally decomposed at about 1000°C.
- Figure 2.14c – an organometallic compound such as the acetylacetonates of Fe, Co and Mn {ex. Iron (III) acetylacetonate ($Fe[CH_3COCHCOCH_3]_3$)}.

Figure 2.15 shows the distribution of fibre length for various precursors (iron III nitrate or ferric nitrate – $Fe(NO_3)_3$; ferrocene – $Fe(C_2H_5)_2$; iron III sulphate or ferric sulphate – $Fe_2(SO_4)_3$) [64].

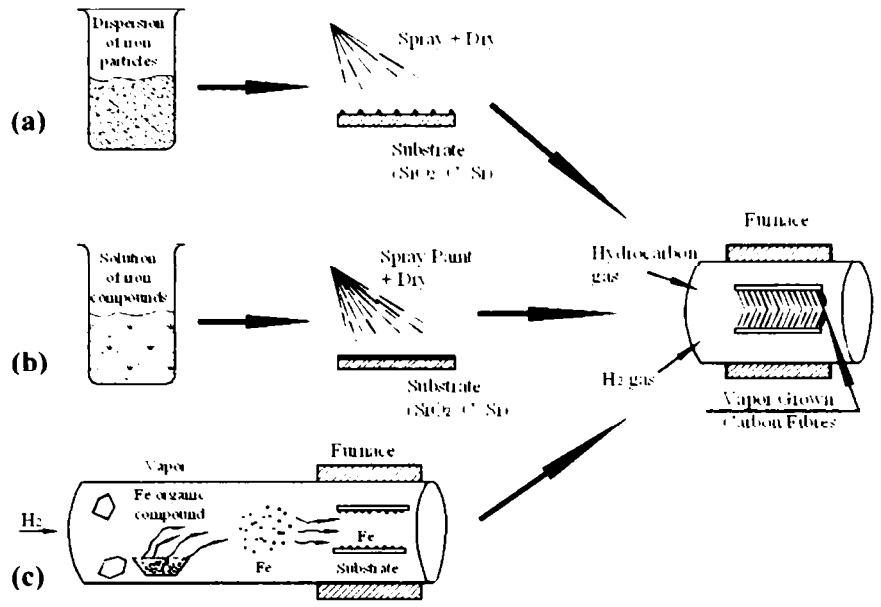

Figure 2.14 Dispersion of iron catalyst particles by three methods: (a) spaying and drying a suspension of Fe particles; (b) thermal decomposition of an inorganic Fe compound on heated substrate; (c) thermal decomposition of an organometallic compound on heated substrate [63].

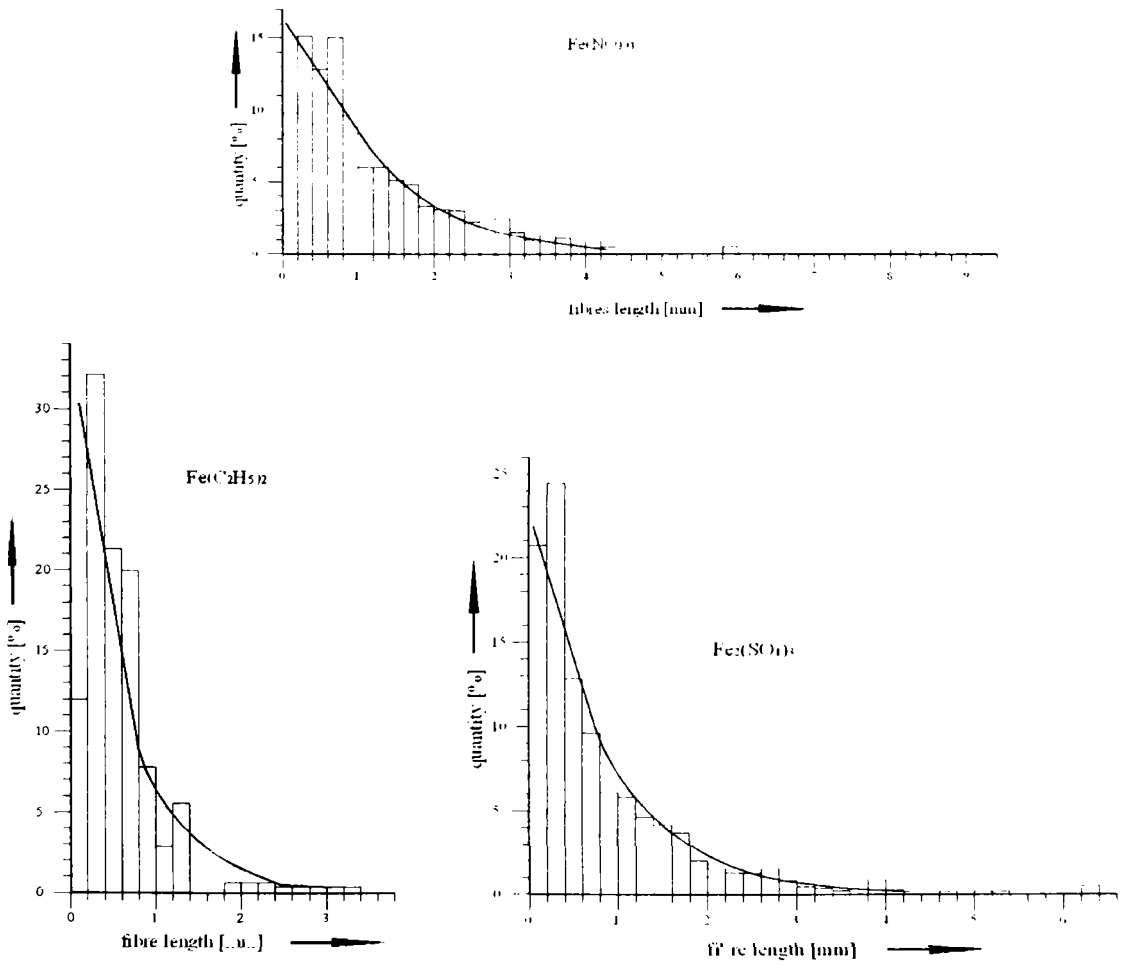

Figure 2.15 Fibre length distributions obtained from various precursors [57].

A simplistic view of the fibres growth mechanism is depicted in Figure 2.16 [57]. It can be observed that, in the first stage occurs the germination of the solid catalyst particle. In the second stage takes place the melting of the catalyst particle with formation of short filaments. Further the filament grows in length (third stage) and finally when the furnace temperature is higher than 1050°C, or the atmosphere is poisoned with oxygen or other ratio gases the filament will grow in diameter resulting the fibre (stage fourth).

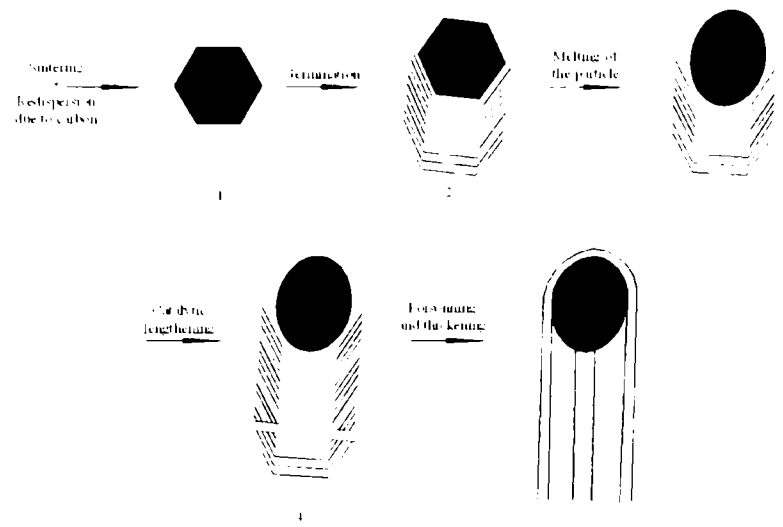

Figure 2.16 Fibre growth mechanisms [64].

R. T. K. Baker et al. already in 1972 showed a mechanism for growing the VGCF by the pyrolysis of the acetylene in the presence of Nickel particles [65]. Baker and co-workers deduced that the filaments had a duplex structure, with a disordered core surrounded by an outer graphitic skin [66]. This mechanism involved decomposition of acetylene on the exposed face of the metal particle (M) by an exothermic reaction, forming carbon (C) and releasing hydrogen (Figure 2.17). The newly formed carbon dissolves in the particle to form a eutectic of about 4.3% carbon and then diffuses through the particle to be re-deposited at the cooler end via an endothermic reaction, permitting filament growth to occur. The filament growth in length is stopped when the catalyst particle is poisoned.

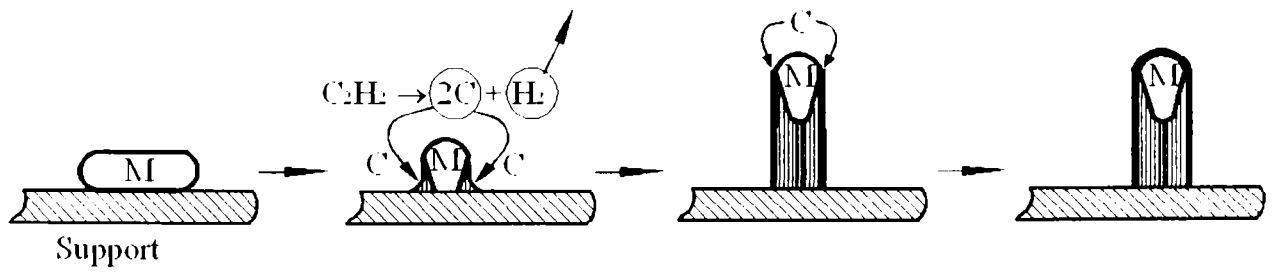

Figure 2.17 The most common growth mechanism of carbon fibres obtained through the pyrolysis of acetylene on a metal particle (M) [65].

The mechanism described above is the most common growth process of carbon fibre formation from the pyrolysis of acetylene, but is not the only one. Baker and Waite [67] have described a mode of growth called also extruded filament growth, where a Fe catalyst is deposited on a Pt support and the carbon which is formed by the breakdown of acetylene (C_2H_2) rapidly diffuses through to form a filament by upward growth (Figure 2.18).

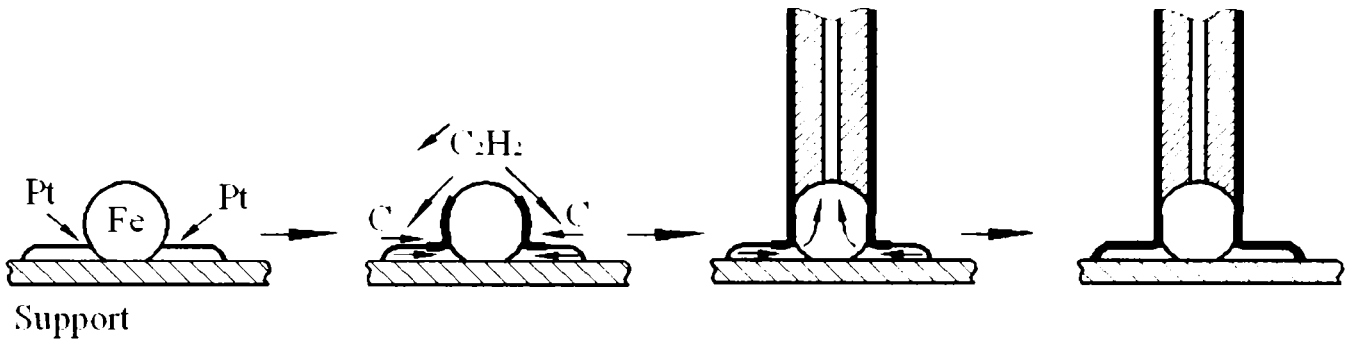

Figure 2.18 Fibre growth mechanisms in the Pt/Fe/C_2H_2 system [67].

Figure 2.19 shows the growth curves of CF from benzene by CCVD process [68]. It can be observed that, depending on the growing rate, the curves can be divided into three regions:

- first region – the growth rate has an initial acceleration rate. The fibre nucleation and elongation starts at about 1000°C (Figure 2.19a), the fibre starts to grow in length and the carbon layers are concentric;
- second region – a period of constant growth rate. The fibre stops to grow in length and the thickening process is started, when the hydrocarbons are decomposed at about 1040°C (Figure 2.19a).
- third region – a slowing down phase. The thickening process is very low after a time of exposition of more than three hours.

TEM – examinations of the vapour grown carbon nanofibres demonstrated that the diameter of the hollow tube within the ultra-thin fibres is bellow than that of the catalyst particle (Figure 2.20). The dense particle at the tip was identified as Fe_3C and was probably formed during the cooling stage at the end of the growing process [60].

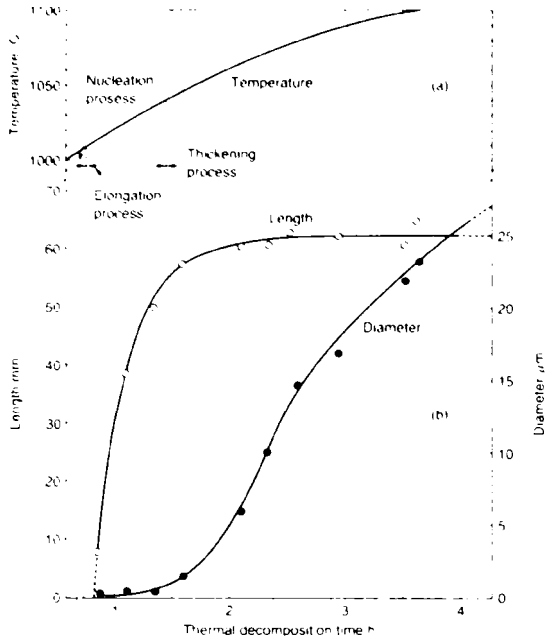

Figure 2.19 Typical growth curves of carbon fibre from benzene by CCVD:
(a) substrate temperature vs. growth time;
(b) fibre length and thickness vs. growth time.

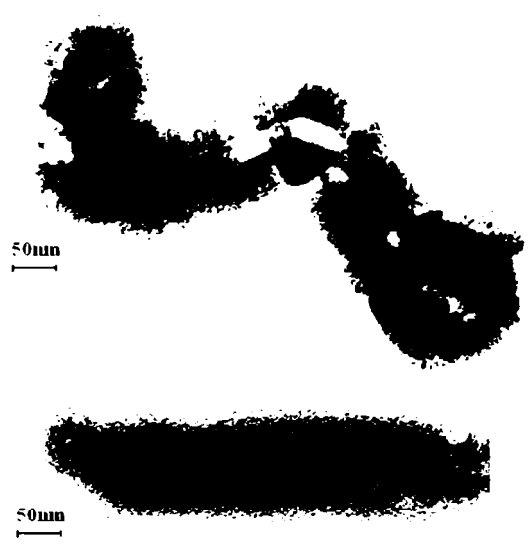

Figure 2.20 TEM – micrograph of the VGC. s...w...g ... ...ll w ub. nd the catalyst particle.

2.6.3 Structure of VGCFs

Graphite consists of layers of hexagonally arranged carbon atoms in a planar condensed ring system with each carbon 0.142 nm from its three nearest neighbours. The chemical bonds between each carbon atom are covalent with sp^2 hybridization. The graphene layers are stacked parallel to each other in a three-dimensional structure. Between these planes are 0.335nm and they are held only with weak forces – van der Waals forces [60].

The stacking of the layer planes occurs in two quite similar crystal forms: hexagonal and rhombohedral. The hexagonal form is the most common form (Figure 2.21).

The turbostratic layer is defined like a network of substantially perfect hexagons with parallel layer planes. Ideal graphite does not exist and the ideal crystal forms invariably contain defects, such as vacancies due to a missing atom (Figure 2.22a) or other defects include screw (Figure 2.22b) and edge dislocations (Figure 2.22c) [69].

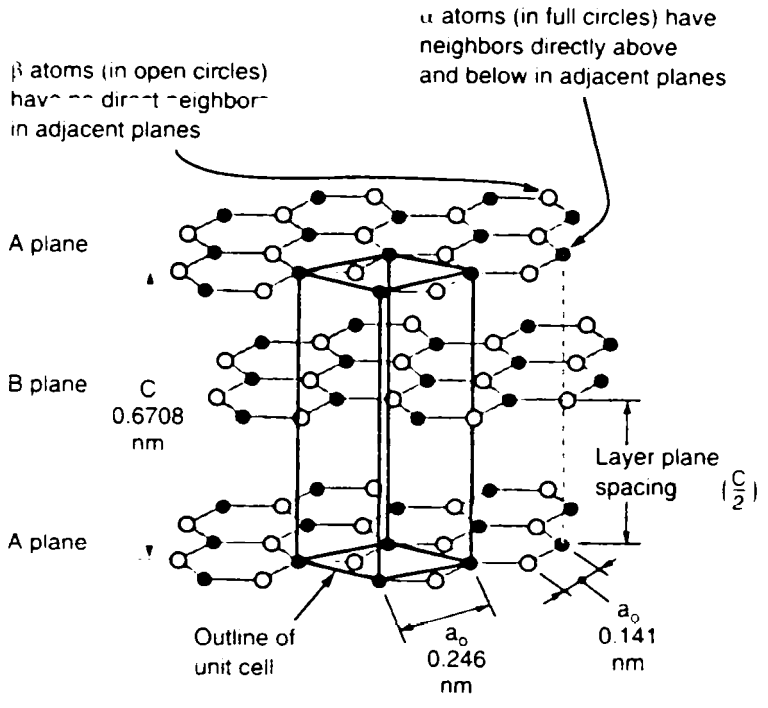

Figure 2.21 Hexagonal unit cell of graphite [60].

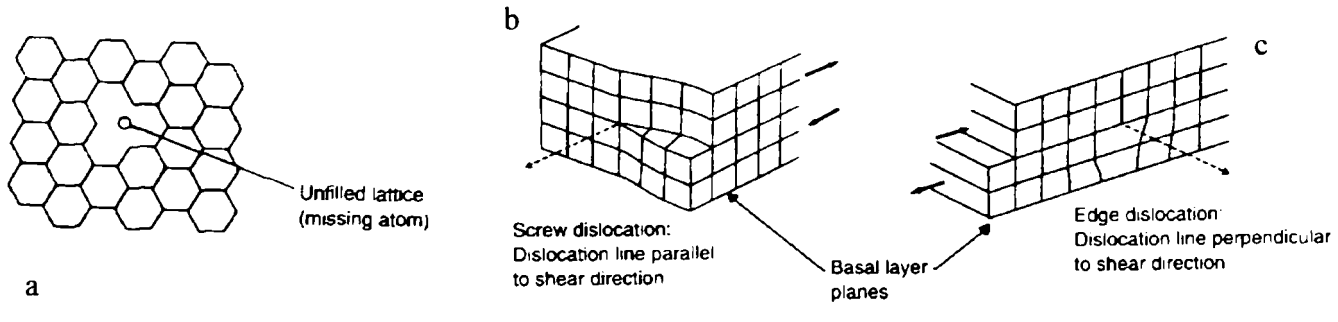

Figure 2.22 Schematic presentations of crystallite imperfections in graphite: (a) vacancies, (b) screw dislocations and (c) edge dislocations.

The structure of a carbon nanofibre can be conceptualized by rolling a perfect layer of graphite (called graphene) into a seamless cylinder (Figure 2.23). There are many ways to roll a graphene sheet into a single-wall nanotube (Figure 2.24). The way the graphene sheet is rolled is represented by a pair of indices (*n*,*m*) called the chiral vector. The integers *n* and *m* denote the number of unit vectors along two directions in the honeycomb lattice of graphene. If *m*=0, the nanotubes are called "zigzag". If *n*=*m*, the nanotubes are called "armchair". Otherwise, they are called "chiral" [70].

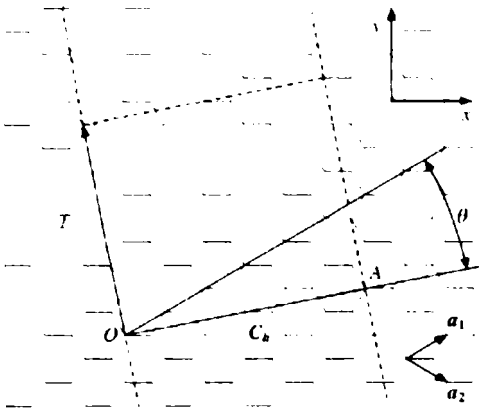

Figure 2.23 Sketch of the way to make a CNT, starting from a grapheme sheet [71].

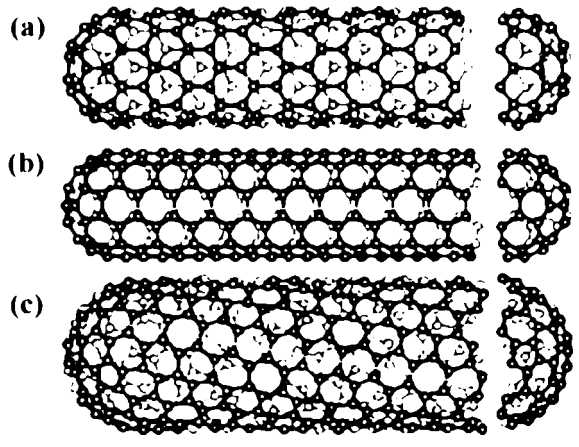

Figure 2.24 Basis type of CNT structure: (a) a zig-zag-type; (b) an armchair-type; (c) a helical nanotubes. The pink line represent the imaginary rolling-up grapheme sheet [72].

Figure 2.25 shows schematic the structure of carbon fibre growth by CCVD technique. The fibre consists of graphene layers nesting together as a series of concentric cylinders. The carbon layers form a three ring structure around a central core region. HRTEM micrographs (Figure 2.26) show the inner fibre core to have a disordered structure (Figure 2.26b), while the microstructure of the outer fibre core shows very well ordered, long parallel planes (Figure 2.26c) and the microstructure in the as-grown sheath region (Figure 2.26d) is somewhat more disordered than that shown in Figure 2.26c [73].

The structure of carbon nanofibre can be classified in terms of the angle of the graphene layers with respect to the filament axis, Figure 2.27 [74].

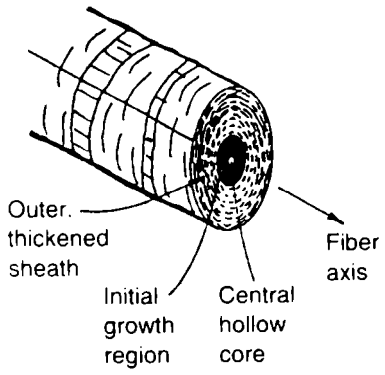

Figure 2.25 Sketch illustrating structure of CCVD filament – as grown at 100°C [69].

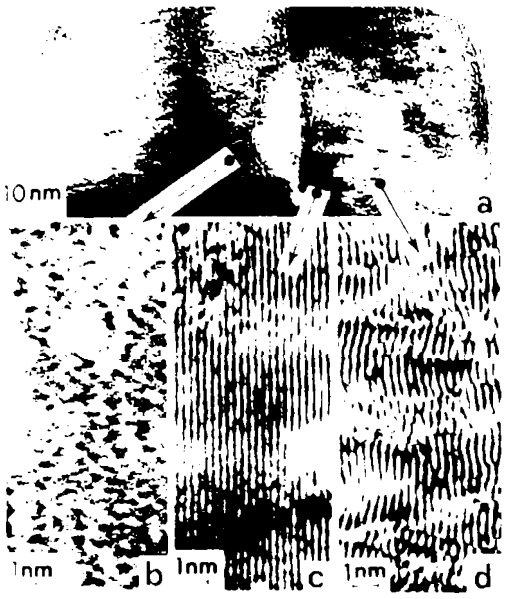

Figu.. 2.26 Microstructure of VGCF derived by benzene: (a) view along the fibre axis; (b) fringes from a disordered region; (c) (002) fringes near the hollow tube and (d) fringes in the external part of the fibre [73].

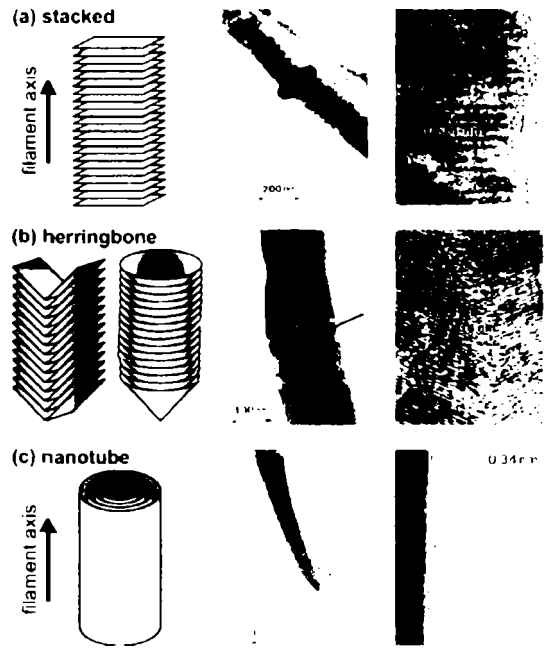

Figure 2.27 Structure of carbon nanofibre: (a) stacked, (b) herringbone and (c) tubular graphene walls [74].

2.6.4 Properties of VGCFs

2.6.4.1 Electrical Properties

Vapour grown carbon nanofibres and single-, or multi-wall carbon nanotubes have the most interesting property that they are metallic or semiconducting, depending on the diameter, graphitisation degree and chirality of the tube [75]. Figure 2.28 shows the electrical resistivity of the VGCFs as a function of the fibre diameters [76]. It can be observed that, the resistivity of the thin fibres (2-5 μm) is very low ($\approx 1\times10^{-5}\Omega m$) in comparison with the fibres with the diameter more than 15μm ($\rho\approx 1\times10^{-3}\Omega m$).

Curves of the electrical resistivity as a function of temperature are very useful for categorizing the lattice perfection of the fibre. Figure 2.29 shows the electrical resistivity of benzene-derived fibres growth by CVD method with single crystal graphite as a function of temperature [77]. These results can be discussed in terms of three distinct regimes:

- the fibre with an ideal structure (without defects) have the electrical resistivity less than $5\times10^{-6}\Omega m$, that means it can be approach with the resistivity of single crystal graphite ($>1\times10^{-7}\Omega m$).
- when the carbon fibre is partially carbonised the resistivity will increase with decreasing temperature. The resistivity is above $10^{-4}\Omega m$.
- between these two extremes, therefore $5\times10^{-6}\Omega m < \rho < 10^{-4}\Omega m$ the fibre resistivity is nearly independent of temperature.

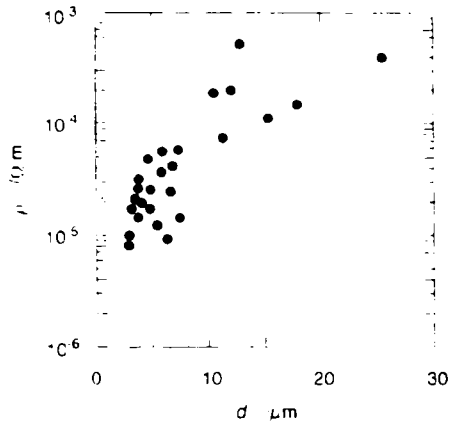

Figure 2.28 Electrical resistivity of the VGCF as a function of fibre diameters [76].

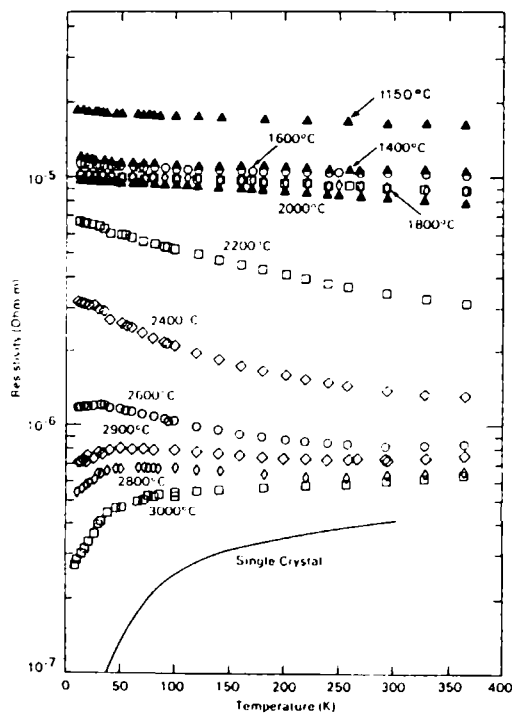

Figure 2.29 The electrical resistivity vs. temperature of VGCFs. Curves are draw for fibres with several heat treatment temperatures (the as-grown fibres are labelled 1150°C) and results are compared to single crystal graphite [77].

It can be concluded that the electrical resistivity of the carbon fibres can not attain the resistivity of the single crystal graphite, because the fibres present residual defects in structure. The effect of temperature treatment onto the fibre can be also remarked. If the heat treatment temperature is less than 2000°C, the resistivity vs. temperature is almost flat because both the carrier density and mobility are approximately independent of temperature in this range. The heat treatment leads to increasing the graphitisation degree of the fibre. Heat treatment about ~3000°C results in almost complete graphitisation.

The most important applications of carbon fibres utilize their high strength-to-weight ratio and therefore mechanical properties are of special interest. Figure 2.30 shows the tensile stress vs elastic modulus for different types of carbon fibres and other filaments [78]. First measurements of the mechanical properties of VGCFs were published by Koyama who reported the tensile strength between 1 – 3 GPa and Young's modulus 180-400 GPa [79]. The mechanical properties of the carbon fibres varied with fibre diameter [80, 81]. The tensile strength and elastic modulus decrease with the increase in fibre diameter. Tibbetts and Beetz measured the mechanical properties of VGCFs as a function of diameter, Figure 2.31. They observed that, the thicker fibres were obtained from a region of the furnace where growth rate was higher, and the resulting material had less orientation alignment of the graphene sheets.

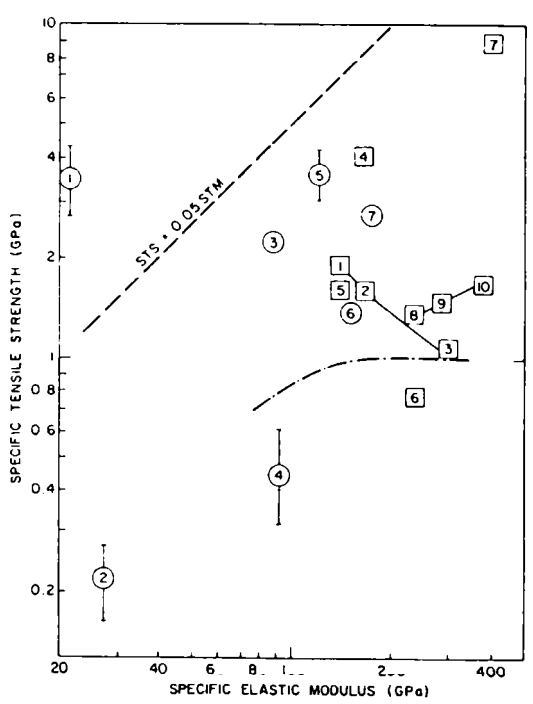

F.gu.e 2.30 Tensile strength vs. elastic modulus for various carbon fibres and other filaments, where: ① silica (whiskers), ② steel, ③ aramid, ④ alumina, ⑤ polyethylene (experimental), ⑥boron, ⑦silicon carbides, [1] high tensile CF (ex-PAN), [2] intermediate modulus CF (ex-PAN), [3] ultra high modulus CF (ex-PAN), [4] ex-PAN (experimental), [5] VGCF as-grown, [6] VGCFs with T_{HT}=3000°C, [7] graphite whiskers, [8] ex-pitch Carbonic HM50, [9] ex-pitch Carbonic HM60, [10] ex-pitch Carbonic HM 80, the dash-dot curve refers to ex-mesophase-pitch fibres and dash line refers to the "theoretical limit" between specific tensile strength (STS) and specific tensile modulus (STM) [60].

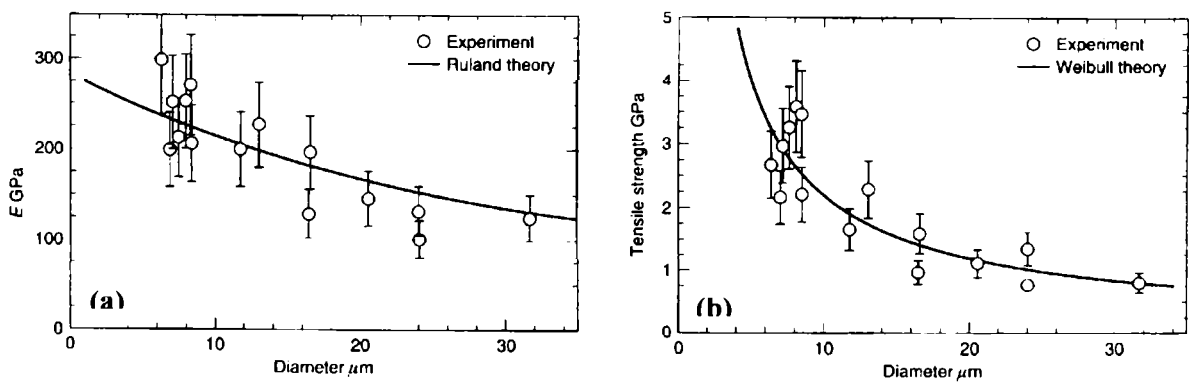

Figure 2.31 Young's modulus (a) and tensile strength (b) of VGCFs as-grown as a function of diameter [80].

CHAPTER III

FIBRE / MATRIX INTERFACES

3.1 Introduction

The interface between a fibre and a matrix can be defined as the bounding surface between these elements. The interface is very important because the area occupied is quite extensive. Considering a fibre in a certain matrix one can write that the surface-to-volume ratio of the fibre, ignoring the fibres end is as follows:

$$\frac{S}{V} = \frac{2\pi rl}{\pi r^2 l} = \frac{2}{r} \qquad (3.1)$$

where r is the radius of fibre and l is the length, respectively. Therefore, the interfaces area per unit volume increases with decreasing the fibre diameter [82].

When a load is applied to the carbon fibre composite, the stress is transferred from one carbon filament to another via the matrix material. If a weak fibre-matrix bond is present, then it will result in poor mechanical properties. This problem can be overcome by some form of surface treatment of carbon fibres. The wettability of the fibres by the surrounding matrix may be increased through different surface treatments.

3.2 Type of Bonding

It is important to be able to control the degree of bonding between the matrix and the reinforcement. The important types of interfacial bonding can be classified as follows [82]:

- mechanical bonding;
- physical bonding;
- chemical bonding;
  - dissolution bonding;
  - reaction bonding.

3.2.1 Mechanical Bonding

The interlocking effects between two surfaces can lead to a considerable degree of bonding. Any contraction of the matrix onto a central fibre would result in a gripping of the fibre by the matrix. This contraction can be obtained in situation in which the matrix in a composite radially shrinks more than the fibre on cooling from a high temperature [82]. This would lead

to a gripping of the fibre by the matrix even in the absence of any chemical bonding (Figure 3.1).

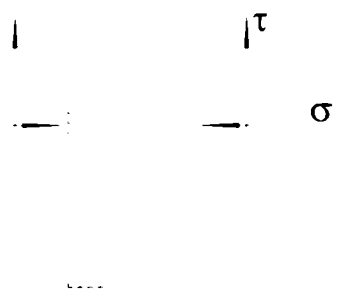

Figure 3.1 Mechanical gripping due to radial shrinkage of a matrix in a composite more than the fibre on cooling from a high temperature [82].

The interfacial shear stress (τ_i) is direct proportional with the radial gripping stress (σ_r) and the friction coefficient, (μ=0.1 – 0.6) (3.2).

$$\tau_i = \mu\sigma_r \qquad (3.2)$$

In general, mechanical bonding is a low-energy bond compared with the chemical bonding, i.e., the strength of a mechanical bond is lower than that of a chemical bond. Mechanical bonding could add, in the presence of reaction bonding, to the overall bonding. Also, mechanical bonding is efficient in load transfer when the applied force is parallel to the interface [83].

3.2.2 Physical Bonding

Any bonding involving weak, secondary or van der Waals forces, dipolar interactions, and hydrogen bonding can be classified as physical bonding. The bond energy in such physical bonding is approximately 8-16 kJ/mol [84].

Electrostatic attraction is another example of physical bonding (Figure 3.2). Forces of attraction occur between two surfaces when one surface carries a net positive charge and the other surface a net negative charge [85].

3.2.3 Chemical Bonding

A chemical bond is formed between a chemical group on the fibre surface and a compatible chemical group in the matrix (Figure 3.3). Atomic or molecular transport, by diffusion process, is involved in chemical bonding [86]. Solid solution and compound formation may occur at the interface, resulting in a reinforcement/matrix interfacial reaction zone with certain

thickness. This includes all types of covalent, ionic, and metallic bonding. Chemical bonding involves primary forces and the bond energy in the range of approximately 40-400kJ/mol. There are two main types of chemical bonding [87]:

- *dissolution bonding*: interaction between components occurs at an electronic scale. Because these interactions are of rather short range, it is important that components come into intimate contact on an atomic scale. This implies that surfaces should be appropriately treated to remove any impurities. Any contamination of fibre surfaces, or entrapped air or gas bubbles at the interface, will hinder the required intimate contact between the components.
- *reaction bonding*: a transport of molecules, atoms, or ions occurs from one or both of the components to the reaction site, that is, the interface. This atomic transport is controlled by diffusion processes. Such a bonding can exist at a variety of interfaces, e.g., glass/polymer, carbon/polymer, metal/metal, metal/ceramic, or ceramic/ceramic.

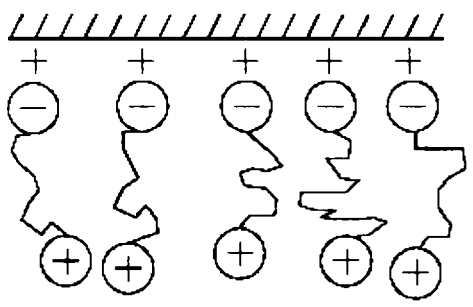

Figure 3.2 Cationic groups at ends of molecules attracted to anionic surfaces resulting in polymer orientation at the surface [85].

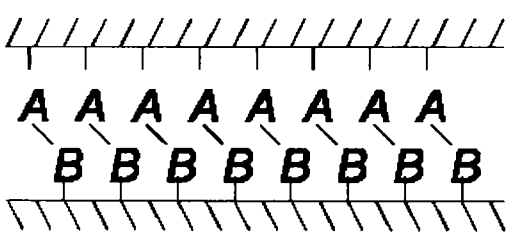

Figure 3.3 Schematically chemical bond formed between groups A on one surface and groups B on the other surface [86].

3.3 Optimum Interfacial Bond Strength

Two general ways of obtaining an optimum interfacial bond involve fibre or reinforcement surface treatments or modification of matrix composition [82].

Very weak interface or fibre bundle (No Matrix): This extreme situation will prevail when it has no matrix and the composite consists of only a fibre bundle. The bond strength in such composites will only be due to inter-fibre friction.

Very strong interface: The other extreme in interfacial strength is when the interface is as strong as or stronger than the higher-strength component of the composite, generally the reinforcement. In this case, of the three components - reinforcement, matrix, and interface – the interface will have the lowest strain to failure. The composite will fail when any weak cracking occurs at a weak spot along the brittle interface.

Optimum interfacial strength: An interface with optimum interfacial bond strength will result in a composite with an enhanced toughness, but without a severe penalty on the strength parameters. Such a composite will have multiple failure sites, most likely spread over the interfacial area, which will result in a diffused or global spread of damage, rather than a very local damage.

3.4 Wettability

Wettability gives information's about the ability of a liquid to spread on a solid surface. The wettability of a given solid by a liquid can be measured by considering the equilibrium of forces in a system consisting of a drop of liquid on a plane solid surface in the appropriate atmosphere [88]. This situation is presented schematic in the Figure 3.4. The liquid drop will spread and wet the surface completely only if this results in a net reduction of the system free energy. Note that a portion of the solid/vapor interface is substituted by the solid/liquid interface. Contact angle (θ) of a liquid on the solid surface fibre is a convenient and an important parameter to characterize wettability. Commonly, the contact angle is measured by putting a sessile drop of the liquid on the flat surface of a solid substrate [89].

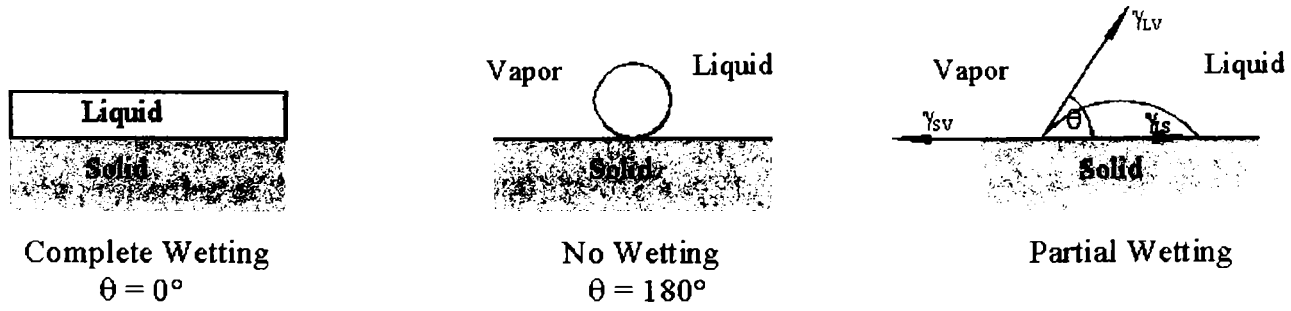

Figure 3.4 Different conditions of wetting: complete wetting, no wetting, and partial wetting [88].

The contact angle is obtained from the tangents along three interfaces: solid/liquid, liquid/vapor, and solid/vapor. The contact angle θ can be measured directly by a goniometer or calculated by using trigonometric relationships involving drop dimension. Therefore,

wetting can be understood in terms of two simple equations. The Dupré equation (3.3) for the thermodynamic work of adhesion, W_A, of a liquid to a solid states that

$$W_A = \gamma_1 + \gamma_2 - \gamma_{12} \qquad (3.3)$$

where γ_1 and γ_2 are the surface free energies of the liquid and solid respectively and γ_{12} is the free energy of the liquid-solid interface. This equation can be related to the physical situation of a liquid drop on a solid surface, using the Young equation (3.4). When the forces at a point A are resolved in the horizontal direction, then Young's equation states:

$$\gamma_{SV} = \gamma_{SL} + \gamma_{LV} \cos\theta \qquad (3.4)$$

where γ is the specific surface energy, and the subscripts SV, LS, and LV represent solid/vapor, liquid/solid, and liquid/vapor, respectively. If this process of substitution of the solid/vapor interface involves an increase in the free energy of the system, then complete spontaneous wetting will not result. Under such conditions, the liquid will spread until a balance of forces acting on the surface is attained; that is a partial wetting. Lower values of θ implies good wetting. The extreme cases being $\theta = 0°$, corresponding to perfect wetting, and $\theta = 180°$, corresponding to no wetting. In practice, it is rarely possible to obtain a unique equilibrium value of θ. Also, there exists a range of contact angle between the maximum or advancing angle, θ_a, and the minimum or receding angle, θ_r. This phenomenon, called the contact angle hysteresis, is generally observed in polymeric system. Among the sources of this hysteresis are: chemical attack, dissolution, inhomogenity of chemical composition of solid surface, surface roughness, and local adsorption.

Wettability is very important in polymer matrix composites because in the PMC manufacturing the liquid matrix must penetrate and wet the fibres. Among polymeric resins that are commonly used as matrix materials, thermoset resins have a viscosity in the 1-10 Pa range. The melt viscosities of thermoplastic are two or three orders of magnitude higher than those of thermoset and they show, comparatively, poorer fibre wetting characteristics and poorer properties of the composites [90].

3.5 Surface Treatment of Carbon Fibres

The high performance characteristics of composites depend not only on the physical properties of the composite components (fibres and matrix) but also on the interfacial region

(interface) that exists between these dissimilar components [91-94]. Effective fillers require good bonding (chemical, mechanical and physical) between the fibres and the matrix. It is known that the adhesion is controlled mainly by the chemical bonds [82]. Thus, chemical or physical treatments are applied to the carbon fibres and/or the polymer matrix in order to improve the fibre/matrix adhesion [95-99]. Surface modifications can increase the density of the functional groups on the carbon fibres and/or polymer matrix surface, improving the adhesion between these components and the wetting characteristics by additional chemical bonding [100].

3.5.1 Classification of Surface Treatments

Treatments can be applied by a batch or continuous process and can be divided in two big classes, the oxidative and the non-oxidative surface treatment. The following tree structures show the oxidative and non-oxidative surface treatments (Figure 3.5) [101-111].

3.5.2 Plasma Treatment

The field of plasma chemistry deals with the occurrence of chemical reactions in a partially ionised gas composed of ions, electrons and neutral species [112]. In a discharge, free electrons gain energy from an imposed electric field and lose this energy through collisions with neutral gas molecules. The transfer of energy to the molecules leads to the formation of a variety of new species including metastables, atoms, free radicals and ions. These products are all active chemically and can serve as precursors to the formation of new stable compounds.

Figure 3.6 shows the characteristics for a number of man-made as well as naturally occurring plasmas in terms of the electron temperature and density [113]. "Glow discharge" and "arcs" plasma present the great interest in industry. It can be observed that the plasma produced in glow discharge is characterised by average electron energies of 1-10eV and electron densities of $10^{9} - 10^{12}$ cm^{-3}.

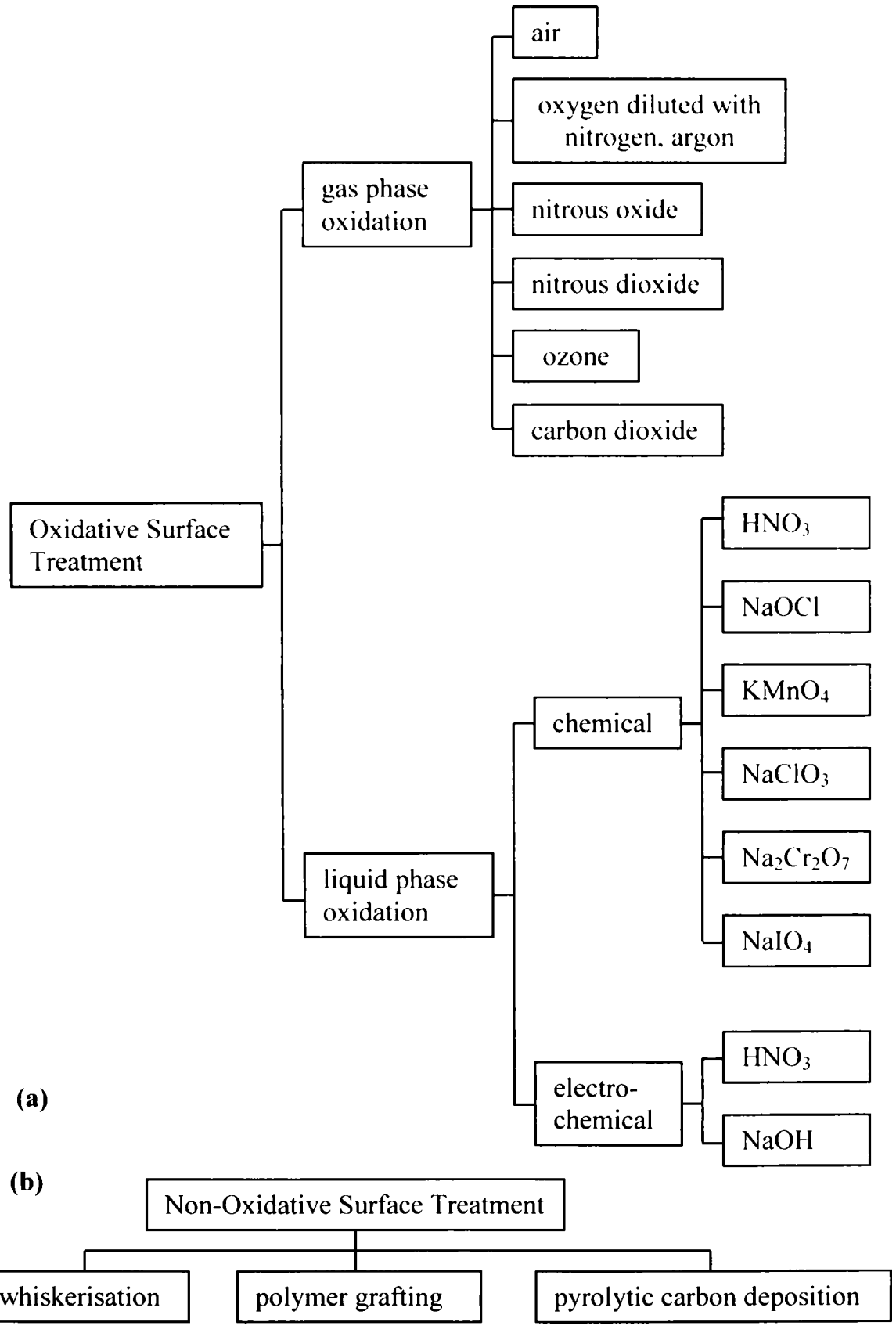

Figure 3.5 Surface treatment classification: (a) oxidative, and (b) non-oxidative.

3.5.3 Low Pressure Plasma Treatment

The low-pressure plasma can be created artificially by exposing gases to high-frequency electromagnetic fields in a vacuum chamber and causing them to discharge. The gas will become ionized and generate chemical radicals and ultraviolet radiation (Figure 3.7). In this manner a highly reactive process gas is created, which reacts with the surface of the material to be treated [114].

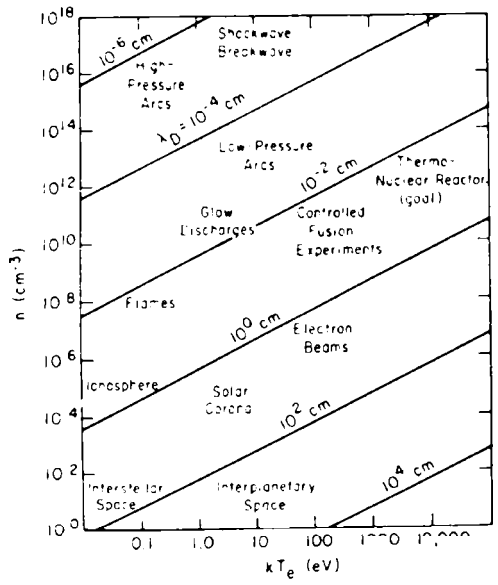

Figure 3.6 Typical plasma characterised by their electron energy and density [113].

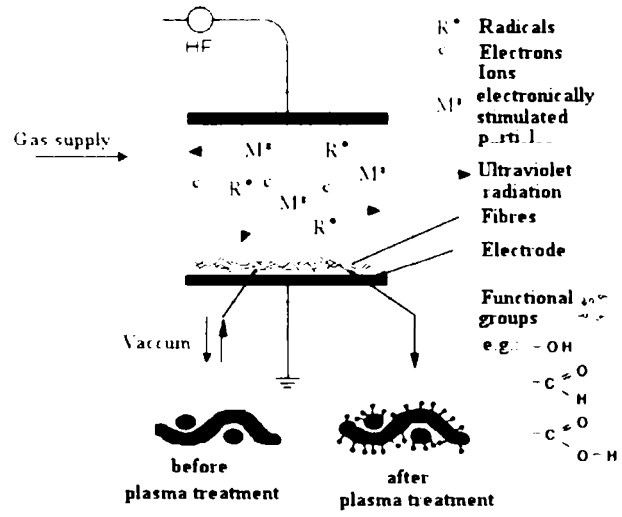

Figure 3.7 Low pressure plasma surface treatment principle (radio frequency discharge) [114].

The low pressure plasma can be generated in range of more frequency. The most popular excitation frequencies are in the radio frequency (RF) and the microwave (MW) range:

- the setup for RF excitation at frequencies above 1MHz is the simplest one. The energy can be fed to the plasma indirectly by capacitive or inductive coupling. The frequency for plasma experiments is limited below 200MHz and it is preferred to work with

fixed frequency and adjustable power (usually is sufficient a power outputs up to 300W) [115]. In the case of a capacitive coupled RF discharge two electrodes are mounted into a vacuum chamber. A process gas with a typical pressure of some Pascal is introduced. When the RF voltage exceeds a certain value in the range of some hundred volts depending on gas, pressure and reactor geometry, the discharge ignites. The major drawbacks of RF discharges are the need of electrodes and the relatively low degree of ionization.

- microwave discharge has the electromagnetic radiation frequency in the gigahertz range. The outputs power in the case of microwave generator is from a few watts up to a kilowatt. In the case of MW excitation no electrodes are necessary. In general a higher degree of ionization is achieved for MW discharge.
- RF and MW excitation can be used simultaneously which results in a *dual frequency discharge*. This configuration offers some specific advantages with respect to the accessible range of plasma conditions [116].

3.5.4 Chemical Reactions Occurring in Plasma Surface Treatment

Plasma surface treatment is a dry reaction process and depending on the process conditions, can have the following effects onto the carbon fibres surface [53]:

- cleans the outside surface of CF, creating a hydrophilic surface for enhanced bonding;
- removes the surface layer by a micro-etching process;
- penetrates the top few molecular layers and modifies the surface, creating a new surface chemistry, enabling improved composite interface;

A broad spectrum of reactions has been observed to take place in plasmas. The reactions are between electrons and molecules, ions and ions, ions and molecules, and electrons and ions. Figure 3.8 illustrates the typical plasma reactions occurring in low pressure plasma oxygen discharge [117].

The following table presents the typical gases used to treatment the carbon nanofibres and the possible functional groups created on the carbon fibres surface (Table 3.1). The functional groups lead to increase the wettability and the polar component of the surface energy of the VGCFs [118-120].

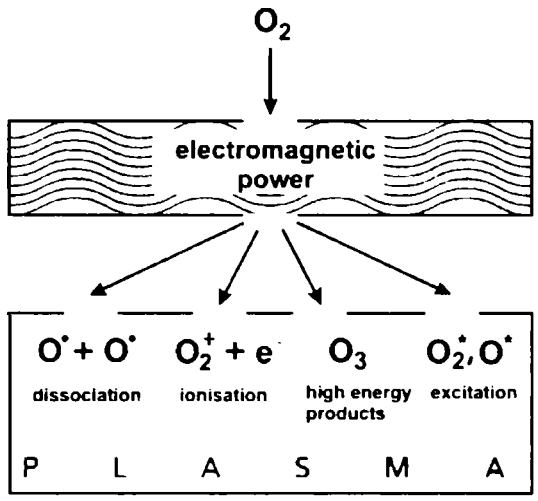

Figure 3.8 Typical plasma reactions occurring in an oxygen discharge [117].

Table 3.1. Typical gases used to create plasma.

Plasmas Gas	Functional groups detected on the carbon fibre surface
Air	–COOH, –OH
Oxygen	–OH, =O, –C=O, –COOH, –COOX, $-CO_3$
Ammonia, Nitrogen	$-CNH_2$, –C=NH
Argon	Cleaning effect

Jones and Sammann studied the effect of low power plasma on the carbon fibre [121]. They exposed the highly oriented pyrolytic graphite, ex-PAN and pitch based carbon fibres by air, ammonia and nitrogen plasma. The fibre was treated under following parameters: the plasma power is less than 1W, the resonator frequency is approximate 15MHz and the pressure is kept constant at 13.35Pa. The functional groups created onto the fibres surface were analysed by X-ray photoelectron spectroscopy. They found that the air plasma is more reactive to the fibres surface than nitrogen or ammonia plasma. Hydroxyl and carboxyl groups were detected on PAN based fibres while only hydroxyl groups were detected on pitch based fibres and HOPG. Both ammonia and nitrogen plasmas were successful in introducing aliphatic and aromatic amines ($C-NH_2$) together with small number of immines (-C=NH).

Shi and He have investigated the coating of carbon nanofibres by plasma polymerisation [122]. Styrene is used as the monomer for the plasma polymerization. The plasma polymerization treatment was between 15 – 20 minutes, plasma power 10 – 80 W and plasma pressure 40 – 60 Pa. They observed an ultra-thin film (approx. 2 – 7 nm) surrounding complete the VGCNFs by HRTEM analysis. The mechanical behaviour of composites containing 1, 3 and 5wt.% untreated and plasma treated shows an increasing of tensile strength up to 80% in the case of plasma coated fibres.

Fukunaga et al treated the pitch-based ultra high modulus carbon fibres by oxygen and argon plasma [123]. They observed that the fibres exposed to oxygen plasma have a smooth surface. They observed that the tensile strength of the filament before and after plasma treatment remain constant, therefore no damage of fibre was observed. The physical surface area was measured by krypton adsorption. The physical surface area was increased with only 23% due the O_2 plasma treatment. The oxygen groups on the surface treated fibres were seven times higher than that of the untreated fibres.

Boudou et al used microwave oxygen plasma to modify the surface of pitch-based isotropic carbon fibres [97]. Oxygen plasma was generated using 2.45GHz microwave radiation. The plasma power and treatment time were as follows: 20W/1min, 50W/1min, 75W/3min, and 150W/5min. They analysed the effect of plasma treatment by SEM, STM, gas adsorption, Raman spectrometry, XPS, and temperature – programmed desorption. They observed that the plasma treatment involved an increasing in nanometre scale surface roughness. XPS and TPD measurements indicate that the oxygen concentration reached its maximum after a short treatment time and lower plasma power (50W/1min), while a severe treatment (150W/5min) lead to a lower quantity of oxygen groups.

CHAPTER IV

METHODS OF PROCESSING THERMOPLASTIC COMPOSITES CONTAINING VGCFs

4.1 *Introduction*

Processing is the generic term for converting raw polymer and its adducts (additives, colorants, stabilizers, minor amount of other polymers, fillers, reinforcements, and so on) to useful products of commerce. The raw thermoplastic polymer (powder or granulate) such as polypropylenes, polyamides and polyethylenes mixed with different adducts such as additives and carbon fibres is converted to pellets by compounding (usually the extrusion process is used). The pellets are then converted into continuous finish goods by a second extrusion step or into discrete shapes by injection moulding. Polymer (composite) interaction is most important for development of the final product properties. There are two major concerns in the manufacture of any product:

- will the finish part meet all required and specified design criteria?
- can the part be produced at the minimum cost for the projected market size?

These two criteria are strongly interrelated and usually require complex technical and marketing analysis [124].

Polymer processes can be catalogued in many different ways. Table 4.1 present the typical thermoplastic processing as a function of polymer viscosity, production rate, and capital costs.

Table 4.1 Thermoplastics processing ways [124].

Process	**Viscosity**	**Production volume/year**	**Costs**	
			Equipment	**Tooling**
Blow moulding	Medium	10^4 - 10^7	M → H	L → M
Calendering	Medium	10^4 - 10^7	VL	
Casting	Very low	$10 - 10^2$	VL	VL
Extrusion, film	Medium	10^5 - 10^7	H → VH	H
Extrusion, profile	Medium	10^4 - 10^7	M → H	M
Extrusion, sheet	Medium	10^6 - 10^7	H → VH	H
Injection moulding, compact	Low to medium	$*10 - 10^2$ / $**10^4 - 10^7$	M → VH	M → H
Injection moulding, foam	Low to medium	$10^3 - 10^5$	VH	M → H
Machining		$10 - 10^2$	L	VL
Melt flow stamping	Low to medium	$10^3 - 10^5$	M → H	M
Rotational moulding	Medium to low	$*10 - 10^2$ / $**10^4 - 10^6$	M → H	L
Thermoforming	Medium	$*10 - 10^2$ / $**10^4 - 10^7$	M → H	L

Where: VL (very low) < 20,000$; L (low) < 50,000$; M (medium) < 100,000$; H (high) < 250,000$, VH (very high) > 250,000$; * - hand unit; ** - automatic unit.

4.2 Extrusion

Extrusion is the most widely used way of fabricating plastic products. The polymer materials (powder or granulate) are frequently mixed with additives, colorants, stabilisers, and/or fibres. In the process known as compounding, this mixture is heated to fluid state, mixed and shaped into pellets [125].

Extruders in the polymer industry come in many different designs. The screw extruder is the most common one. The screw extruders are divided into single screw, twin screw and multi screw extruder (more than two screws). The single screw extruder is the most important type of extruder used in the polymer industry. Its key advantages are relatively low cost, straightforward design, ruggedness and reliability and favourable performance / cost ratio. But has disadvantages, too. The single screw extruder can not ensure a good compounding (to mix polymer with filler), the devolatilisation, chemical reactions and to extrude profile thermally sensitive materials (e .g. PVC). The twin screw extruder can cover the disadvantages of the single screw extruder [126].

4.3 Twin Screw Extruder

The main function of an extruder is to develop sufficient pressure in the material to force the material through the die. The pressure necessary to force a material through the die depends on the geometry of the die, the flow properties of the material, and the flow rate.

The twin screw extruders based on the geometrical configuration of screws are divided as shown in Figure 4.1 [127]. Figure 4.2 shows schematically the intermeshing and nonintermeshing co– and counter– rotating twin screw extruder.

The solid polymer (pellets or powder) is fed in the hopper, and by gravity flows into the barrel, where an Archimedes type screw rotates at a given speed. Consequently, the solid polymer is dragged along the screw's helical channel, where it starts melting. The molten material subsequently accumulating in a pool, segregated from the surviving solids. Fillers are often added to a downstream feed port at a point where the polymer material is melted. This

melt is homogenized, pressurized and forced to pass through the die, which gives the desired shape to the product, Figure 4.3. The product is cooled in water bath and then is cut in pellets for further processing, like injection moulding.

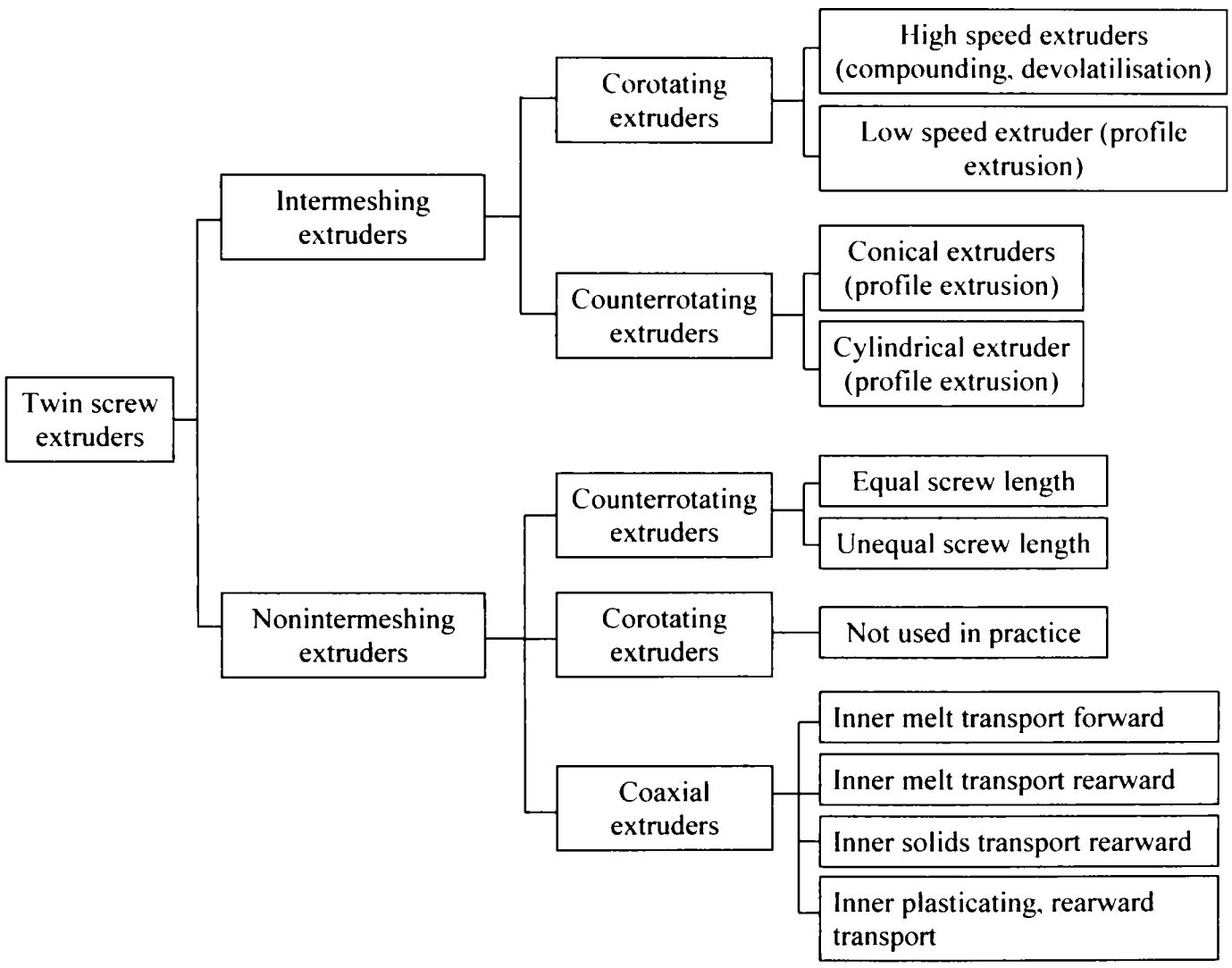

Figure 4.1 Classification of twin screw extruders.

Figure 4.4 shows the typical components of the twin screw extruder and are the following [128]:

- the extruder drive unit;
- the extruder screw;
- the extruder barrel;
- the extruder hopper;
- the extruder throat;
- the extrusion die;
- barrel heating and cooling;
- screw heating and cooling;

- the screen pack;
- the breaker plate;
- the reducer;
- gear pumps;
- instrumentation and control.

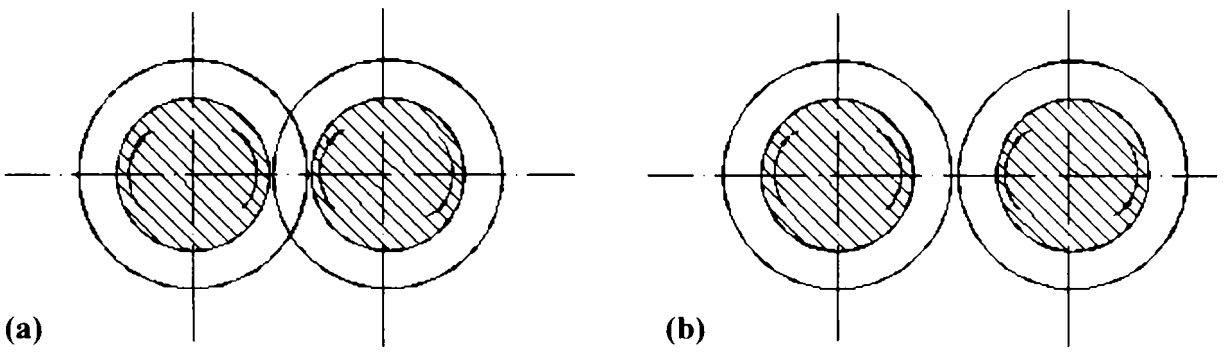

Figure 4.2 Schematically presentation of the intermeshing (a) and nonintermeshing (b) co– (blue arrows) and counter– rotating (black arrows) twin screw extruder.

To compound the polymer materials with vapour grown carbon fibre is very important not to destroy the fibres during the extrusion process. Therefore, an optimal screw geometry should be choose for each functional zone to not grind the fibres. The extruder should also have a barrel with several feed opening. In the following section the extruder barrel and the screw geometry are described.

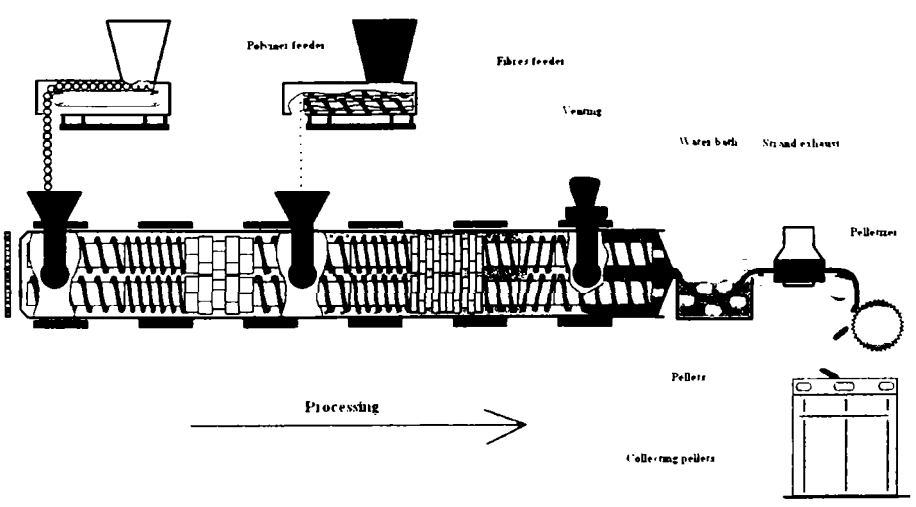

Figure 4.3 Compounding line [129].

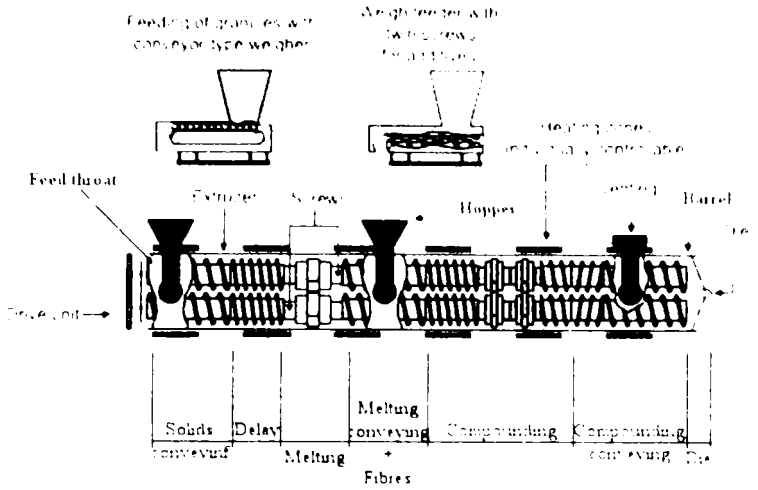

Figure 4.4 Twin screw extruder components [129].

4.4 The Extruder Barrel and Feed Throat

The extruder barrel is the cylinder that surrounds the extruder screw. The barrel is a straight cylinder usually equipped with a bimetallic liner. This liner is a hard, integral layer with high wear resistance (normally the wear resistance of the barrel is better than that of the screw, because is much easier to rebuild and replace the screw than the barrel).

The barrel may have at least one feed opening and can have a vent opening through which volatiles can be removed from the melting polymer (this process called devolatilisation), Figure 4.5. An extruder with a vent port should use a special screw geometry to keep the plastic melt from coming out of the vent port. The vent port is often connected to a vacuum pump; a high level of vacuum improves the removal of volatiles from the plastic. Figure 4.6 shows schematically an extruder barrel with three feed opening. The VGCFs can be mixed with the PP in three ways (Figure 4.6), as follow:

- PP powder or granulate and VGCFs mechanically mixed together and feed in the first hopper. In this way, it is possible that the fibres will be grinded during the first phase of the extruder – feed section. The advantage is that the extruder has a modest complexity and do not required a second feeder for fibres, therefore relatively a low cost.
- VGCFs can be introduced in the second hopper that means the fibres are introduced in the melted polymer – compression zone. The shearing possibility is not so strong like in the first case;

- VGCFs can be introduced in the last hopper, before the extruder die - metering zone. The shearing possibility is fast non-existence, but the problem which can occur is the way how the fibres are distributed and dispersed in matrix. In this situation is very hard to achieve an uniform distribution of the fibres in the polymeric matrix.

The engineers must to be able to solve this problem, to predict the process performance for a given combination of polymer properties, fibres properties, screw geometry and operating conditions (screw speed and barrel temperature profile), that to obtain the best extruder performance and the highest composite properties [130].

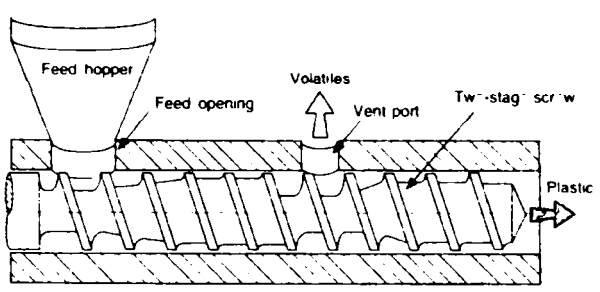

Figure 4.5 An extruder barrel with one feed opening and a vent port [125].

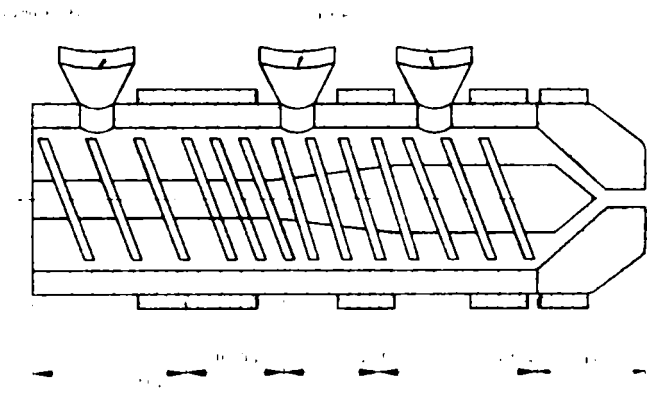

Figure 4.6 An extruder barrel with three feed opening.

The feed throat in connected to the barrel and contains the feed opening through the polymer (powder or pellets) materials is introduced in extruder.

4.5 The Extruder Screw

The single most important mechanical element of a screw extruder is the screw. The proper design of the geometry of the extruder screw is of crucial importance to the proper functioning of the extruder.

In many discussions of extrusion, reference is made to a so-called standard extruder screw, Figure 4.7. The general characteristics of the standard extruder screw are as follow (these dimensions are approximate, but the majority of the extruder screws used today have these characteristics) [128]:

- total length 20D – 30D (D – screw diameter);
- length of feed section 4D – 8D;
- length of metering section 6D – 10D;

- number of parallel flights 1;
- flight pitch 1D (helix angle 17.66°);
- flight width 0.1D;
- channel depth in feed section 0.10D – 0.15D;
- channel depth ratio 2 – 4;

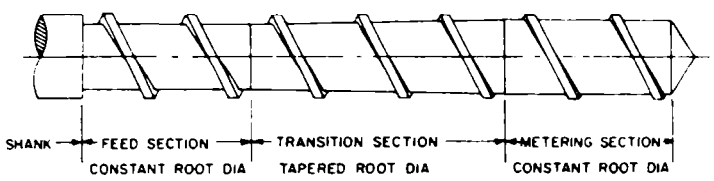

Figure 4.7 The standard extruder screw [128].

The standard screw design is by no means an optimum screw design. It was developed over the last several decades mostly in an empirical fashion and works reasonably well with many polymers. There are a large number of modifications of the standard extruder screw in use today. Figure 4.8a shows the standard screw with an additional flight in the feed section. The additional flight is intended to smooth out the pressure fluctuation caused by the flight interrupting the in-flow of material the feed hopper every revolution of the screw, and the forces which acting on the screw are balanced, thus the screw deflection is less likely to occur. On the negative side, the additional flight reduces the open cross-sectional channel area and increases the contact area between solid bed and screw. Figure 4.8b shows a variable pitch extruder screw. The varying pitch allows the use of the locally optimum helix angle, i. e. optimum helix angle for solids conveying in the feed section and optimum helix angle for melt conveying in the metering section of the screw.

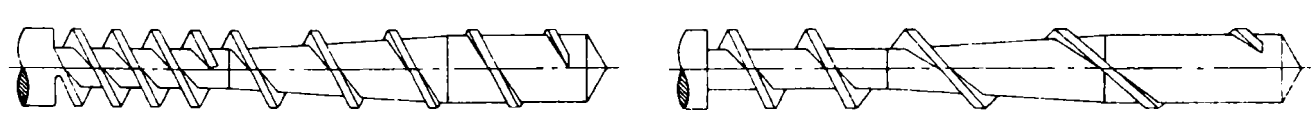

(a) (b)

Figure 4.8 Standard screw with additional flight in feed section (a) and with variable pitch (increasing pitch) (b) [128].

Mixing can be defined as a process to reduce the non-uniformity of a composition. The basic mechanism of mixing is to induce physical motion of the ingredients. The types of motion that can occur are molecular diffusion, turbulent motion and convective motion. A significant mixing takes place only when the polymer is in the molten state. Therefore, the mixing zone in the extruder extends from the start of the plasticating zone to the end of the die.

The mixing capacity of standard extruder screws is relatively limited. Therefore, many modifications have been made to improve the mixing capacity of the standard screw. The mixing section can be divided into distributive and dispersive mixing section. The distributive mixing refers to mix fluid components and which do not exhibit a yield point. If the component exhibiting a yield point is a solid, this type of mixing is referred to as dispersive mixing. Dispersive mixing elements are used when agglomerates or gels need to be broken down. Figure 4.9 show several mixing screw design.

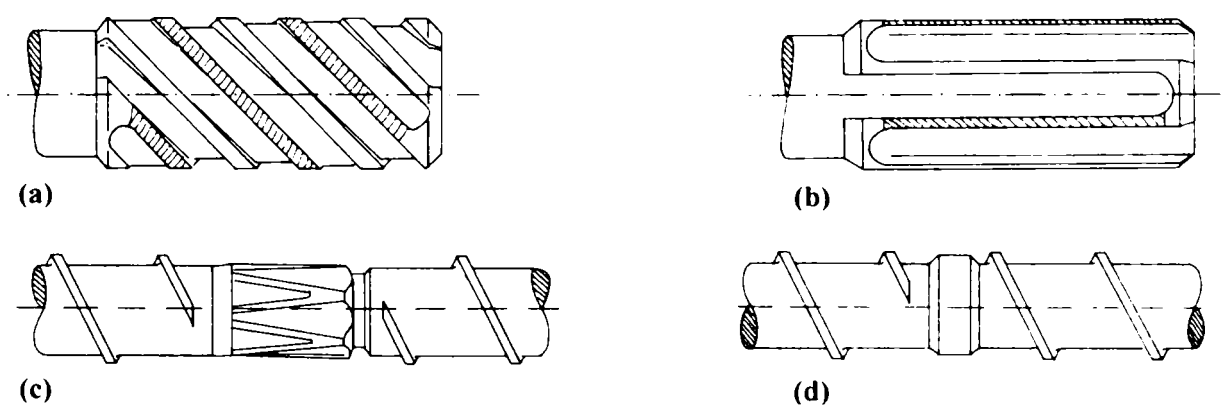

Figure 4.9 Various designs of the dispersive mixing elements: (a) Egan mixing section; (b) Union Carbide mixing section; (c) dray mixing section; (d) blister ring [128].

4.6 Injection Moulding

Injection moulding is the second most widely used polymeric fabrication process. It involves the cyclic injection of a molten or liquid resin into a hollow cavity under pressure.

The injection moulding process of thermoplastics composite can be divided into several stages in the case of the most common reciprocating screw machine, Figure 4.10. The plasticating unit operates pretty much as an extruder, melting and homogenising the material in the screw/barrel system. This stage is called the plasticization stage. The screw is allowed to retract, to make room for the moulted material in the space between the screw tip and a closed valve of the nozzle, called as the melted material reservoir. In the second stage, the injection stage, the screw is used as a ram for the rapid transfer of the moulded material from the reservoir to the cavity of the closed mould unit. In the last stage, ejection stage, the mould is kept at a temperature below the solidification temperature of the injected material, and after the cooling the mould can be open and the injected product is ejected. The cooling of the

material in the mould is often the limiting time factor in injection moulding, because of the low thermal conductivity of polymers [131].

Figure 4.11 shows schematic the most commonly reciprocating screw machine [132]. Two distinct unit referred to as feed unit [F] and the mould unit [M], are mounted on a frame (F`). The operation is primarily hydraulic with pumps (H) driven by electrical motors (M), used in conjunction with hydraulic cylinders, motors, valves, accumulators and tanks. Sophisticated computer based control system are now increasingly used to improve the quality and uniformity of products. The feed unit [F] consists of the plastification/injection cylinder (C), the axial screw drive (D) and the rotational screw drive (D`). The whole unit (I) is sometimes mounted on a carriage for limited axial displacement along the machine frame. The screw is normally fitted with a non-return valve. The mould unit generally consists of two stationary vertical platforms (P) and (B) connected by four cylindrical bars or columns (R), and a moving platen (P`) driven by a clamping mechanism (C`). The stationary and moving halves of the tool (T) are fastened to the platens (P) and (P`).

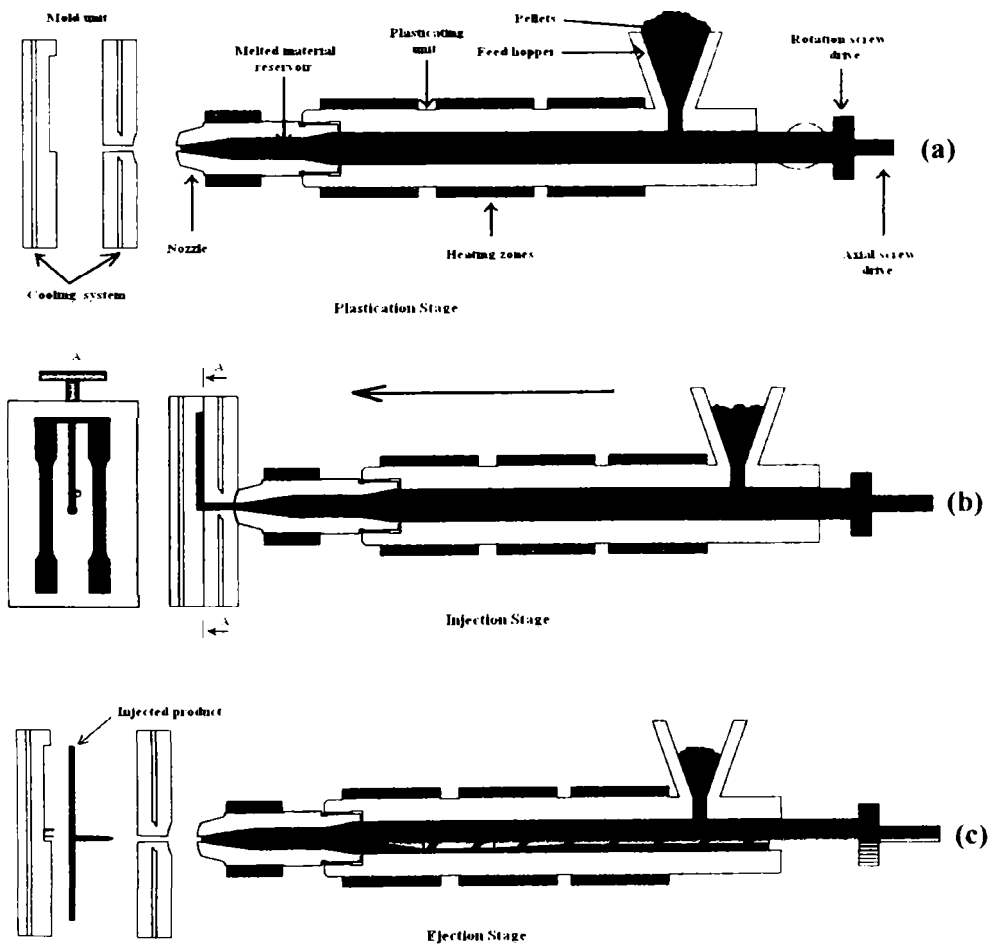

Figure 4.10 Injection moulding principle: plasticization stage (a), injection stage (b), and ejection stage (c) [133].

System of clamping mechanism is usually mechanic, hydraulic or hydromechanical. Figure 4.12 shows schematic a hydromechanical injection moulding clamp mechanism [134].

The geometry of the mould cavity depends on the dimensions of the product. When a part is large compared with the plasticating and transfer capacity of the injection press, than only one unit is moulded at a time. If the part is small, many units can be formed at one time. Each mould cavity is connected to the mould sprue by a runner-gate system, Figure 4.13. If all cavities are connected to the sprue via runners of the same length and cross-sectional dimension, the runner system is called balance system, if not is called unbalance system (Figure 4.13b, c) [124].

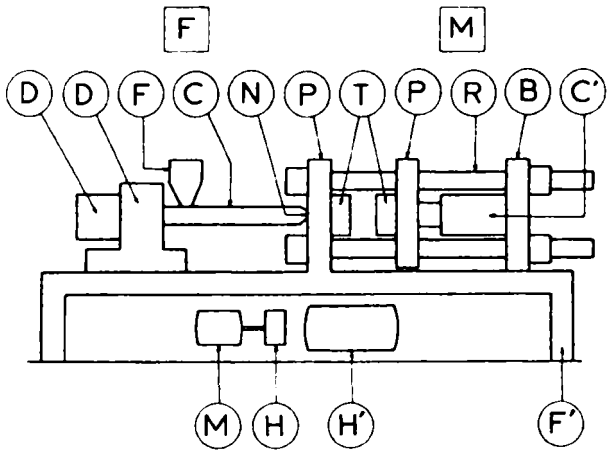

Figure 4.11 Injection moulding machine: [F] feed unit; [M] mould unit; (D) axial screw drive; (D`) rotational screw drive; (F) feed hopper; (C) plastication/injection cylinder; (P) stationary platen; (T) mould; (P`) moving platen; (R) tie bars; (B) back platen; (C`) mould clamping mechanism; (F`) machine frame (H`) hydraulic pump; (M) electric motor; (I) injection unit [132].

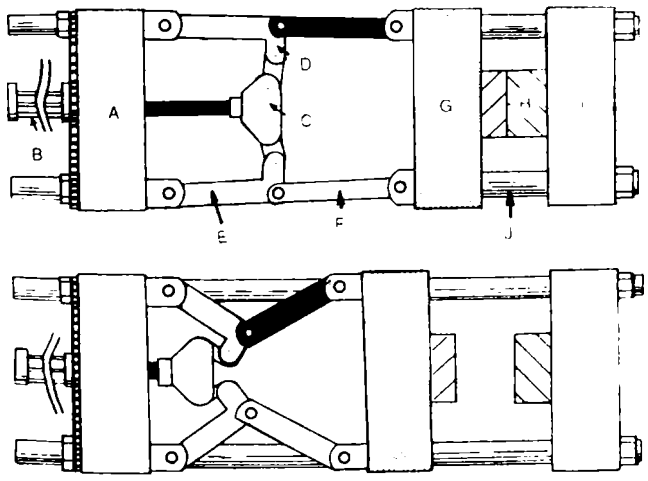

Figure 4.12 Hydromechanical injection machine clamp schematic: (A) ils ock platen; (B) actuating cylinder; (C) crosshead; (D) crosshead link; (E) back link; (F) front link; (G) moving platen; (H) Mould; (I) stationary platen; (J) tie rod [134].

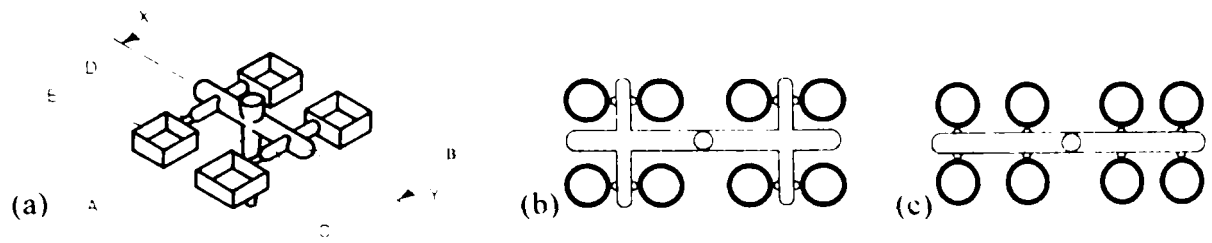

Figure 4.13 (a + b) Four cavity balanced runner system (symmetry line XY): A – sprue, B – primary runner, C – secondary runner, D – gate, E – cavity; (c) unbalanced runner system [124].

CHAPTER V

ANALYSIS AND CHARACTERISATION OF VAPOUR GROWN CARBON NANOFIBRES

5.1 Introduction

The vapour grown carbon nanofibres were characterised by several investigation methods. The morphology as well as the structure of VGCNFs were studied by scanning electron microscopy (SEM) and transmission electron microscopy (TEM). The graphitisation degree of the fibres was measured by X – ray diffraction (XRD). The thermal stability and the electrical properties of the fibres were analysed by thermogravimetrical measurement and DC electrical measurements.

5.2 The Morphology and the Structure of VGCNFs

The VGCNFs studied in these experiments are provided from two different manufacturers. These are Pyrograf® III from Applied Sciences, Inc. (ASI), Cedarville, Ohio and GANF®1 from Grupo Antolin Ingenieria S.A, Burgos, Spain.

Pyrograf®-III is a patented, very fine, highly graphitic, yet low cost, carbon nanofibres. Pyrograf®-III is available in diameters ranging from 60 and 150 nm and a length estimated to be 30-100 μm [135]. Table 5.1 summarises the typical characteristics of these fibres.

Table 5.1 Pyrograf®-III (PR-24) - typical characteristics [135].

Properties	Values	Unit
Fibre diameter	60 – 150	nm
Fibre length	30 – 100	μm
N_2Surface area	50 – 60	m^2/gm
Moisture content	<5	%
Iron content	<14000	ppm
PAH content	<1	mg PAH/g fibre

Grupo Antolin Carbon Nanofibres (GANF®) are s-VGCF, (submicron vapour grown carbon fibres) with a very small diameter, an excellent aspect ratio and a highly graphitic structure, (graphitisation degree about 70%). They are characterised by high transport properties (exceptionally high electric and thermal conductivity) [136]. The Grupo Antolin fibres were produced in different processes: SEMANA (pilot fibres) and GANF®1 stripped and debulked (the commercially available fibres on the market). Table 5.2 summarises the typical characteristics of the GANF®1 fibres.

Table 5.2 GANF®1 - typical characteristics [136].

Properties	Values	Unit
Fibre diameter	20 – 80	nm
Fibre length	>30	μm
Bulk density	>1,97	g/ccm
Apparent density (as grown)	0.009	g/ccm
Apparent density (stripped and debulked)	0.060	g/ccm
Specific surface area (N_2)	150 – 200	m^2/g
Surface energy (stripped and debulked)	≈ 200	mJ/m^2
Young modulus (theoretic)	230	GPa
Tensile strength (theoretic)	2.7	GPa

5.2.1 Scanning Electron Microscope

The morphology of the VGCNFs was studied by scanning electron microscopy. The SEM, with a typical magnification of X300,000 and a resolution of 3 nm in the high vacuum (HV) mode and 5 nm in the low vacuum (LV) mode, has a much greater depth of field than either the optical microscope (OM) or the transmission electron microscope (TEM).

Using a W – or LaB_6 cathode, an electron gun is generated at the top of the electron column. The beam is focused into a small spot, which is scanned over the specimen in a raster pattern. The specimen is mounted in a vacuum chamber. The magnification is determined by the area of the sample scanned by the beam. Secondary electrons are produced by the interaction of the primary electron beam with the sample; a positively biased detector collects these secondary electrons. Secondary electron (SE) images have excellent depth of field, allowing the depiction of complex topographical features on fracture surfaces, fibres, powders and cross-sections samples. The high-quality back-scattered electron (BSE) images provide atomic number contrast and, in some cases (depending on the surface finish), crystallographic contrast [137].

The scanning electron microscope used in this research is from Philips model XL 30 ESEM TMP. The XL 30 microscope is equipped with a field emission gun operating at an acceleration voltage up to 30kV and is able to achieve a very high resolution (2nm). Its useful magnification range is about 1,000-250,000X. The microscope is equipped with secondary electron and backscattered electron detector, energy dispersive X-Ray spectrometry (EDX) and electron beam backscatter patterns (EBSP) system [138].

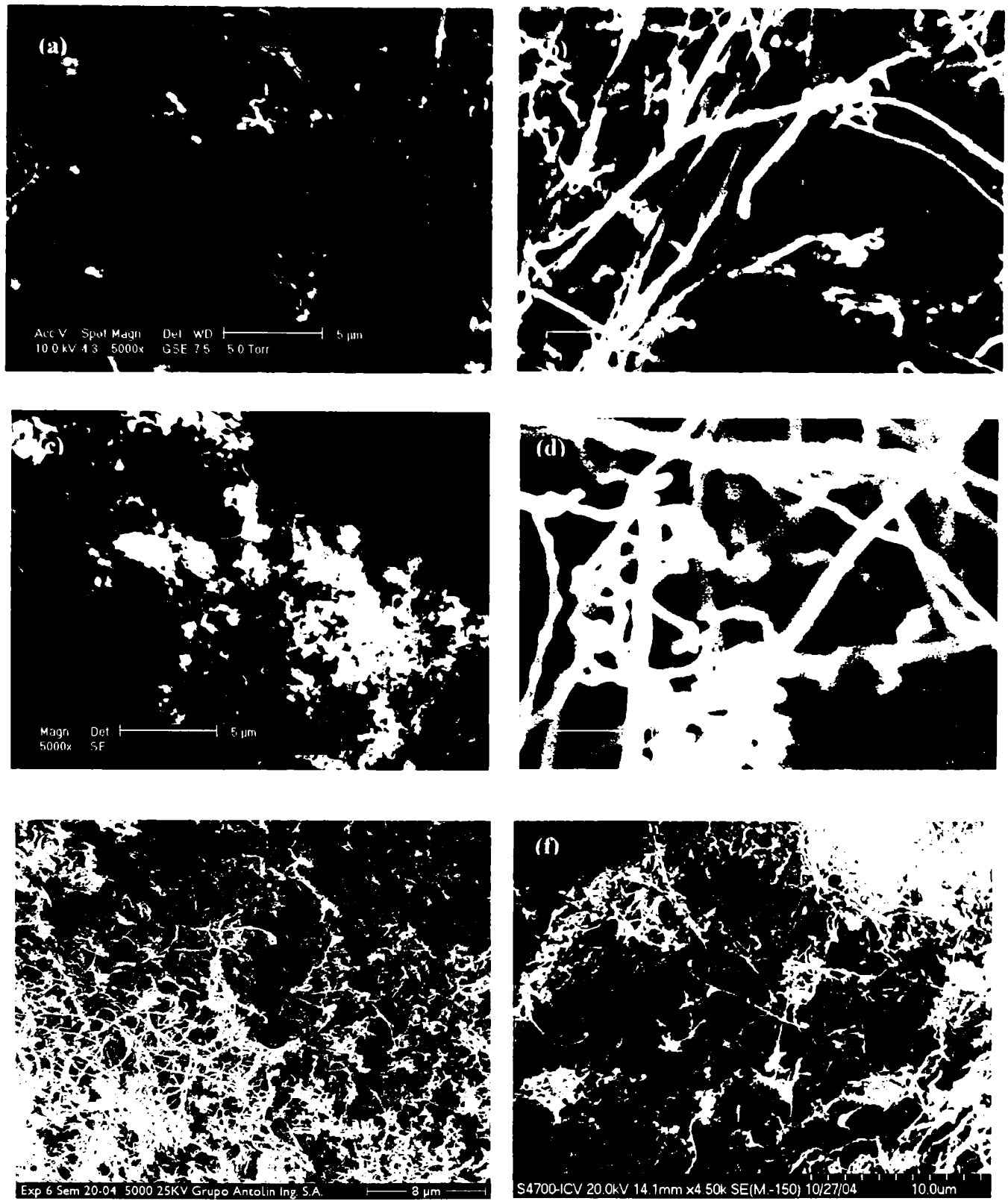

Figure 5.1 SEM – micrograph: (a) + (b) Pyrograf; (c) + (d) Semana; and (e) + (f) GANF.

The fibres were fixed on the sample holder and were examined by SEM at 10 – 15kV, a working distance of 10 mm, using the SE detector.

Figure 5.1 shows the morphology of the VGCFs in the as grown status. The Pyrograf fibres are characterised by a homogeneous diameter, about 50-200 nm and a length up to 150 µm. The fibres are debulked (Figure 5.1a+b). Semana fibres have a diameter up to 150 nm and a

length less than 80μm. These fibres are agglomerated, Figure 5.1c. GANF fibres are thinner than Pyrograf and Semana fibres and have a homogenous diameter up to 80nm and a length between 30 – 100μm, Figure 5.1e+f.

5.2.2 Transmission Electron Microscope

A transmission electron microscope (TEM) is basically transmission light microscope using electrons instead of light, and has a resolution of some thousand times greater than a transmission light microscope. These advantages make that the TEM can be used for objects as small as a few angstroms to be studied [139].

A transmission electron microscope is comparable in design to an inverted light microscope. An electron gun at the top of the column produces a beam of electrons, which are accelerated down the column, and focused into a coherent beam by electromagnetic lenses onto the sample. The specimen, mounted on a small copper grid, must be thin enough to allow the beam to pass through it. The objective lens forms an image of the sample, which is further magnified by the imaging lenses below. The image is projected onto the fluorescent screen at the bottom of the column. In various positions in the column are a series of apertures, which serve to eliminate any stray electrons from the image forming process [140].

The transmission electron microscope used to analyse the structure of VGCNFs is from Philips, model CM 200. The Philips CM200 transmission electron microscope can operate at accelerating voltages of up to 200 kV and can achieve a resolution of 2 Angstroms (2,000,000X) with ultrathin specimens. The VGCNFs are embedded in colourless resin matrix and subsequently cut in ultrathin samples by Ultra Microtome. The sample size is 3 mm in diameter and the thickness less than 100 nm [141].

The TEM-micrograph shows the structure of the Pyrograf fibres, Figure 5.2. It can be observed that the fibres have a hollow core structure. They are multi wall carbon nano-tubes. The nanofibres are generally composed of concentric cylindrical graphene tubules, each with the structure of role-up sheet and have a smooth surface. The outer carbon layers are disoriented and the VGCNFs have an amorphous structure. In order to reduce the degree of amorphous carbon supplementary heat treatment could be applied to the carbon fibres. This kind of morphology is very favourable when nanofibres are used as filler materials in order to improve electrical conductivity and tensile properties of the composites.

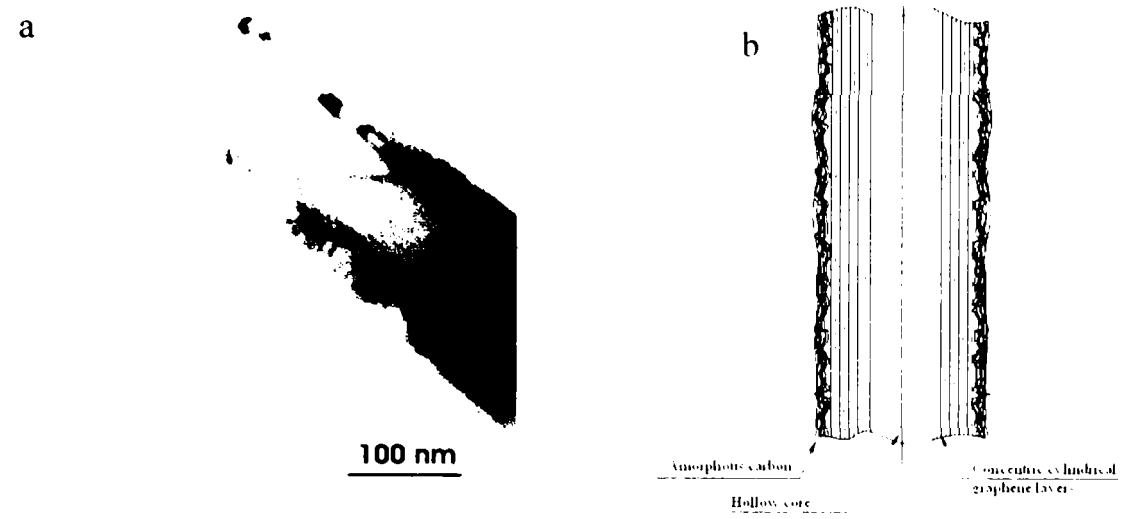

Figure 5.2 Pyrograf: (a) TEM-micrograph and (b) schematic image.

Figure 5.3 shows the structure of Semana and GANF fibres. It can be observed that, in the VGCNFs the graphitic carbon layers form a herringbone structure around a void core region. Figure 5.3c shows clearly the hollow core structure of the nanofibres. Also, it can be observed that the thickness of the fibres wall is small in comparison with the inner diameter. The herringbone structure of the VGCNFs is not so adequate for improvement of tensile properties of the final composite, because the bondings between graphene layers are weak. The high graphitisation degree makes this type of structure to be favourable to improve the electrical or thermal conductivity of the polymeric composites.

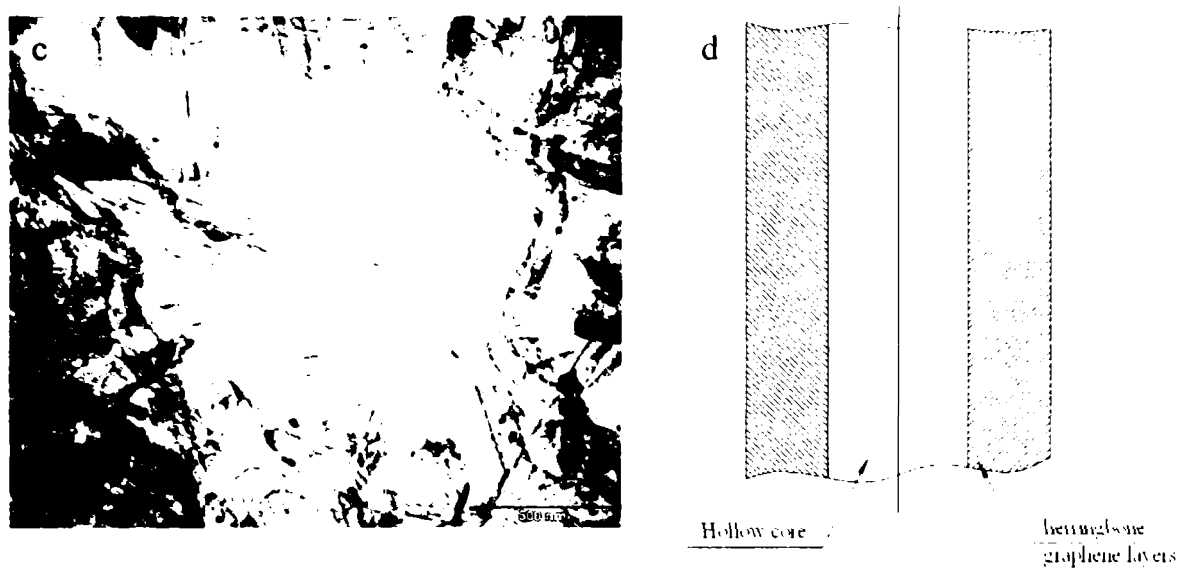

Figure 5.3 (a) Semana and (b) GANF fibres TEM-micrographs; (c) lower magnification of GANF fibres; (d) schematic image.

5.3 X-Ray Diffraction

An X-ray or Roentgen ray is a form of electromagnetic radiation with a wavelength in the range of 10 nanometers to 100 picometers (corresponding to frequencies in the range 30 PHz to 3 EHz). X-rays are primarily used to diagnostic medical imaging and crystallography [142]. When a sample is irradiated, X-rays are diffracted in a way that is characteristic of the phases present in the sample under analysis. The atomic lattice acts as a three dimensional diffraction grating, causing the X-ray beams to be refracted at specific angles related to interatomic spacings. The type and the amount of the sample constituents can be determined by measuring the angles and intensities at which diffraction peaks occur. The spacings in the crystal lattice can be determined using Bragg's law (Bragg's relation 5.1, Figure 5.4) [143].

$$n\lambda = 2d\sin(\theta) \quad (5.1)$$

where:

n – is an integer (n=1, 2, 3 ….);

λ - is the wavelength of the incident X-ray beam (CuK_{α});

d - is the distance between atomic layers in a crystal;

θ - is the angle between the incident rays and the scattering planes.

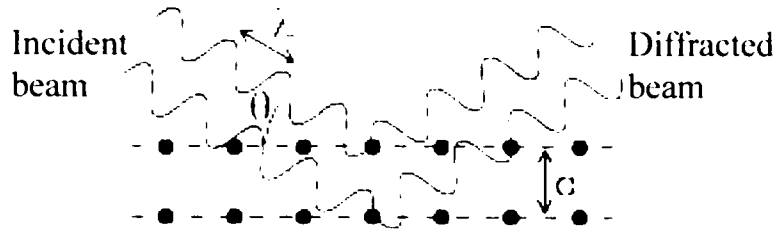

Figure 5.4 Derivation of Bragg's Law [143].

The distance between carbon layers was measured by X-Ray diffractometry using an apparatus from Philips, model X'Pert. The fibres are mixed with silicon powder as reference and pressed in the sample holder. The silicon powder is used as standard element. The voltage applied during the measurements was 55kV, and the 2θ angle was between 10 and 50°. X-ray diffractogram of the GANF fibres is presented in Figure 5.5. The intensities and the angles of the graphite can be observed on the pattern. The first signal corresponds to the graphite 002, and its intensity is used for further mathematical calculation.

The graphitisation degree of the vapour grown carbon nanofibres is calculated using the following formula [144]:

where:

$$g_p = \frac{0.344 - c}{0.344 - 0.3354} \qquad (5.2)$$

$$\tilde{c} = \frac{3.1354 - \tilde{c}'}{\tilde{Si}} \qquad (5.3)$$

0.344 nm - the interatomic distance of the carbon – axis characteristic for the turbostratic layers (TG – graphite);

0.3354 nm - the interatomic distance of the carbon – axis for the perfect graphite (HOPG – highly ordered pyrolytic graphite);

$\tilde{c}$ - the interatomic distance of the carbon – axis calculated (Formula 5.3) and adjusted with the Silicon powder;

$\tilde{c}'$ - the interatomic distance of the carbon – axis measured;

$\tilde{Si}$ - the interatomic distance of the silicon – axis measured.

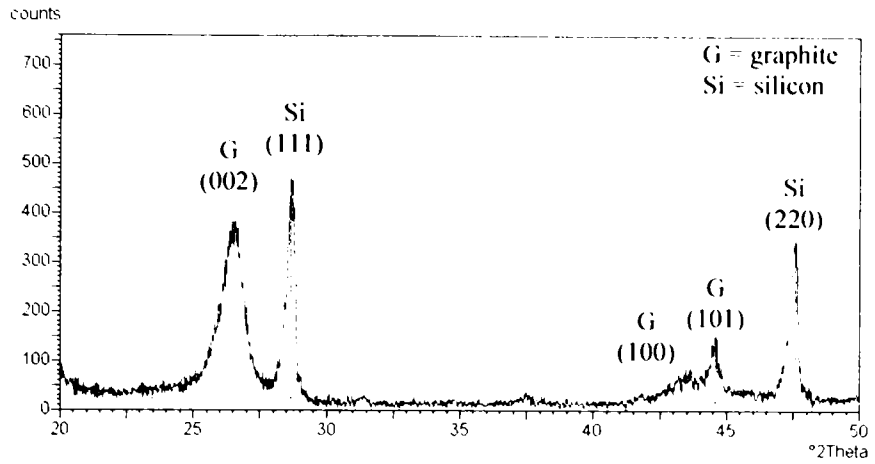

Figure 5.5 GANF fibres – X-ray diffractogram.

The graphitisation degrees of the analysed fibres using XRD method described previously are presented in Table 5.3.

Table 5.3 Graphitization degree of the VGCNFs.

VGCNFs	g_p [%]
Pyrograf	**30.54**±3%
Semana	**10.13**±3%
GANF	**65.26**±3%

5.4 Thermogravimetric Analysis

Thermogravimetric analysis (TGA) measures weight changes in a sample material as a function of temperature (or time) under a controlled atmosphere. A furnace heats the sample while a sensitive balance monitors loss or gain of sample weight due to chemical reactions, decomposition, and solvent or water evaporation. The decomposition can be a thermal decomposition, e.g. nitrogen gas, or an oxidative decomposition (air or oxygen) [145].

TGA is used primarily for determining thermal stability of polymers. The most widely used TGA method is based on continuous measurement of weight on a sensitive balance (called a thermobalance) as sample temperature is increased in air or in an inert atmosphere. This is referred to as nonisothermal TGA. Data are recorded as a thermogram of weight versus temperature.

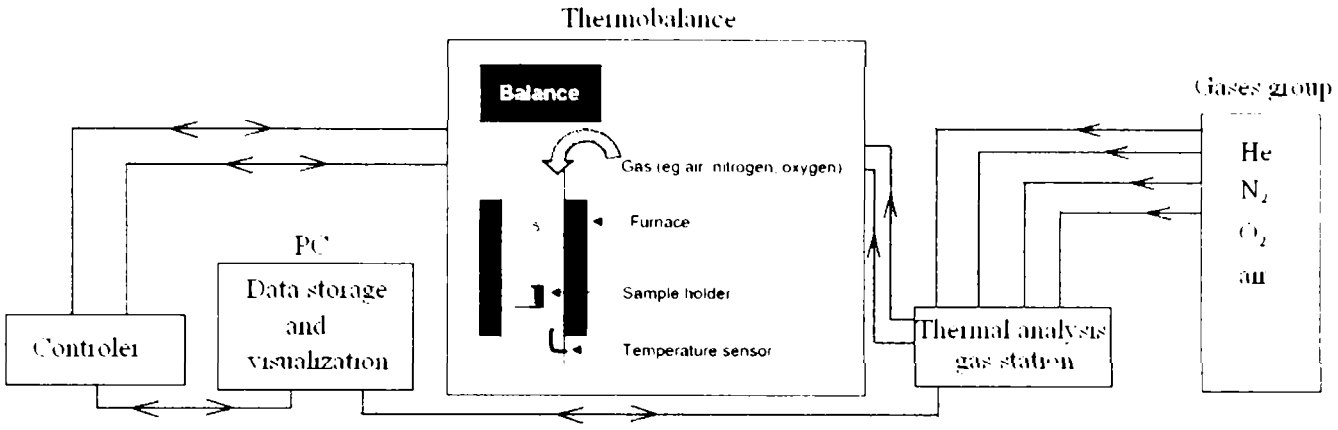

Figure 5.6 Principle of the TGA measurements.

The thermal stability and the quantity of catalyst particles and/or impurities by thermogravimetrical measurement were determined. The thermogravimetric analysis were performed in a thermobalance from PerkinElmer, model TGA 7. Figure 5.6 shows schematically the principle of TGA measurements [146].

The same quantity of VGCFs (cca. 20 – 25 milligrams) was used for each measurement. The samples were heated from 100°C to 800°C in a synthetic air atmosphere, 25 ml/min, with a heating rate of 5°C/min. The measurements start from 100°C in order to avoid the moisture effect. Figure 5.7 shows the curves obtained from TG measurements. It is known that a higher graphitisation degree of the fibres leads to a better thermal stability. Therefore the fibre with the highest graphitisation degree (GANF fibres – G_p= 65% ±3%) has a higher thermal stability (burning temperature, T_B=535°C ±3%) compared with the Semana fibres (G_p=10% ±3%) which the thermal degradation starts at 460°C ±3%. Also, it can be observed that, at around 190°C the Semana fibres start to lose slightly in weight, Figure 5.8. This loss in weight is due to the burning of hydrocarbons. Hydrocarbons on the fibre surface are formed in the growing process. After complete burning of the carbon fibres, a certain quantity of catalyst particles remained in the crucible. This can be observed also on the TG – curves, Figures 5.7 and especially 5.8, where the mass of the remained catalyst particles was calculated in percent.

Figure 5.9 shows the morphology of the catalyst particles remained in the crucible after thermogavrimetrical measurements.

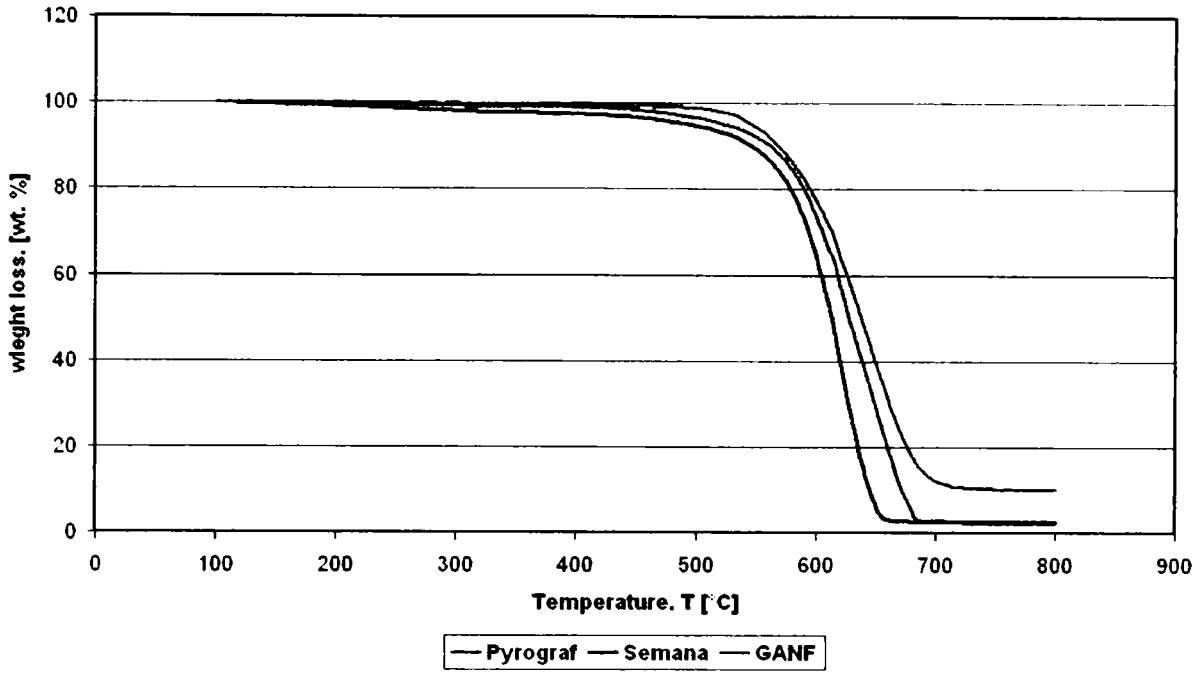

Figure 5.7 Thermogravimetrical measurements of the carbon nanofibres.

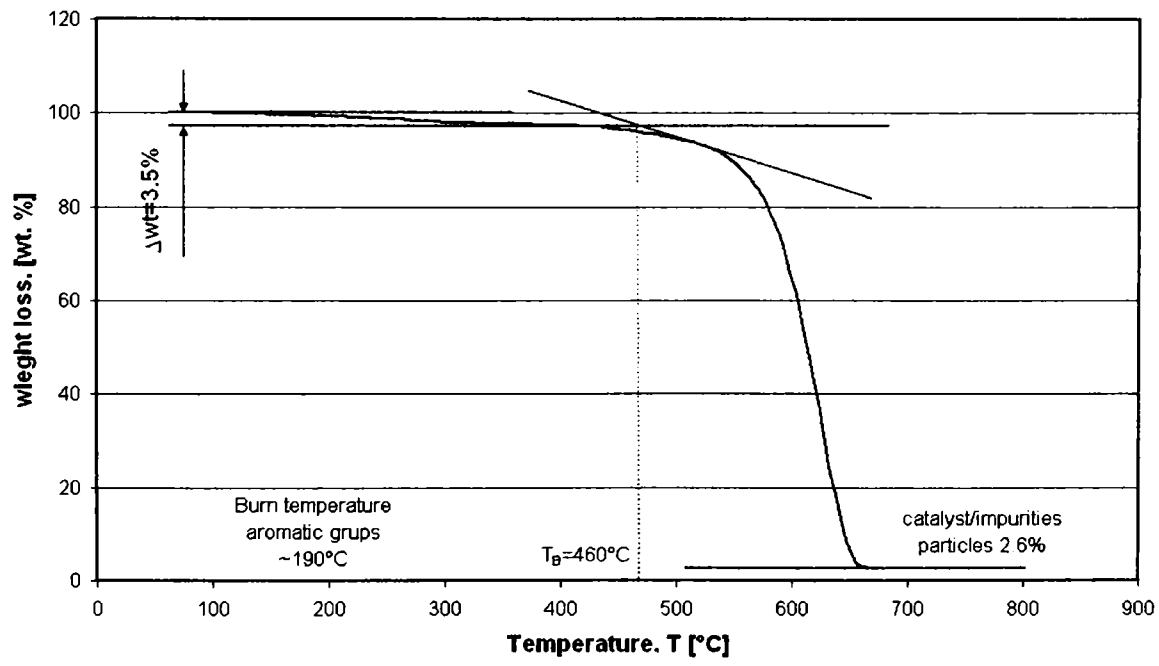

Figure 5.8 Semana fibres – TGA.

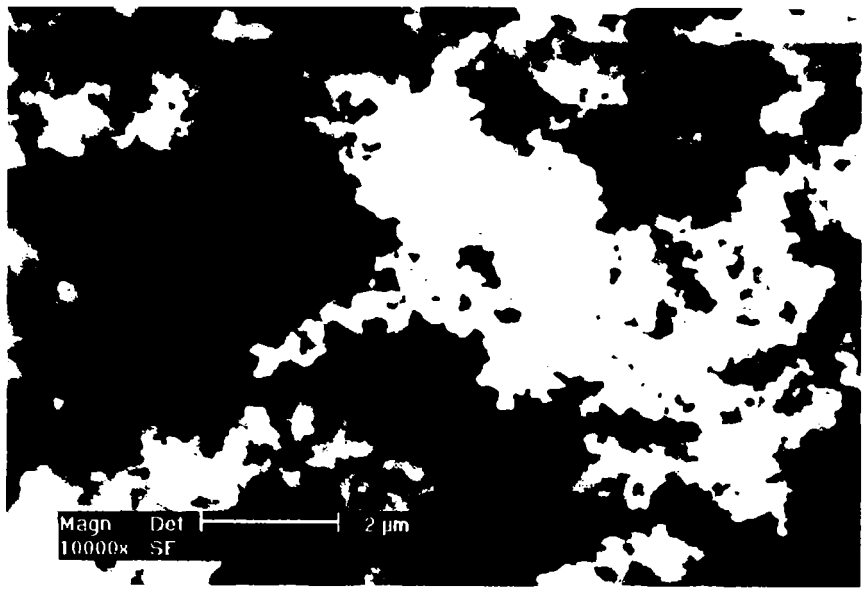

Figure 5.9 SEM-micrograph of the catalyst particles.

The burning temperatures and the quantities of catalyst particles that remained after TG analysis are presented in Table 5.4. The GANF fibres showed the best thermal stability but have a high content of catalyst particles. A good purification process of the fibres after growing should reduce the catalyst content under at least 5%.

Table 5.4 TGA – Thermal stability and catalyst particle quantity of the VGCNFs.

VGCFs	Burning Temperature [°C]	Catalyst Particles [%]
Pyrograf	505 ±3%	2.1 ±3%
Semana	460 ±3%	2.6 ±3%
GANF	535 ±3%	10.2 ±3%

5.5 Volume Electrical Resistivity

Electrical resistivity (also known as specific electrical resistance) is a measure indicating how strongly a material opposes the flow of electric current. A low resistivity indicates a material that readily allows the movement of electrons. The SI unit for electrical resistivity is the ohm metre [147].

In general, electrical resistivity of metals increases with temperature. The electrical resistivity was measured at constant temperature in order to avoid the resistivity dependence of the temperature. Electrical resistivity measurements at room temperature (20°C ±1) were performed using a standard DC electrical resistance method. The method used for measurements of specific electrical resistivity is the constant voltage method. The basic

configuration of the constant voltage method is shown in Figure 5.10. In this method, a constant voltage source (VS) is placed in series with the unknown resistor (sample), R, and an electrometer ammeter, A, and in parallel is placed a voltmeter, V, in order to measure the potential tension on the sample. Since the voltage drop across an electrometer ammeter is negligible, essentially all the voltage appears across R. The resulting current is measured by the ammeter and the resistance is calculated using Ohm's law [148].

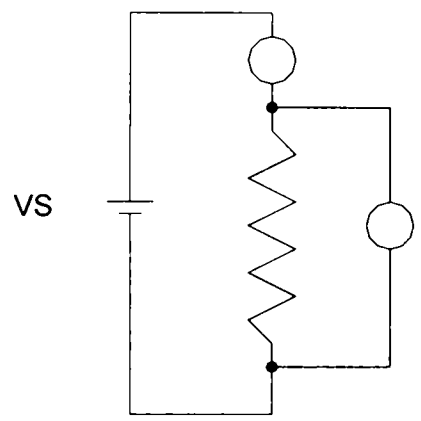

Figure 5.10 Electrical circuit used to measure the electrical resistivity of the VGCNFs.

The resistivity of the vapour grown carbon nanofibre was not measured for one fibre but was measured as volume resistivity. The volume resistivity is measured by applying a voltage across the sample and measuring the resulting current. The resistivity is calculated from the geometry of the electrodes and the thickness of the sample.

The measurements were performed as follow:

- the glass tube (inner diameter 4.7 mm) was filled with VGCNFs (cca. 0.020-0.030 g) depending on the nanofibres type. At the end of the tube the electrodes were mounted (Figure 5.11) and subsequently pressed into a vice with the same force. The density was almost the same for each type of carbon nanofibres;
- the applied voltage on the sample was 0.2 V;
- the electrical current, I, flowing through the sample was measured using an ammeter;
- the electrical resistivity of the nanofibres was calculated using Ohm's law:

$$\rho = R\frac{A}{l}[\Omega m] \qquad [5.4]$$

where:

ρ – is the electrical resistivity (measured in ohm metres);

R – is the electrical resistance of the sample (measured in ohms);

$$R = \frac{U}{I}[\Omega] \qquad [5.5]$$

A – is the cross-sectional area of the sample (measured in square metres);

L – is the length of the sample (measured in metres).

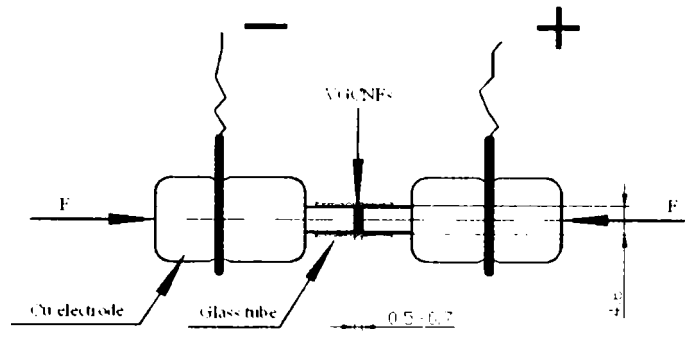

Figure 5.11 Specific electrical resistivity measurements, schematically.

For each type of fibres several measurements (at least 7 measurements) were performed. Table 5.5 shows the electrical resistivity of the fibres in as grown status. The electrical resistivity can be correlated with the fibres graphitisation degree. Therefore it can be seen that, the fibres with a higher graphitization degree, have a lower volume electrical resistivity (a better electrical conductivity).

Table 5.5 Electrical resistivity of the VCGNFs.

VGCNFs	Electrical resistivity ρ [Ω m] x 10^{-3}
Pyrograf	1.995
Semana	3.145
GANF	1.523

CHAPTER VI

PLASMA CHEMICAL FUNCTIONALISATION OF VAPOUR GROWN CARBON NANOFIBRES

6.1 Introduction

One of the main aims of this thesis is to functionalise the outer surface of the VGCNFs, to increase their wettability in order to improve the fibres – matrix adhesion. The wetting behaviour of the plasma treated VGCNF was characterized by the contact angle and the surface energy measurements. After submission of the VGCNFs to plasma treatment, the fibre surface will become highly hydrophilic. A good functionalisation of the fibre surface is characterized by a lower water contact angle and a higher surface energy. The quantity of functional groups was determined by titration and X-ray photoelectron spectrometry (XPS) measurements. TEM and BET analysis were performed in order to characterise the structure of the modified surface and the specific surface area before and after plasma chemical treatment of the fibres.

6.2 Plasma Chemical Treatment

The fibres were treated in a plasma reactor from Plasma Finish model V 15-G (Figure 6.1). The plasma device consists of the following main components:

- housing – DIN 40 050;
- process chamber – aluminium chamber (L x W x H) 250 x 250 x 250 mm. Description:
    - on the top side is the microwave feed (1);
    - on the bottom side is the flange connection with the main valve of vacuum system (2);
    - gas inlet (3);
    - pressure measurement (4) ;
    - rotary quartz barrel (dimension: ϕ = 150 mm and L = 150 mm) in order to ensure a homogenous treatment (5). The barrel rotating speed is 4 min^{-1};
    - high frequency electrodes (6).
- rotary vane vacuum pump from Leybold model TRIVAC D 25 BCS. The plasma reactor is a low pressure plasma, chamber pressure is between 0.01 – 3 mbar;
- process gas supply – consists of gas valve and mass flow controller (MFC). The gas supply in process chamber can be made alternatively in two ways. First, through 2

stainless pipes in the top of the chamber and second way is directly in rotary barrel (Figure 6.2). The reactor is equipped with 4 gas drain, Figure 6.2. The work gases and the maximum flow rate is as following:

  - O_2 – MFC < 300 ml/min;
  - CO_2 – MFC < 200 ml/min;
  - NH_3 – MFC < 300 ml/min;
  - Ar – MFC < 300 ml/min;

- pressure measurement device – the pressure measurement takes place via as gas-kind-independent absolute pressure receiver (the Pirani). The measuring range of the Pirani is between 0.01 – 100mbar;
- MW – generator (microwave generator) – from F&M with a magnetron of 850W, which works at industry frequency of 2.45GHz. The plasma power is up to 500W;
- high frequency (radio frequency) generator from Hüttinger model PFG 300 RF, which works at a frequency of 13.56 MHz ±0.05% and a maximum power up to 300W;
- actuators and sensors;
- control system – from Bernecker & Rainer, model PP41;
- electrical switch and control equipments.

The process steps of the plasma chemical treatments are as follow:

1. the VGCNFs are introduced in the quartz barrel in the case of using the RF – generator or are put on the quartz plate in the case of MW – generator and the door chamber is closed. For each experiment, the same quantity of fibres (1g in the case of Pyrograf and Semana fibres; 1.2g – GANF fibres, respectively) was treated. The same quantity is used in order to not introduce another parameter, the fibres quantity;
2. the necessary parameters are setup;
3. the process starts with chamber evacuation, to obtain a basic vacuum. The basic vacuum is lower than the working pressure;
4. gas stabilisation. A certain time should be set for the mass flow controller (MFC) in which they should be able to ensure the necessary flow rate with 1% error. Also, the vacuum pump must ensure the desire chamber pressure during the treatment;
5. setting of the effective treatment time, beginning when the plasma starts to burn;
6. evacuation using the soft ventilation which is important when the MW – generator is used, because the fibres are treated on the plate and when the venting starts they can be blown;

7. ventilation, the Ar gas fill the chamber up to atmospheric pressure (~1 bar), than the samples can be removed from the plasma chamber.

The fibres were treated using the following parameters:

- treatment time 1 up to 60 min;
- plasma power:
  - RF – generator: 50 – 180 W;
  - MW – generator: 50 – 150 W;
- chamber pressure (vacuum): 0.5 – 1 mbar;
- gas flow rate:
  - oxygen: 50 – 200 ml/min;
  - ammonia: 10 ml/min.

Initially the plasma device was equipped with the ventilation system direct from air (Figure 6.2a – red line). After treatment with different parameters (plasma power between 100 – 150W and treatment time up to 20 minutes) no functionalisation was achieved. It was observed that the functional groups were destroyed during ventilation with air. The ventilation system was modified (Figure 6.2b – red line) and connected with the inert gas, like argon.

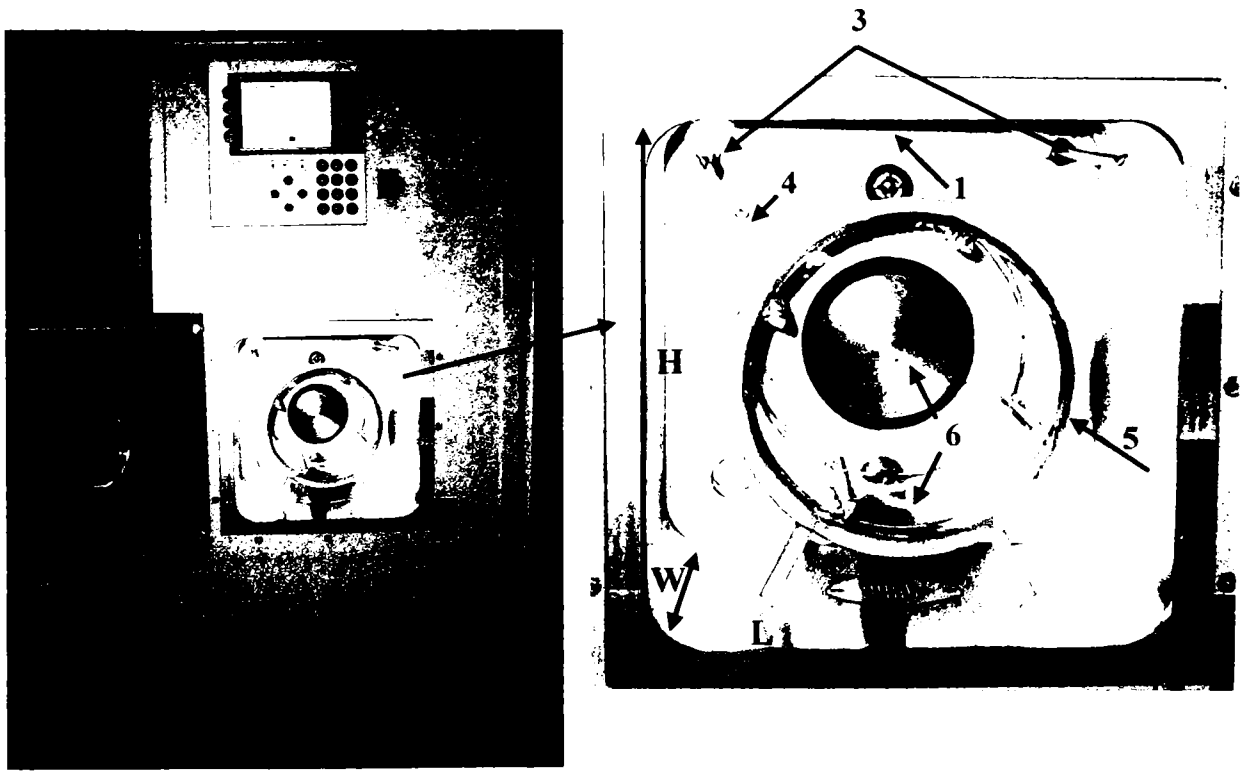

Figure 6.1 Plasma reactor V 15-G.

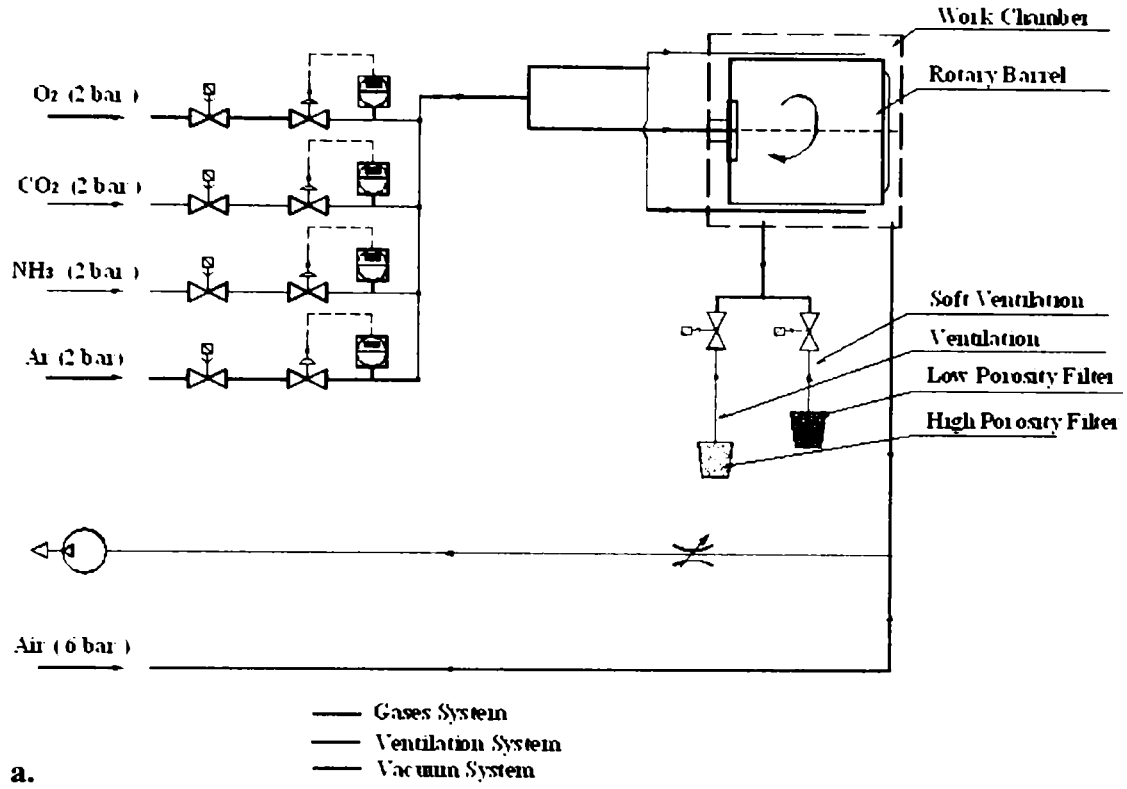

a.

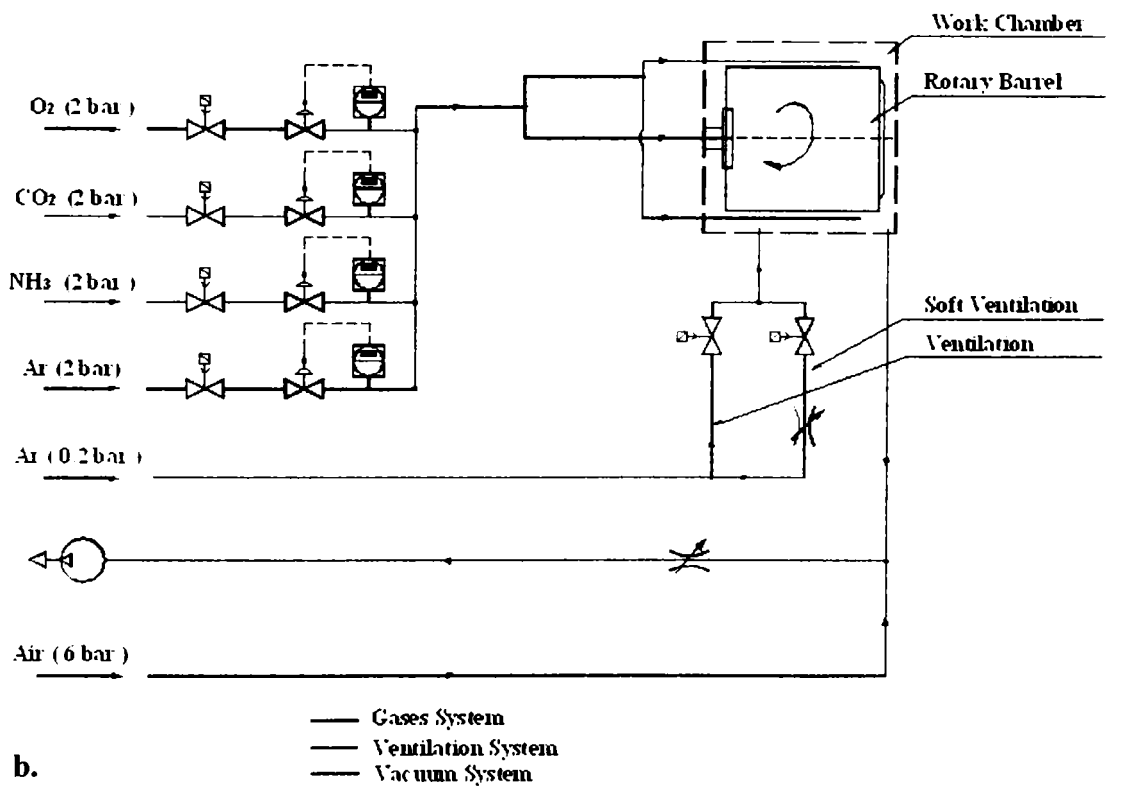

b.

Figure 6.2 Pneumatic system of the plasma reactor; blue line – vacuum system, red line – ventilation system and dark blue line gases supply.

6.3 Water Contact Angle Measurements

The wettability of the fibres was determined by water contact angle measurements (gravimetric method), using an electronic balance DCAT 11 from DataPhysics Instruments. The powder method was used for these measurements and the contact angles were determined using the extended Washburn equation. The Washburn's equation describes capillary flow in porous materials [149]. It is:

$$L^2 = \frac{\gamma D t}{4\eta} \qquad (6.1)$$

Where:

L – measures the volume of liquid soaked up;

γ – is a measure of surface tension;

D – is the diameter of the holes the liquid runs through;

t – is the length of dunking time;

η – is a measure of the viscosity of the liquid.

To perform these measurements the sample preparation requires some special attention. The VGCNFs are pressed into the glass tube (Figure 6.3). The glass tube has at the bottom part a glass frit (sintered permeable glass filter). For precise measurements it is very important to have the same density of the sample. Therefore, always the same amount of vapour grown carbon nanofibres must be filled and to compress than equally, because small differences in the packing density cause big differences in the permeability. The sample vessel is filled with the desired test liquid (for example n-hexane, water, etc.) and put on the balance table. Subsequently, the glass tube is suspended in the balance (Figure 6.4). The table with test liquid is climbing up to some millimetres below the bottom of the glass tube. After the vessel contacted the glass frit, the speed at which the liquid rises through the bulk fibres is measured by recording the increase in weight as a function of time.

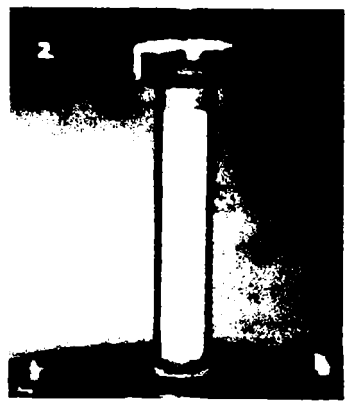

Figure 6.3 Glass tube for the contact angle measurement of the powder materials, according to Washburn.

The balance is connected to a personal computer using a serial RS 232C cable. The information from balance to PC is taken by SCAT software. To measure the contact angle of nanofibres it is important to determine the constant c which is a material factor (mainly dependent on the porous architecture of the nanofibres). The constant can be measured in a first step using a total wetting liquid such as *n-Hexane*. This step is called calibration of the constant. After that, the test liquid is changed with water or other polar liquids. The sample is changed too, and the measurement has been repeated. The contact angle is automatic calculated drawing the tangent to the obtained curve (Figure 6.5) and using the determined calibration constant.

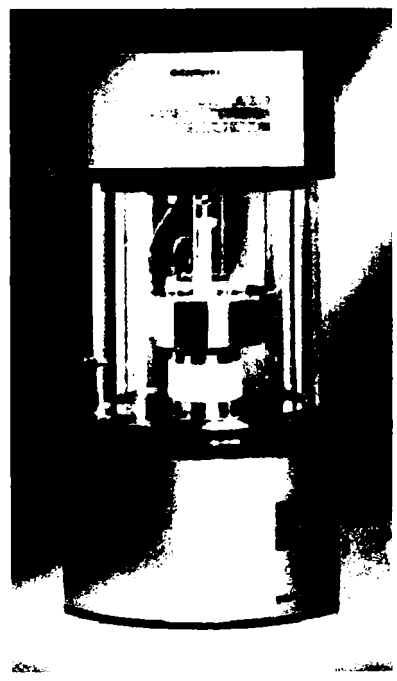

Figure 6.4 Water contact angle measurements of the VGCNFs using a dynamic contact angle meter and tensiometer DCAT 11.

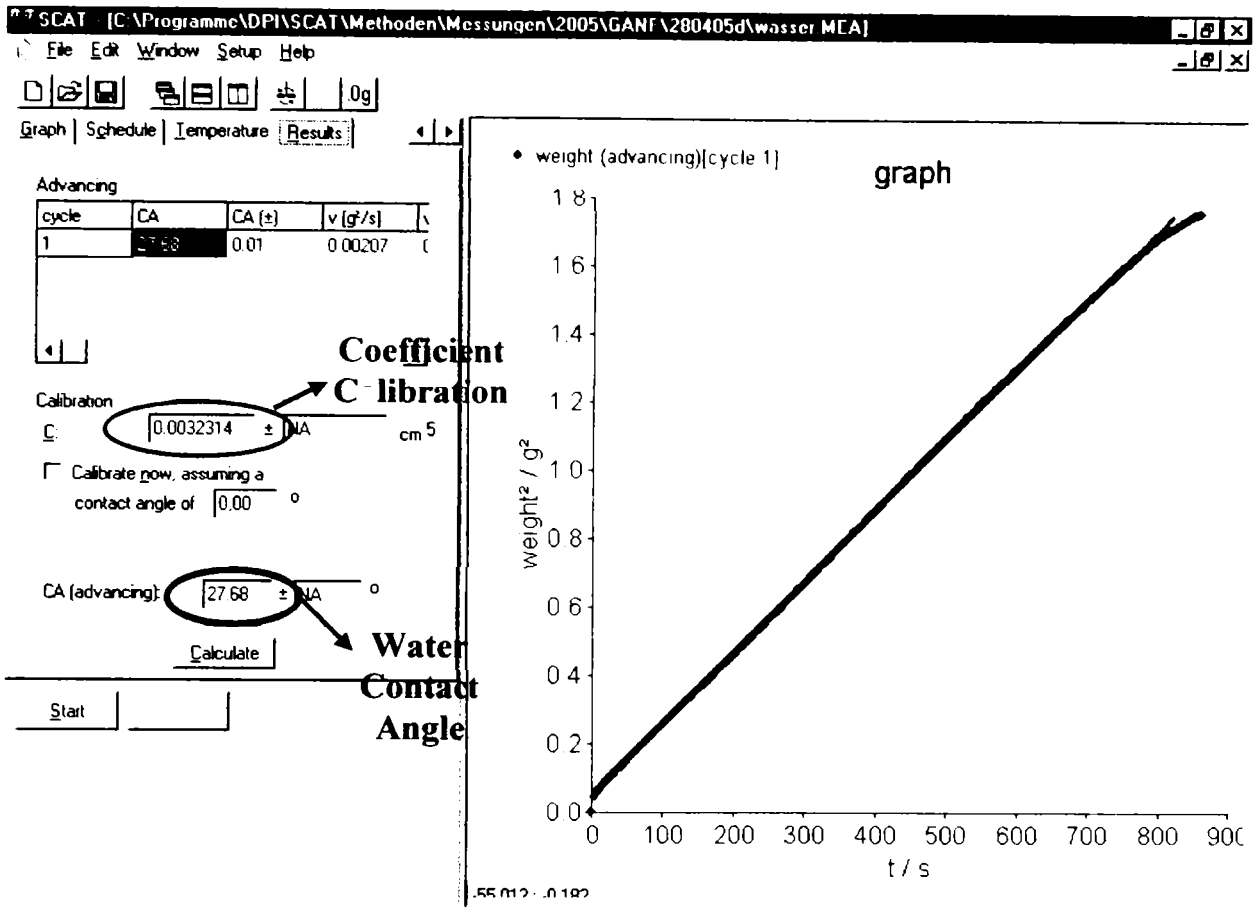

Figure 6.5 Water contact angle calculations of the VGCNFs.

6.4 *Surface Energy Measurements*

The surface energy of the vapour grown carbon nanofibres was calculated from contact angles based on the Owens-Wendt method (dispersion & polar force contributions) [150]. For determination of the fibres surface energy, measurements of the contact angle in at least three different liquids of known surface tension (water (density = 0.9982 g/cm³, viscosity = 1.00 mPa, surface tension = 72.75 mN/m), isopropanol (density = 0.7855 g/cm³, viscosity = 2.29 mPa, surface tension = 23.00 mN/m) and diiodmethane (density = 3.3254 g/cm³, viscosity = 2.76 mPa, surface tension = 50.80 mN/m) or formamide (density = 1.1334g/cm³, viscosity = 3.81mPa, surface tension = 58.20mN/m)) were carried out. The fibres surface energy was calculated using the SCA10 software from DataPhysics Instruments (Figure 6.6). The increase of the fibres surface energy (especially the polar component), is a direct result of introducing polar functional groups onto fibre surface during the oxygen plasma treatment. The surface

energy has two important components: the dispersive component (γ^d) and the polar component (γ^p). The latter component respectively the polar component is correlated with the amount of functional groups on the fibre surface [100].

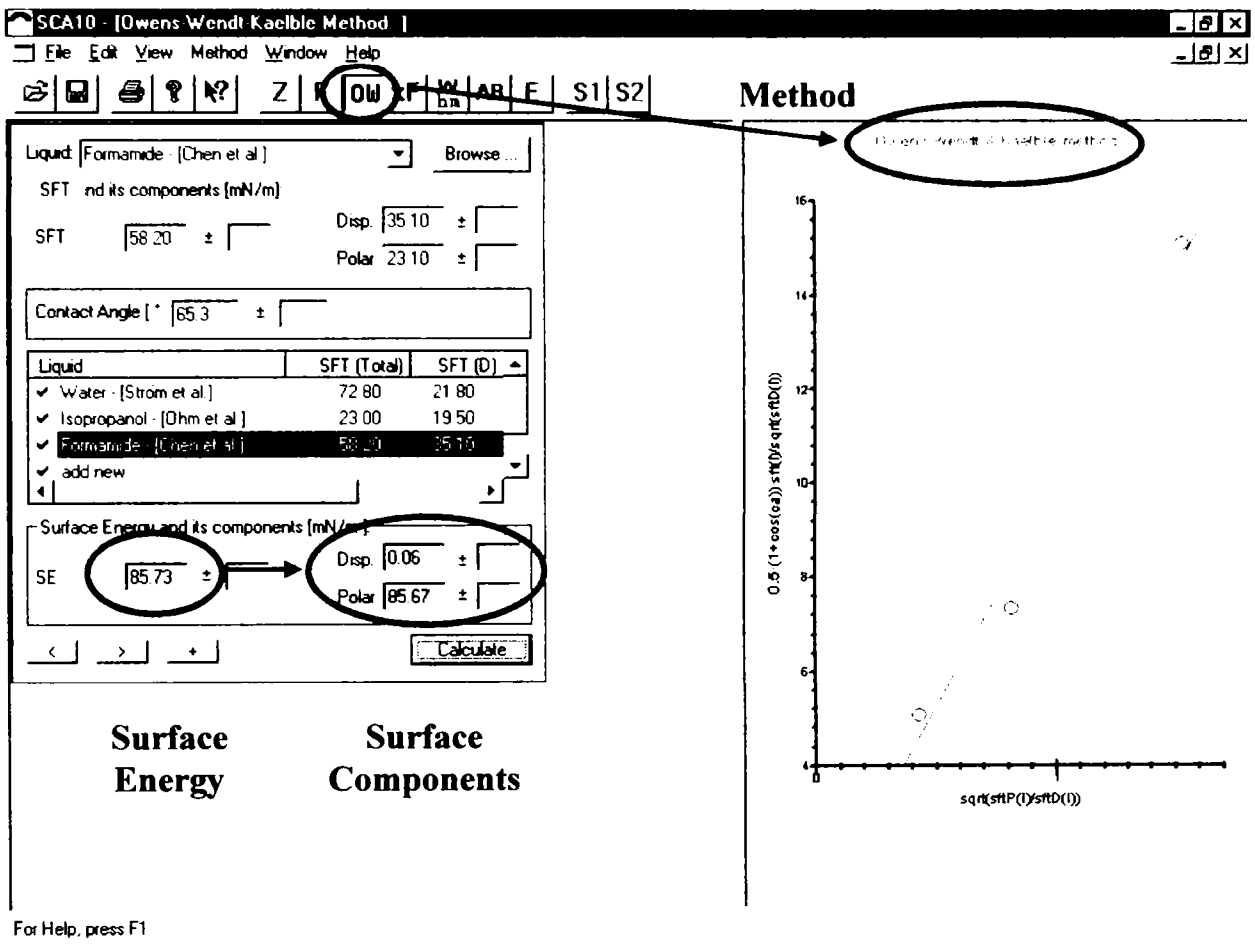

Figure 6.6 Surface energy calculations of the VGCNFs according to Owens – Wendt method.

6.5 *NaOH Titration*

The total amount of functional groups on the surface, consisting of carboxylic, carbonylic and phenolic or hydroxylic groups, generated in oxygen plasma treatment was determined by NaOH – titration according to Boehm [151]. The same quantities of VGCNFs for each experiment (0.1g) were stirred for 24 h in 0.1 M NaOH under inert atmosphere (Figure 6.7) and subsequently vacuum filtered. The obtained solution was back – titrated with HCl 0.1 N and using the value for the necessary titration volume, the total amount of oxygen containing acidic functional groups was calculated with the following Formula 6.2:

$$t_{afg} = \left(V_{NaOH} - V_{NaOH+CnF}\right) \cdot 10^2 \, mmol / gFibre \qquad [6.2]$$

where:

t_{afg} – total amount of acidic functional groups

V_{NaOH} – the necessary volume for titration of pure solution NaOH, 0.1M (0.198)

$V_{NaOH+CnF}$ - the necessary volume for titration of solution NaOH, 0.1M after extraction of the acidic groups.

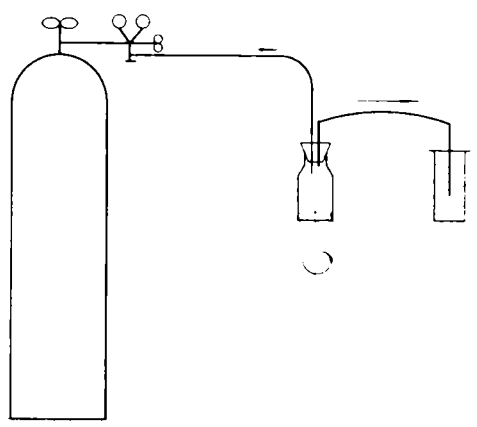

Figure 6.7 Titration stall.

6.6 *X-ray Photoelectron Spectrometry*

X-ray Photoelectron Spectroscopy (XPS), also known as Electron Spectroscopy for Chemical Analysis (ESCA) is a widely used technique to investigate the chemical composition of surfaces. Surface analysis by XPS requires irradiating a solid in an Ultra-high Vacuum (UHV ~1×10^{-8} – 1×10^{-12} mbar) chamber with monoenergetic soft X-rays and analyzing the energies of the emitted electrons. The emitted electron signal is plotted as a spectrum of binding energies. The photon is absorbed by an atom, molecule or solid leading to ionization and the emission of a core electron. Analysis will reveal the composition from a depth of 2 – 20 atomic layers and the electronic state of the surface region of the sample. XPS has the ability to identify different chemical states resulting from compound formation, which are revealed by the photoelectron peak positions and shapes [53]. XPS can detect all elements except H and He (owing to the absence of core orbital) [152].

XPS technique can be used with success in order to determine the levels and nature of oxidation in VGCNFs. XPS revealed the presence on the fibres surface of =C=O; =C–OH, =C=C=, etc., Figure 6.8 [63].

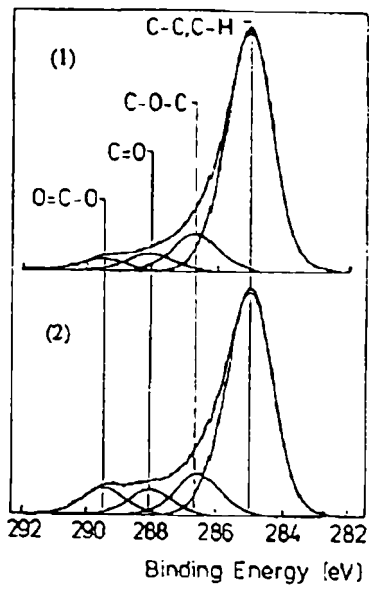

Figure 6.8 XPS spectra of the differently functionalisation degree of carbon fibres.

6.7 *BET Analysis*

BET comes from the initials Brunauer, Emmett and Teller, the men's who invented a straight-forward method, and a complicated-looking accompanying theory, to determine the effective surface of solid materials with complicated shapes, such as porous powders, by using adsorbed gas molecules as rulers. The observation of the so-called adsorption and desorption isotherms is used to determine the amount of gas molecules adsorbed to a surface. Knowing the size of a molecule, one can then calculate the entire effective surface [153].

The gas adsorption technique may be used to measure the specific surface area and pore size distribution of powder or solid materials. The dry sample is usually evacuated of all gas and cooled to a temperature of -196°C, the temperature of liquid nitrogen. At this temperature inert gases such as nitrogen, argon and krypton will physically adsorb on the surface of the sample. This adsorption process can be considered to be a reversible condensation or layering of molecules on the sample surface during which heat is evolved. Nitrogen gas is ideal for measuring surface area and pore size distribution [154].

Surface area measurements of the VGCNFs at -196°C with N_2 as the absorbate, were performed using Quantachrome Nova 2000 surface area analyzer (Quantachrome, Inc., Boynton Beach FL). The necessary quantity of the fibres for BET measurements was 5 – 10g.

6.8 Plasma Treatment of the Pyrograf Fibres

In order to functionalize the carbon nanofibres a plasma chemical treatment was applied. A good wetting behaviour of the plasma treated VGCNF is characterized by a lower value of the water contact angle and a higher surface energy.

The plasma parameters which have an important influence onto the functionalisation degree of the vapour grown carbon nanofibres are as follow:

1. plasma power;
2. treatment time;
3. chamber pressure;
4. oxygen flow rate;
5. type of plasma generator (RF – and MW – generator);
6. plasma gas;
7. fibres quantity.

The first four parameters can be setup easily using the software control of the plasma device. To optimise the effect of the plasma parameters on the functionalisation degree of the fibres it is essential to modify for one series of experiments only one parameter whereas the other parameters will be kept constant. The fibres quantity was also kept constant for each experiment, 1g.

The optimisation of the plasma parameters will be presented as a function of the plasma gas and the type of plasma generator.

6.8.1 Oxygen Plasma Treatment of the Pyrograf Fibres

The VGCFs were exposed to a RF – generated oxygen plasma treatment. Two kinds of methods were used to optimise the plasma parameters in order to obtain a high functionalisation degree. The first method use a statistical software based on the mathematical modelation. This method can estimate the effect of plasma parameters on the functionalisation degree of the VGCNFs. After determination of the plasma parameters which have a strong influence on the fibre functionalisation, the optimisation of these parameters was performed with the step by step method (one parameter is variable while the other parameters are constant).

6.8.1.1 Oxygen Plasma Treatment using Mathematical Modelation

Statgraphic software was used for the statistical experimental planning. Four factors are considered: plasma power, treatment time, chamber pressure and oxygen flow rate. The plasma parameter limits are shown in Table 6.1. This experiment employed a Draper-Lin small-composite response surface design (Face Centred Design) to determine the optimal dimensional-factor levels for the fibres treatment.

Table 6.1 Plasma parameters and theirs limit.

Plasma Parameter	Notation	Minimum	Maximum	Units
Plasma Power	A	50	220	W
Treatment Time	B	60	1200	sec
Oxygen Flow Rate	C	60	200	sccm
Chamber pressure	D	70	110	Pa

The plasma parameter limits must be correlated between them. A very high plasma power will destroy the fibres, or a very long treatment time (hours) may lead to a very expensive fibres functionalisation process and in this case, the process at industrial scale will not represent any interest. The chamber pressure and the oxygen flow rate must be also correlated. The plasma device is not able to work at a high vacuum, like 0.3 mbar, and high oxygen flow rate, 250sccm.

The random Draper-Lin small-composite experimental design (Face Centred Design) is presented in the Table 6.2. The number of centre points is 3, and totally are 19 measurements. The estimate effect of the treatment parameters (plasma power, treatment time, oxygen flow rate, chamber pressure) are shown in Table 6.3. It can be seen that, the plasma power, treatment time and their square multiplication (plasma power – plasma power and treatment time – treatment time) have the higher influence in the optimization of VGCNFs functionalisation. The chamber pressure in combination with plasma power and treatment time is the third important plasma parameters.

Table 6.2 Design experiments and water contact angle of the VGCNFs.

No. Block Experiment	No. Experiment	Plasma Power [W]	Treatment Time [sec]	O_2 flow rate [sccm]	Chamber Pressure [Pa]	Water Contact Angle [°]
1	1	135	630	130	90	69.85
1	2	220	1200	200	70	81.65
1	3	135	630	60	90	67.92
1	4	135	1200	130	90	68.28
1	5	50	60	60	70	88.93
1	6	50	60	200	70	88.94
1	7	135	630	200	90	69.81
1	8	135	60	130	90	88.67
1	9	220	630	130	90	68.08
2	10	135	630	130	90	68.88
2	11	50	630	130	90	88.70
2	12	220	60	200	110	85.86
2	13	220	60	60	110	88.96
2	14	50	1200	60	110	88.97
2	15	135	630	130	110	68.83
2	16	50	1200	200	110	87.72
2	17	135	630	130	70	68.66
2	18	220	1200	60	70	74.73
2	19	135	630	130	90	65.33

Pareto chart is used to graphically summarize and display the relative importance of plasma parameters, Figure 6.9. The Pareto chart is a specialized version of a histogram that ranks the categories in the chart from most important to least important parameter. This chart helps us to prioritize which parameter or which combination of the parameters should be focused in order to obtain a high functionalisation degree of the vapour grown carbon nanofibres. The plasma power and the treatment time are the most important parameters. The chamber pressure does not influence so much the functionalisation degree, but its combination with the plasma power and the treatment time plays an important role.

Table 6.3 Estimated effects of the plasma parameters.

Parameters	Parameter Effect s	Tolerance
Average	68.9637	+/-0.72
A (plasma power)	-20.62	+/-2.72
B (treatment time)	-20.39	+/-2.72
C (O_2 flow rate)	0.896	+/-1.22
D (chamber pressure)	0.17	+/-2.72
AB	-4.145	+/-3.05
AC	1.265	+/-1.36
AD	-15.485	+/-3.05
BC	2.19	+/-1.36
BD	-14.78	+/-3.05
CD	-2.82	+/-1.36
AA	17.9754	+/-2.42
BB	18.1454	+/-2.42
CC	-1.07455	+/-2.42
DD	-1.31455	+/-2.42
Standard error estimated from total error with 4 d.f. (t = 2.77743)		

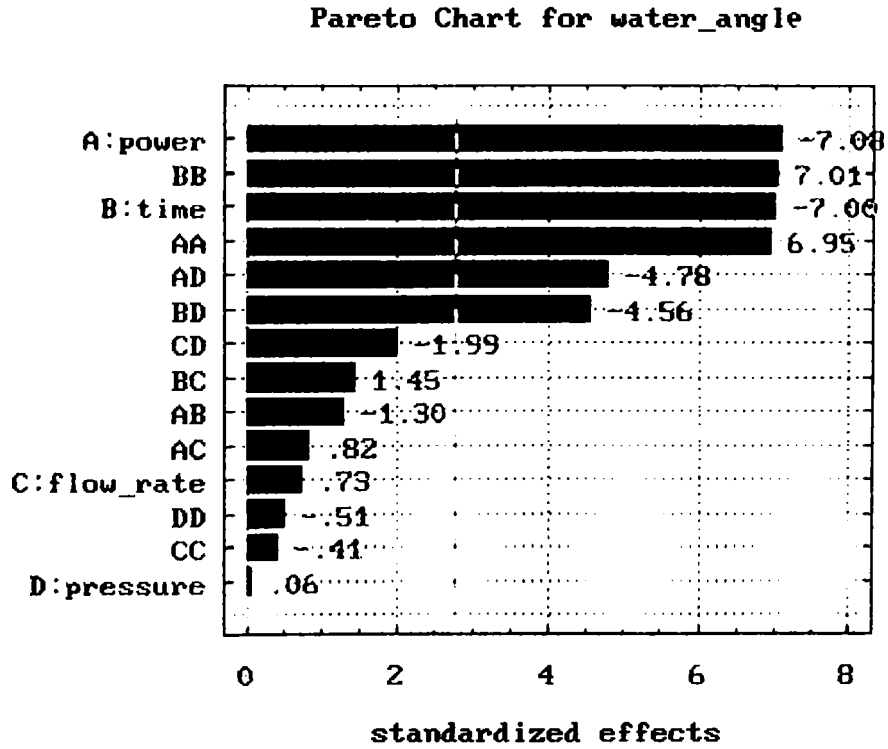

Figure 6.9 Pareto Chart.

The estimated response of the water contact angle depending on the plasma power and treatment time is plotted in Figure 6.10. A lower water contact angle can be obtained if is applied high plasma power (higher than 120W) correlated with a long treatment time. If the fibres are treated with an extremely higher plasma power (more than 160W) for a long time (longer than 10 minutes) the lowest contact angle can be reached (≈62°). But in this case the outer graphene layers of the fibres or more than these layers, respectively the complete fibres can be burned during the treatment. This means, a high functionalisation degree of the fibres can not be achieved without destruction of the fibres surface. In order to obtain a good functionalisation degree without supplementary etching effect of the fibres, it is important to accord a full attention to the correlation between the plasma power and the treatment time.

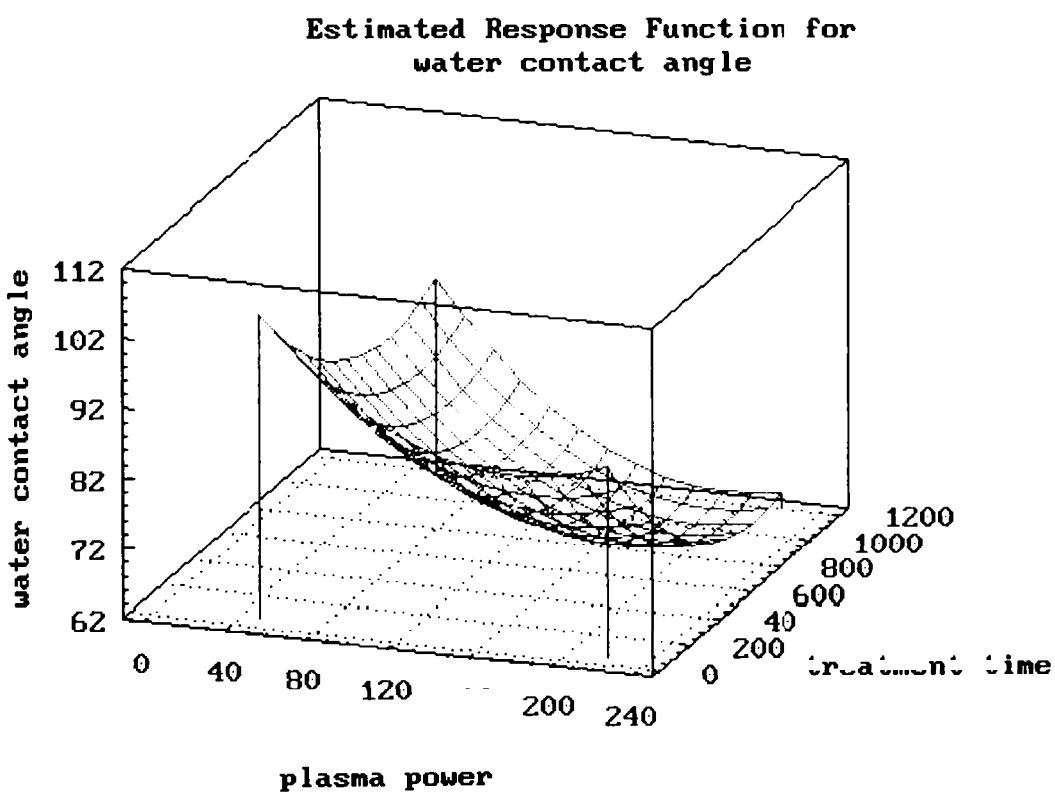

Figure 6.10 Estimate response of the VGCNFs water contact angle depending on the plasma power and treatment time.

Further estimations of the mathematical modelation design are presented in the annexes. The analysis of variance (ANOVA) table is presented in Annex 1. The estimate response of the water contact angle depending on the others plasma parameters are plotted in Annex 2-4, like: treatment time – chamber pressure (Annex 2), plasma power – chamber pressure (Annex 2), oxygen flow rate – chamber pressure (Annex 3), plasma power – oxygen flow rate (Annex 3),

treatment time – oxygen flow rate (Annex 4) and plasma power – treatment time – chamber pressure (Annex4).

6.8.1.2 Oxygen Plasma Treatment using Step by Step Method

The plasma power and treatment time are the parameters which require a special attention. Table 6.4 shows the plasma parameter used for vapour grown carbon nanofibres functionalisation.

Table 6.4 Plasma Parameter

Plasma Parameter	Minimum	Maximum	Units
Plasma Power	50	180	W
Treatment Time	1	60	min
Oxygen Flow Rate	50	200	sccm
Chamber Pressure	0.5	1	mbar

6.8.1.2.1 Influence of the Treatment Time

The oxygen plasma functionalisation of the VGCNFs was performed considering plasma power and treatment time variable while the other parameters were kept constant (chamber pressure (1 mbar) and oxygen flow rate (100 sccm O_2)). Figure 6.11 shows the water contact angle of the Pyrograf fibres as a function of plasma power and treatment time. In each graphic is presented the water contact angle for two different plasma powers: 50 W and 80W – Figure 6.11a; 100 W and 120 W – Figure 6.11b; 150 W and 180 W – Figure 6.11c as a function of the treatment time (variable parameter).

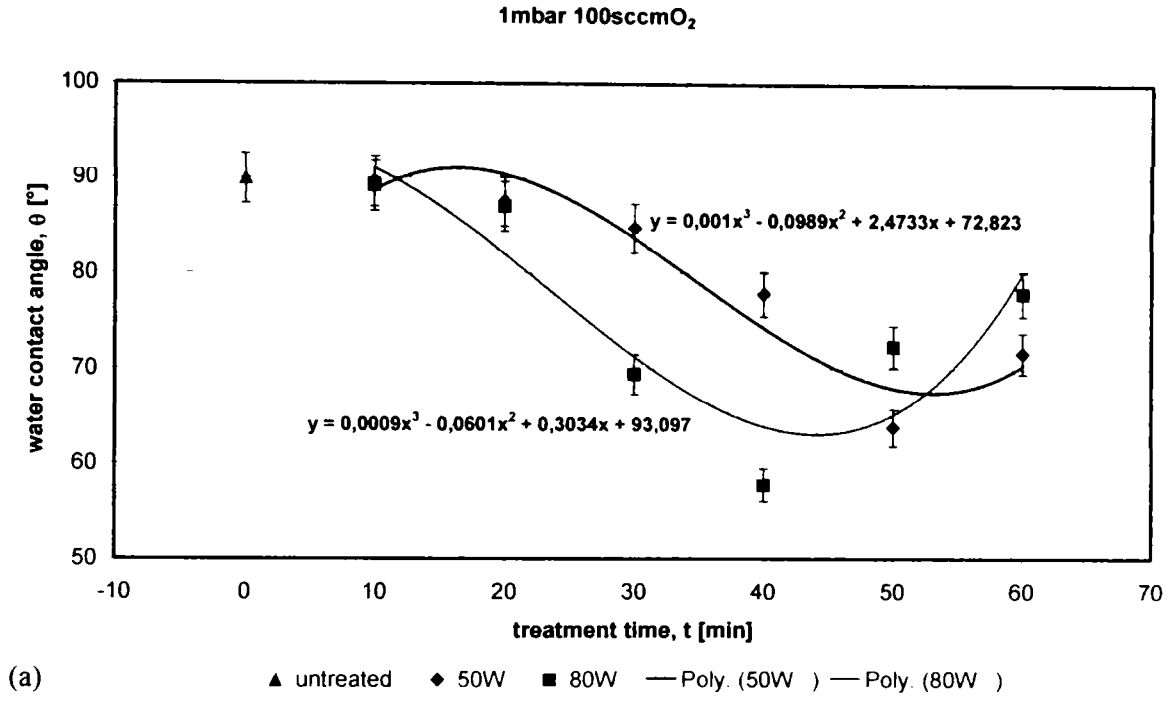

(a)

1mbar; 100sccmO2

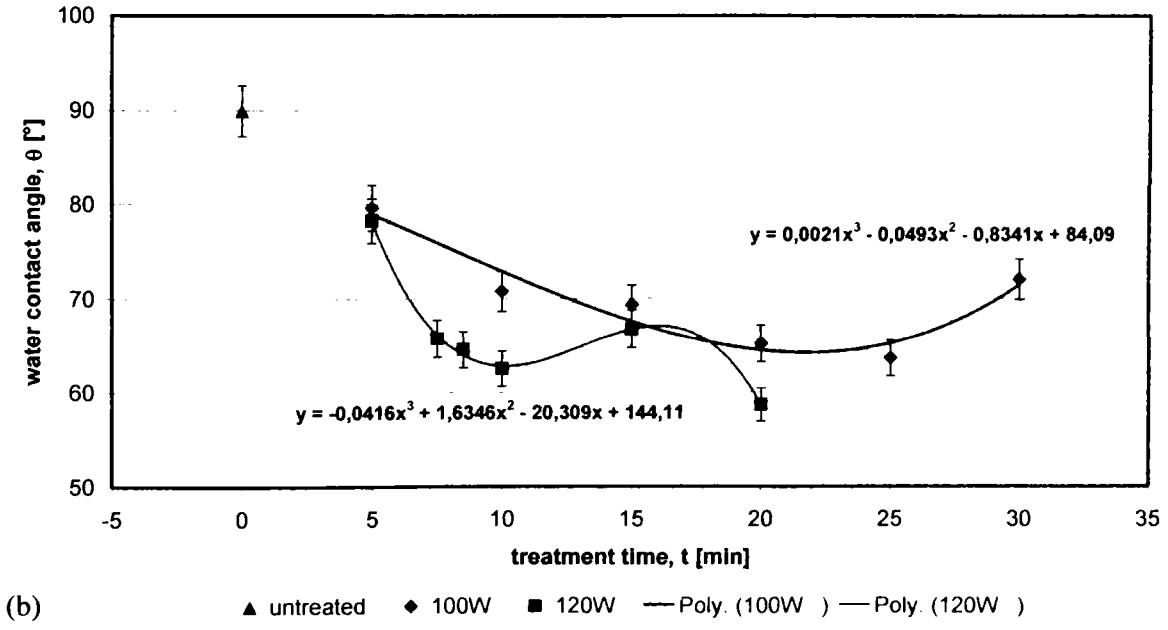

(b)

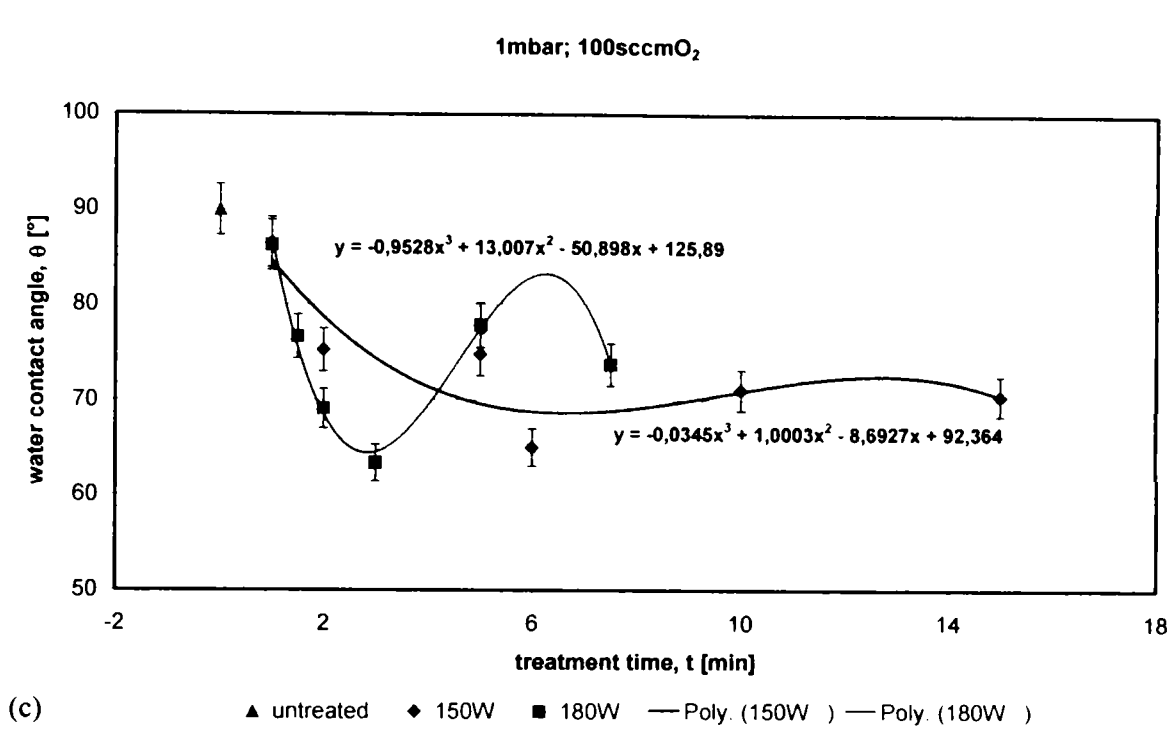

Figure 6.11 Water contact angle as function of treatment time and plasma power: (a) 50W + 100W; (b) 100W + 120Wand (c) 150W + 180W.

The water contact angle (WCA) of the fibres begins slowly to decrease after minimum 20 min when the fibres are treated at 50W plasma power. The lowest value for the water contact angle was achieved only after 50 minutes, 63.87° ±4%. Increasing the plasma power to 80W, the lowest value for WCA was obtained after 40 min (57.75° ±4%), Figure 6.11a. Increasing further the plasma power to 120W, the water contact angle of the VGCNFs decreased already after a few minutes. Comparing figure 6.11a with b, one can observe that same values for WCA were achieved either using 120W plasma power for 7.5 minutes treatment time, or using lower values for plasma power, like 50W for longer treatment time, 50 minutes. If the vapour grown carbon fibres are treated at 180W, a lower water contact angle of 63.38° ±4%, was obtained in only 3 minutes (Figure 6.11c).

The hydrophilicity of the plasma treated VGCNFs was increased up to 35% (sample treated by 80W, 40 min, 1mbar, 100sccm O_2 - θ =58°) compared with the untreated fibres, θ = 89.9°. These graphics reveal also the water contact angle tendency during the plasma treatment as function of treatment time. The water contact angle (WCA) decreased up to a certain point (treatment time) than the WCA have the tendency to remain constant or to increase.

A long treatment time correlated with a high plasma power lead to etching the outer surface of the fibres. The etching effect on the outer graphene layers of the VGCFs treated for a long time is shown in the TEM – micrograph from Figure 6.12. The arrows indicate a minimal

etching of the fibres surface using shorter treatment times, whereas by increasing the exposure time, the fibres could be deeply etched. This phenomenon should be avoided in order to keep the original properties of the fibres.

Figure 6.12 TEM – micrograph of the oxygen plasma treated fibres for 30 min (a) and 60 min (b).

Figure 6.13 shows the treatment parameters which were set in order to obtain similar lower values for water contact angle. These samples were used further for calculation of the total surface energy according to the Wendt – Owens method. These results are plotted in Figure 6.14.

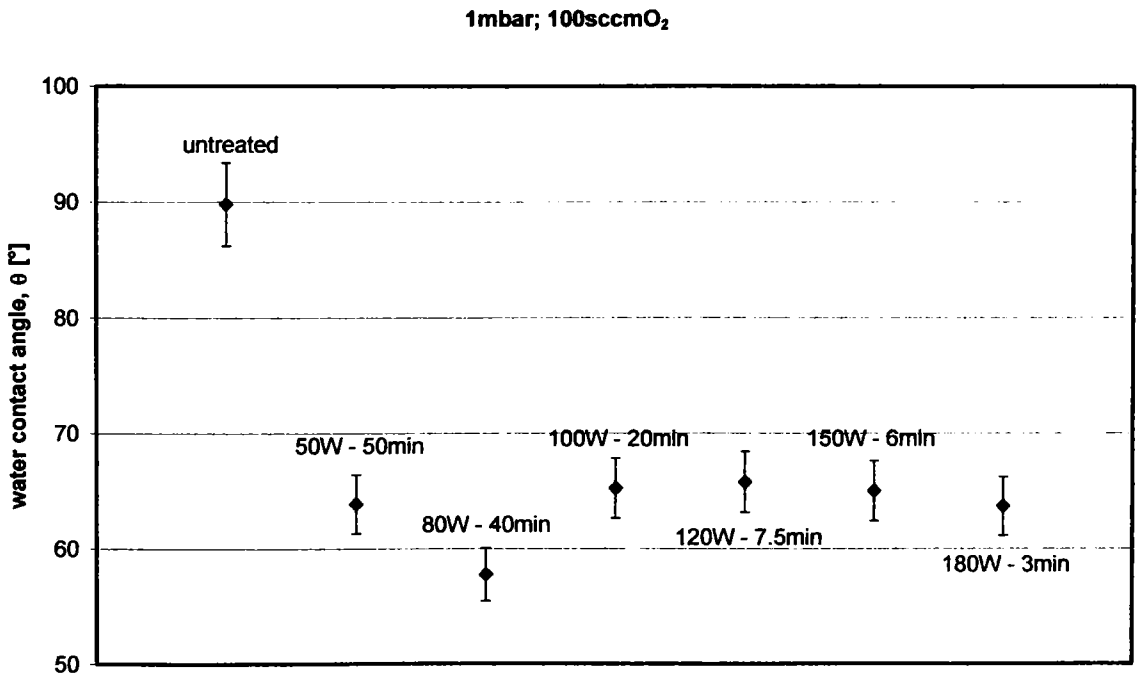

Figure 6.13 The approx. same water contact angle obtained for different plasma power (50W – 180W) and treatment time (3min – 50min).

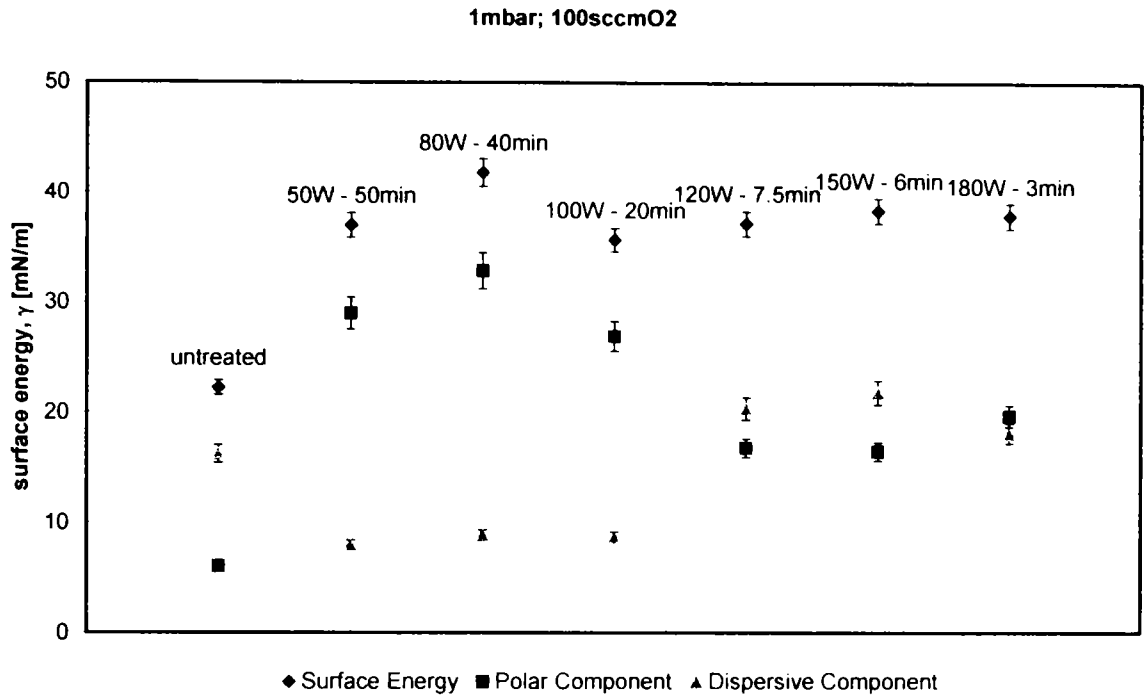

Figure 6.14 Surface energy of the oxygen plasma treated fibres.

The surface energy of the treated fibres increased with more than 80% (sample 80 W – 40 min, γ=41.79 mN/m) compared with the untreated fibres (γ = 22.25 mN/m). It can be observed that for similar values of water contact angle of the fibres (63° ±3°) are corresponding also similar values of the total surface energy (38 mN/m ±3 mN/m) indifferently of the used plasma treatment parameters. The surface energy has two important components: the dispersive component (γ^d) and the polar component (γ^p). The later one correlates with the total amount of functional groups onto the fibres surface [100].

Although, the total surface energy is almost constant indifferent if the VGCNFs were treated for a long time (50 min) at 50 W or short time (3 min) at 180 W, but the polar component is strongly influenced by those two parameters (treatment time – plasma power). The untreated fibres have the polar component only 6.03 mN/m and after the plasma treatment for longer time and at lower values for plasma power this component is increased up to 450%. Also, in order to obtain a higher value for the polar component of the surface energy, a lower plasma power and a longer treatment time is indicated (samples 50 W – 50 min, 80 W – 40 min and 100 W – 20 min). For the production of polymer composites, a larger quantity of plasma treated carbon nanofibres is necessary. Therefore, in order to avoid an expensive functionalisation process a reduction of treatment time plays an important role. Increasing the plasma power, the suitable treatment time will be shorter but the value for the polar component (the functionalisation degree) will slowly decrease (samples 120 W – 7.5 min,

150 W – 6 min and 180 W – 3 min). For example the value of the polar component for the sample treated at 120 W for 7.5 minutes is 16.81 mN/m in comparison with that of the sample treated at 80 W for 40 min, 32.89 mN/m.

The polar component can be correlated with the values obtained from the titration measurements. A lower value of the polar component means a reduced amount of functional groups containing oxygen or nitrogen atoms on the nanofibres surface. The same conclusion is revealed from the NaOH titration measurement, Figure 6.15. In the case of untreated samples, the amount of oxygen groups on the outer graphene layer is very low (0.2 mmol/g) compared with the oxygen plasma treated samples. Therefore, after oxygen plasma treatment the amount of oxygen groups was increased up to 9 times (sample 80 W – 40 min).

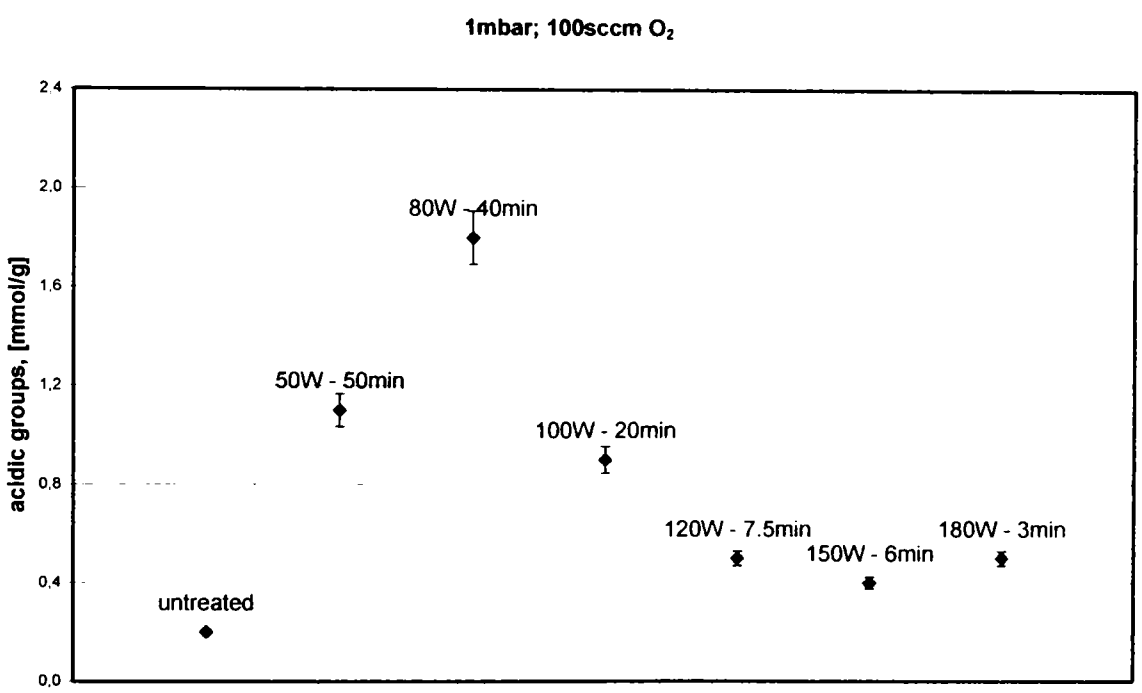

Figure 6.15 Back titration measurements of the oxygen plasma treated fibres.

The results from XPS measurements can be correlated very well with the polar component of the total surface energy and with the values from back titration measurements. Figure 6.16 shows the XPS measurements results. The sample which has the highest polar component, respectively contains the highest amount of acidic groups has also the highest at.% O_2. The samples treated at higher plasma power (> 120W) have the content of functional groups (O + N At.%) lower than the samples treated at lower plasma power (50-100W). This phenomenon can be explained as a result of etching effect onto the fibres surface.

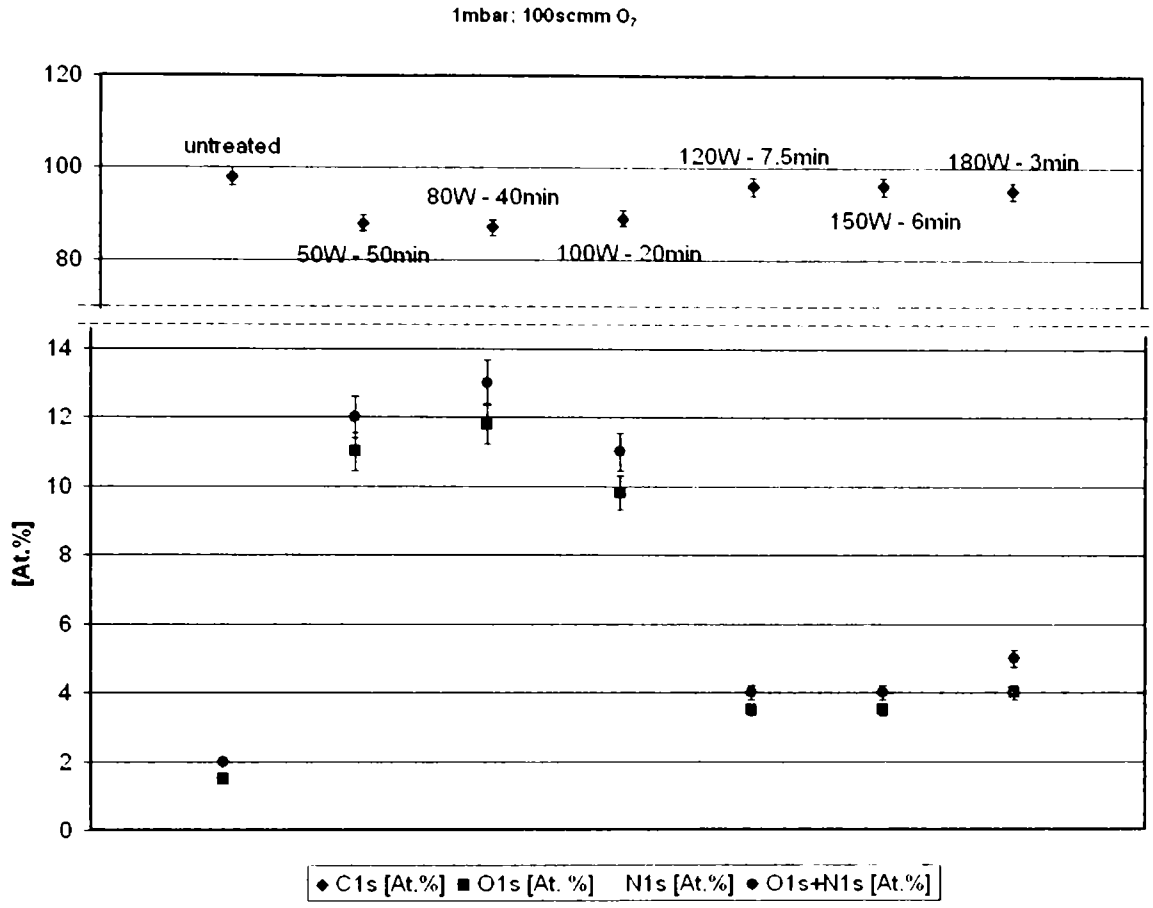

Figure 6.16 XPS measurements of the oxygen plasma treated fibres.

The BET measurements and TEM – micrographs explain very well the etching effect of the fibres surface. Figure 6.17 shows the values for specific surface area of the untreated and plasma treated vapour grown carbon nanofibres. The specific surface area of the fibres can be correlated with the values for dispersive component of the surface energy. The untreated fibres having the value of the dispersive component of 16.22 mN/m, the value for the surface area is about 44.92 m^2/g. The plasma treated fibres at 150 W for 6 min have the highest value for the dispersive component (21.87 mN/m) and nevertheless the determined surface area (43.21 m^2/g) is lower than of untreated fibres. Normally, a higher dispersive component corresponds to a higher surface area. This fact can be explained knowing that the untreated fibres have the outer carbon layers amorphous (see chapter V, section 5.2.2). The surface energy measurements are based on contact angle measurements in different liquids. The liquids having a higher molecule cannot penetrate the layers. For example, considering the water (H_2O) as testing liquid. The water molecule formed from one oxygen molecule and two hydrogen molecules (molar mass: $H_2O = O_2 + 2H_2 = 15.999 + 2\times1.008 = 18.015$ g/mol) is larger than nitrogen gas molecule (atomic mass $N_2 = 14.007$ g/mol) which is used for BET measurements (gas chromatography). It should be also mentioned, that the amorphous carbon layers burned easily during the oxygen plasma treatment.

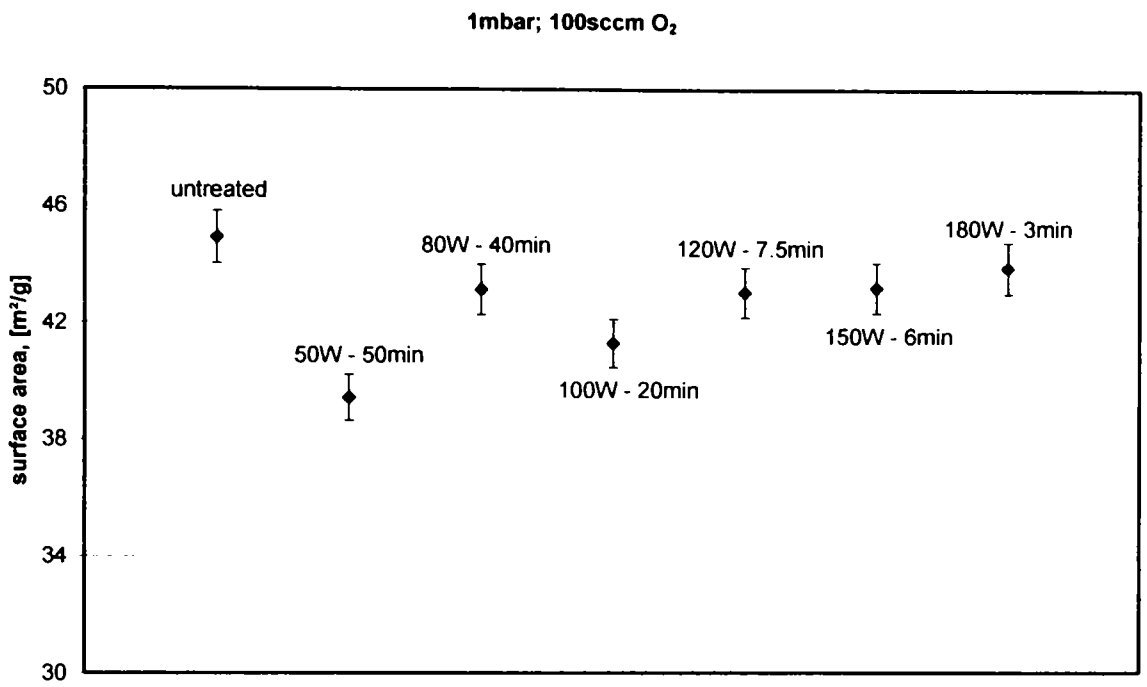

Figure 6.17 BET measurements of the oxygen plasma treated fibres.

Therefore, a lower water contact angle or a high surface energy of the VGCNFs doesn't mean always that the fibres have a good functionalisation degree. The important component of the surface energy, which reflects a good functionalisation degree, is the polar component γ^p. Figure 6.18 shows the transmission electron microscopy analysis for the oxygen plasma treated nanofibres. The etching effect of the oxygen plasma treatment on the VGCNFs (such as pitting etching or micropores) was more or less evident depending on the treatment parameters.

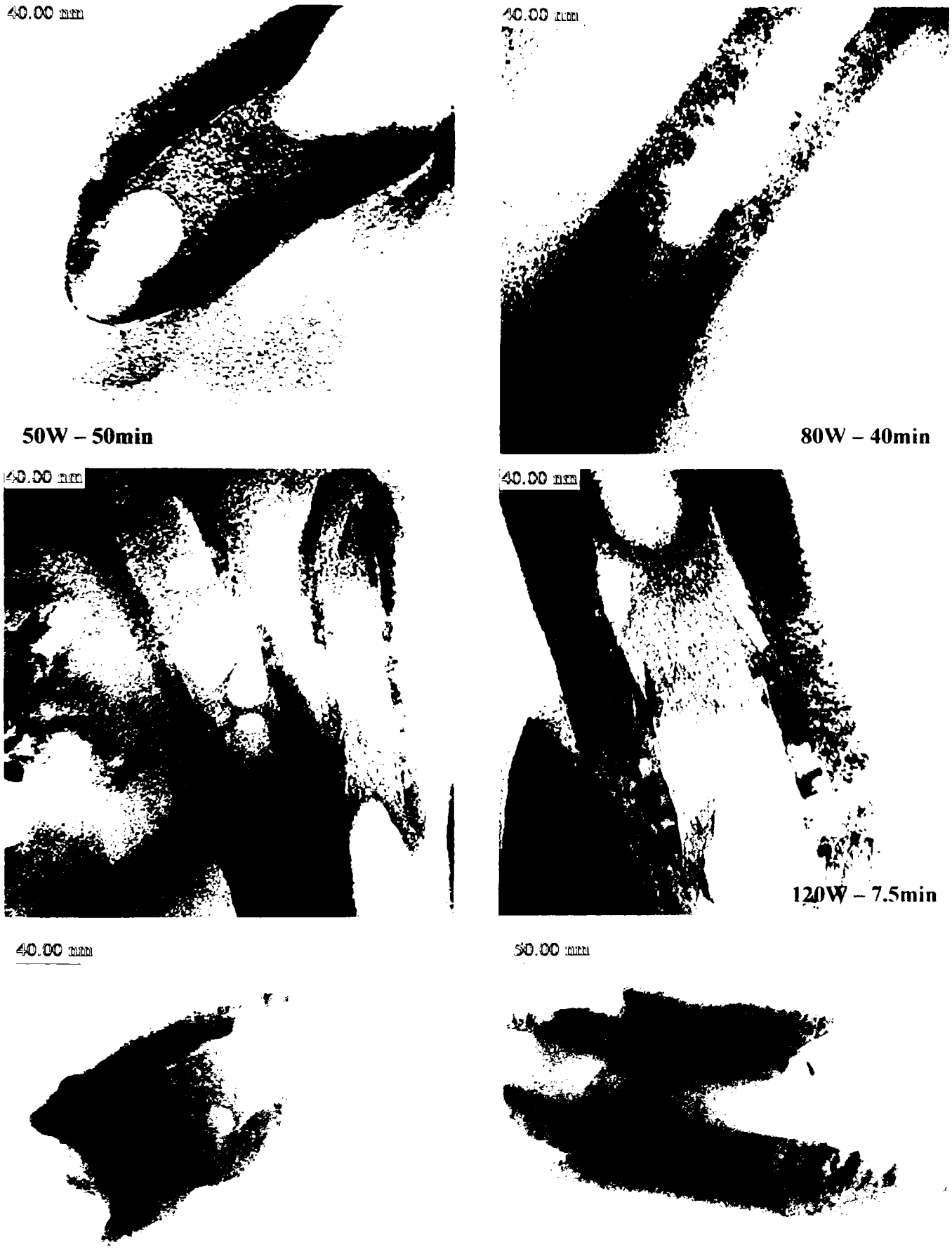

Figure 6.18 TEM – micrograph of the oxygen plasma treated fibres.

The specific electrical resistivity for these samples was calculated, Figure 6.19. The higher functionalisation degree of the fibres is, the higher is electrical resistivity (lower electrical conductivity).

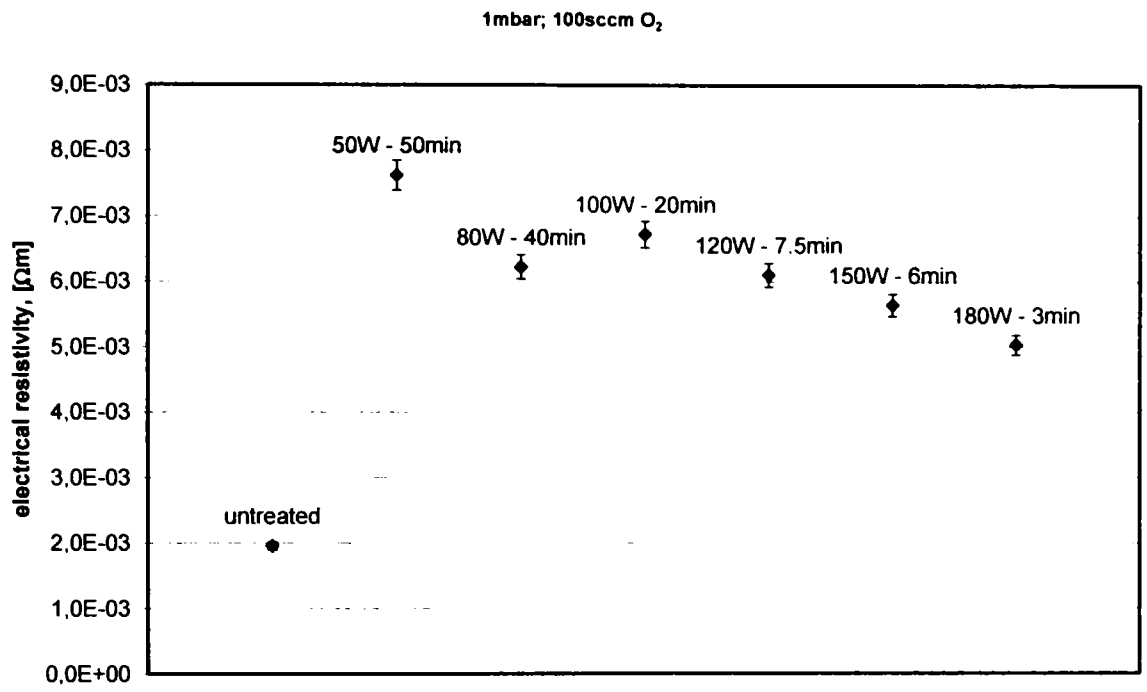

Figure 6.19 Volume electrical resistivity of the oxygen plasma treated fibres.

The water contact angle was estimated using mathematical modelation from Matlab based on the results of the water contact angle obtained from step by step method, Figure 6.20. The blue colour shows a water contact angle up to 30° for plasma power range from 160 to 180W and treatment time between 30 – 60 min.

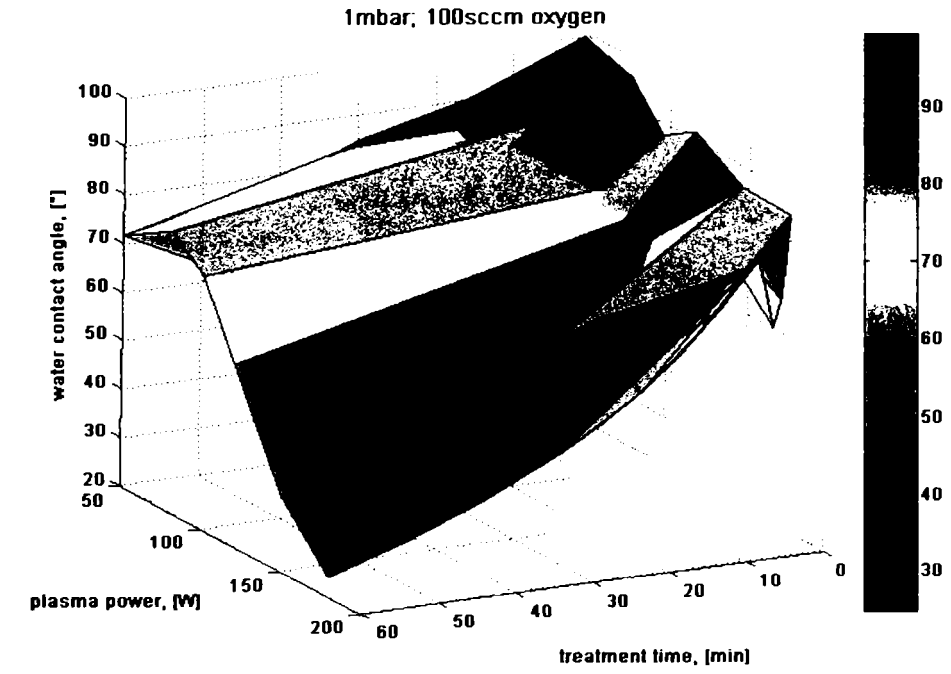

Figure 6.20 Estimation of water contact angle for the oxygen plasma treated fibres.

These values for water contact angle where estimated up to 30° and if are correlated with the values from titration and polar component (surface energy). It can be observed that the fibres are totally burned, Figure 6.21a and b. The total amount of acidic groups and the polar component estimations show even negative values for samples treated in the domain of high plasma power combined with long treatment time. This thing indicates that the fibres are not functionalised but destroyed although have a lower contact angle.

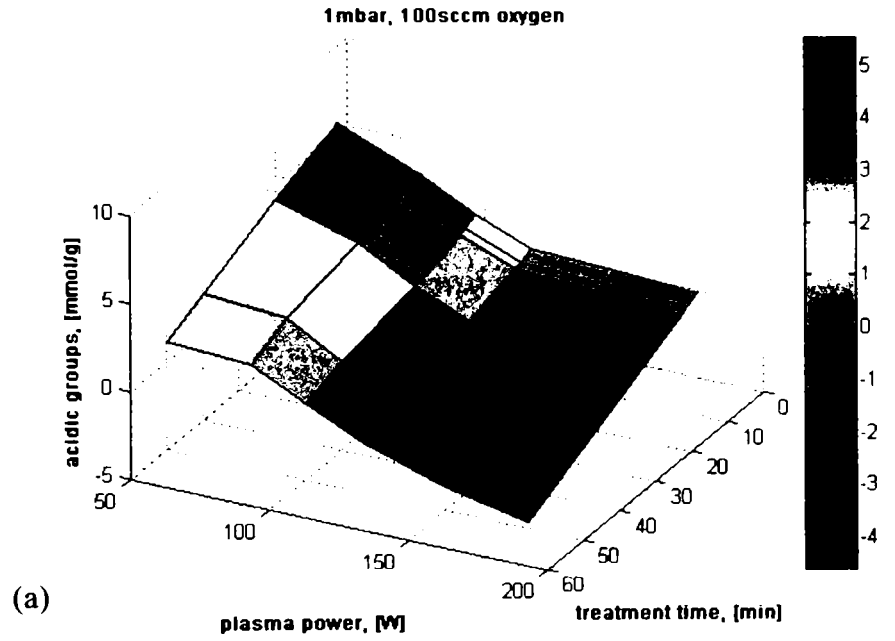

(a)

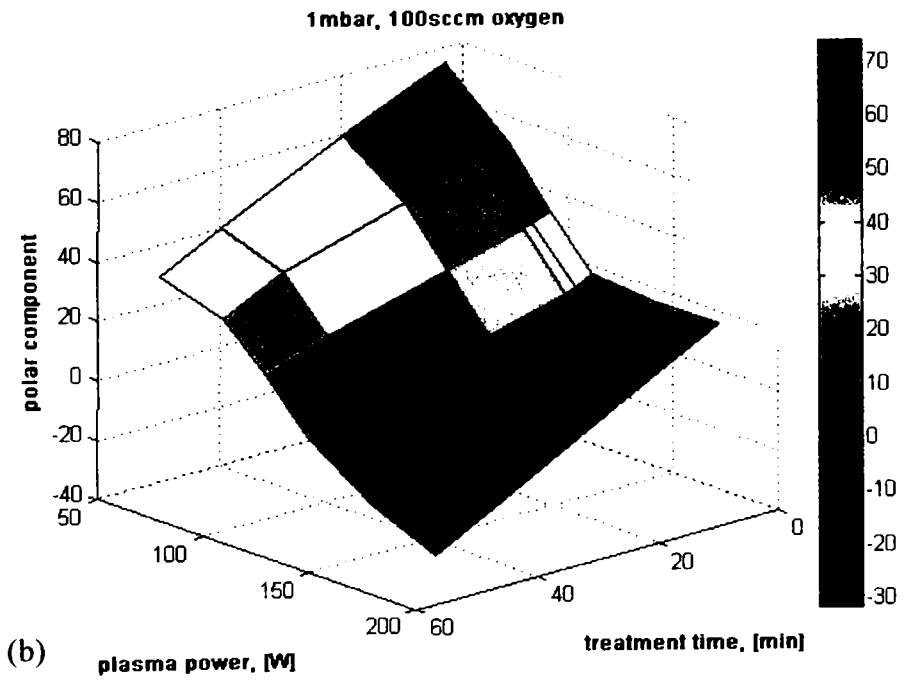

(b)

Figure 6.21 Estimation of total acidic groups (a) and the polar component (b) for the oxygen plasma treated fibres.

The estimation for surface energy, dispersive component, BET and XPS analysis are presented in annexes, Annex 5, 6.

6.8.1.2.2 *Influence of the Plasma Power*

The Pyrograf fibres were treated at a constant treatment time (5, 10 and 20min), chamber pressure (1mbar) and oxygen flow rate (100sccm). The variable parameter was plasma power, from 50 to 180W. A relatively low treatment time (mauve points), 5min, leads to a water contact angle of only 74.8° while a double time (yellow points), 10min, leads to a water contact angle of 62° at a plasma power of 120W, Figure 6.22. A further increase of the treatment time, up to 20 minutes will not enhance very much the functionalisation degree of the treated fibres comparing with the fibres treated for 10 minutes.

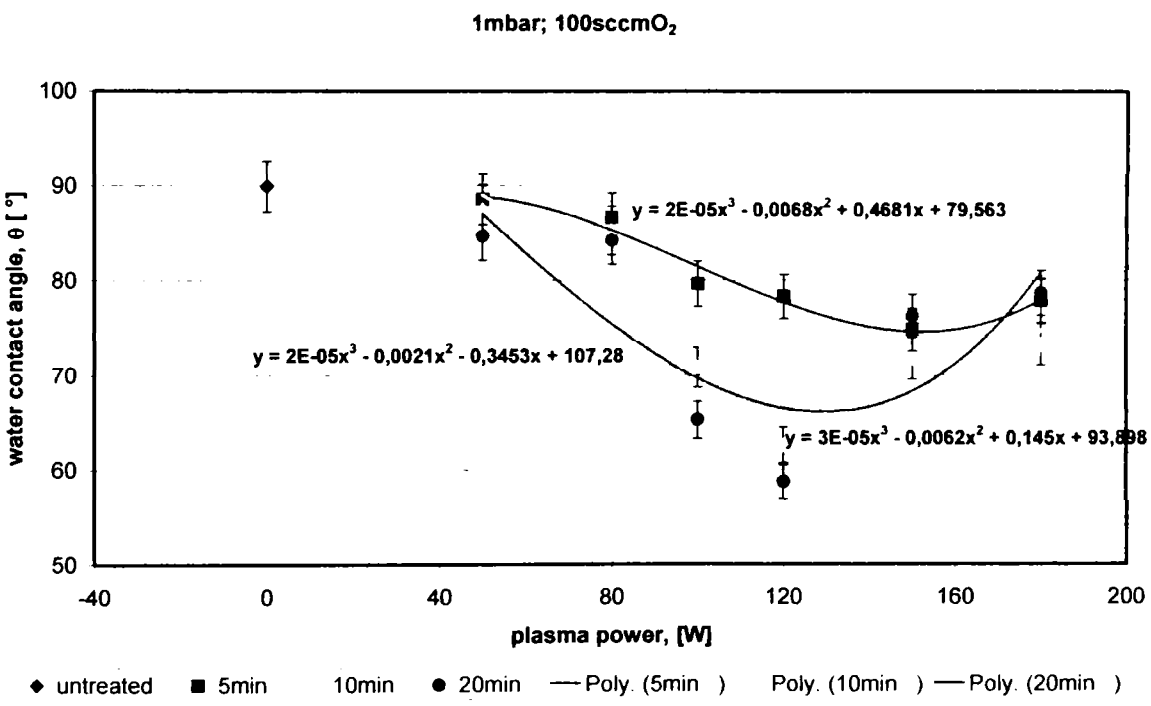

Figure 6.22 Water contact angle as function of plasma power (50 – 180W).

6.8.1.2.3 *Influence of the Oxygen Flow Rate*

The following treatments were performed at different oxygen flow rates from 50 sccm to 200 sccm, treatment time up to 20 minutes and chamber pressure of 0.5 mbar.

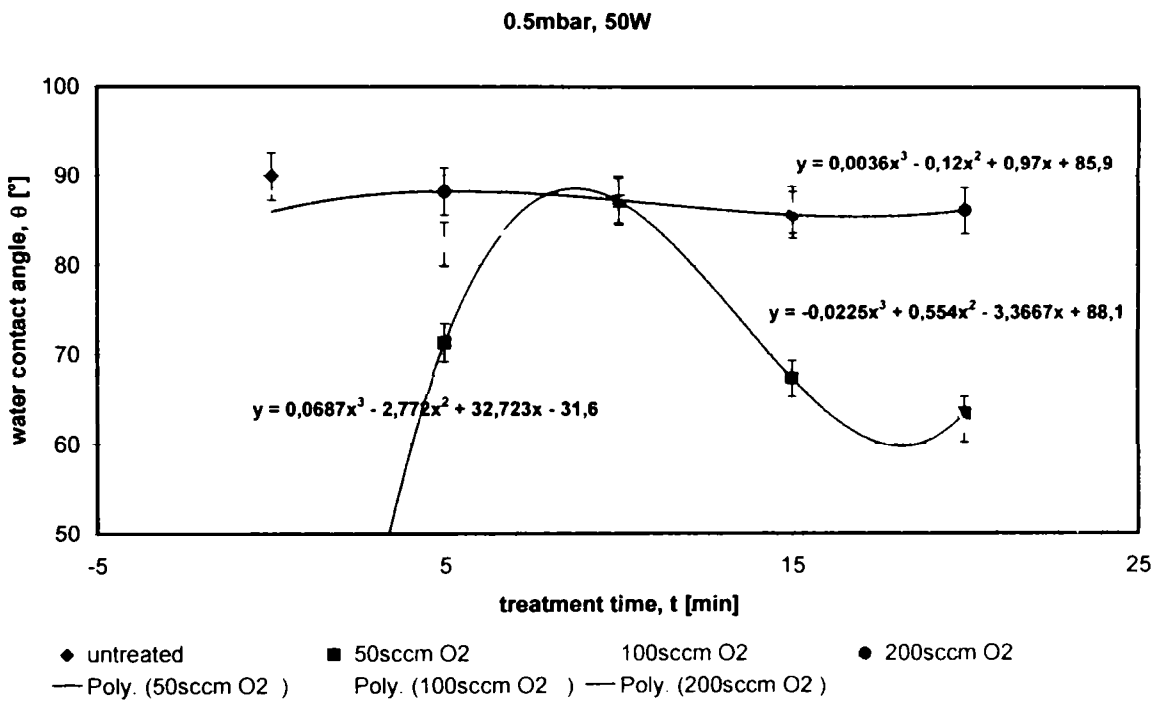

Figure 6.23 Water contact angle as function of oxygen flow rate (50 – 200sccm).

It is consider the following correlation between flow rate and chamber pressure as a function of their ratio: 50 sccm O_2 and 0.5 mbar means ratio 1:1, 100 sccm O_2 and 0.5 mbar means 1:2 and respectively 200 sccm O_2 and 0.5 mbar is ratio 1:4. No functionalisation of the fibres was obtained at 50W and ratio 1:4, Figure 6.23. At low plasma power and high flow rate it wasn't obtain a plasma discharge. The O_2 molecules can not be divided in two O atoms. Increasing the plasma power to 100W (Figure 6.24) similar water contact angle for ratio 1:1 and 1:2 can be observed. A water contact angle of 62° was obtained at ratio 1:4 for 10 min treatment time compared with the values obtained for ratios 1: or 1:2 for the same treatment time. A further increase of the treatment time under the same conditions will not lead to a better value for water contact angle.

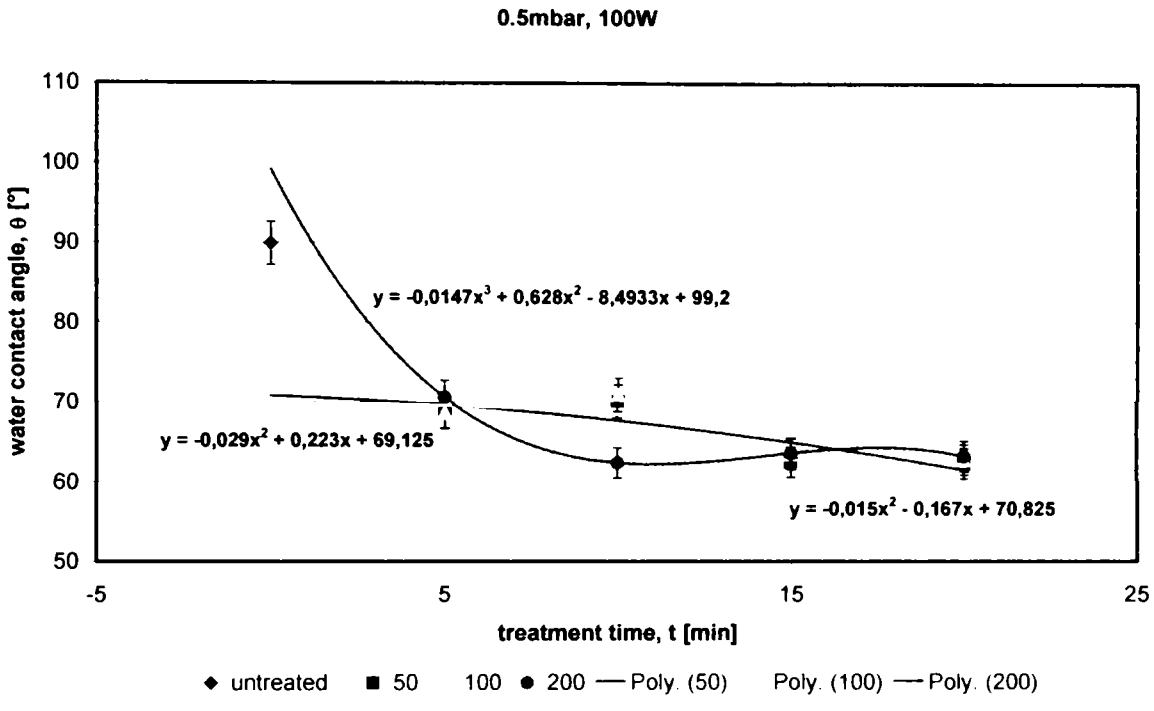

Figure 6.24 Water contact angle as function of oxygen flow rate (50 – 200sccm), at 100W.

6.8.1.2.4 *Influence of the Chamber Pressure*

The values of water contact angle of the VGCNFs treated by two different chamber pressures are presented in Figure 6.25. The fibres treated at low chamber pressure can achieve a water contact angle of 71° at low plasma power 50W. Considering the values for oxygen flow rate and chamber pressure the ratio for these measurements is 1:0.5. The lowest value for water contact angle was obtained at 100W. At higher plasma power (150W) the chamber pressure has not a strong influence on the water contact angle.

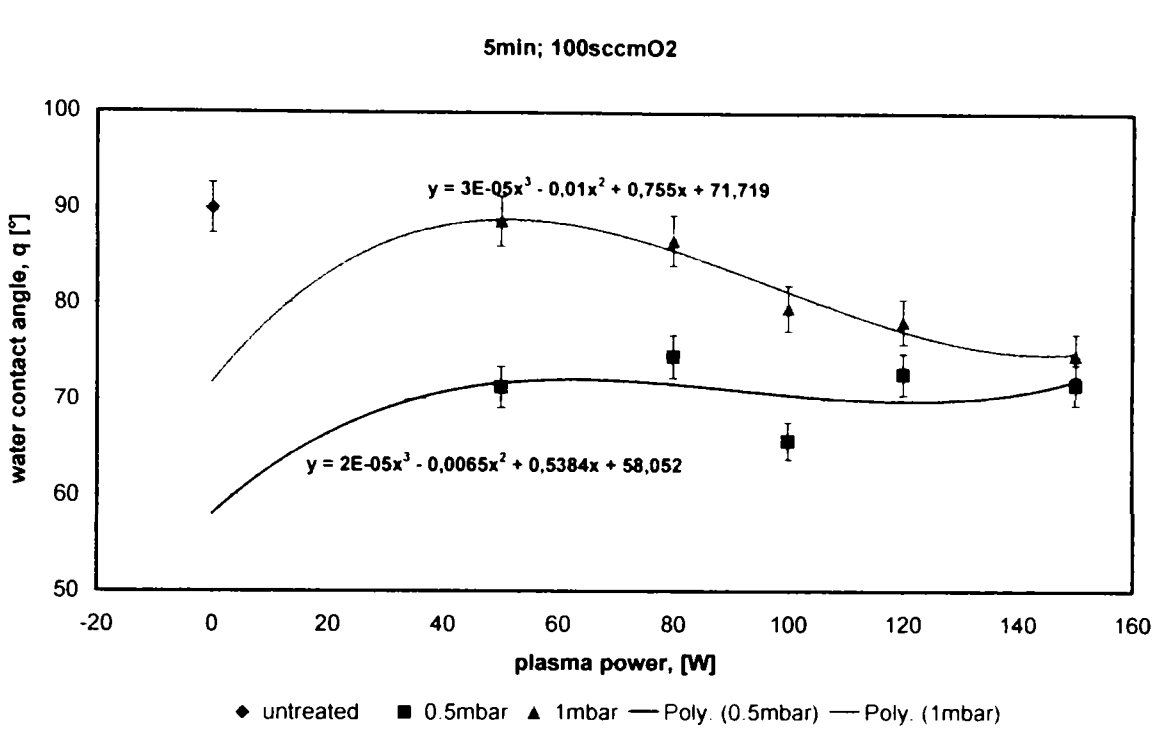

Figure 6.25 Water contact angle as function of chamber pressure, 0.5 – 1mbar.

6.8.2 Ammonia Plasma Treatment of the Pyrograf Fibres

The following treatments of vapour grown carbon nanofibres were performed by ammonia plasma treatment. The chamber pressure and ammonia flow rate was maintained constant, 1 mbar and 10 sccm NH_3. A higher ammonia flow rate can't be reached from plasma device for the same chamber pressure of 1 mbar.

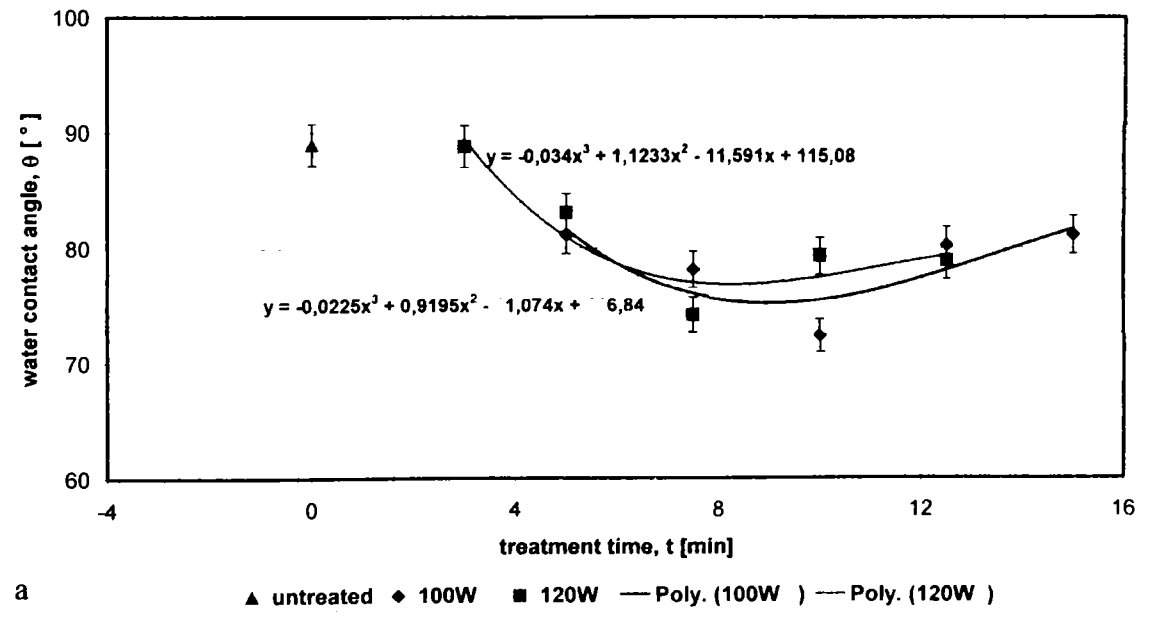

a

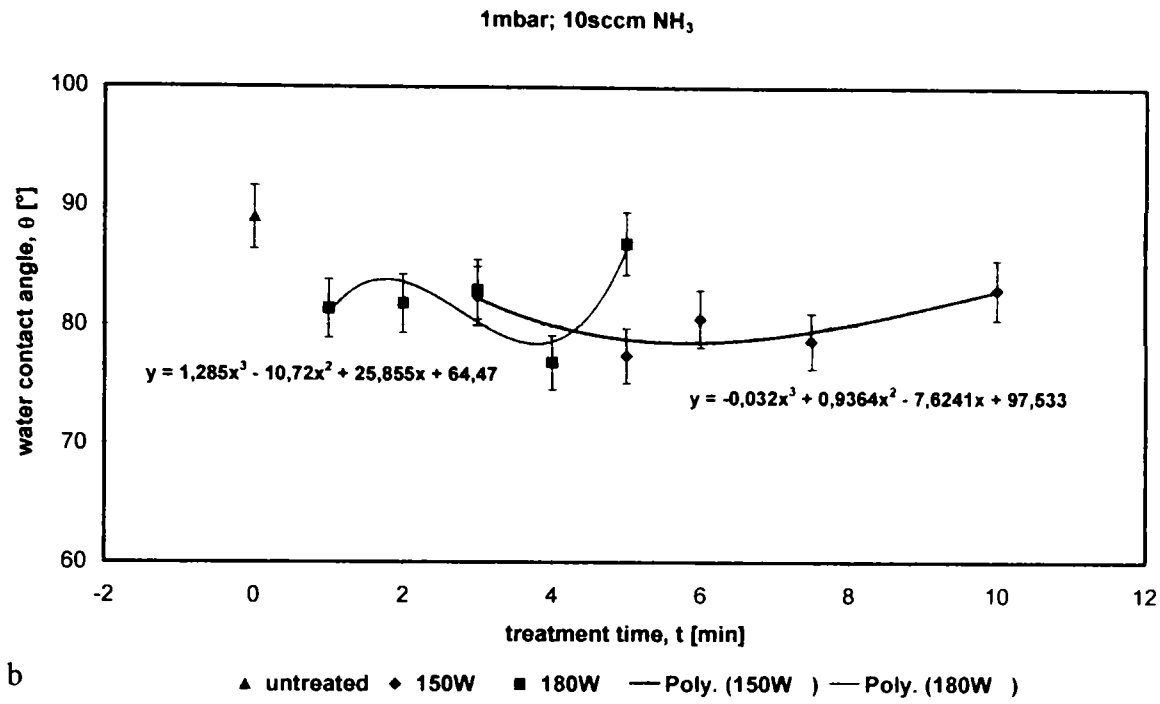

Figure 6.26 Water contact angle as function of treatment time, (a) 100 and 120W, (b) 150 and 180W.

The best value for water contact angle was obtained at 120W plasma power and 7.5 minutes treatment time (Figure 6.26). Increasing the plasma power up to 180W a water contact angle of 77° for 5 minutes treatment time was obtained.

The ammonia plasma treatment should be more intensively researched with different ammonia flow rate and different chamber pressure. Also, is very important to analyse the effect of ammonia plasma treatment on the VGCNFs by XPS and titration measurements.

6.8.3 Combined Gases Plasma Treatment of the Pyrograf Fibres

The fibres were pre-activated in argon plasma for 2 minutes and subsequently were treated by ammonia and oxygen plasma. Figure 6.27 shows the values of water contact angle for the best obtained samples. The fibres were treated at 120W plasma power, and 1 mbar chamber pressure. It can be observed that a lower contact angle was obtained for fibres treated in combined plasma gases (2.5 min in oxygen and 2.5 min in ammonia), therefore 5 minutes treatment time compared with the fibres treated for 5 min only in oxygen or in ammonia plasma. Also, if the fibres are treated first in oxygen plasma and than in ammonia plasma, the values for water contact angle is lower than in the case when the fibres are treated first by ammonia and than in oxygen plasma. The lowest water contact angle (66°) was obtained for the fibres treated 5 min in oxygen and 5 min in ammonia plasma, total 10 min treatment time.

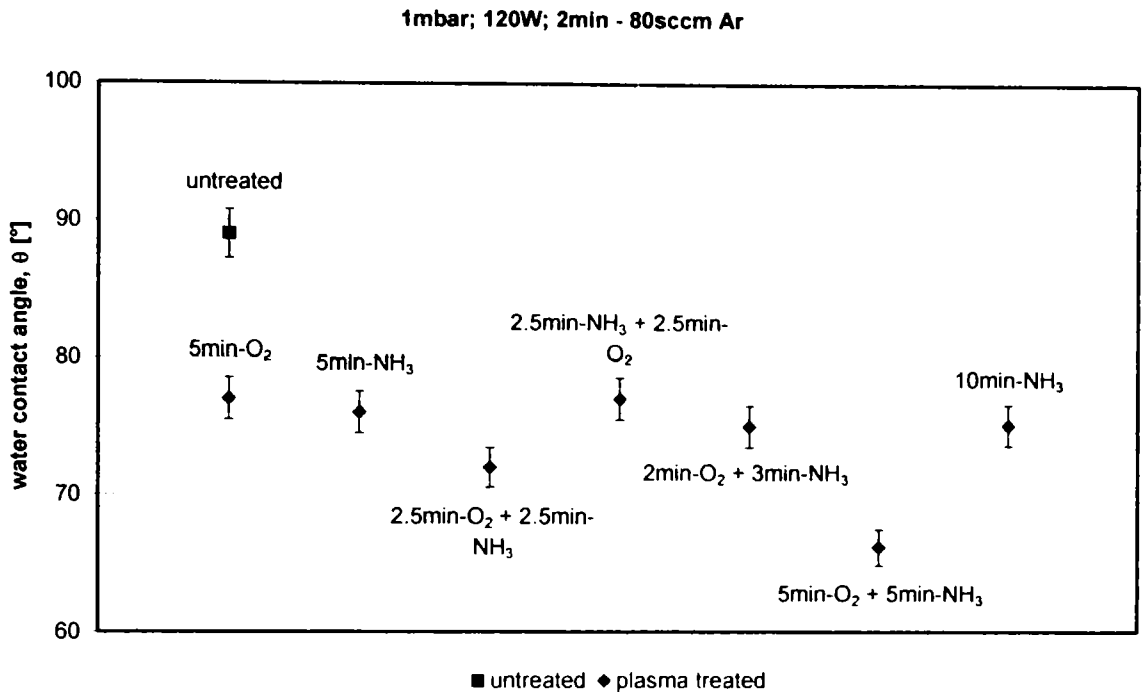

Figure 6.27 Values for water contact angle of the fibres treated in combined plasma gases.

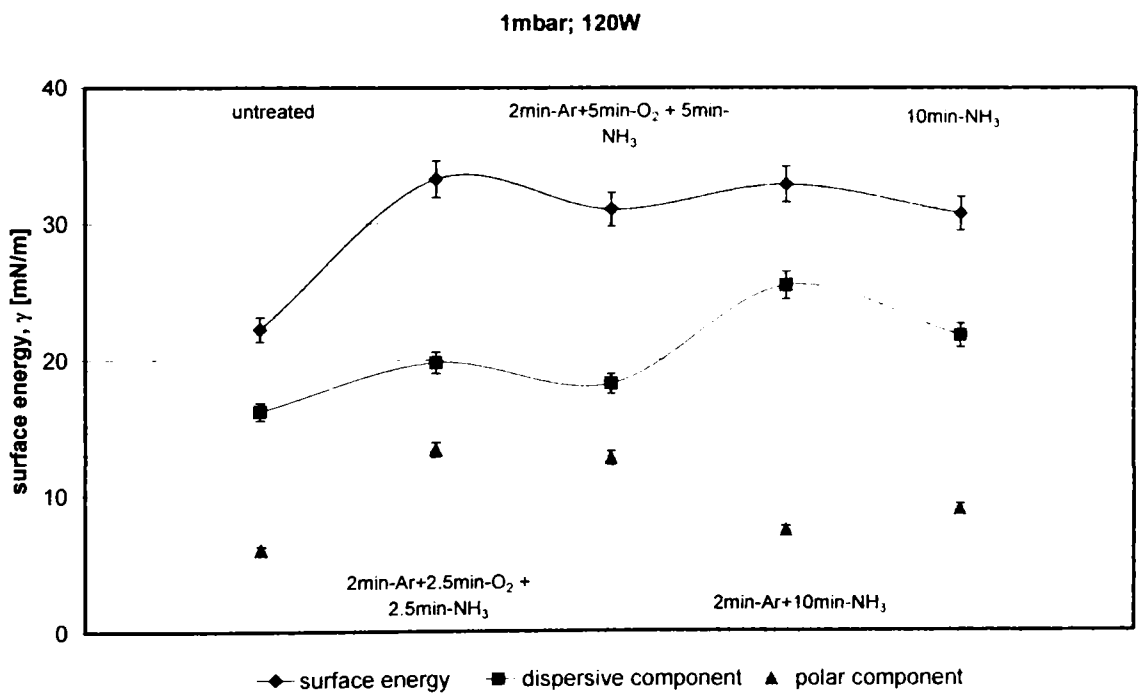

Figure 6.28 Values for surface energy of the fibres treated in combined plasma gases.

The surface energy (Figure 6.28) and XPS (Figure 6.29) measurements for the best samples were performed. The values for the polar component of the surface energy are higher for the fibres treated for a short time, 5 minutes or 10 min combined plasma gases, than that of the fibres treated only in ammonia plasma for 10 min. Generally, this component increased up to an average of 50% compared with untreated fibres. The XPS measurements reveal the same

conclusion for the functional groups. The values of nitrogen atoms percent from total functional groups for the fibres treated by oxygen and than ammonia plasma is lower than in the case of fibres treated only in ammonia plasma. The amount of acidic functional groups of the treated fibres increased up to 6 times more than untreated fibres, Figure 6.29.

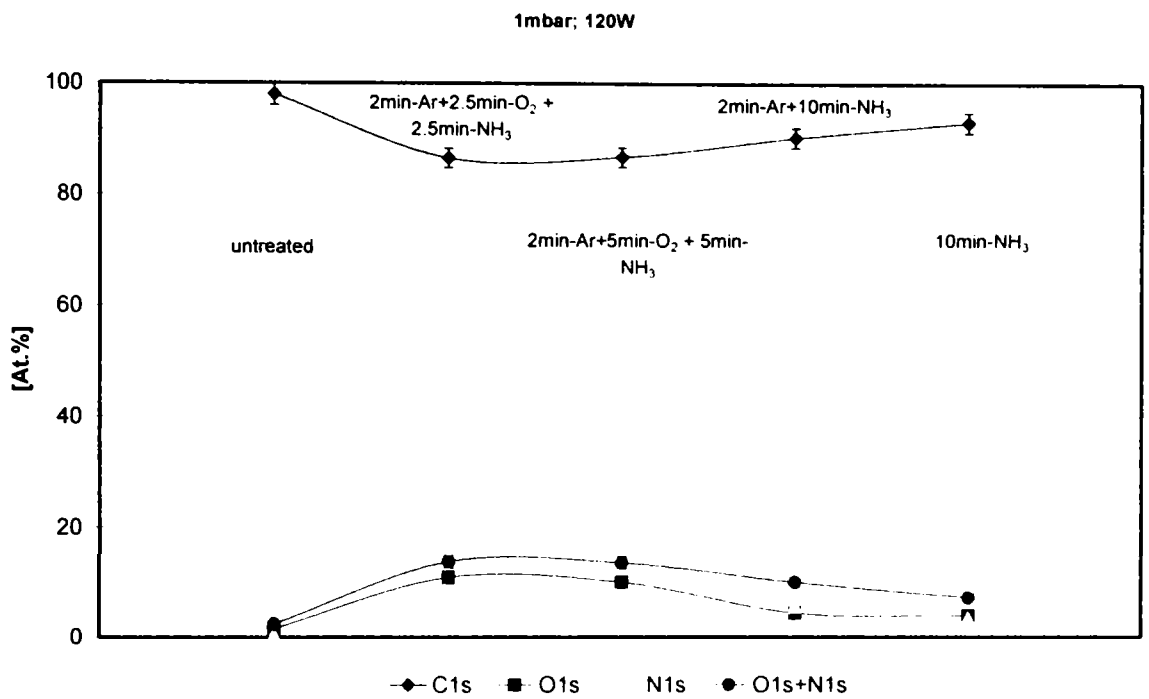

Figure 6.29 XPS measurements of the combined plasma treated fibres.

6.9 *Oxygen Plasma Treatment of the Semana Fibres*

For the surface activation of the Semana Fibres the RF – generator as well as MW – generator were used during the oxygen plasma treatment. The quantity of fibres used for one treatment was 1g.

From the thermogravimetrical characterisation of the Semana fibres it was observed that the TG curve showed a loss in weight at about 190°C. This phenomenon is due to the burning-off process of the polyaromatic groups which still exist on the outer surface of the fibres (Figure 5.8, Chapter 5). The fibres were treated at radio frequency (RF) and high values of the plasma power, between 120 and 180W in order also to clean and subsequently to functionalise the outer surface layers.

The values for water contact angle are presented in Figure 6.30. A water contact angle lower than 72° can not be achieved for the fibres treated by RF generated oxygen plasma. In order to reach better values for water contact angle, it was necessary to treat the fibres using microwave generated oxygen plasma.

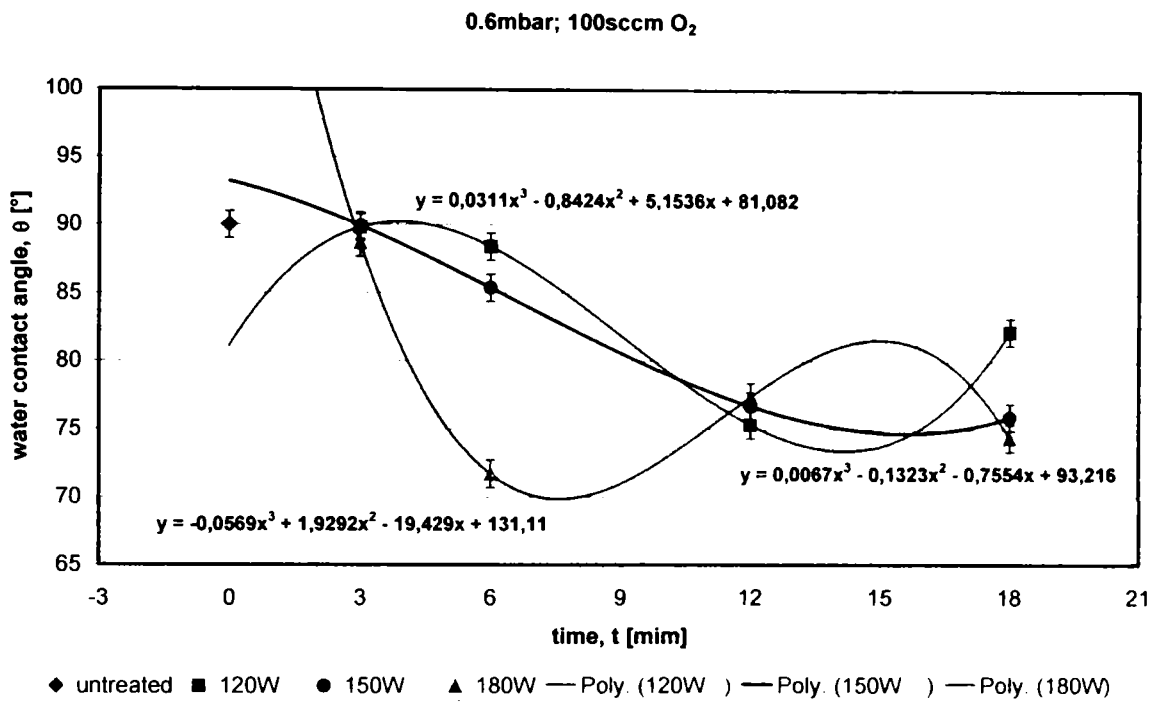

Figure 6.30 Values for water contact angle of the fibres treated in RF generated oxygen plasma.

Using the MW – generator, the fibres were treated at different plasma power (80 – 120W) and up to 7 minutes treatment time. The chamber pressure and oxygen flow rate were maintained constant at 0.4 mbar, and 80 sccm oxygen, respectively. The chamber pressure of 0.4 mbar was selected because in the case of microwave generated plasma, the plasma burn very intensive due to the high frequency in this domain [155]. The ratio chamber pressure / O_2 flow rate was set 1:2 according to our earlier experience and to literature. A high concentration of the working gas leads to a better functionalisation of the fibres. In the case of MW generated plasma the fibres were treated on the plate. For an uniform treatment of the fibres surface, there is necessary to mix manually the fibres. Therefore, it is necessary to interrupt the process at equal interval of time. An effectively 7 min treatment time requires more than 12 min. The soft ventilation was setup to 1 min in order to avoid the blowing of the fibres.
Figure 6.31 shows the values for water contact angle of the treated VGCNFs. Already after 3 minutes of treatment, the water contact angle is lower than in the case of fibres treated by RF generated oxygen plasma for 18 minutes and plasma power 180W. Increasing the treatment time up to 7 min a water contact angle of 29° was obtained.

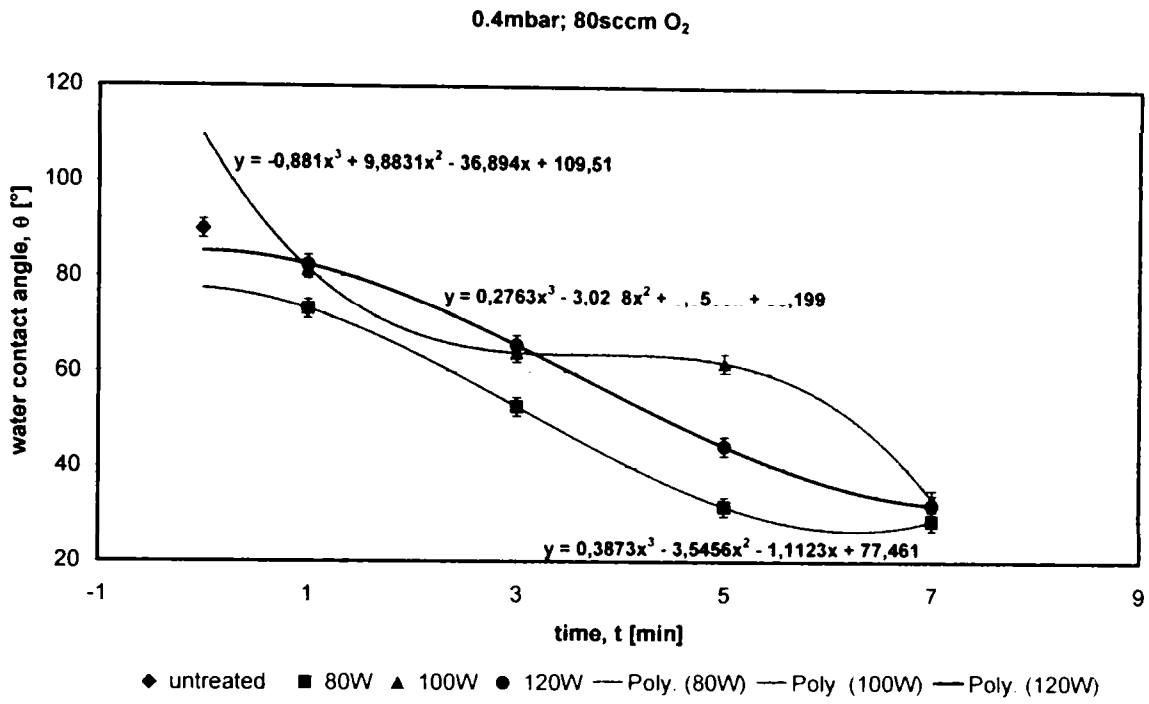

Figure 6.31 Results of water contact angle measurements of the fibres treated in MW generated oxygen plasma.

The best water contact angle was obtained for the fibres treated at 80 W, Figure 6.31. The surface energy was measured for the samples series treated at 80 W, Figure 6.32.

Figure 6.32 Results of surface energy measurements of the fibres treated in MW generated oxygen plasma (80 W, 0.4 mbar and 80 sccm oxygen).

An increase of the total surface energy up to 74 mN/m was obtained. Surprising, the polar component increased up to 69 mN/m even if the treatment time was 7 min. The dispersive component decreased from 20mN/m (untreated fibres) to 5 mN/m (fibres treated for 7 minutes). The titration measurements showed also an increase in the total amount of acidic groups up to 2.4 mmol/g, Figure 6.33. The results from titration measurements are perfect correlated with the polar component of the total surface energy.

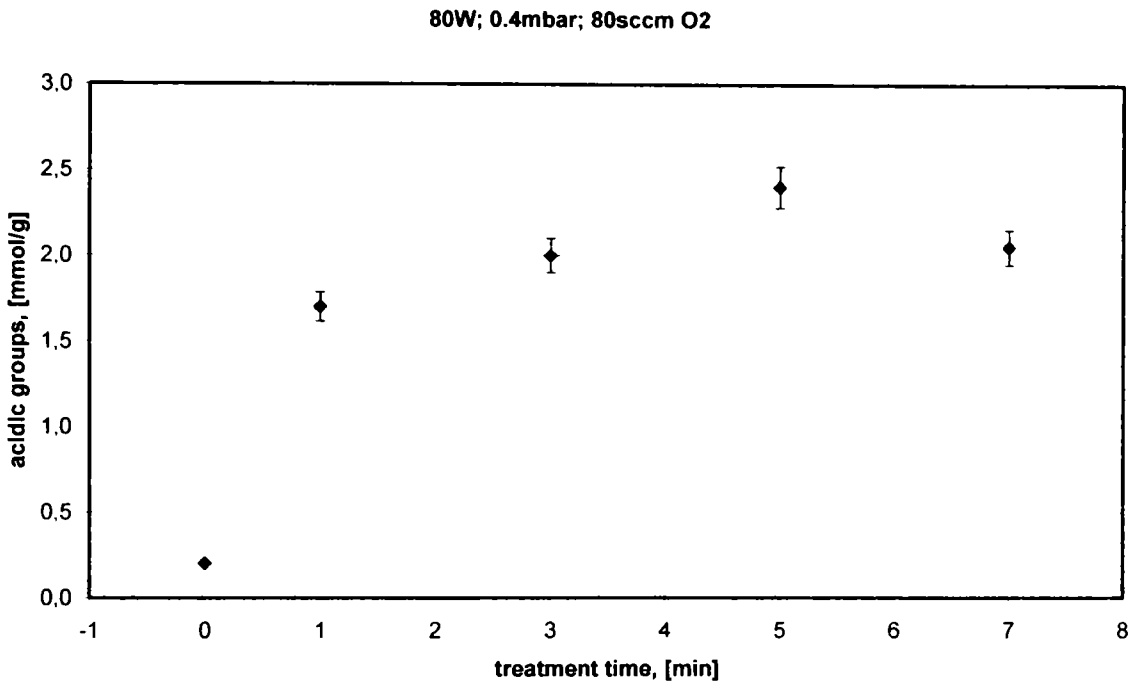

Figure 6.33 Results of the titration measurements of the fibres treated in microwave generated oxygen plasma (80 W, 0.4 mbar and 80 sccm oxygen).

The influences of the chamber pressure onto water contact angle of the VGCNFs are presented in Annex 7. A lower value of water contact angle was obtained at a plasma power of 100 W and 120 W for 3 minutes treatment time. It can be concluded that the fibres treated at a lower chamber pressure (high vacuum) 0.2 mbar, a higher plasma power (100 and 120 W) is necessary in comparison with the samples treated at 0.4 mbar chamber pressure where a plasma power of 80 W should be applied.

6.10 Oxygen Plasma Treatment of the GANF Fibres

The GANF fibres were treated by plasma power up to 150 W and treatment time up to 10 minutes. The quantity of fibres for each treatment was 1.2 grams. The oxygen plasma used is high frequency generated. It was tried also to functionalise the fibres with the microwave

generated plasma, but this fibres have the bulk density very low and are blown from the plate during the soft ventilation.

6.10.1 Influence of the Treatment Time

Figure 6.34 shows the water contact angle of the treated fibres in comparison with the untreated fibres. It can be observed that the untreated fibres have a lower water contact angle in comparison with the untreated Pyrograf and Semana nanofibres. The untreated fibres have already a value of water contact angle of 66°. This phenomenon is due to the debulking and stripping processes made from the manufacturer in order to cleaning and purify the fibres.
The water contact angle measurements shown a surprising value of zero degree in the case of fibres treated at 100W for 2.5 min. This treatment was repeated at least 3 times and always the value for water contact angle was between 0° and 6°. Increasing the treatment time, it can be observed that the water contact angle is between 50° and 65°. At lower plasma power (50 and 80W) the water contact angle is slightly decreased in comparison with the untreated fibres.
A water contact angle of 52° was obtained for the fibres treated at 150W for 5 minutes, Figure 6.35. If the fibres are treated at a higher plasma power, 150W it can be observed that the values for water contact angle are increased more than that of the untreated fibres, e.g. fibres treated at 150W for 7.5 minutes.

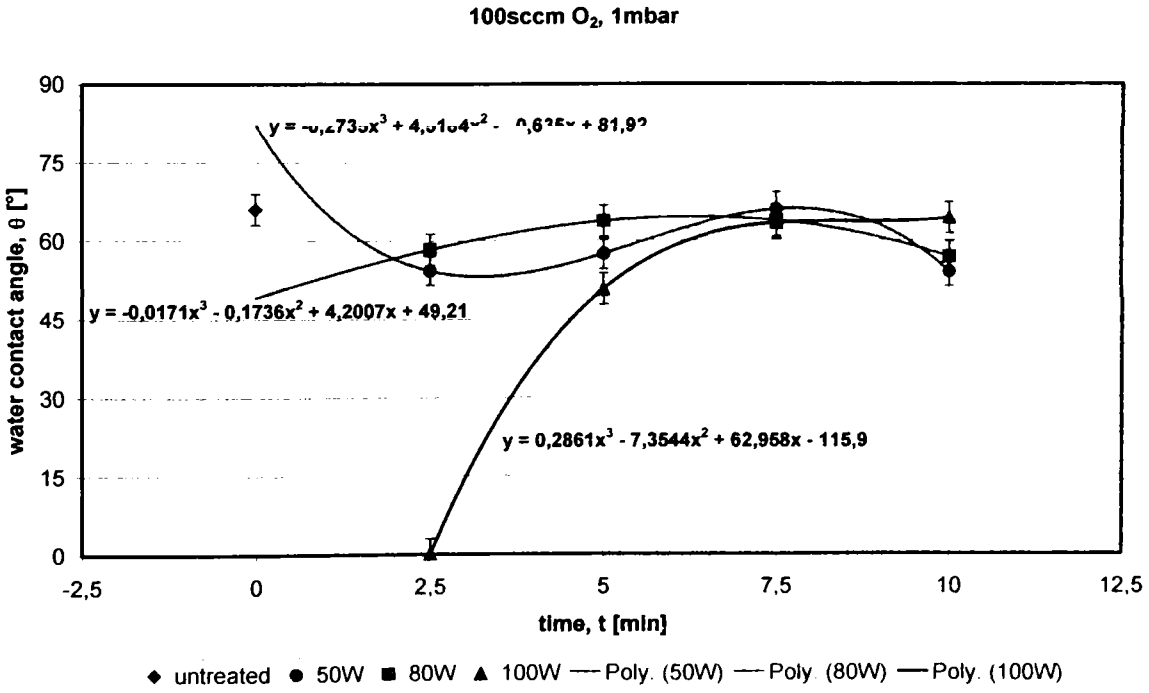

Figure 6.34 Water contact angle as function of treatment time and plasma power (50 – 100W).

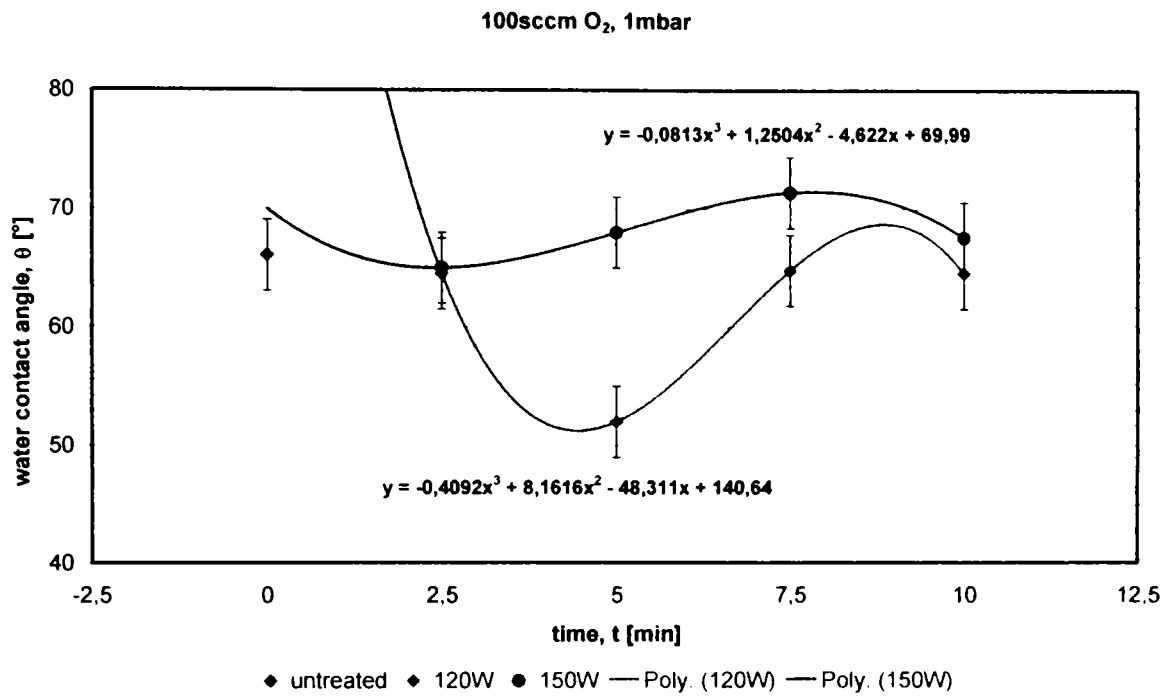

Figure 6.35 Water contact angle as function of treatment time and plasma power (120 – 150W).

Further investigations were made on the sample series treated at 100W. The fibres were treated also for 1.5 min and 3.5 min. A contact angle of 59° for 1.5 min treatment time and 40° for the sample treated for 3.5 min was obtained, Figure 6.36.

Figure 6.36 Water contact angle as function of treatment time.

The surface energy measurements for the samples treated at 100W were performed (Figure 6.37). The untreated fibres have already a surface energy of 40mN/m. This value is comparable with the surface energy obtained for the treated Pyrograf fibres.

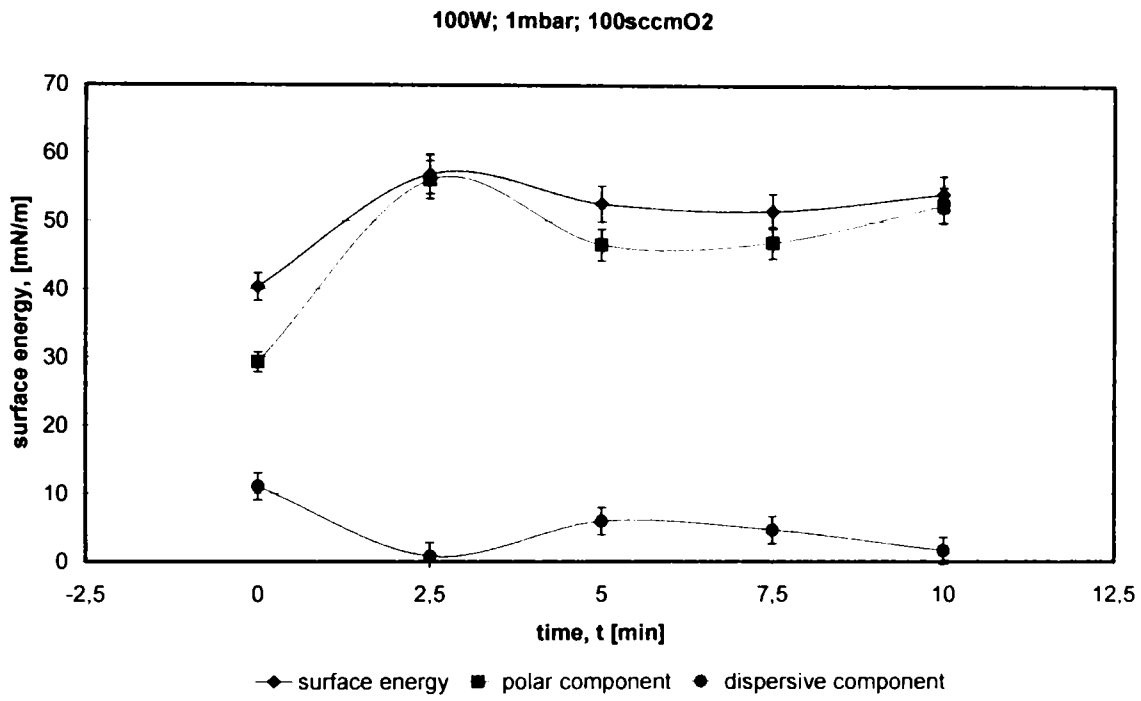

Figure 6.37 Surface energy of the oxygen plasma treated fibres at 100W.

The sample with the 0° water contact angle has also the highest value of the total surface energy. A special attention is accorded to the polar component. The value of the polar component is almost equal with the value for the total surface energy. That reflects a higher functionalisation degree. The titration measurements reveal the same conclusion. For this sample a total amount of acidic groups of 2.2 mmol/g was obtained (Figure 6.38).

Further investigations on the oxygen plasma treatment of GANF fibres at lower chamber pressure and different oxygen flow rate were performed. The influences of the chamber pressure on the water contact angle of the fibres are presented in Annex 8. Like in the case of Pyrograf, GANF fibres present the same tendency of a lower contact angle when of high vacuum chamber is used. In annex 9 are presented the influences of the oxygen flow rate and chamber pressure ratio (0.5:1; 1:1; and 1:2) on the water contact angle.

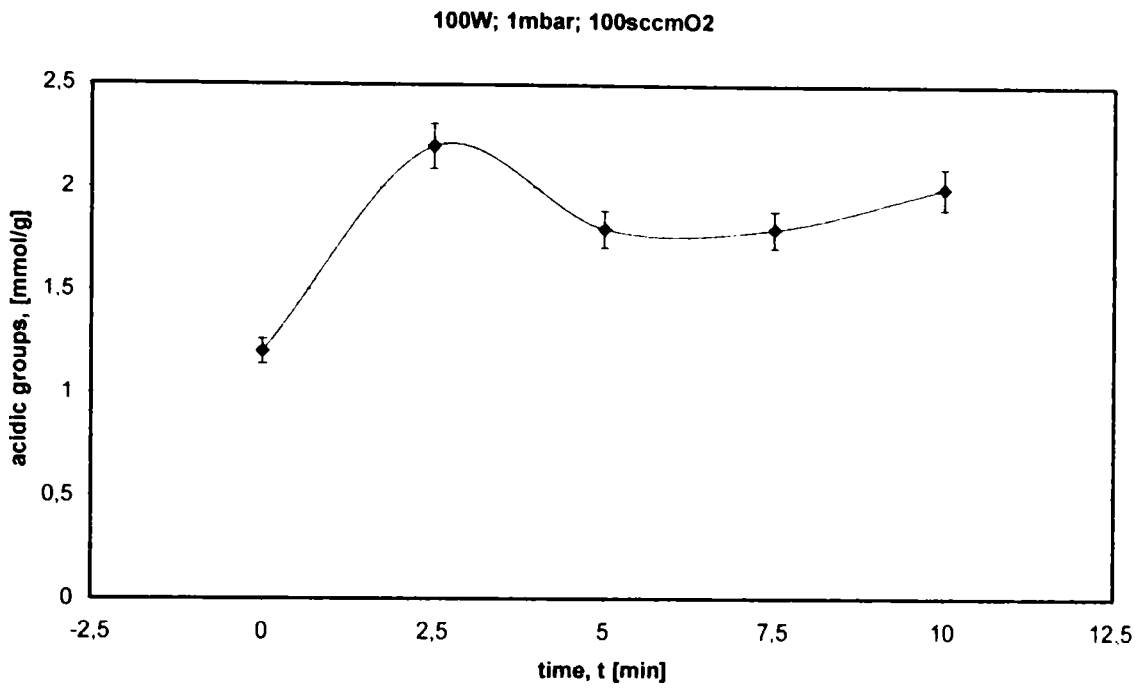

Figure 6.38 Total acidic groups of the oxygen plasma treated fibres.

6.11 Conclusions

The influences of the treatment parameters of the oxygen plasma on the activation of the vapour grown carbon fibres are presented in this chapter. Various suitable techniques for analysis of the wettability and the functionalisation degree of the fibre are also described. The plasma chemical treatments lead to an increase of the wettability as well as in surface energy of VGCNFs.

The importance of the plasma treatment parameters was determined using a statistical software. The Pareto chart shows the importance of plasma treatment parameters. Therefore, the most important parameter is the plasma power followed by the treatment time and the combination plasma power – chamber pressure and treatment time – chamber pressure.

The wettability of the Pyrograf fibres was increased up to 35% . This fibres wettability can be obtained by the correlation of the low plasma power (50W – 80W) and long treatment time up to 50 min, or high plasma power (180W) and short treatment time (~ 3 min). The surface energy reveals that not always a lower water contact angle means a high functionalisation degree. The polar component from surface energy shows an increase in the case of long treatment time at lower plasma power, and than decreased with the increase of the plasma

power. The polar component can be very well correlated with the values from titration and XPS measurements. The titration measurements prove an increase on the total amount of functional groups up to 9 times in comparison with the untreated fibres. The dispersive component of the total surface energy gives information about the porosity of the fibres. BET measurements and TEM micrographs reveal that a higher plasma power combined with a long treatment time lead not only to the destruction of the functional groups generated in the first minutes of treatment but also to burning the outer graphite layers even the complete destruction of the fibres.

The microwave generated oxygen plasma leads to an increase of wettability of VGCNFs up to 70% in relative short treatment time (5 – 7 minutes) and plasma power of 80 – 120W in the case of Semana Fibres. The polar component values are also increased up to 12 times more than that of the as grown fibres. The amount of total acidic groups increased from 0.2 up to 2.4 mmol/g.

The GANF Fibres were treated by different plasma parameters in high frequency generated oxygen plasma. The lowest obtained water contact angle of the treated fibres was 0°. The surface energy and the polar component were both increased up to 56mN/m. That means that the polar component is fast equal with the surface energy, therefore dispersive component is almost zero means a very low etching effect of the fibres (no fibres porosity).

In all cases the polar component from the surface energy is very well reverberate in the titration measurements. Therefore, if the surface energy measurements are performed the titration measurement loses its significance. The XPS measurements are important because are giving information's about what kind of functional groups are created on the fibres surface.

In all cases the adequacy of oxygen and ammonia plasma treatment to improve the wettability and the functionalisation degree of the vapour grown carbon fibres has been demonstrated in the present researches.

CHAPTER VII

ANALYSIS OF THE POLYPROPYLENE COMPOSITES CONTAINING VAPOUR GROWN CARBON NANOFIBRES

7.1 Introduction

The polypropylene and the vapour grown carbon nanofibres were compounded by extrusion technique. The samples for mechanical testing were manufactured by injection moulding. The dispersion and orientation of the VGCNFs in PP matrix were investigated by SEM. The adhesion between fibres and matrix was analysed by scanning electron microscope investigations of the samples in cross section. The mechanical properties of the composites were determined by the following tests (short time duration tests): tensile strength and impact resistance. The thermal stability and conductivity of the composites were also investigated. The electrical measurements of the composites were analysed by DC electrical measurements.

7.2 Extrusion

The composites with different weight percent nanofibres were manufactured in a twin screw extruder from firma Berstorff, ZE 25. The technical data of the extruder are presented in Table 7.1 [156]. The twin screw extruder is equipped with 9 heat sensors and 8 heating zones. The extruder is equipped also with a twin screw feeder system from Brabender, model DDW-H0 / DDSR 20-30, connected to a microcomputer – Congrav "C". The feeder system has four modes of operation: "gravimetric metering feeders", "volumetric metering feeders", "run dry, RD", and "charge" [157].

In order to compound the PP with VGCNFs, these materials were mixed manually together. The composites containing Pyrograf fibres have as matrix granular polypropylene (RA 1 E 10, notated PP1) while the composites containing Semana and GANF fibres have as matrix powder PP (P9400, notated PP2).

The first composites containing Pyrograf and Semana fibres were manufactured by the company SABIC Polyolefin GmbH (before was DSM Polyolefin GmbH), Germany. The configuration of the screw geometry and the setup of the temperature in each heating zone were optimised by this company. The parameters used in order to compound the PP with VGCNFs are as follow:

- screw rotation 200 min^{-1};
- current 14 – 18 A, depending on the concentration of nanofibres in composite;
- mass temperature 230°C;

- mass pressure 36 bar;
- mass flow 2.5 – 3 kg/h;
- master balance – run dry 15%
- temperature in heating zone:
  - zone 1: 33°C;
  - zone 2: 190°C/190°C (theoretic temperature / real temperature);
  - zone 3: 200°C/200°C;
  - zone 4: 210°C/210°C;
  - zone 5: 210°C/225°C;
  - zone 6: 210°C/210°C;
  - zone 7: 210°C/210°C;
  - zone 8: 200°C/200°C;
  - zone 9: 190°C/190°C;

Table 7.1 Berstorff ZE 25 – technical data [156].

Component		Value	Units
Extruder	screw diameter	25	mm
	inside diameter	17	mm
	axes distance	21.5	mm
	max. rotation speed	450	min^{-1}
	max. torsion moment	60	Nm
	max. drive power with max. permissible torsion	6	KW
extruder drive	tension	3 × 380	V
	rated speed	450	min^{-1}
	torsion moment	0 – 58	Nm/screw
gear box	reduction	7	
	driving speed	3000	min^{-1}

The composites containing 5 wt.% untreated and plasma treated VGCNFs were manufactured in our laboratory using the same extruder. Compounding of the PP with VGCNFs was performed using different extrusion parameters, especially by different screw rotation (100 – 200 min^{-1}) and different percent of feeder (10 – 25 %) (run dry method). The screw rotation and feeder parameters must be correlated. A low screw rotation (100 min^{-1}) and a high feeder

percent (25 %) lead to overloading of the extrusion process or a high rotation screw (250 min^{-1}) and a low feeder percent (10 %) lead to a low efficiency of the extrusion process. The cross section of the obtained pellets was examined by stereo microscope, Leica MZ12. The composites were also tested by tensile strength measurements. Figure 7.1 shows the morphology of the composites containing 5 wt.% fibres. It can be observed that the pellets have some voids inside, because the compounding process was performed without venting of the volatile gases. The pellets have more voids inside if were compounded at a high screw rotation (200 min^{-1}) and a high feeder percent (25%), Figure 7.1b. Figure 7.2 shows the tensile properties of the composite containing 5 wt.% untreated fibres. It can be concluded that an optimal rotation of screw is 200 min^{-1} and a feeder of 20%. The processing temperature in each heating zone was the same like at SABIC.

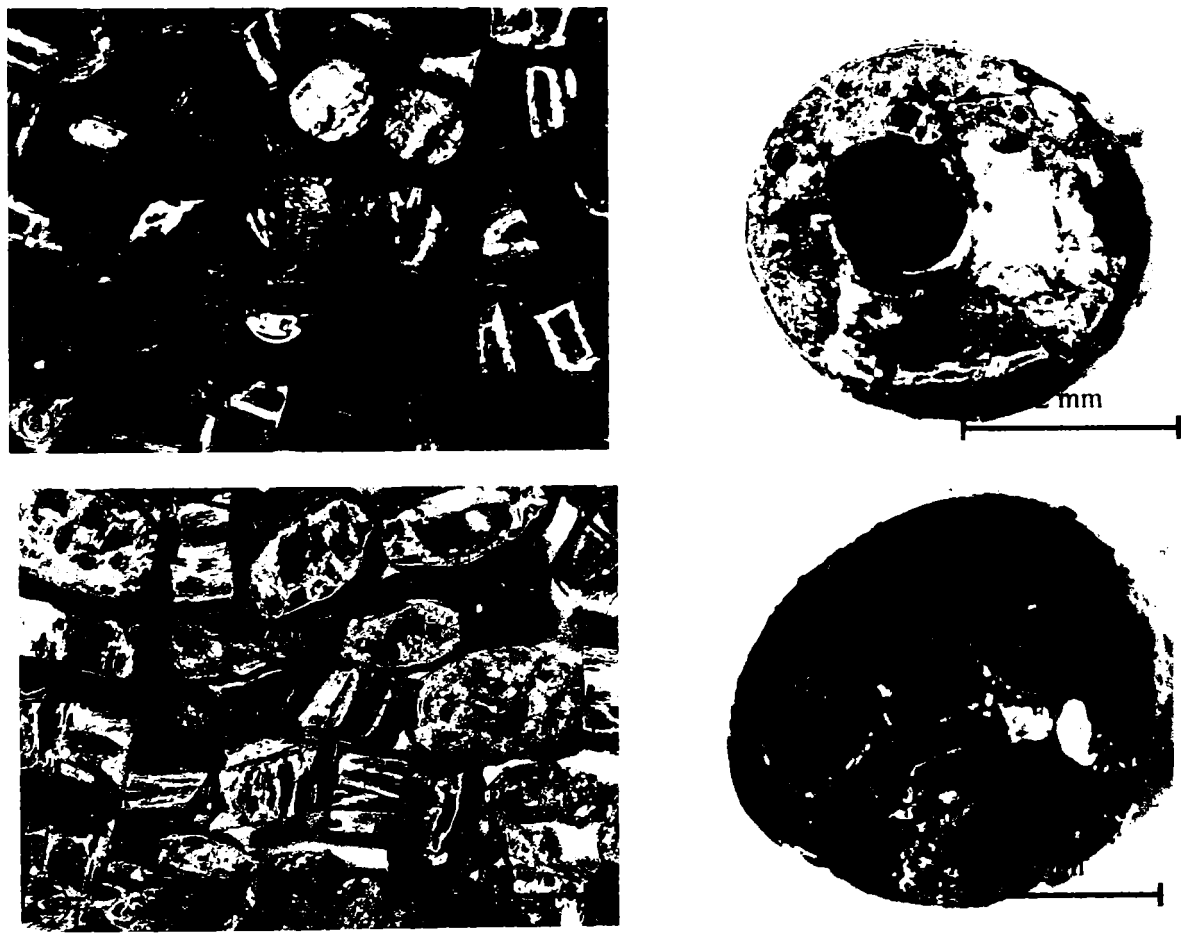

Figure 7.1 SM – micrographs of the PP composites containing 5 wt.% untreated GANF fibres as a function of extrusion parameters, (a) screw rotation 150 min^{-1} and RD = 15 %; (b) screw rotation 200 min^{-1} and RD = 20 %.

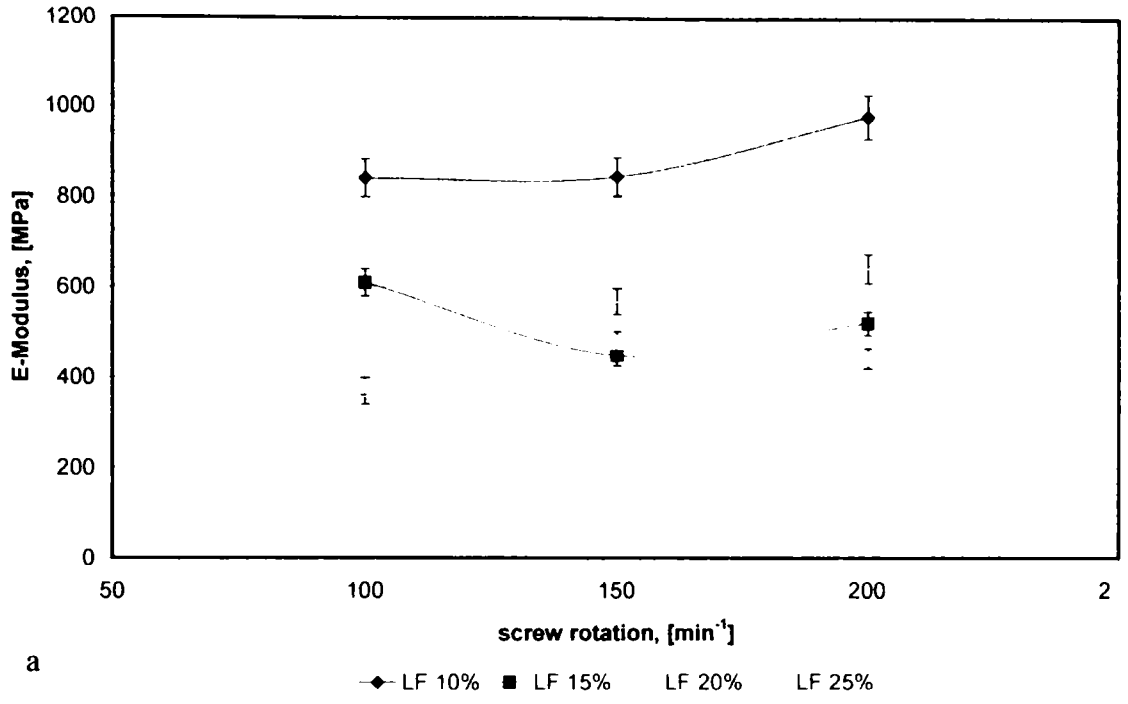

a

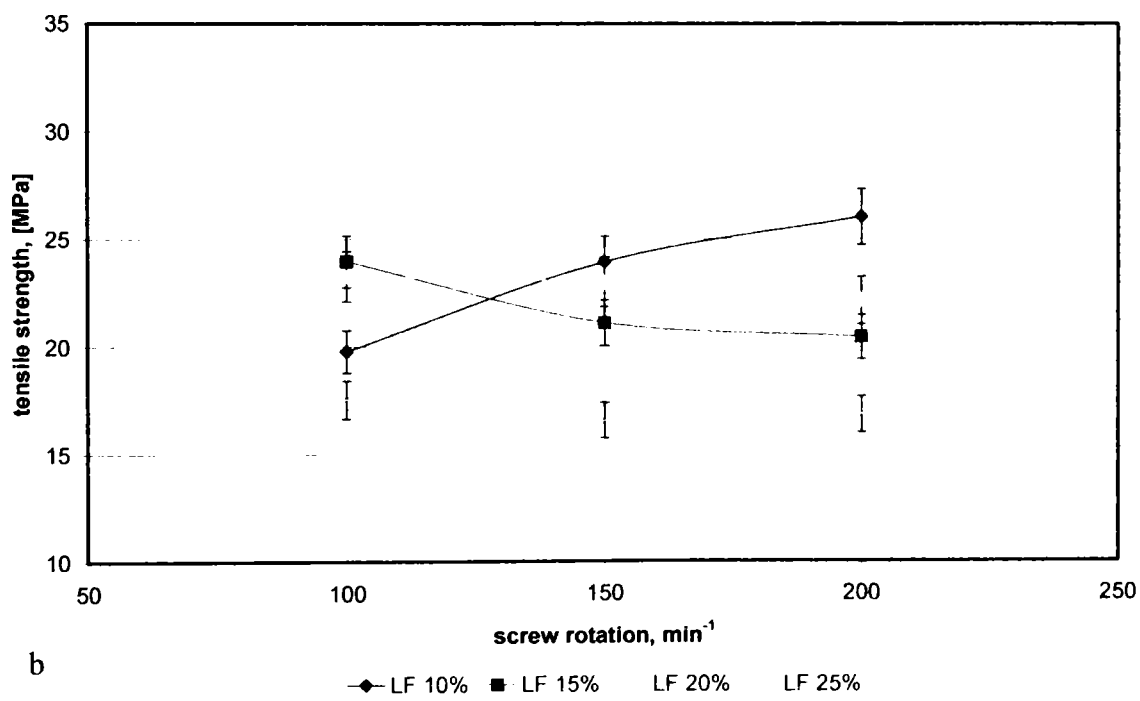

b

Figure 7.2 Tensile properties of the PP composite containing 5wt% fibres as a function of extrusion process; (a) E-Modulus and (b) tensile strength.

Table 7.2 presents the polypropylene composites containing untreated and oxygen plasma treated vapour grown carbon nanofibres which were manufactured by extrusion and injection moulding.

Table 7.2 Polypropylene composite containing vapour grown carbon nanofibres.

PP	VGCNFs	Content	Status	Parameters
PP1	*Pyrograf*	5wt.%	untreated	as – grown
PP1	*Pyrograf*	7.5wt.%	untreated	as – grown
PP1	*Pyrograf*	10wt.%	untreated	as – grown
PP1	*Pyrograf*	5wt.%	plasma treated	HF – generator, 120 W; 7.5 min; 100 sccm O_2; 1 mbar
PP2	*Semana*	5wt.%	untreated	as – grown
PP2	*Semana*	10wt.%	untreated	as – grown
PP2	*Semana*	5wt.%	plasma treated	MW – generator; 80 W; 5 min; 80 sccm O_2; 0.4 mbar
PP2	*GANF*	5wt.%	untreated	stripped and debulked
PP2	*GANF*	5wt.%	plasma treated	HF – generator; 100 W; 2.5 min; 100 sccm O_2; 1 mbar

In order to determine the content of VGCNFs in the composite, the samples were submitted to thermogravimetrical measurements. The composite was heated up to 600°C in an inert atmosphere (nitrogen). The polypropylene at this temperature is decomposed while the fibres are not affected, because carbon fibres have a thermal stability up to 3000°C in an inert atmosphere. The values obtained from TG measurements are presented in Table 7.3. The weight concentration of the fibres in the granular polymer composite was up to 1wt.%, because the granules have a large diameter and is heavy in comparison with the nanofibres. The composites having powder PP as matrix, a good precisely weight percent in the sample was obtained.

Table 7.3 Weight percent of VGCNFs in polymer composites.

Sample	**wt.% VGCNFs**	
	theoretical	**Real**
PP granular + 5wt.% Pyrograf	5	4.21
PP granular + 10wt.% Pyrograf	10	9.06
PP powder + 5wt%. Semana	5	4.92
PP powder + 10wt%. Semana	10	9.86

To manufacture the composite (5 kg) with 5 wt.% nanofibres are necessary 250 grams fibres. In order to treat this quantity of fibres, one should treat 250 charges of fibres (1g/charge). The optimisation of fibres quantity in one charge was done in order to obtain the same functionalisation degree of the fibres. The maximum quantity of fibres treated in one charge was up to 10 grams.

7.3 Injection Moulding

The samples for mechanical tests (tensile and impact measurements) were manufactured by injection moulding of the composite pellets. The principle of injection moulding process was discussed in Chapter IV, section 4.6.

The composites were injected at the SABIC Company. The injection moulding machine used was from Klöckner Ferromatik Desma, model Klöckner FM 110. The technical data of the injection moulding machine are presented in Table 7.4.

Table 7.4 Klöckner FM 110 – technical data.

	Component	Value	Units
injection unit (single screw extruder)	screw diameter	45	mm
	screw rotation	300	min^{-1}
	injection pressure	2400	bar
	shot volume	150	ccm
	clamping force	110	kN

In Table 7.5 are presented the injection moulding parameters used for the production of the tensile and Charpy samples.

Table 7.5 Injection moulding parameters.

Parameter	Values	Units
Mass temperature	265 ± 5	°C
Mould cavity temperature	30 ± 5	°C
Pressure p_2	60 - 70	bar
Pressure p_3	50 - 60	bar

The shape of the samples for tensile test measurements was chosen according to DIN EN 20179 (Figure 7.3) and the mould unit was a two cavity mould, Figure 7.4.

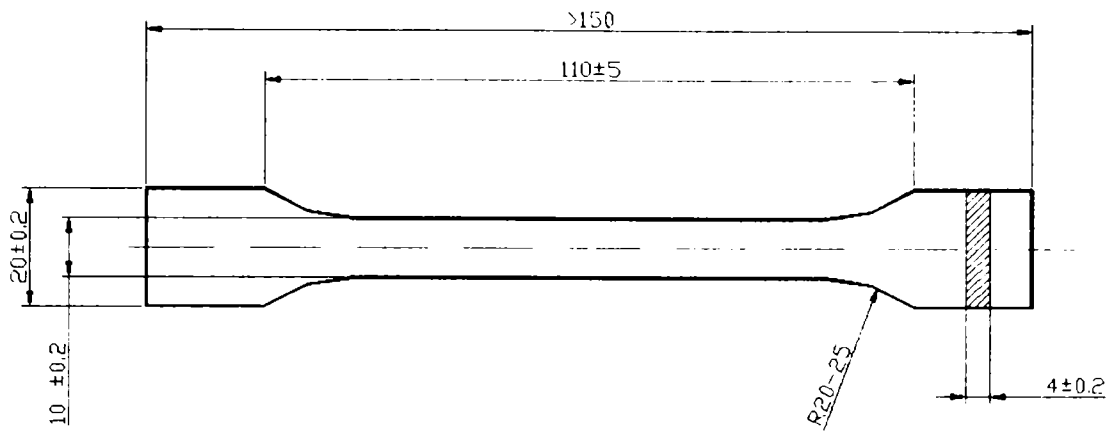

Figure 7.3 The type and dimensions of the tensile samples.

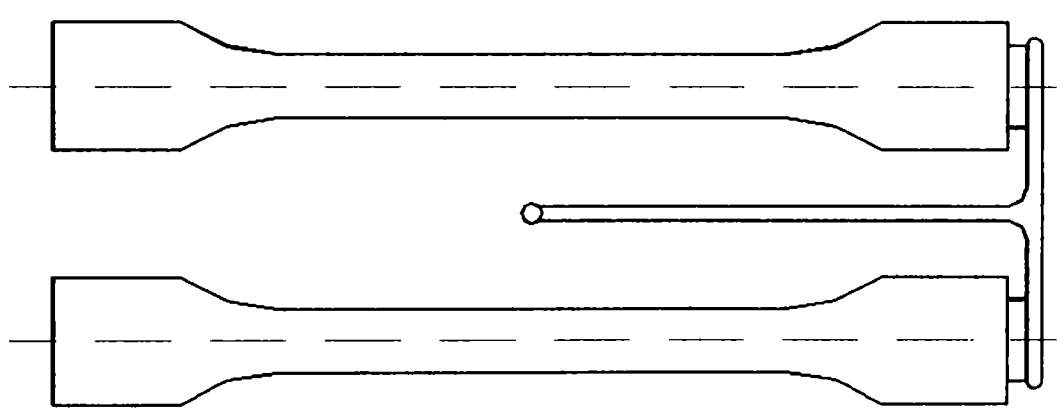

Figure 7.4 Two tensile samples injected in one cycle.

The Charpy specimens used for impact measurements have the geometry according to ISO 179:1993(E), Figure 7.5a. The number of samples injected in one injection cycle in the unit mould was four, Figure 7.5b.

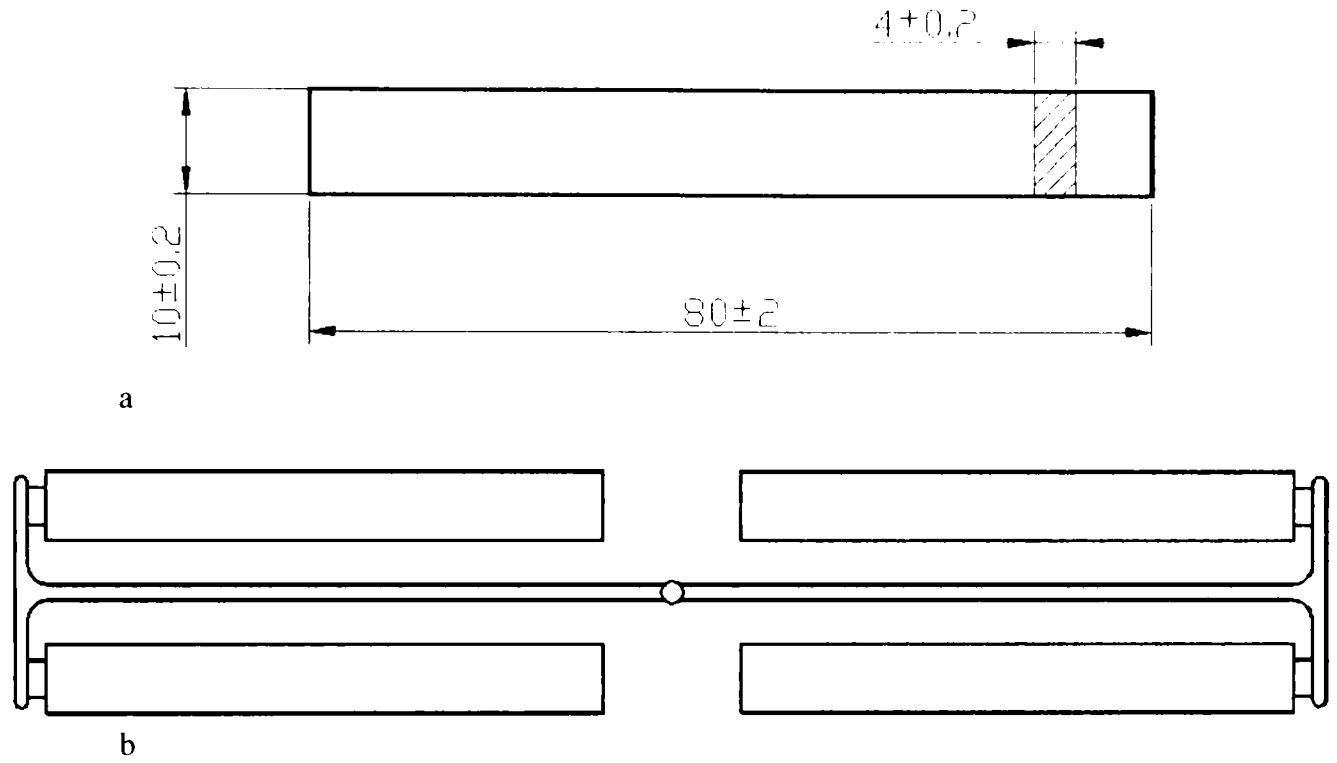

Figure 7.5 (a) The type and dimensions of the Charpy samples; (b) Four Charpy samples injected in one cycle.

7.4 Morphology of the Composites

The first manufactured composite has as reinforcement untreated Pyrograf carbon nanofibres. The morphology in the cross section (fracture of the dog-bone samples under liquid nitrogen, -196°C) of the extrudated and injection-moulded PP composites with 5; 7.5 and 10 wt.% nanofibres was studied by SEM. The presence of fibres pull out proves a weak adhesion between PP and as-grown fibres, Figure 7.6. The orientation and dispersion of the fibres in matrix can be also observed. The fibres are in some places agglomerated (Figure 7.6a) but in generally are well dispersed in polypropylene matrix.

A better adhesion was observed in the cross section SEM-micrograph of the polypropylene composite containing 5 wt.% plasma treated Pyrograf fibres, Figure 7.7. It can be observed how the polymer matrix covers the fibres (see arrows). Comparing the composite containing 5 wt.% untreated fibres (Figure 7.6a) with the composite containing 5 wt.% plasma treated fibres (Figure 7.7) can be easily observed how the pull out effect of the fibres was strongly reduced in the case of composite containing treated fibres.

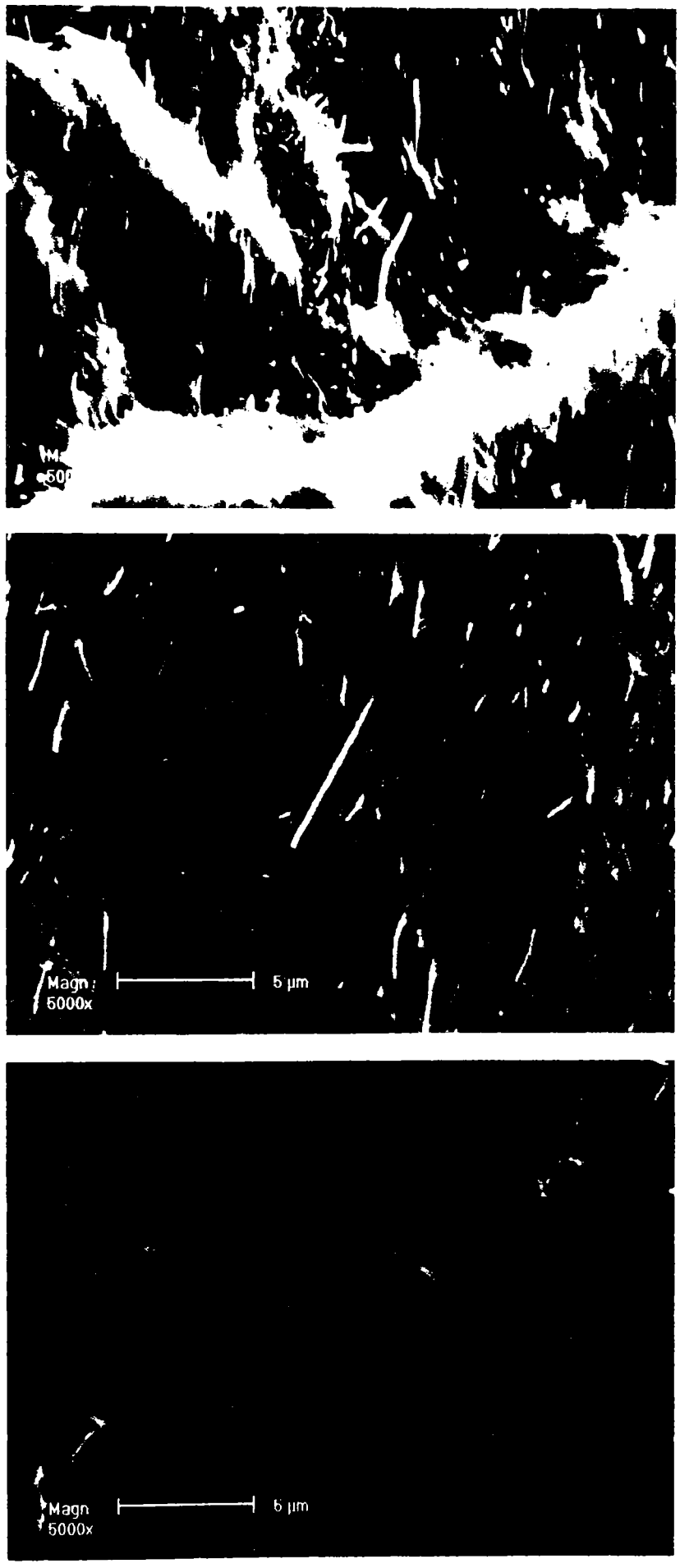

Figure 7.6 SEM – micrographs of the PP composites containing untreated fibres: a. 5 wt.% fibres; b. 7.5 wt.% and c. 10 wt.%.

Figure 7.7 SEM – Micrographs of the PP composite containing 5 wt.% plasma treated.

Therefore the effect of the oxygen plasma treatment of the fibres is an adequate process in order to improve the adhesion (interface) between PP and VGCNFs. The chemical acidic groups formed on the surface of carbon nanofibres during the plasma treatment are able to produce strong chemical bonds at the interface VGCNFs/PP. Figure 7.8 shows schematically the fundamental interaction mechanism between PP chains and treated VGCNFs. The polypropylene chain is very stable but due to the mechanical shearing during the extrusion process it could break and form active points which will bond with the most reactive groups present on the fibre surface (generally the carboxylic groups).

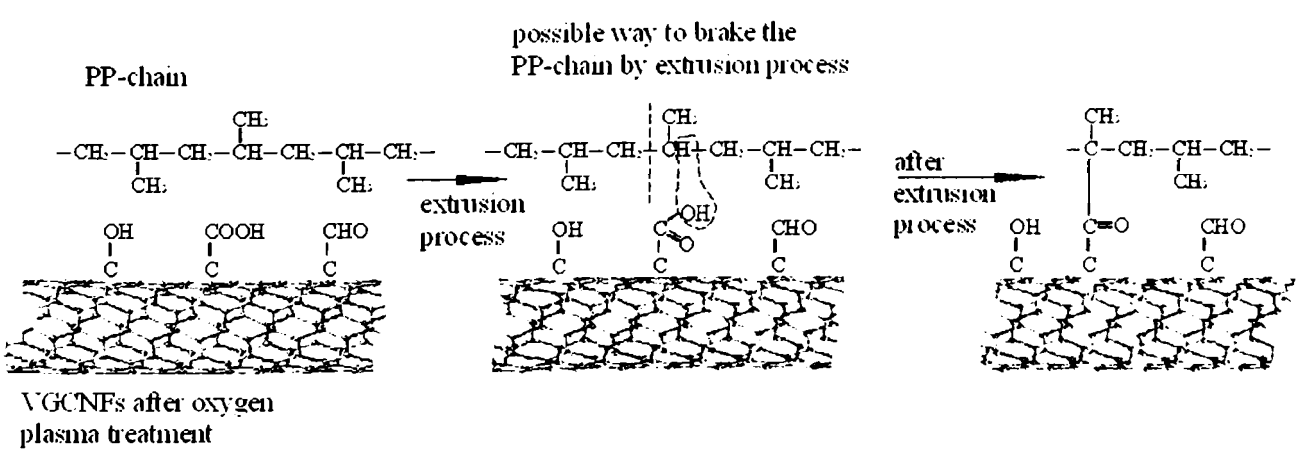

Figure 7.8 Possible interactions between PP-chain and functionalised VGCFs.

The SEM – micrographs of the composites containing untreated and plasma treated Semana fibres shows the same results, a weak adhesion in the case of untreated fibres and a good adhesion of the treated fibres to the PP (Annex 10). The composites containing untreated

GANF fibres present a better adhesion than composites containing Pyrograf and Semana fibres, because these fibres have already a water contact angle of 66° and a value of surface energy of 40 mN/m (γ_p = 29.5 mN/m), Figure 7.9. The PP containing oxygen plasma treated fibres shows also a very good adhesion.

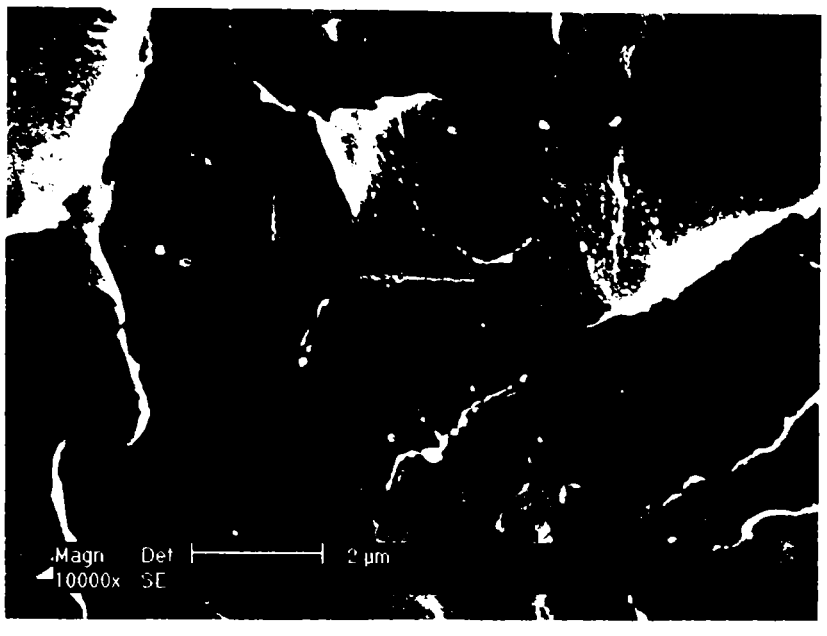

Figure 7.9 Fracture cross section SEM micrographs of the composites containing 5wt.% untreated GANF fibres.

In order to visualise the fibres orientation and distribution in the composites, the polymeric matrix was burned-off in an oxygen plasma. Figure 7.10 shows a top-view SEM-micrographs of the injected composites containing 5 wt.% untreated and oxygen plasma treated Semana fibres. It can be seen that the fibres are oriented in the injection moulding direction showing an uniform distribution in the PP matrix, specially in the case of plasma treated fibres.

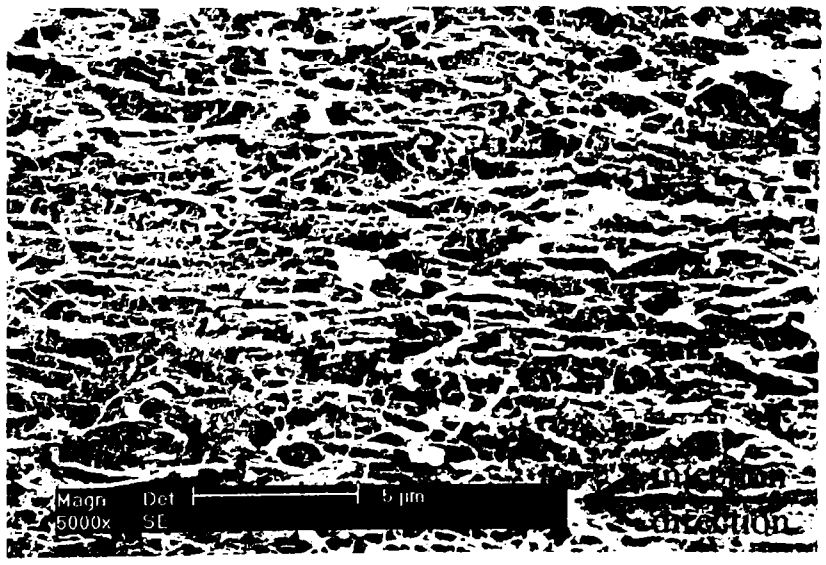

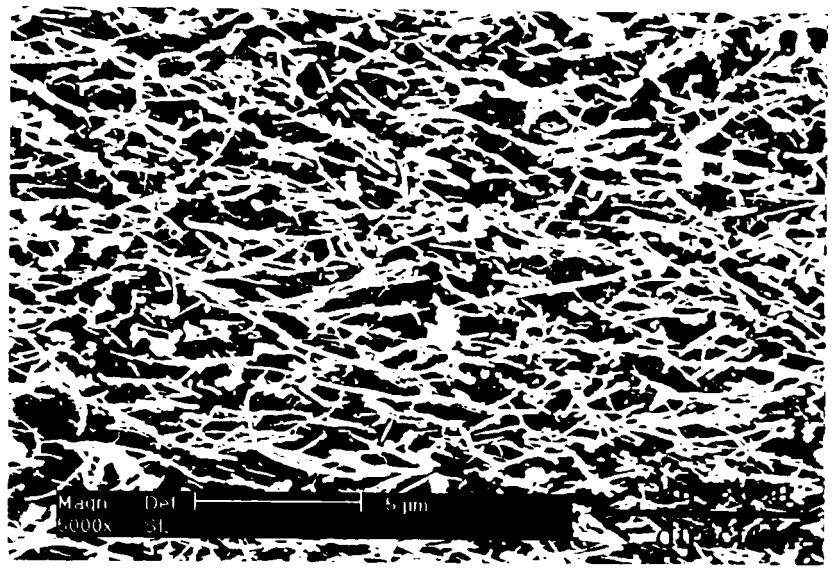

Figure 7.10 SEM micrographs of the composites containing 5wt.% untreated (a) and plasma treated vapour grown carbon nanofibres (b).

7.5 Mechanical Properties of the Polypropylene Composites Containing Vapour Grown Carbon Nanofibres

The PP composites containing different weight percent of untreated and oxygen plasma treated VGCNFs were tested by tensile and impact measurements.

7.5.1 Tensile Strength Measurements

Among the many mechanical properties of composite materials, tensile properties are probably the most frequently considered, evaluated, and used throughout the industry.

The tensile tests were performed using a tensile strength machine from Instron, model 5584 and Zwick, model 1120. The measurements for tensile strength were made according to EN ISO 527 – 1 : 1996 with the following parameters (Figure 7.11) [158]:

- previous force 5N;
- traction speed for previous force 1 mm/min;
- traction speed for E-Modul 5 mm/min;
- traction speed for tensile strength 50 mm/min;
- E-Modulus 0.05-0.25 %;

- distance between grips (transverse distance), l 115 mm;
- measure distance, l_0 50 mm.

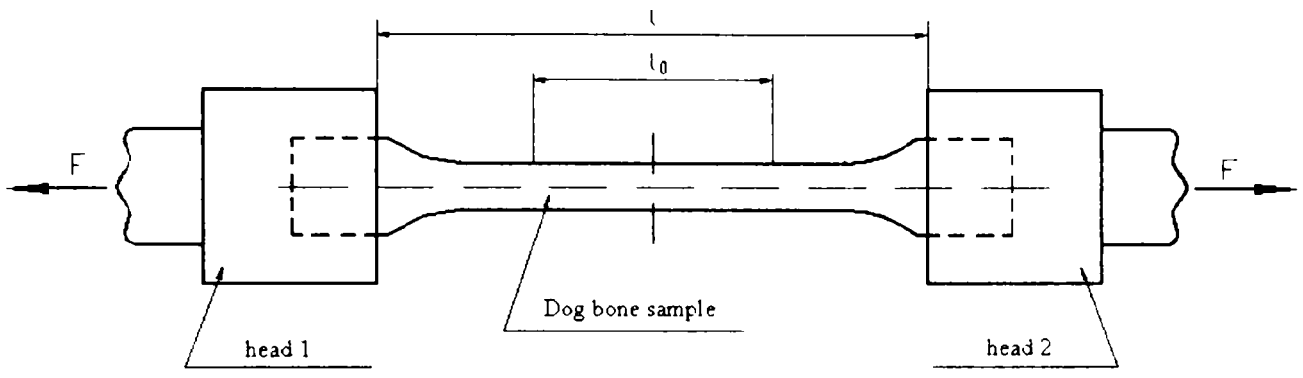

Figure 7.11 Tensile measurements.

The tensile strength was calculated with the following formula:

$$\sigma = \frac{F}{A} \text{ [MPa]} \quad (7.1)$$

where

F – force at failure, [N];

A – area of cross-section, [mm^2].

The tensile strain, ε, was calculated with the following formula

$$\varepsilon = \frac{l_1 - l_0}{l_0} \times 100[\%] \quad (7.2)$$

where:

l_0 – initial length of the specimen, [mm];

l_1 – length of the specimen at failure, [mm].

The elastic modulus was calculated using the following formula:

$$E = \frac{\sigma_2 - \sigma_1}{\varepsilon_2 - \varepsilon_1}[MPa] \quad (7.3)$$

where:

σ_1 – tensile measured in MPa at strain $\varepsilon_1 = 0.05\%$;

σ_2 – tensile measured in MPa at strain $\varepsilon_2 = 0.25\%$.

In order to reduce the errors for the measurements of tensile properties, for each series of composite were tested at least 7 samples. The highest and the lowest value of the tensile properties were also eliminated and than the average value was calculated.

The values of tensile strength of the polypropylene and polypropylene composites containing 5, 7.5 and 10 wt.% untreated Pyrograf fibres and also the composite containing oxygen plasma treated Pyrograf fibres are presented in Figure 7.12. The weak adhesion between fibres and matrix in the case of composites containing untreated fibres was proved from the values of tensile strength and can be correlated with the SEM micrographs in cross section of the composite. It can be observed that, a slight increase of the tensile strength of 2.6% for the composite containing 5wt.% untreated fibres compared with the polypropylene occurred. The composite containing 10 wt.% untreated Pyrograf fibres has the value for tensile strength of 33.6 MPa, that means an increase up to 7.4% in comparison with PP. The composite containing 5 wt.% plasma treated fibres present an increase of tensile strength up to 19% in comparison with PP and also an increase up to 15% compared with composite containing 5 even 10wt.% untreated fibres.

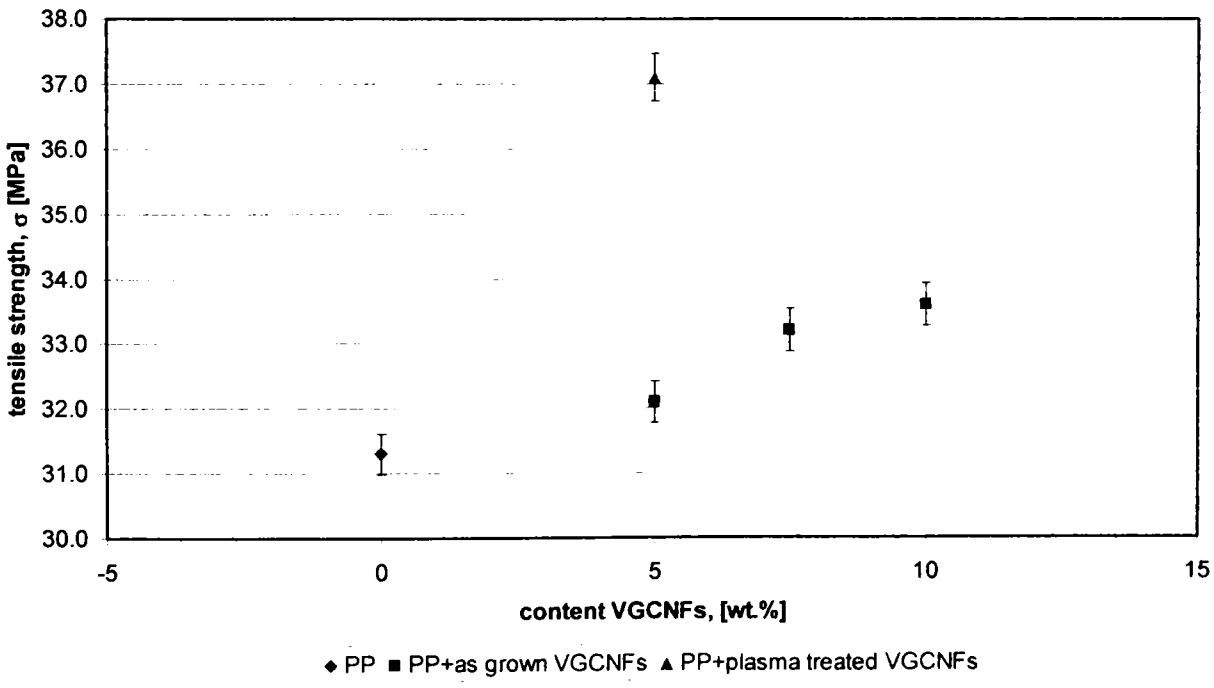

Figure 7.12 Tensile strength of PP and PP composite containing untreated and oxygen plasma treated Pyrograf fibres.

The elastic modulus of the composites containing untreated fibres shows the same tendency like the tensile strength, an increase up to 70% for the composites containing 10 wt.% untreated fibres in comparison with PP can be observed (Figure 7.13). The composites containing 5 wt.% plasma treated fibres has the elastic modulus higher than PP and PP + 5 wt.% untreated fibres but lower than the composites containing untreated 10 wt.% Pyrograf fibres.

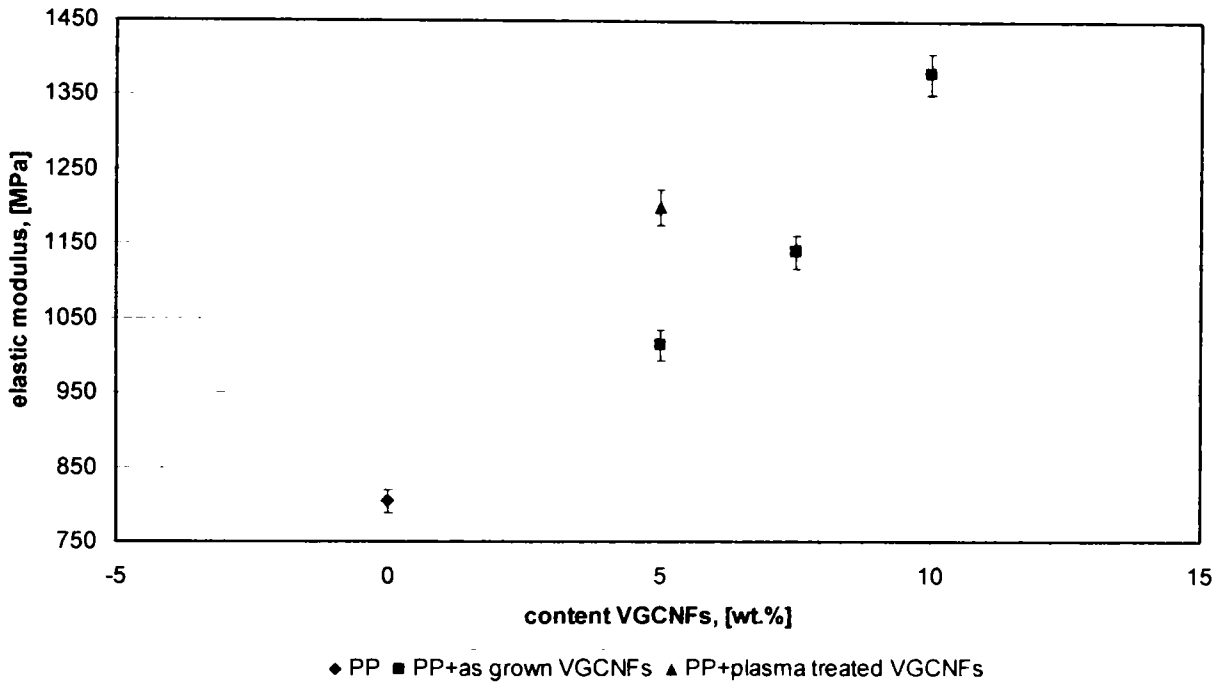

Figure 7.13 Elastic modulus of PP and PP composite containing untreated and oxygen plasma treated Pyrograf fibres.

The values of tensile strength of the polypropylene and composites containing 5 and 10 wt.% untreated and 5 wt.% treated fibres are presented in Figure 7.14. It can be seen that activation of the VGCFs surface by oxygen plasma treatment increases the tensile strength of the polymeric composite with 15% in comparison with the composite containing untreated fibres. The elastic modulus of the composite containing Semana fibres increased with the increase of the weight percent of fibres in composite, Figure 7.15. The composites containing 5 wt.% plasma treated fibres have the same E-modulus as the composites containing 5. wt.% untreated fibres. Figure 7.16 shows the stress-strain curve for polypropylene and PP composites containing 5wt.% untreated and oxygen plasma treated fibres. It can be seen that the plastic domain of the composites increased with approximate 22-25% compared with PP.

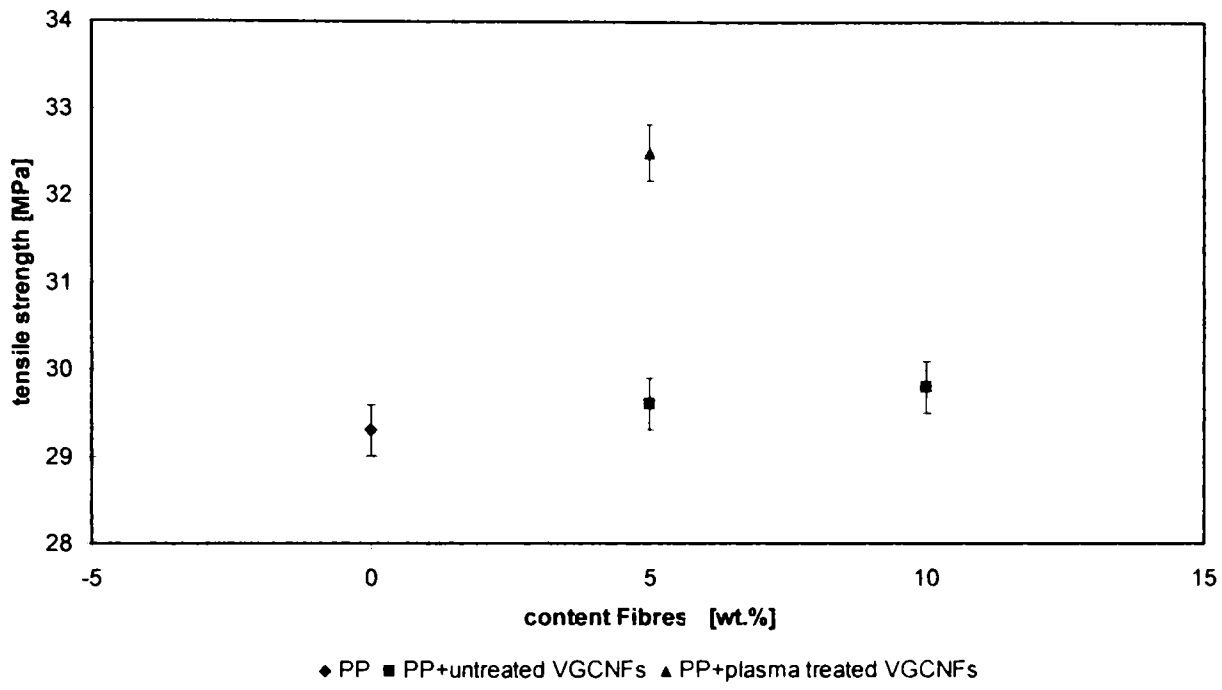

Figure 7.14 Tensile strength of PP and PP composite containing untreated and oxygen plasma treated Semana fibres.

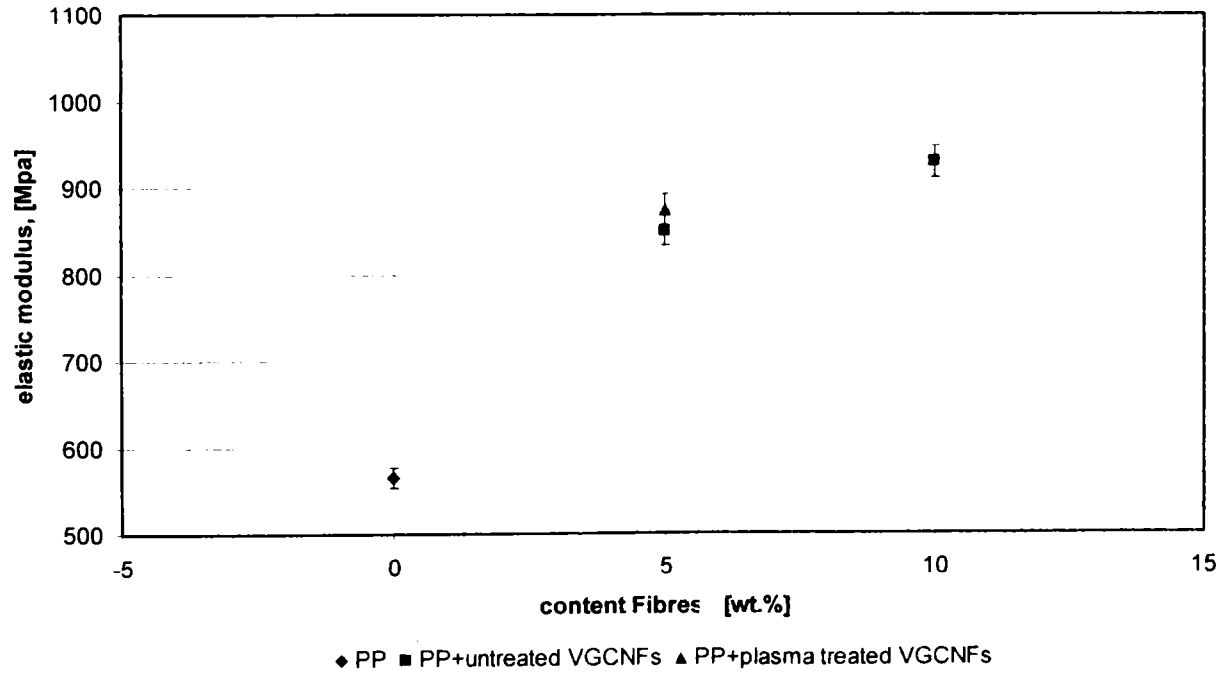

Figure 7.15 Elastic modulus of PP and PP composite containing untreated and oxygen plasma treated Semana fibres.

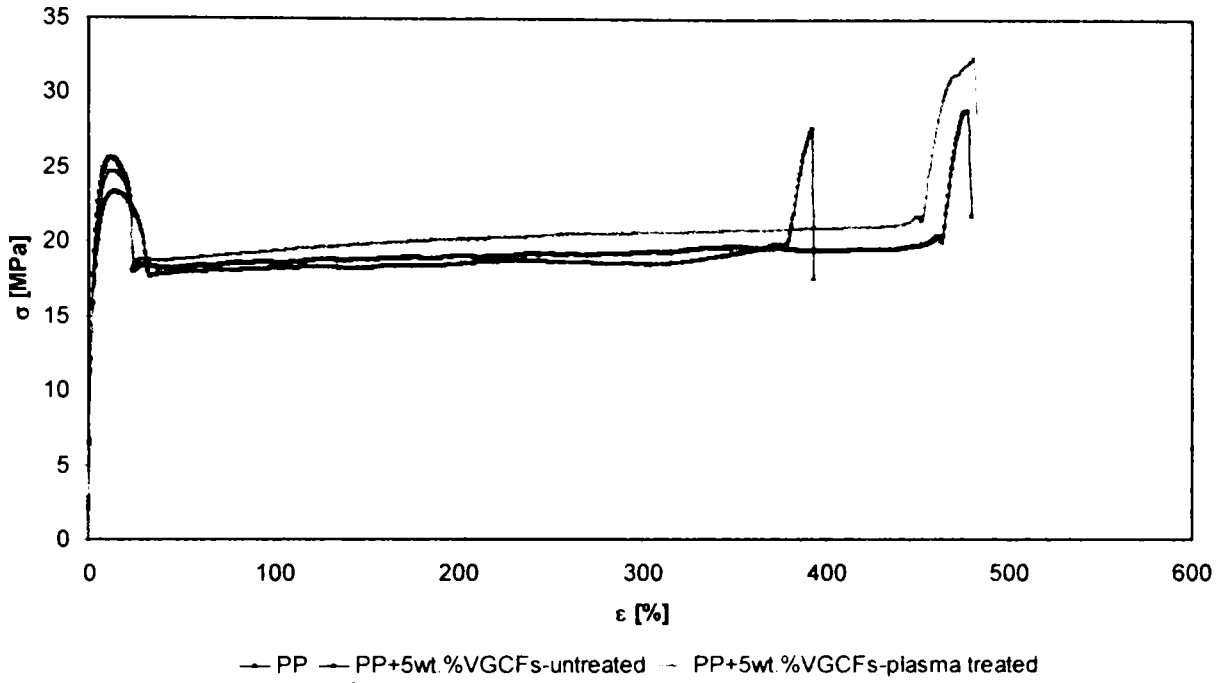

Figure 7.16 Stress-strain curves for PP and PP/VGCFs composites.

The results of the composites containing 5 wt.% untreated and oxygen plasma treated GANF fibres are presented in Figure 7.17 and 7.18. The composites containing untreated fibres have already a better tensile strength than polypropylene. The tensile strength is increased up to 18% in the case of composite containing 5 wt.% untreated fibres than PP because these fibres after debulking process have the value of surface energy of 40mN/m. The tensile strength of the composites containing 5 wt.% oxygen plasma treated fibres was also better than the composites containing 5 wt.% untreated fibres but only with 3.2%. An increase of surface energy of the fibres very high does not lead always to an increase (linear or exponential) of the tensile properties, because the interface becomes stronger than the fibres. In this case, the interface will have the lowest strain to failure behaviour. The composite will fail when any weak cracking occurs at a weak spot along the brittle interface. The elastic modulus of the composite containing plasma treated fibres was increased up to 1.4 times more than PP.

The adequacy of oxygen plasma treatment as functionalising process used in order to improve the adhesion between VGCFs and PP especially through the chemical bonding at the interface was demonstrated.

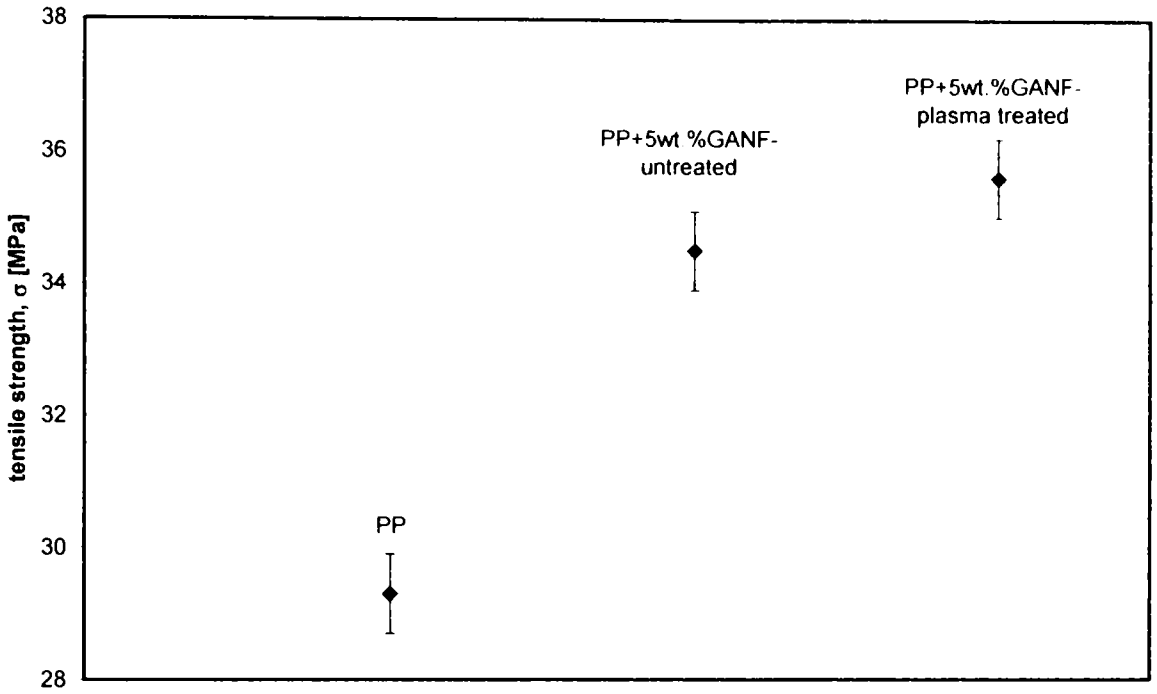

Figure 7.17 Tensile strength of PP and PP composite containing untreated and oxygen plasma treated GANF fibres.

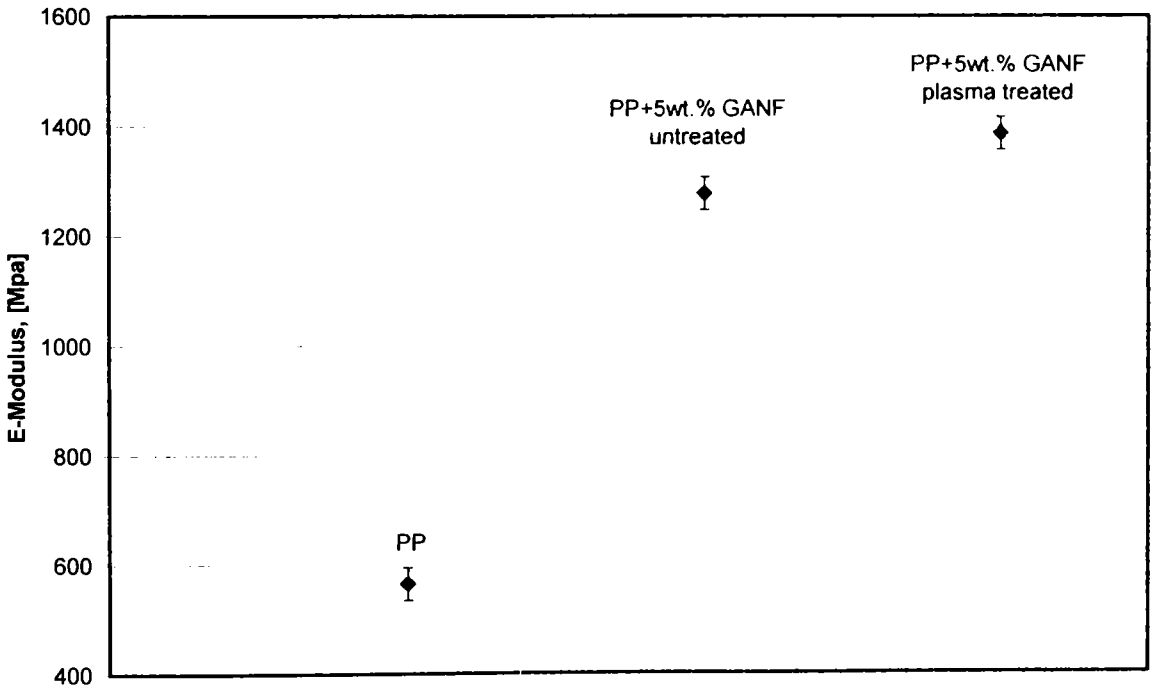

Figure 7.18 Elastic modulus of PP and PP composite containing untreated and oxygen plasma treated GANF fibres.

7.5.2 Impact Strength Measurements

Charpy impact strength of unnotched samples is defined as the impact energy absorbed in breaking an unnotched sample, referred to the original cross sectional area of the specimen. The principle of the Charpy impact strength of unnotched samples is presented in Figure 7.19. The test sample, supported as horizontal beam, is broken by a single swing of a pendulum, with the line of impact midway between the supports.

The Charpy impact strength measurements were performed using an apparatus from Zwick, model 5102. The measurements for Charpy impact were made according to ISO 179:1993 and were calculated with the following formula [159]:

$$a_{cU} = \frac{W}{b \cdot h} \times 10^3 \, KJm^{-2} \qquad (7.4)$$

where:

a_{cU} – Charpy impact strength of the unnotched samples, [kJ/m];

W – corrected energy absorbed by breakage the test sample, [J];

b – the width of test sample (10±0.2mm), [mm];

h – the height of test sample (4±0.2mm), [mm].

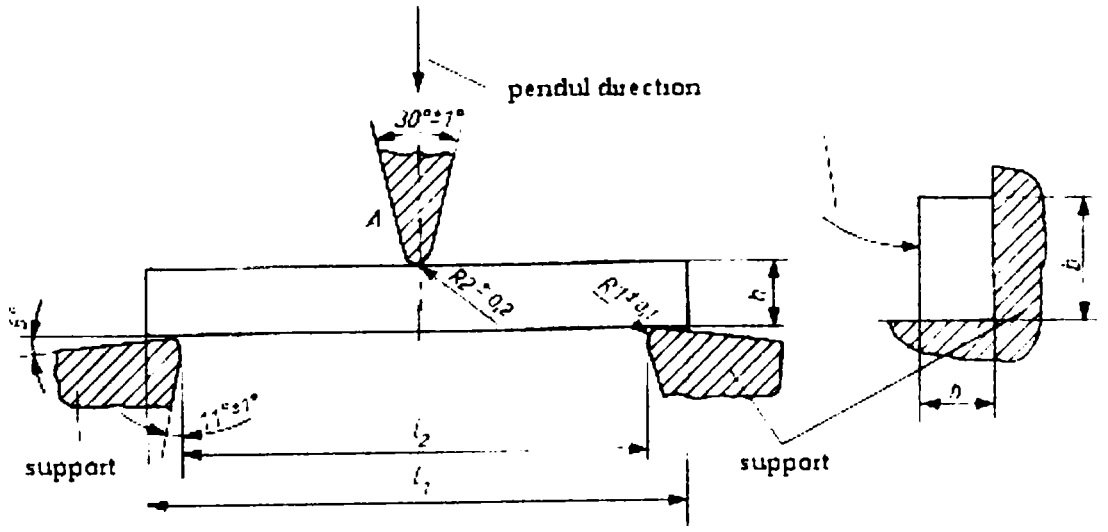

Figure 7.19 Charpy impact test.

The shape of the necessary sample for impact measurements is shown in Figure 7.5. The shape of the sample is prismatic, 80 x 10 x 4 mm. The span (distance between supports, l_2) is $62_0^{+0.5}$ mm, see Figure 7.19.

The Charpy impact tests of the polypropylene composites containing untreated and plasma treated Semana fibres were performed at two different temperatures: room temperature (22°C)

and low temperature, 0°C. The samples for impact measurements at low temperature were cooled at 0°C for 2 hours in a refrigerator from Corola and immediately were tested. The values of Charpy impact resistance of the polypropylene and polypropylene composites containing 5 and 10 wt.% untreated Semana fibres and also the composite containing 5 wt.% oxygen plasma treated Semana fibres are presented in Figure 7.20. The composites containing 5 wt.% untreated fibres have the impact strength at room temperature only with 3% better than polypropylene, Figure 2.20a. The composites containing 10 wt.% untreated Semana fibres show an increase of impact at room temperature strength up to 16.5% in respect of polypropylene. The composites containing plasma treated fibres have the highest impact strength at room temperature. The Charpy impact strength was increased up to 19% compared with PP and was better with 15.5% than composite containing the same quantity of untreated fibres. All these samples which were tested are not broken during the experiments. It can be concluded that the composites containing untreated fibres become tougher at room temperature with the increase of content of VGCNFs than PP. At low temperature (T = 0°C) the composites containing untreated fibres become brittle with the increase of the fibres content, but the Charpy impact strength was better in comparison with polypropylene (Figure 7.20b). The composites containing oxygen plasma treated fibres have the highest Charpy impact strength at low temperature.

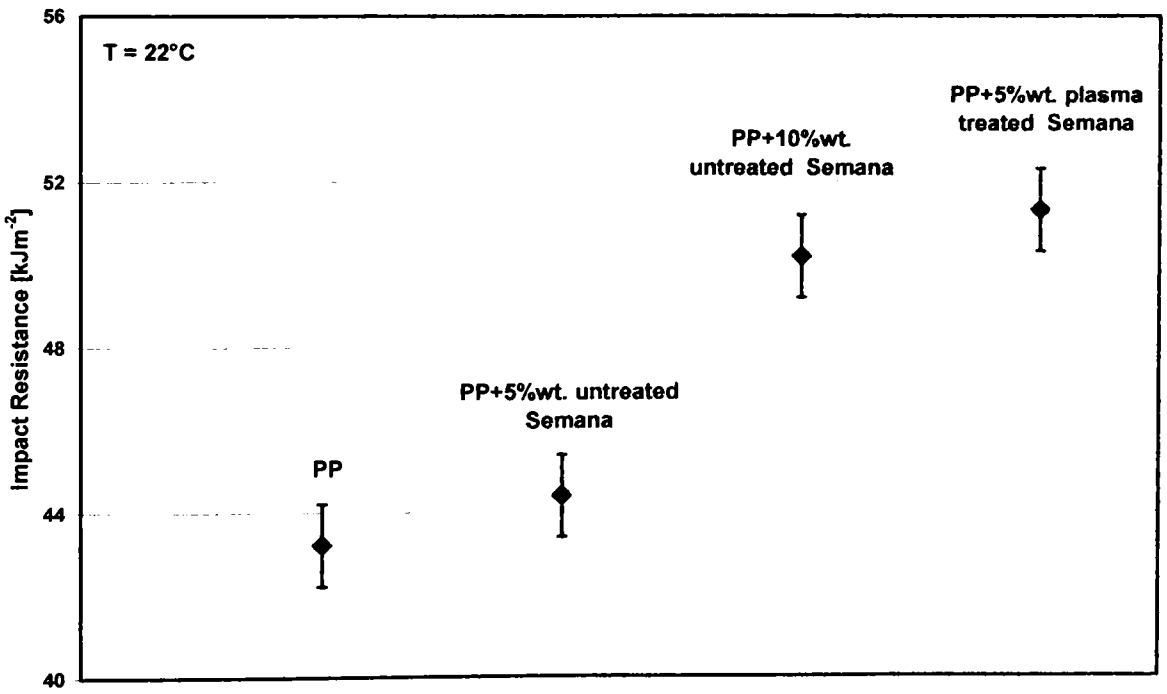

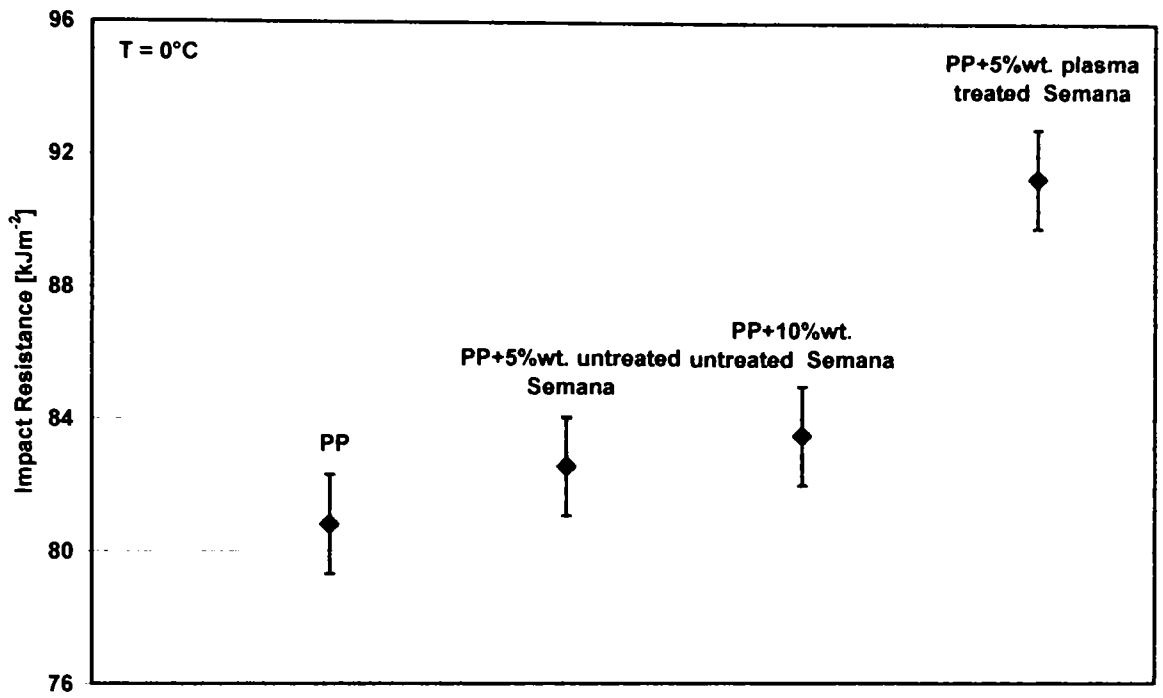

Figure 7.20 The values of Charpy impact strength at room temperature, T = 22 °C (a) and low temperature, T = 0°C (b) of the PP and composites containing untreated and plasma treated fibres.

The Charpy impact measurements of the composites containing untreated and oxygen plasma treated GANF fibres were performed at three different temperatures, room temperature (22°C), low temperature (0°C) and very low temperature. The desired very low temperature was -40°C because at this temperature the polypropylene is in the brittle solid region (glassy region). The PP has the T_g = -18°C (theoretic), below this temperature the PP is brittle solid and above T_g the isotactic PP is rubbery – crystalline. The laboratory refrigerator used can refrigerate theoretic up to -40°C, but unfortunately the minimum temperature obtained was -22 – -25°C.

The results of the Charpy impact strength measurements are presented in Figure 7.21. The impact strength at room temperature of the composites containing 5 wt.% plasma treated fibres is equal with the composites containing 5 wt.% untreated fibre and both are better than polypropylene with 64% (see Figure 7.21a). In the case of measurements at low and very low temperature, the composites containing untreated and plasma treated fibres were brittle than polypropylene. The PP was still ductile at these temperatures. Therefore, the Charpy impact strength of the composite containing untreated fibres decreased up to 85% in comparison with the PP. A possible explanation of this lower value of the Charpy impact strength is that the fibres lead to an increase of the glass transition temperature of polypropylene, therefore the

composites were in brittle solid domain. Further investigation of the glass transition temperature of composite are required in order to sustain the upper explanation.

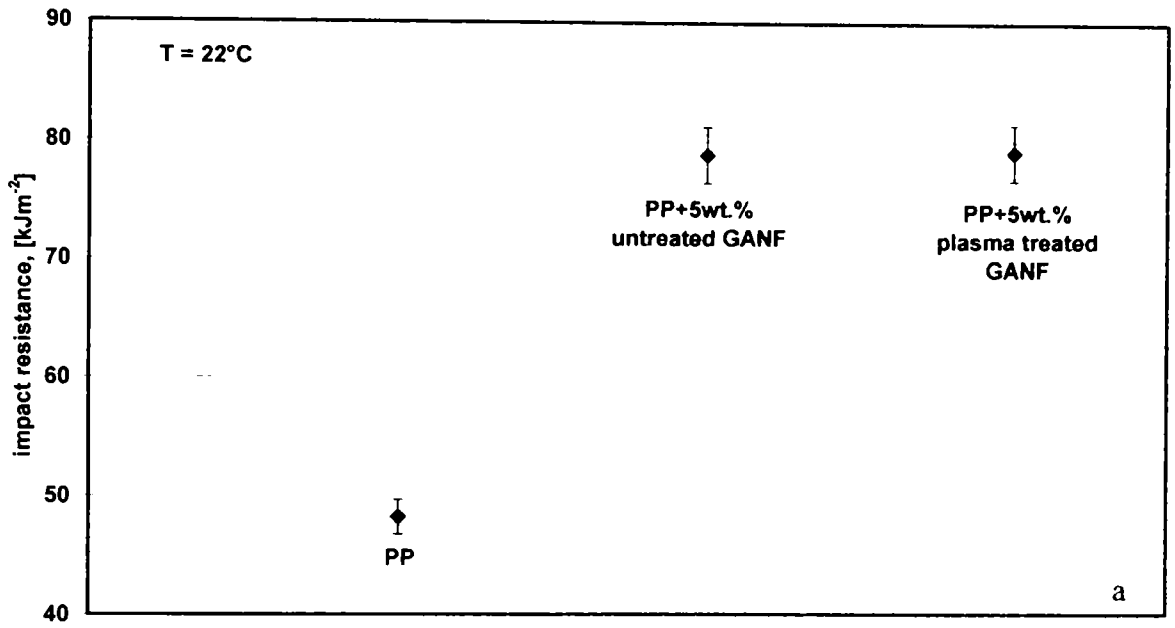

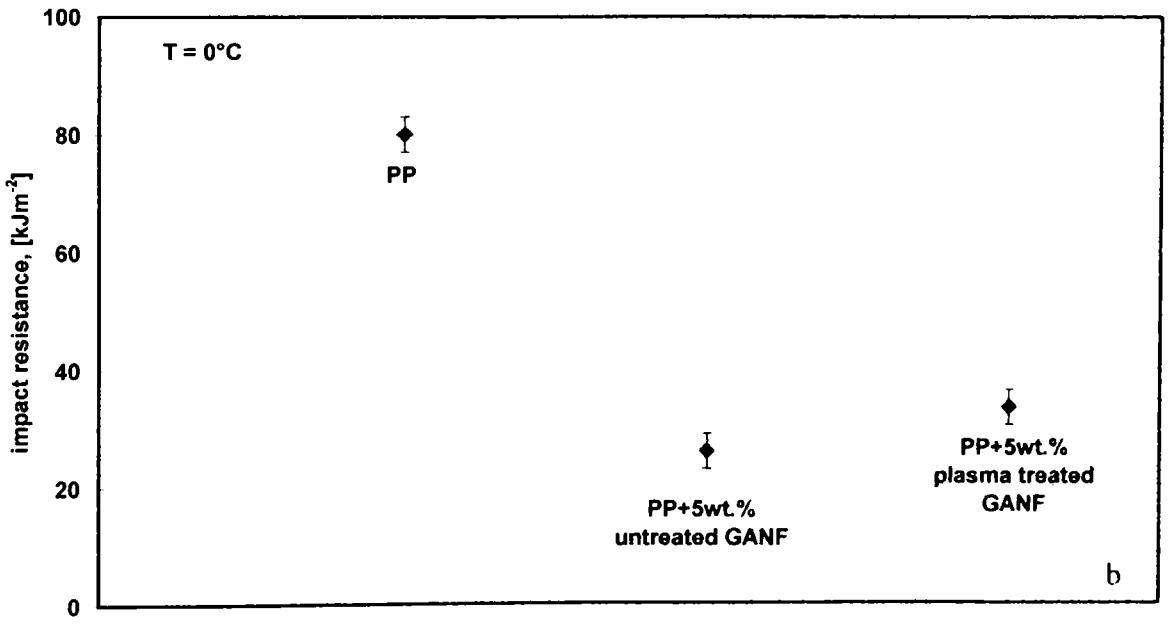

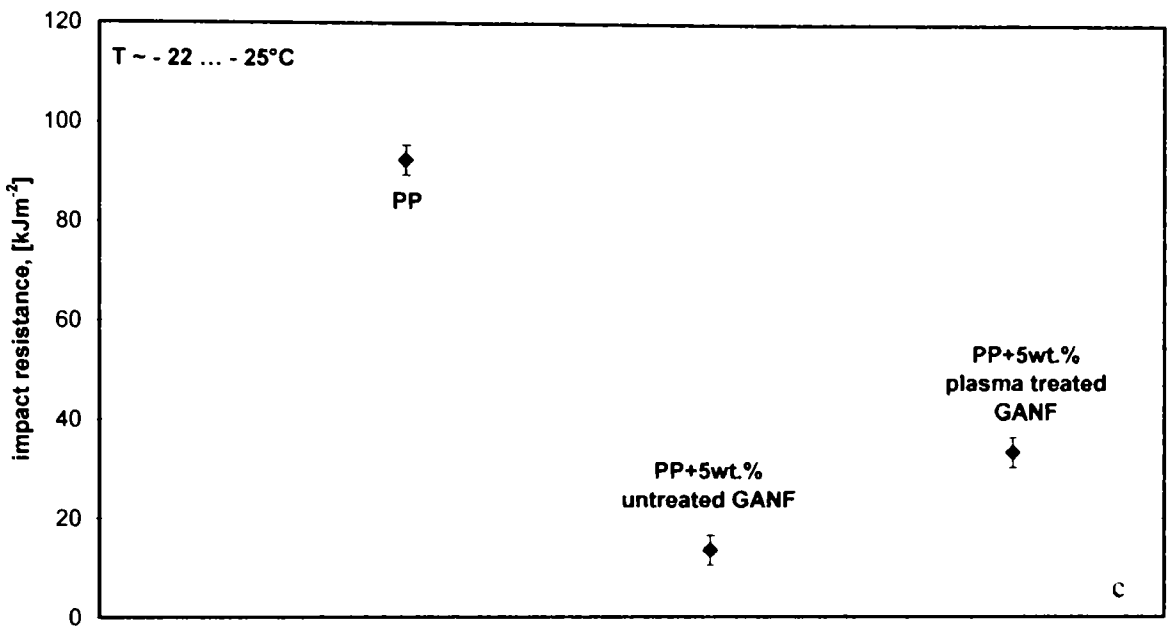

Figure 7.21 The values of Charpy impact strength at room temperature, T = 22 °C (a), low temperature, T = 0°C (b) and very low temperature (c) of the PP and composites containing untreated and plasma treated fibres.

7.6 Thermal Properties of the Polypropylene Composites Containing Vapour Grown Carbon Nanofibres

7.6.1 Thermal Conductivity

Thermal conductivity is defined as the mechanism of energy transfer from a warm portion of solid body to its cooler portion. Thermal conductivity is the quantity of heat, Q, transmitted through a thickness L, in a direction normal to a surface of area A, due to a temperature difference ΔT, under steady state conditions and when the heat transfer is dependent only on the temperature gradient (see formula 7.5).

$$\lambda = \frac{Q \times L}{A \times \Delta T} \left[\frac{W}{mk}\right] \quad (7.5)$$

The thermal conductivity measurements were performed using a heat conductivity apparatus from NETZSCH, model TCT 416. The measurement principle of TCT 416 is presented in Figure 7.22 [160]. Previously to measure the thermal conductivity the heat conductivity

apparatus was calibrated using Stainless Steel - AISI 304 (Fe/Cr18/Ni10) in order to determine a device constant. The sample was fixed between cooper plate and a force of 25N was applied in order to measure the thermal conductivity of the composites. The temperature of heating block was 60°C and the temperature of the second thermostat was 25°C (environment temperature).

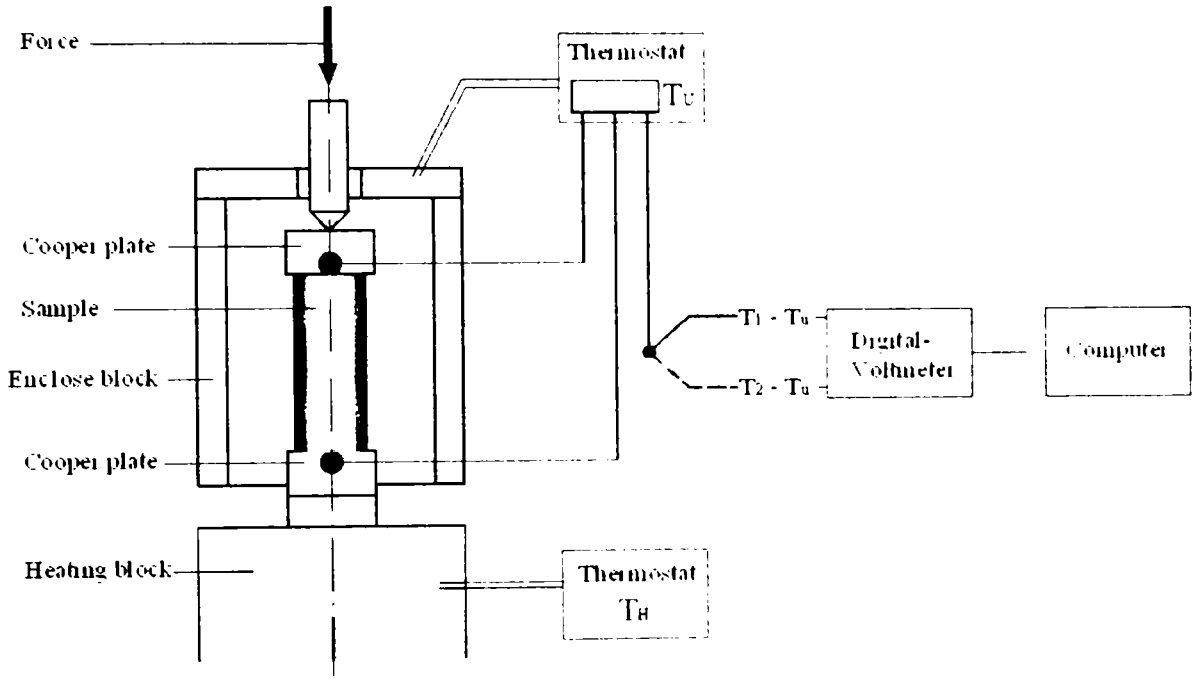

Figure 7.22 Measurement principles of the TCT 416 apparatus [160].

The necessary samples for thermal conductivity measurement were cut in prismatic shape (4 × 5 × 20 mm) from dog bone samples (tensile samples) using a minitom from Struers, Figure 7.23a. The samples were cut in two directions in respect of "dog bone" samples, see Figure 7.23b.

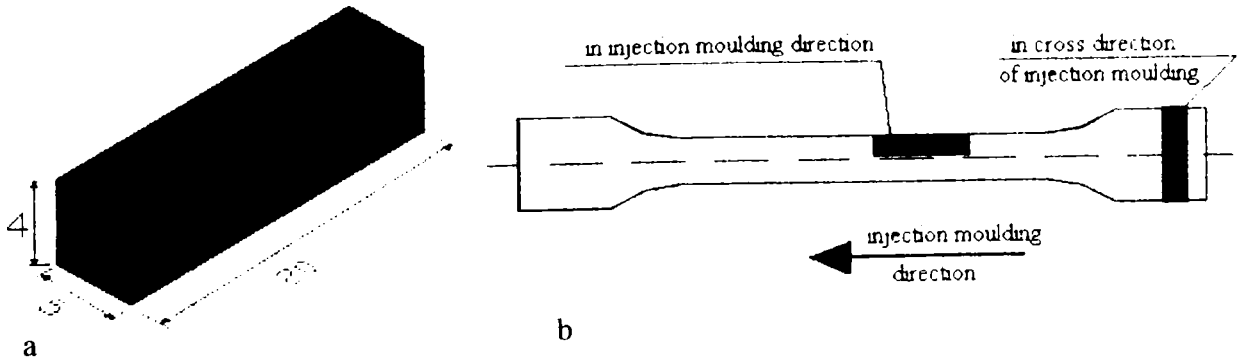

Figure 7.23 Dimension and shape of the sample for thermal conductivity measurements (a) and (b) cutting direction of the sample in respect of tensile sample (injection moulding direction).

The results of thermal conductivity of the composites containing Pyrograf and Semana fibres show that the values of thermal conductivity increased with the increase of VGCNFs contents in composite. The composites containing 10 wt.% untreated Pyrograf fibres cut in the cross direction of injection moulding shows an increase of the thermal conductivity up to 15% in comparison with the PP and an increase up to 10% compared with the PP composites containing 5 wt.% untreated Pyrograf fibres, Figure 7.24. The measurements of the composites cut parallel with the injection moulding direction reveal an increase of thermal conductivity in comparison with the composites cut in the cross direction of injection moulding. For example, the composites containing 10 wt.% untreated fibres and cut parallel with the injection moulding direction have the thermal conductivity better with 27.3% (±5%) than the same sample which was cut normal to the injection moulding direction. Between the composites containing 5 wt.% untreated and plasma treated weren't significant differences, Figure 7.25. For example in cross section the composites containing 5 wt.% plasma treated fibres have the value of thermal conductivity of 24.7 $Wm^{-1}K^{-1}$ and the composites containing 5 wt.% untreated fibres have 25 $Wm^{-1}K^{-1}$. A slight decrease of thermal conductivity of the composite containing oxygen plasma treated fibres is normally because the fibres are well aligned and uniform distributed in the matrix than in the case of the composites containing untreated fibres. In this way the fibres doesn't make a network (they form no bounds, connections).

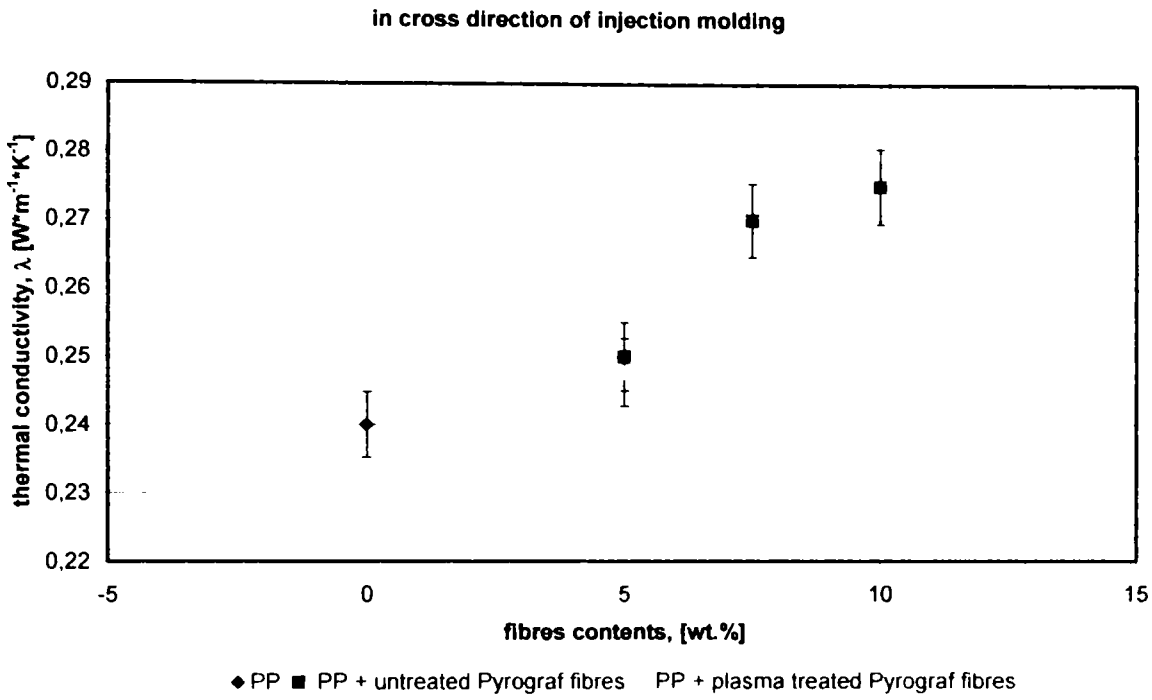

Figure 7.24 Thermal conductivity of the PP and PP composite containing untreated and plasma treated Pyrograf fibres measured in cross section.

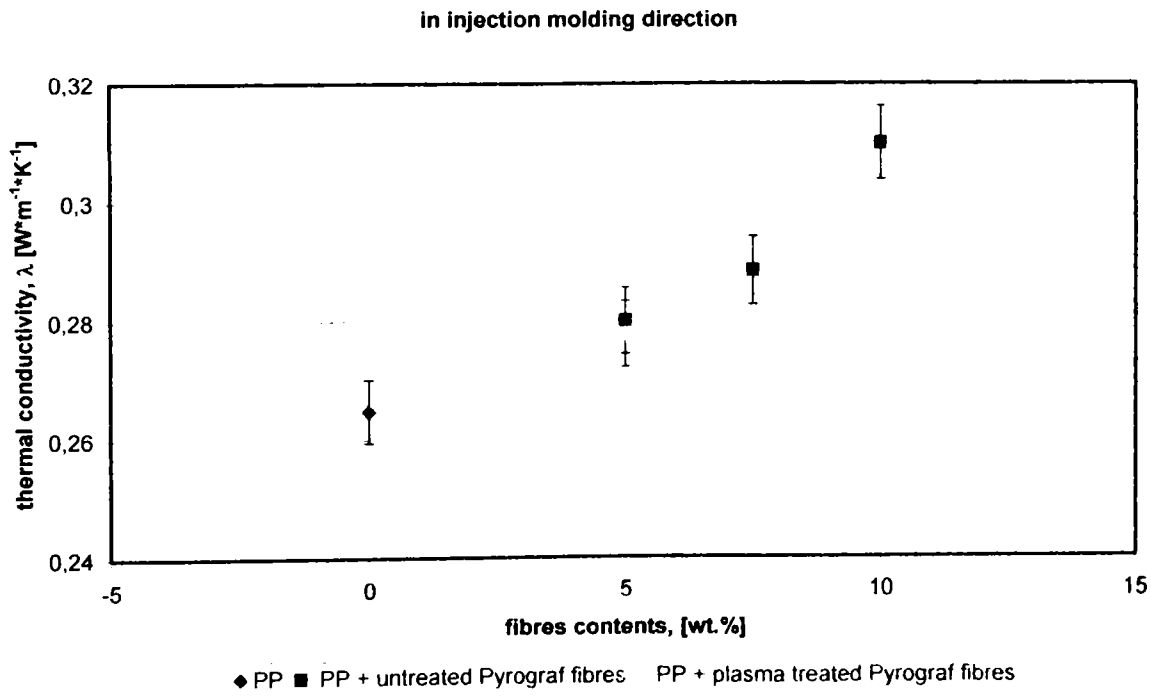

Figure 7.25 Thermal conductivity of the PP and PP composite containing untreated and plasma treated Pyrograf fibres measured in parallel with the injection moulding direction.

The same remarks are available also for the composites containing Semana fibres, see Figure 7.26.

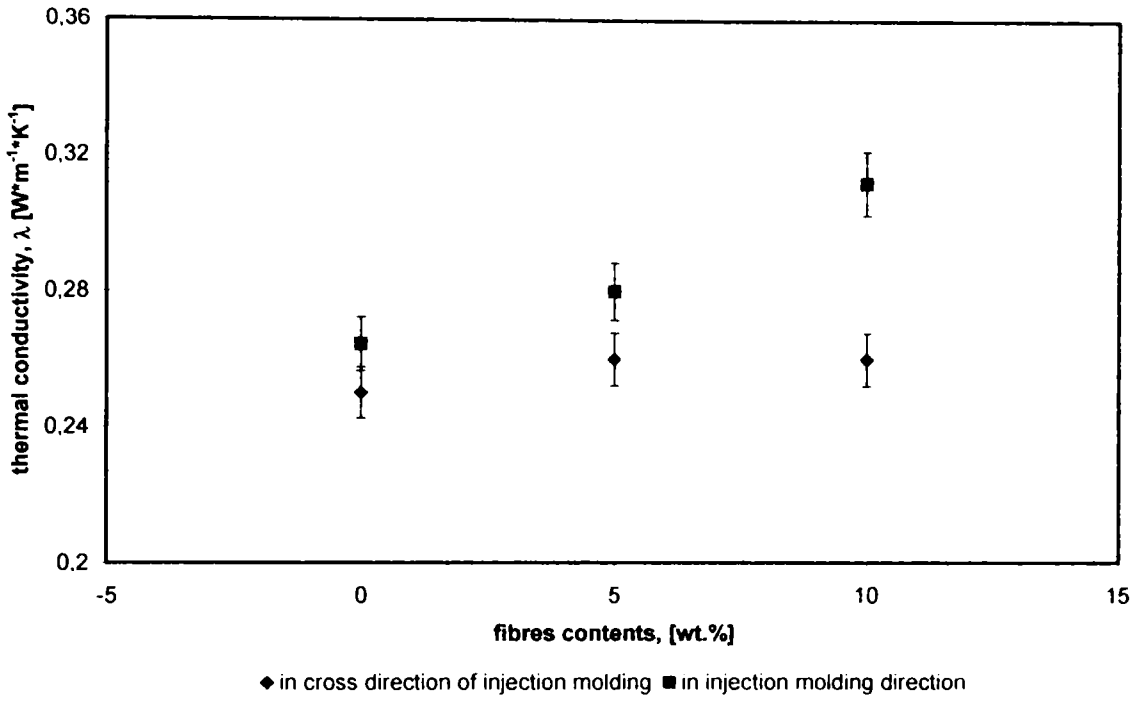

Figure 7.26 Thermal conductivity of the PP and PP composite containing untreated and plasma treated Semana fibres.

7.6.2 Thermal Stability

The thermal stability of the composites was determined by thermogravimetrical measurements. The samples were heated in an oxidative atmosphere up to 800°C with a heating rate of 5°C/min and oxygen flow rate of 25sccm.

Figure 7.27 shows the thermal stability of the composites containing 5 wt.% untreated GANF fibres manufactured by extrusion and injection moulding process. The composites manufactured by injection moulding have a slightly better thermal stability than the extruded composites. The extruded composites have some voids inside (see Figure 7.1) and this leads to a larger surface which is exposed during TG measurements.

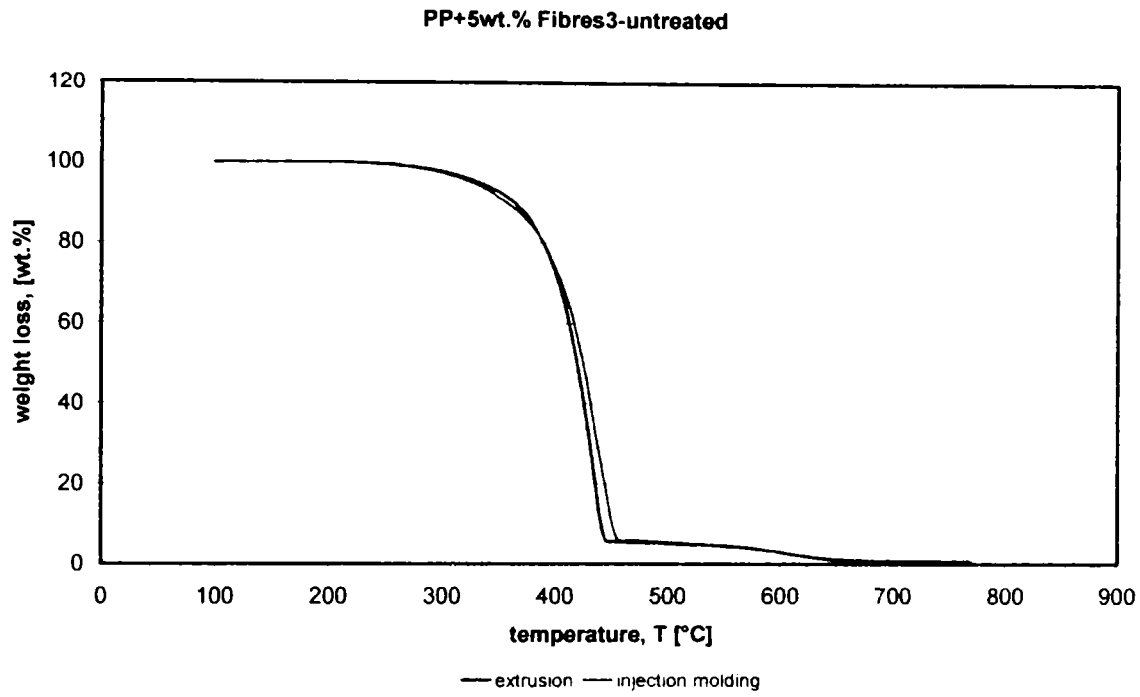

Figure 7.27 Thermal stability of the PP composite containing untreated GANF fibres.

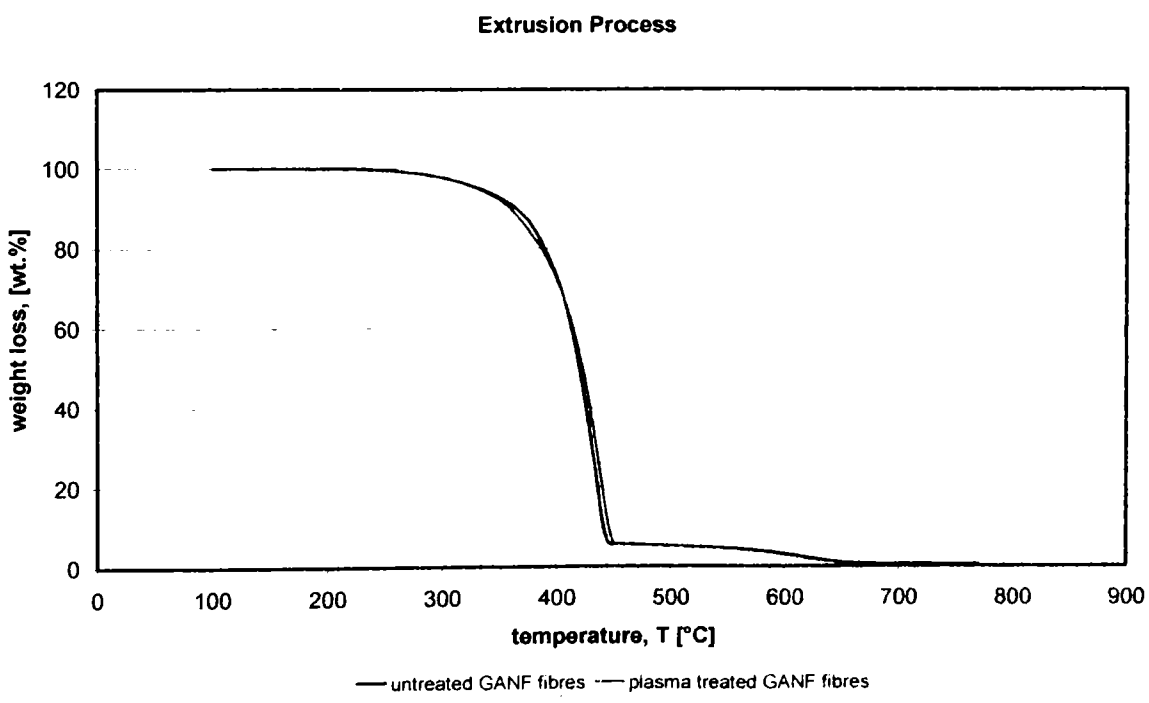

Figure 7.28 Thermal stability of the extruded PP composite containing untreated and plasma treated GANF fibres.

The thermal stability of the extruded composites containing untreated and plasma treated fibres presents no significant differences, Figure 7.28. The thermal stability of the composites containing untreated and plasma treated fibres manufactured by extrusion and injection moulding process and also of the injection moulded composites containing untreated and plasma treated GANF fibres are presented in Annex 11.

Polypropylene composites containing 5, 10 and 20 wt.% untreated GANF fibres were manufactured manually in laboratory. The PP mixed with the desired fibres contents was heated and melted on a oven from Ikamag, at 190°C for 5 minutes and permanently was mixed with a glass stick only in one direction in order not to destroy of the fibres. The thermal stability of the composite increased with the increase of the fibres contents in composites (see Figure 7.29).

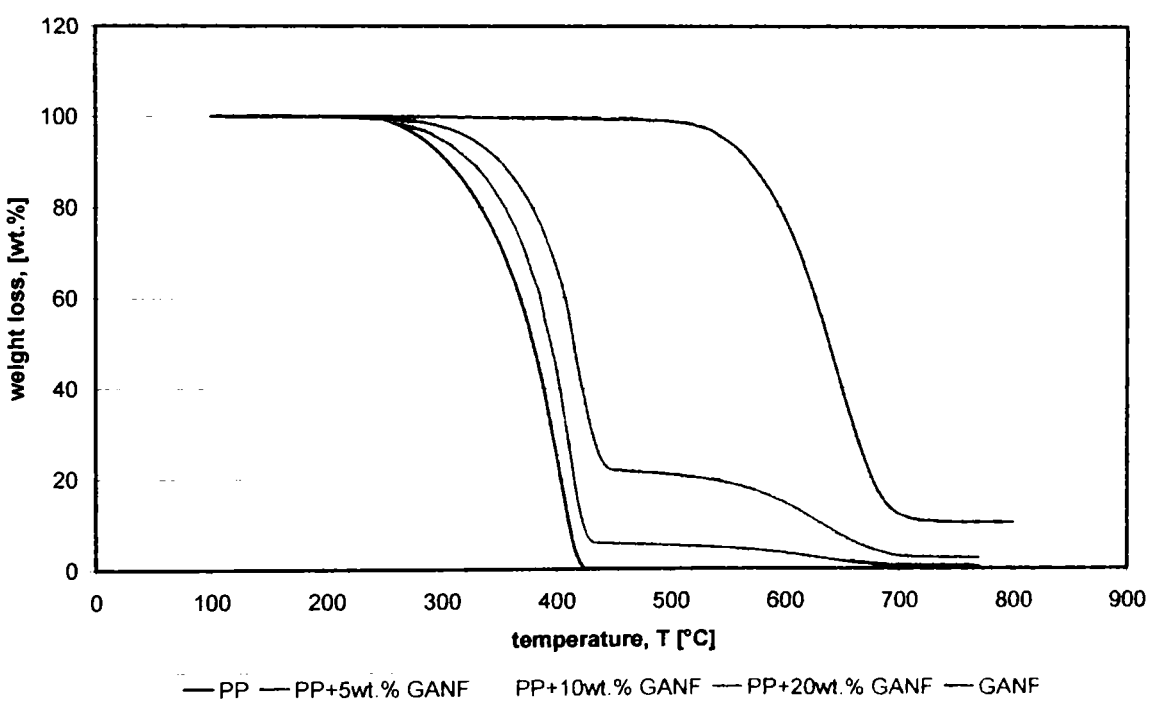

Figure 7.29 Thermal stability of the PP composite as a function of fibres contents.

7.7 Electrical Properties of the Polypropylene Composites Containing Vapour Grown Carbon Nanofibres

Polymers are considered to be ideal dielectric insulators. Their applications include integrated circuit "packaging", wire and cable insulation, industrial electrical switching, and high-voltage capacitor insulation. Sometimes is necessary that the polymers to be electrical conductive. Applications for automotives sector require paintable plastics using the

electrostatic painting methods; conductive adhesives, fuel tanks and fuel lines (pipe). For example, electrical conductive fuel tanks and fuel lines are necessary in order to avoid the electrostatic discharges which can lead to ignition of these components.

The volume electrical conductivity measurements were performed at room temperature using a standard DC electrical resistance method (see Figure 5.10). The electrical resistivity of the composites containing untreated GANF fibres manufactured manually in our laboratory is presented in Figure 7.30. The volume electrical resistivity of the PP was taken from literature ($\rho \approx 1 \times 10^{12} - 10^{14}$ Ωm). The composites containing 5 wt.% untreated GANF fibres have already the volume electrical resistivity of 2.9×10^{3} Ωm which is a decrease of ten orders of magnitude larger than that of the pure PP matrix. Increasing further the amount of VGCNFs in PP composite at 10 wt.% the volume electrical resistivity was decreased up to 6.4 Ωm. This may be ascribed primarily to the large aspect ratio of the conductive nanofibres. Percolation theory predicts that there is a critical concentration or percolation threshold at which a conductive path is formed in the composite, causing the material to convert from an insulator to a conductor. As the weight percentage is increased, the number of internanofibre connections increases and many conductive paths become available. The percolation threshold is reached when a conductive path of interconnected nanofibres is formed across the volume of the composite.

Y. Yang and co-workers described in their work the electrical properties of the polystyrene composites containing carbon nanofibres [161]. They show the volume electrical conductivity of the composites as a function of amount of VGCNFs in PS matrix. The percolation threshold for this material resides between 0.5 and 3 wt.% nanofibre contents.

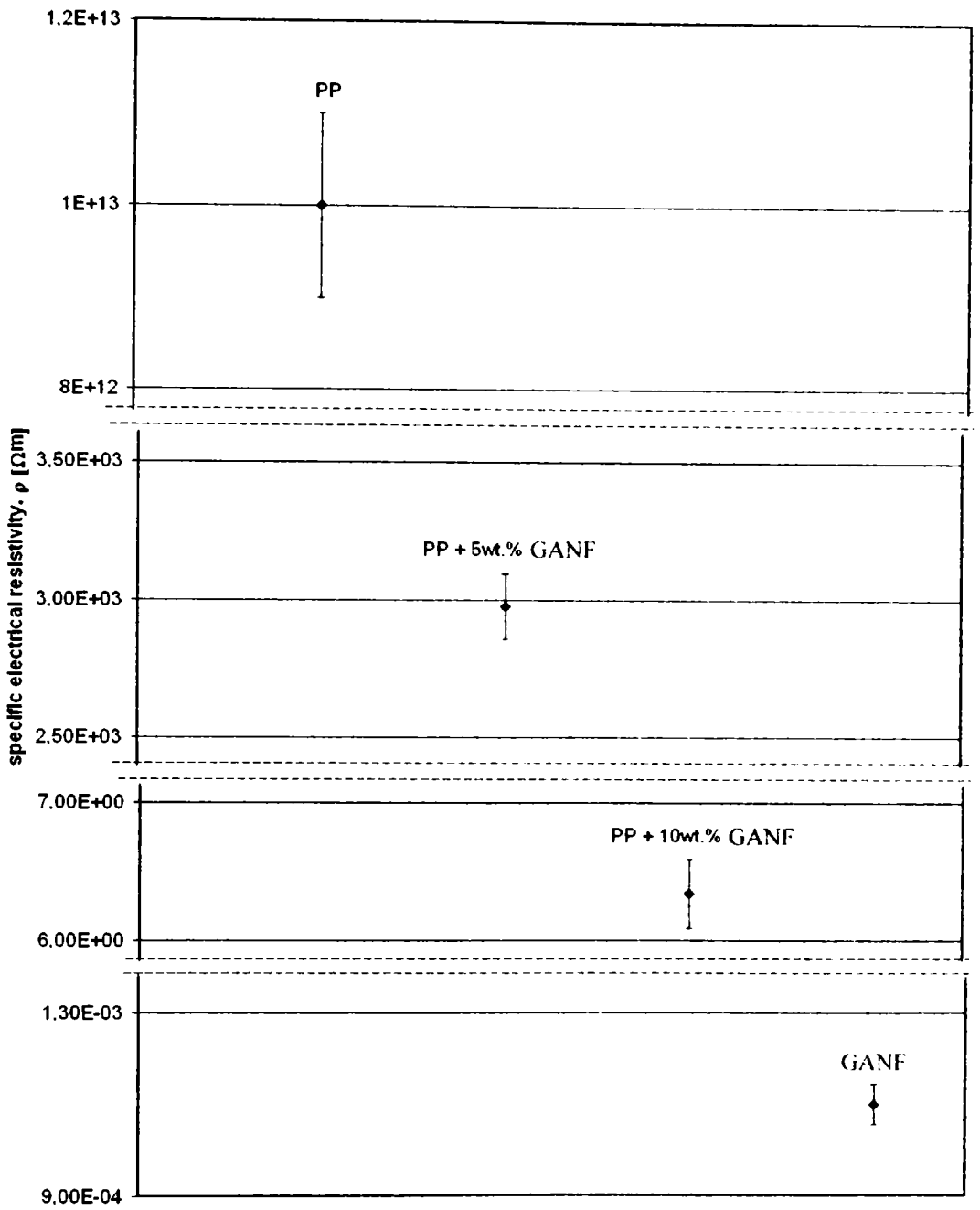

Figure 7.30 Volume electrical resistivity of the PP composites containing VGCNFs.

Figure 7.31 shows the volume electrical resistivity of the composites containing 5 wt.% untreated and plasma treated fibres. The composites containing plasma treated fibres have the value of volume electrical resistivity greater than composites containing untreated fibres, that means a higher electrical resistivity (lower thermal conductivity) than PP + VGCNFs untreated. This phenomenon is valid because the fibres during the oxygen plasma treatment were oxidised (the oxide interrupts the electrical flow).

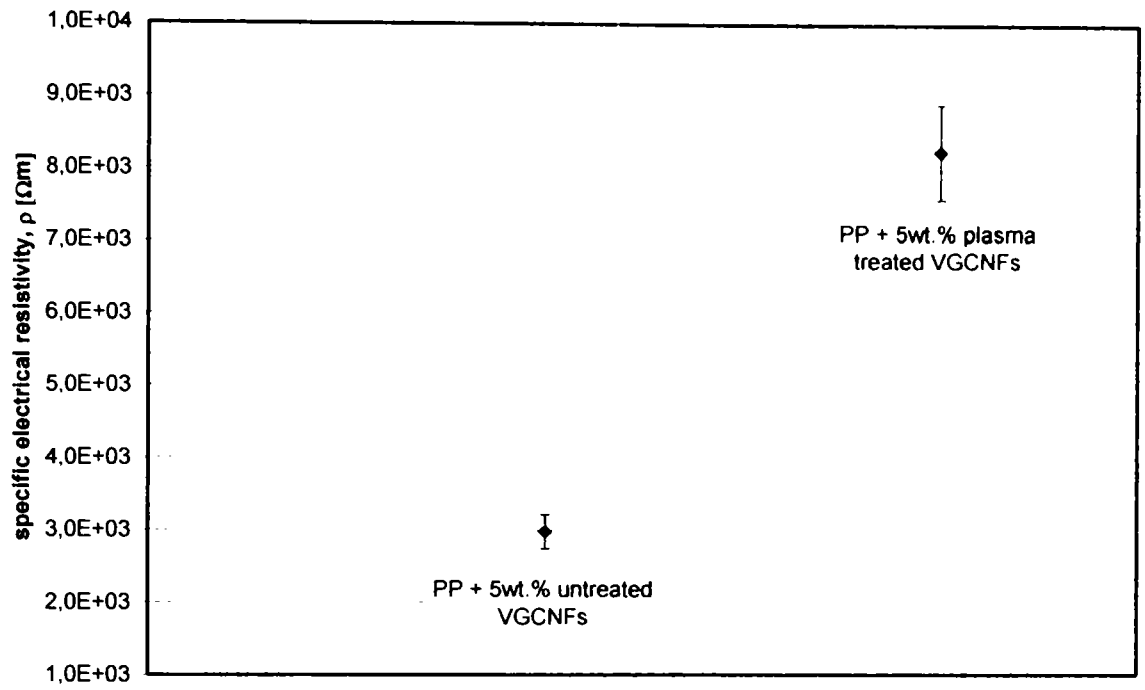

Figure 7.31 Volume electrical resistivity of the PP composites containing untreated and oxygen plasma treated VGCNFs.

The volume electrical resistivity of the injection moulded composites was measured using the same method. The injection moulded composites containing 5 wt.% and even 10 wt.% untreated fibres were insulators. The fibres are very well dispersed and oriented in PP matrix after injection moulding. This thing perhaps leads to the isolating of fibres in matrix and the fibres don't make a conductive network. Anyway, the volume electrical resistivity and surface electrical resistivity of the polymer composites containing vapour grown carbon fibres manufactured through extrusion and injection moulding should be further investigated.

7.8 Conclusions

The VGCNFs and PP composites were manufactured by extrusion and injection moulding process. The influence of the amount of vapour grown carbon nanofibres in polypropylene composites on the mechanical, thermal and electrical properties and also the morphology of these composites were presented in this chapter. The effect of oxygen plasma treated fibres on the mechanical and physical properties of the composites was also discussed.

The composites were investigated in cross section by SEM in order to observe the adhesion of the untreated and oxygen plasma treated fibres to the polymeric matrix. A weak adhesion was

observed in the case of untreated fibres (as grown fibres) whereas the cross section SEM micrograph of the composites containing oxygen plasma treated fibres showed a good adhesion. The introduction of oxygen containing functional groups is favourable to form strong chemical bonds between fibres as reinforcement material and polymer matrix of the composite.

The as grown and oxygen plasma treated VGCNFs were uniform dispersed in PP matrix after injection moulding process. The fibres were oriented in the injection moulding direction, phenomenon which leads to an increase of tensile properties of the composites in this direction. With other words, the injection moulded composites containing fibres as reinforcing material are anisotropic materials (mechanical properties are not the same in all directions).

The good adhesion between these two components of the obtained composite which was observed by SEM investigations, could be very well correlated with the mechanical properties, especially the tensile strength. The tensile strength of the composites containing 5 wt.% oxygen plasma treated fibres was increased up to 22% in comparison with pure polypropylene and was also better than the value for the composites containing 5wt.% even 10 wt.% untreated vapour grown carbon nanofibres. The elastic modulus of the composites containing untreated carbon nanofibres increased with the increase in the fibres amount. The composites containing 5 wt.% oxygen plasma treated fibres have the E – modulus slightly higher than the composites containing 5 wt. % untreated fibres. The stress – strain curves proved that the composites containing 5 wt.% untreated and plasma treated fibres are more ductile than pure polypropylene.

The impact strength measurements were performed at three different temperatures (22, 0 and -22…-25°C). The composites containing oxygen plasma treated GANF fibres have the highest impact strength at room temperature, while at low temperatures (0 and -22…-25°C) the composites containing untreated and plasma treated GANF fibres became brittles than pure polypropylene. The highest impact strength at room and even at low temperature was measured for the samples having 5 wt.% oxygen plasma treated Semana fibres as reinforcement material.

The thermal conductivity of the composites increases with the increase of the amount of fibres. The anisotropy of the injection moulded polypropylene composites containing nanofibres are reflected also by the thermal conductivity properties. The thermal conductivity

of the composites measured in the injection moulding direction is higher than of the samples measured normal to injection moulding direction. The thermal conductivity of the composites containing 10 wt.% carbon nanofibres increased up to 15% in comparison with pure polypropylene. No significant variation of the thermal conductivity was observed between the composites containing 5 wt.% oxygen plasma treated fibres and respectively untreated fibres.

The thermal stability of the composites increases with the increase of the contents of VGCNFs in PP matrix. The pure polypropylene starts to burn at around 250°C while the PP containing 20 wt.% VGCNFs burns at around 300°C. Between composites containing untreated and oxygen plasma treated fibres is no significant difference, both start to burn at around 265°C.

The PP composites containing VGCNFs show a spectacular improvement of the electrical conductivity. The electrical resistivity of the pure polypropylene was decreased from $\approx 1 \times 10^{13}$ Ωm (theoretic value) to 3×10^{3} Ωm in the case of composites containing 5 wt.% untreated fibres and up to 7×10^{0} Ωm for composites containing 10 wt.% untreated fibres (these composites were manufactured manually having an disordered orientation of carbon nanofibers). The electrical resistivity of the composites containing 5 wt.% plasma treated fibres increased slighter in comparison with the composites containing the same amount of untreated fibres.

The composites which were manufactured through extrusion and injection moulding exhibit a high orientation and distribution of the VGCNFs in the polymeric matrix and in this case, the necessary conductive fibres network is not formed. Therefore, these composites remain insulator even in the case of 10 wt.% (20 vol.%) amount of fibres (the electrical resistivity is higher than 1×10^{8} Ωm).

CHAPTER VIII

CONCLUSIONS

8.1 Conclusions

Adhesion at the nanofibres – matrix interface in vapour grown carbon nanofibres reinforced composites plays an important role in controlling the mechanical properties and overall performance of composites. Effective fillers require good bonding (chemical, mechanical and physical) between the fibres and the matrix. The chemical bonds are the most important one. Chemical or physical treatments are applied to the carbon fibres or the polymer matrix in order to improve the fibre/matrix adhesion. Among the many available treatments applicable to the reinforcement materials, the plasma treatment has the advantage of being a modern technique capable to improve the functionalisation degree of nanofibres in a short time.

The VGCNFs used in this research were provided from two different manufacturers: Pyrograf® III from Applied Sciences, SEMANA and GANF® 1 from Grupo Antolin. The nanofibres were characterised using the following methods: SEM, TEM, X-ray diffraction, TG and DC measurements. The SEM micrographs show the morphology of the nanofibres and reveal a relative homogenous diameter with an aspect ratio (length/diameter) up to 1:1000. The Pyrograf fibres are characterised by concentric cylindrical graphene layers while the Semana and GANF fibres have a herringbone structure around a void core region. The graphitisation degree of the fibres can be very well correlated with the electrical and the thermal properties. The fibres with the highest graphitisation degree have the best electrical conductivity (lower electrical resistivity) and thermal stability.

The VGCNFs were treated at two different plasma frequencies: high frequency (radio frequency) 13.56 MHz and microwave frequency 2.45 GHz. The wettability and the functionalisation degree of the nanofibres were investigated by several methods, like: water contact angle, surface energy, titrations, and XPS measurements. The surface structure modifications of the treated fibres were analysed by TEM and BET methods.

The importance of the plasma treatment parameters (plasma power, treatment time, oxygen flow rate, and chamber pressure) on the functionalisation degree of the nanofibres was determined using mathematical modelation (Statgraphic – statistical software) and step by step methods.

The PARETO chart obtained from the mathematical modelation showed that the plasma power and the treatment time are the most important parameters. The combination between

chamber pressure – plasma power and chamber pressure – treatment time had also a strong influence on the functionalisation degree of the nanofibres.

The as grown nanofibres had the water contact angle of about 90° and a surface energy of about 23 mN/m (Pyrograf and Semana fibres). The Pyrograf fibres were treated in oxygen and ammonia plasma. After plasma treatment the fibres became highly hydrophilic and the wettability was increased up to 35%, the value of water contact angle was about 62°, respectively. This wettability of the fibres was obtained by different plasma power correlated with different treatment time, for example a long treatment time (50 min) and a lower plasma power (50 W) or a short time (3 min) and a high plasma power (180W). The surface energy measurements showed that for the same water contact angle obtained for treated fibres with different plasma parameters, the values of the calculated surface energy were similar but its polar component was different. The polar component of the surface energy for the samples treated for longer time (40 min) at 80W plasma power had a higher value (≈33 mN/m) whereas for the samples treated at high plasma power (180W) for shorter time (3 min) the polar component of the total surface energy was about 16 mN/m. A value of 33 mN/m represents an increase up to 450% in comparison with the value for as grown fibres, ≈6 mN/m. The polar component of the surface energy gives information about the functionalisation degree of the fibres surface which could be well correlated with the total amount of functional groups created on the nanofibers after oxygen plasma treatment. Titration and XPS measurements were carried out in order to determine the amount of functional groups. The samples with the highest value of polar component (33 mN/m) had the highest value of functional groups (1.8 mmol/g) which were determined through titration measurements. The XPS measurements showed also an increase (up to 6 times in comparison with the untreated fibres) of the amount of oxygen groups present on the surface of the oxygen plasma treated Pyrograf fibres. The BET and TEM investigations can be very well correlated with the value of dispersive component from surface energy. The nanofibres treated at a high plasma power (more than 150 W) have the value of the dispersive component around 20 mN/m and correspond also a high surface area (44 m^2/g), that indicated an increase in the surface porosity. A good functionalisation degree of the oxygen plasma treated nanofibres means a high oxidation degree of the surface which leads to a certain degradation of the fibres structure which could affect mainly the electrical properties of the treated material in comparison with the untreated nanofibres.

The Semana fibres were treated in microwave generated oxygen plasma for short time (< 7 min) at plasma power of 80 – 120W. It was found that, a lower water contact angle of 30° was obtained for the samples treated at 80 – 120 W plasma power for 7 minutes. The surface energy of the nanofibres was increased up to 2 times in comparison with the untreated fibres. The values for the polar component of the surface energy as well as the amount of acidic functional groups determined for the plasma treated fibres are up to 12 times higher than that of the untreated fibres.

The microwave generated oxygen plasma was more adequate than radio frequency generated oxygen plasma for the treatment of Semana fibres. The upper conclusion is not a general one. The plasma parameters optimised for one type of fibres were not available for another type of fibres. For example, comparing Pyrograf with Semana, it can be observed that the Semana fibres can't be functionalised with the optimised parameters from Pyrograf fibres.

The treatment in MW generated plasma was difficult to make because the fibres having a very low bulk density (< 2 g/cm^3) were blown during the chamber ventilation. The treatments of the nanofibres in a microwave generated plasma can be easy to realise if some modifications of plasma reactor are made, for example the MW generator to be assembled inside in a barrel (especially a rotary one in order to obtain a homougenous treatment).

The GANF fibres were well functionalised using RF generated oxygen plasma. The highest surface energy was obtained in the case of fibres treated for only 2.5 minutes at 100W. The dispersive component of the surface energy of these treated fibres was very low, only 1 mN/m, that indicates a very low etching effect of the fibres.

The adequacy of oxygen plasma treatment (radio- or microwave frequency generated plasma) to improve the wettability and the functionalisation degree of the vapour grown carbon nanofibres has been demonstrated in the present researches. The introduction of oxygen containing functional groups is favourable to form strong chemical bonds between fibre reinforcements and polymer matrix of the composite.

Polypropylene composites containing different quantities of untreated and oxygen plasma treated VGCNFs were manufactured using a co-rotating twin screw extruder and injection moulding.

The fracture surface of the samples analysed in cross section by SEM showed an improve adhesion between fibres and polymer matrix whereas the composites containing untreated fibres had a weak adhesion. The top view SEM micrographs of the injected composites revealed a high orientation of the fibres in injection moulding direction and an uniform dispersion of them in PP matrix. Due to the high orientation of the fibres in one direction, the obtained composites will have better mechanical and physical properties in this direction, phenomenon which is known for anisotropy materials.

The mechanical properties of the PP/VGCNFs composites were improved when plasma functionalized carbon nanofibres were used. The composites containing 5 wt.% oxygen plasma treated fibres proved a higher tensile strength (up to 22% improvement) in comparison with the pure polypropylene and the composites containing 5 wt% even 10 wt.% untreated fibres. The elastic modulus of the composites containing nanofibres increased with the increase of the contents of nanofibres. No significant difference of the E-modulus was observed between the composites containing 5wt.% untreated and plasma treated fibres, the last composite having a higher elastic modulus.

The Charpy impact strength measurements were performed at room and low temperature. The composites containing 5 wt.% oxygen plasma treated Semana fibres had the highest impact strength at room and low temperature in comparison with the PP and the composites containing 5 and 10 wt.% untreated fibres. The composites containing GANF fibres at low temperature were more brittle than the PP, having a low impact resistance.

Composites containing 5, 10 and 20 wt.% GANF fibres were manufactured manually in laboratory. The amount of VGCNFs in the polymer matrix has a strong influence on the thermal stability of composites. The thermal stability of the composites increased with the increase of the contents of VGCNFs in PP matrix. Composites containing 20 wt.% nanofibres had the highest thermal stability (burning temperature starts at 300°C) in comparison with the composites containing 5 wt.% fibres (265°C) and PP (250°C).

The thermal conductivity of the samples was measured in two directions: in the injection moulding direction and normal to the injection moulding direction. The thermal conductivity of the samples measured in the injection moulding direction was higher than that of the samples measured normal to this direction. The thermal conductivity of the injected

composites containing 10 wt.% carbon nanofibres increased up to 15% in comparison with the pure polypropylene.

The composites manufactured through extrusion and injection moulding were insulator because the high orientation and distribution of the fibres in matrix didn't form a conductive network.

The composites manufactured manually showed a high improvement of the electrical conductivity. The composites containing 10 wt.% untreated VGCNFs had the value of electrical resistivity of 7×10^{0} Ωm which was very low in comparison with the value for PP, $1 \times 10^{12} \ldots 1 \times 10^{14}$ Ωm.

A better adhesion between vapour grown carbon nanofibres and polypropylene was obtained for the composites containing oxygen plasma treated fibres. The mechanical properties, especially the tensile strength, were increased without a negative influence on the physical properties of the composites (thermal and electrical properties).

REFERENCES

1. World Wide Web, 27.09.2005, 15:10, Institute of Technology, Banaras Hindu University: http://www.itbhu.ac.in/dcam/details.htm;
2. L. A. Pilato, M. J. Michno, *Advanced Composite Materials*, Springer-Verlag Berlin Heidelber 1994;
3. D. D. L. Chung, *Composite Materials: Science and Applications*, Springer-Verlag London, 2003;
4. D. Banerjee, J. Lao, Z. Ren, *Design of Nanostructured Materials*. M. J. Schulz, A. D. Kelkar, M. J. Sundaresan, editor. Nanoengineering of Structural, Functional, and Smart Materials, Taylor&Francis Group, Boca Raton, 2006;
5. P. M. Ajayan, L. S. Schadler, P. V. Braun, *Nanocomposite Science and Technology*, Willey-VCH Verlag, Winheim, 2003;
6. F. W. Starr, S. C. Glotzer, *Simulations of Filled Polymers on Multiple Length Scales*, Mat. Res. Soc. Symp. Proc. 661, 2001;
7. G. Beaucage, S. Rane, D. W. Schaefer, G. Long, D. Fischer, *Morphology of Polyethylene–Carbon Black Composites*, Journal of Polymer Science: Part B: Polymer Physics 37, 1105 – 1119, 1999;
8. World Wide Web, 20.06.2005, 10:00, *Handbook of Texas Online*: http://www.tsha.utexas.edu/handbook/online/articles/CC/doc1.html;
9. P. Holister, J. W. Weener, C. R. Vos, T. Horper, *Nanoparticles: Technology White Paper nr. 3*, Cientifica, 2003;
10. S. R. Raghavan, M. W. Riley, P. S. Fedkiw, S. A. Khan, *Composite Polymer Electrolytes Based on Poly(ethyleneglycol) and Hydrophobic Fumed Silica: Dynamic Rheology and Microstructure*, Chemistry of Materials 10, 244 – 251, 1998;
11. M. Sumita, T. Shizuma, K. Miyasaka, K. Ishikawa, *Effect of reducible properties of temperature, rate of strain, and filler content on the tensile yield stress of Nylon 6 composites filled with ultrafine particles*, J. Macromol Sci. Phys. B22(4), 396 – 400, 1983;
12. O. Breuer, U. Sundararaj, *Big Returns from Small Fibres: A Review of Polymer/Carbon Nanotube Composites*, Polymer Composites 25 (6), 630 – 645, 2004;
13. T. Engelhardt, *Industrial Application of Nanocomposite Fillers Based on Organic Intercalated Bentonites*, IMA-Europe 2002 Conference, 2002;
14. W. Posthumus, *UV-curable Acrylate Metal Oxide Nanocomposite Coatings*, Technische Universiteit Eindhoven, Eindhoven, 2004.

15. Y. T. Lim, O. O. Park, *Microstructure and Rheological Behavior of Block Copolymer/Clay Nanocomposites*, Korean Journal of Chemical Engineering, 18(1), 21 – 25, 2001

16. S. Musikhin, L. Bakueva, E. H. Sargent, A. Shik, *Luminescent Properties and Electronic Structure of Conjugated Polymer-Dielectric Nanocrystal Composites*, Journal of Applied Physics, 91(10), 6679 – 6683, 2002;

17. D. Schmidt, D. Shah, E. P. Giannelis, *New Advances in Polymer / Layered Silicate Nanocomposites*; Current Opinion in Solid State and Materials Science 6, 205 – 212, 2002;

18. D. M. Schmidt, *Polysiloxane/Layered Silicated Nanocomposites: Synthesis, Characterisation, and Properties*, University Cornell, PhD Thesis, 2003;

19. P. M. Ajayan, T. W. Ebbesen, *Nanometre-size Tubes of Carbon*, Reports on Progress in Physics 60, 1025 – 1062, 1997;

20. Q. Zhao, H. D. Wagner, *Raman Spectroscopy of Carbon-Nanotube-Based Composites*, Phil. Trans. R. Soc. Lond. A 632, 2407 – 2424, 2004;

21. P. Poza, J. P. Rigueiro, M. Elices, J. LLorca, *Fractographic analysis of silkworm and spider silk*, Engineering Fracture Mechanics 69, 1035 – 1048, 2002;

22. S Iijima, *Helical microtubules of graphitic carbon*, Nature 354, 56 – 58, 1991;

23. H. S. Kim1, H -S. Yang, H. J. Kim, H. J. Park, *Thermogravimetric Analysis of Rice Husk Flour Filled Thermoplastic Polymer Composites*, Journal of Thermal Analysis and Calorimetry 76, 395 – 404, 2004;

24. S. Wang, D. P. Kowalik, D D L Chung; *Self-sensing attained in carbon-fiber–polymer-matrix structural composites by using the interlaminar interface as a sensor*, Smart Materials and Structures 13, 570 – 592, 2004;

25. K. S. C. Kuang, W. J. Cantwell, *In situ process monitoring of a thermoplastic-based fibre composite using optical fibre sensors*, Smart Materials and Structures 11, 840 – 847, 2002;

26. H. Barber, Q. Zhao, H.D. Wagner, C.A. Baillie, *Characterization of E-Glass-Polypropylene Interfaces Using Carbon Nanotubes as Strain Sensors*, Composites Science and Technology 64, 1915 – 1919, 2004,

27. R. Mezzenga, L. Boogh, J. A. E. Manson, *A Review of Dendritic Hyperbranched Polymer as Modifiers in Epoxy Composites*, Composites Science and Technology 61, 787 – 795, 2001;

28. R. L. Clark, *Influence of the Interphase on the Mechanical Properties of Nylon 66 Composites*, Faculty of theVirginia Polytechnic Institute, PhD Thesis, 1996
29. K. Joseph, R. D. T. Filho, B. James, S. Thomas, L. Hecker de Carvalho, *A Review on Sisal Fiber Reinforced Polymer Composites*, Revista Brasileira de Engenharia Agrícola e Ambiental 3 (3), 367 – 379, 1999;
30. World Wide Web, 03.09.2005, 15:10, Advanced composite Materials: http://www.nosc.mil/usn/nepmu5/assets/images/Advanced_Composite_Materials_.pdf;
31. K. T. Hsiao, J. Alms, S. G. Advani, *Use of Epoxy/Multiwalled Carbon Nanotubes as Adhesives to Join Graphite Fibre Reinforced Polymer Composites*, Nanotechnology 14, 791 – 793, 2003;
32. T. A. Osswald, G. Menges, Materials Science of Polymers for Engineering, Carl Hanser Verlag, Munich Vienna New Yorg, 1996;
33. H. G. Elias, *An Introduction to Plastics*, VCH Verlagsgesellschaft, Wheinheim, 1993;
34. T. Iclanzan, Plastics Engineering : Processing Technique of the Plastic Materials, Politehnica, Timsisoara, 2003;
35. World Wide Web, 07.06.2005, 13:10, Material Selection Guide: http://www.boedeker.com/mguide.htm;
36. T. M. Pelsoci, *Composites Manufacturing Technologies: Applications in Automotive, Petroleum, and Civil Infrastructure Industries*, NIST GCR 04-863, 2004
37. World Wide Web, 12.09.2005, 09:45, Huntsman Polymers, Polypropylene: http://www.huntsman.com/polymers/index.cfm?PageID=796;
38. World Wide Web, 12.09.2005, 10:45, FiberVision, Polypropylene: http://www.fibervisions.dk;
39. World Wide Web, 12.09.2005, 09:45, Total Petrochemicals USA, Polypropylene: http://www.totalpetrochemicalsusa.com/home/default.asp;
40. World Wide Web, 12.09.2005, 09:45, The Chemistry Encyclopaedia, Polymer banknote: http://www.chemistrydaily.com/chemistry/Polymer_banknote;
41. World Wide Web, 19.07.2005, 10:30, Wikipedia: The Free Encyclopedia: http://en.wikipedia.org/wiki/Polypropylene;
42. L. Cerruti, *Historical and Philosophical Remarks on Ziegler-Natta Catalysts*, International Journal for Philosophy of Chemistry 5(1), 3 – 41, 1999;
43. A. M. Thayer, *Metallocene Catalysts Initiate New Era In Polymer Synthesis*, Chemical and Engineering News 11, 1995, http://pubs.acs.org/hotartcl/cenear/950911/art01.html (12 Feb. 2003);

44. E. Albizzati, U. Giannini, G. Callina, L. Noristi, L. Resconi, *Catalysts and Polymerizations*, E. P. Moore editor, Polypropylene Handbook, Carl Hanser Verlag, Munich Vienna New York, 1996;
45. R. A. Phillips, M. D. Wolkowicz, *Structure and Morphology*, E. P. Moore editor, Polypropylene Handbook, Carl Hanser Verlag, Munich Vienna New York, 1996;
46. E. P. Moore Jr., *Fabrication Processes*, E. P. Moore editor, Polypropylene Handbook, Carl Hanser Verlag, Munich Vienna New York, 1996;
47. World Wide Web, 20.04.2004, 10:00, 3D-Cam: Technical Suport, Materials: http://www.3d-cam.com/materials/polypropylene_molded.asp;
48. World Wide Web, 20.04.2004, 10:30, Azonano: Classification of Nanomaterials, http://www.azonano.com/details.asp?ArticleID=1073#_Introduction_to_Nanoparticles;
49. T. A. Edison, *Electric Lamp*, U. S. Patent 223898, 1879;
50. J. C. Masson, *Acrylic Fibre Technology and Applications*, Marcel Decker, New York, 1995;
51. L. H. Peebles, *Carbon Fibres: Formation, Structure, and Properties*, CRC Press Inc., Boca Raton, 1995;
52. J. Xie, K. Mukhopadyay, J. Yadev, V. K. Varadan, *Catalytic Chemical Vapor Deposition Synthesis and Electron Microscopy Observation of Coiled Carbon Nanotubes*, Smart Materials and Structures 12, 744 – 748, 2003;
53. P. Morgan, *Carbon Fibres and their Composites*, Taylor&Francis Group, Boca Raton, London, New York, Singapore 2005;
54. World Wide Web, 10.11.2005, 10:30, Wikipedia: The Free Encyclopedia: http://en.wikipedia.org/wiki/Electron_microscopy;
55. M. Endo; *Grow Carbon Fibers in the Vapor Phase*, CHEMTECH, American Chemical Society, 568, 1988;
56. G. Tibbetts, *Vapor-Grown Carbon Fibers*, J. L. Figueiredo, C. A. Bernardo, R. T. K. Baker, K. J. Hüttinger editors, Carbon Fibres Filaments and Composites, Kluwer, Dordrecht, 1990;
57. P. Gadelle, *The Growth of Vapour Deposited Carbon Fibres*, J. L. Figueiredo, C. A. Bernardo, R. T. K. Baker, K. J. Hüttinger editors, Carbon Fibres Filaments and Composites, Kluwer, Dordrecht, 1990;
58. R. T. K. Baker, P. S. Harris, *The Formation of Filamentous Carbon*, P. L. Walker, P. A. Thrower editors, Chemistry and Physics of Carbon, Marcel Dekker, New York 1978;

59. E. Fitzer, L. M. Manocha, *Carbon Reinforcements and Carbon/Carbon Composites*, Springer-Verlag Berlin Heidelberg, 1998;
60. M.S. Dresselhaus, G. Dresselhaus, K. Sughihara, I. L. Spain, H. A. Goldberg, *Graphite Fibres and Filaments*, Springer-Verlag, Berlin 1988;
61. G. G. Tibbetts, *Lengths of carbon fibres grown from iron catalyst particles in natural gas*, Journal of Crystal Growth 73(3), 431 – 438, 1985;
62. T. Koyama, M. T. Endo, *Method for manufacturing carbon fibres by a vapour phase process*, Japanese Patent 1982-58, 1985;
63. G. Marginean, *Vapour Grown Carbon Fibres: Morphology and Chemical Plasma Functionalisation*, Bochum University, PhD Thesis, 2004;
64. F. Benissad, F. Gadelle, P. Coulon, L. Bonnetain, *Influence of catalyst on the lengths of vapour grown carbon fibres*, Proc Int Conf Carbon, Newcastle upon Tyne, 1988;
65. R. T. K. Baker, M. A. Barber, P. S. Harris, F. S. Feates, R. J. Waite, *Nucleation and growth of carbon deposits from the nickel catalyzed decomposition of acetylene*, Journal of Catalysis 26, 51 – 62, 1972;
66. R. T. K. Baker, M. A. Barber, P. S. Harris, F. S. Feates, R. J. Waite, Formation of filamentous carbon from iron, cobalt and chromium catalyzed decomposition of acetylene, Journal of Catalysis 30, 86 – 95, 1973;
67. R. T. K. Baker, R. J. Waite, Formation of carbonaceous from the platinum – iron catalysed decomposition of acetylene, Journal of Catalysis 37, 101 – 105, 1975;
68. M. Endo, T. Koyama, Explanation of growth mechanism and physical properties of vapour grown carbon fibres, Kotai Butsuri (in Japanese) 12, 1, 1977;
69. H. O. Pierson, *Handbook of Carbon, Graphite, Diamond and Fullerenes - Properties, Processing and Applications*, William Andrew Publishing/Noyes, New York, 1993;
70. B. Bhushan, *Handbook of Nanotechnology*, Springer Verlag, Berlin Heidelberg, 2004;
71. N. Hamada, S. I. Sawada, A. Oshiyama, *New one-dimensional conductors: Graphitic microtubules*, Physical Review Letters 68, 1579 – 1581, 1992;
72. M. S. Dresselhaus, G. Dresselhaus, P. Eklund, R. Saito, *Carbon nanotubes*, Physics World, January 1998, http://physicsweb.org/articles/world/11/1/9/1;
73. A. Oberlin, M. Endo, T. Koyama, *High resolution electron microscope observations of graphitized carbon fibres*, Carbon 14, 133 – 135, 1976;
74. B. K. T. Kenneth, S. Charanjeet, M. Chhowalla, W. I. Milne, *Catalytic Synthesis of Carbon Nanotubes and Nanofibers*, Encyclopedia of Nanoscience and Nanotechnology 1, 665 – 686, 2004;

75. C. P. Poole Jr., F. J. Owens, *Introduction to Nanotechnology*, John Wiley & Sons Inc., Hoboken, New Jersey, 2003,

76. S. R. Mukai, T. Masuda, K. Hashimoto, *Mechanical and Electrical Properties of Rapidly Grown Vapor Grown Carbon Fibers*, American carbon Society Conference, 564 – 565, 1999;

77. J. Heremans, *Electrical conductivity of vapor-grown carbon fibers*, Carbon 23(4), 431 – 436, 1985;

78. A. A. Bright, L. S. Singer, *The electronic and structural characteristics of carbon fibers from mesophase pitch*, Carbon 17(1), 59 – 69, 1979;

79. T. Koyama, M. Endo, M. Hyshiyama, *Carbon Fibers Obtained by Thermal Decomposition of Vaporized Hydrocarbon*, Japanese Journal of Applied Physics 11, 445 – 449, 1972;

80. G. G. Tibbetts, C. P. Beetz Jr., *Mechanical Properties of Vapour Grown Carbon Fibres*, Journal of Physics D 20, 292 – 297, 1987;

81. J. D. H. Hughes, *The Evaluation of current Carbon Fibres*, Journal of Physics D 20, 276 – 285, 1987;

82. K. K. Chawla, *Composite Materials: Science and Engineering*, 2nd edition, Springer Verlag New York, 1998;

83. A. T. Yokobori Jr., H. Takeda, T. Adachi, J. C. Ha, T. Yokobori, *Characteristics of Fatigue Life and Damage Accumulation of Short Fibre – Reinforced Polymer Composite*, C. J. Spragg, L.T. Drzal editors, Fibre, Matrix, and Interface Properties, ASTM publication, STP 1290, Scranton Pa, 1996;

84. K. C. Seavey, *Lyocell Fiber-Reinforced Cellulose Ester Composites - Surface and Consolidation Considerations, and Properties*, Faculty of the Virginia Polytechnic Institute and State University, Master's Thesis, 1999;

85. J. Sun, Peel, *Test for the Study of the Fibre Polymer Interface*, University of Toronto, Master's Thesis, 2001;

86. J. Xie, N. Zhang, M. Guers, V. K Varadan, *Ultraviolet-curable polymers with chemically bonded carbon nanotubes for microelectromechanical system applications*, Smart Materials and Structures 11, 575 – 580, 2002;

87. World Wide Web, 08.07.2005, 10:00, Free information Society: *Chemical Bonding*, http://www.freeinfosociety.com/pdfs/science/chemicalbonding.pdf;

88. World Wide Web, 07.09.2005, 11:00, Kruess online: *Contact angle measurement – a theoretical approach*, http://www.kruss.info/techniques/contact_angle_e.html;

89. World Wide Web, 08.09.2005, 11:00, KSV Instruments USA: *Contact angle* http://www.ksvinc.com/contact_angle.htm;

90. B. D. Bauman, *Surface-Modified Polymer Particles: Performance Additives for Cast PU*, Advancing International Markets and Technology, Toronto, 2001;

91. R.J. Young, D.J. Bannister, A.J. Cervenka, I. Ahmad, *Effect of surface treatment upon the pull-out behaviour of aramid fibres from epoxy resins*, Journal of Materials Science 35(8), 1939 – 1947, 2000;

92. M.A. Montes-Moran, A. Martınez-Alonso, J.M.D. Tascon, R.J. Young, *Effects of plasma oxidation on the surface and interfacial properties of ultra-high modulus carbon fibres*, Composites Part A - Applied Science and Manufacturing 32, 361 – 371, 2001;

93. P.W.J. van den Heuvel, T. Peijs, R.J. Young, *Failure phenomena in two-dimensional multi-fibre microcomposites. Part 4: a Raman spectroscopic study on the influence of the matrix yield stress on stress concentration*, Composites Part A - Applied Science and Manufacturing 31, 165 – 171, 2000;

94. W.H. Prosser, J.A. Hinkley, J. *Interfaces in Thermoplastic Composites Probed by Laser-Induced Acoustic Emission*, Journal of Materials Science Letters 13, 213 – 214, 1994;

95. V. A. Shelestova, V. V. Serafimovich, P. N. Grakovich, J. X. Hong, Y. S. Jin, *Change in the Surface Properties of Carbon Fibers as a Result of Plasmochemical Modification*, Mechanics of Composite Materials 39(5), 467 – 472, 2003;

96. G. G. Tibbetts, J.C. Finegan, D. G. Glasgow, J.M. Ting, M. L. Lake, *Surface Treatments for Improving the Properties of Vapor-Grown Carbon Fiber/Polypropylene Composites*, Conference on Carbon , Charleston, SC, 58 – 59, 1999;

97. J. P. Boudou, J.I. Paredes, A. Cuesta, A. Martineu-Alonso, J. M. D. Tascon, *Oxygen plasma modification of pitch-based isotropic carbon fibres*, Carbon 41, 41 – 56, 2003;

98. J. P. Boudou. A. Martinez-Alomzo, J. M. D. Tascon, *Introduction of acidic groups at the surface of activated carbon by microwave- induced oxygen plasma at low pressure*, Carbon 38(7), 1021 – 1029, 2000;

99. A. Cuesta, A. Martinez-Alonzo, J. M. D. Tascon, *Carbon reactivity in an oxygen plasma: a comparison with reactivity in molecular oxygen*, Carbon 39(8), 1135 – 1146, 2001;

100. J. B. Donnet, M. Brendle, T. L. Dhami, O. P. Bahl, *Plasma treatment effect on the surface energy of carbon and carbon fibers*, Carbon 24(6), 757 – 770, 1986;

101. N. J. Wadsworth, W. Watt, *Treatment of Carbon Fibres and composite materials including such fibres*, British Patent 1180441, 1968;

102. D. W. Mckee, V. J. Mimeault, *Surface Properties of Carbon Fibres*, P. L. Walker, P. A. Thrower editors, Chemistry and Physics of Carbon, Marcel Decker, New York, 1973;

103. J. Alcañiz-Monge, D. Cazorla-Amorós, A. Linares-Solano, S. Yoshida, A. Oya, *Effect of the activating gas on tensile strength and pore structure of pitch-based carbon fibres*, Carbon 32 (7), 1277 – 1283, 1994;

104. J. C. Goan, L. A. Joo, G. E. Sharpe, *Surface treatment for Graphite Fibres*, 27th Ann Tech Conf Plast/Comp Inst 27, 1972;

105. Z. Wu, C. U. Pittman, Jr., S. D. Gardner, *Nitric acid oxidation of carbon fibres and the effects of subsequent treatment in refluxing aqueous NaOH*, Carbon 33(5), 597 – 605, 1995;

106. . U. Pittman, Jr , G. R. He, B. Wu, S. D. Gardner, *Chemical modification of carbon fibre surfaces by nitric acid oxidation followed by reaction with tetraethylenepentamine*, Carbon 35(3), 317 – 331, 1997;

107. E. D. Perakslis, S. D. Gardner and C. U. Pittman, Jr., *Surface composition of carbon fibers subjected to oxidation in nitric acid followed by oxygen plasma*, Journal of Adhesion Science and Technology 11(4), 531 – 552, 1997;

108. J.R. Lee, M.H. Kim, S. J. Park, *Surface Modification of Carbon Fibres by Anodic Oxidation and its Effect on Adhesion*, Key Engineering Materials 183-187, 2000;

109. T. R. King, D. F. Adams, D. A. Buttry, *Anodic oxidation of pitch-precursor carbon fibers in ammonium sulfate solutions: Batch screening treatment results*, Composites Science and Technology 44(4), 351 – 359, 1992;

110. G. Emig, N. Popovska, G. Schoch, *Chemical vapour deposition of silicon carbide on mesophase pitch-based carbon fibres*, Thin Solid Films 241, 361 – 365, 1994;

111. J. B. Donnet, Carbon Fibres 2nd edition, Marcel Dekker, New York, 1990;

112. J. A. Bittencourt, *Fundamentals of Plasma Physics*, Springer Verlag, New York, 2004;

113. A. T. Bell, *Fundametanls of plasma Chemistry*, J. Hollahan and A. Bell editors, Techniques and Applications of Plasma Chemistry, Wiley & Sons, 1974;

114. Uwe Vohrer, *Glow Discharge Treatments for the Modification of Technical Textiles*, Techtextil Symposiums, Frankfurt am Main, 1997;

115. H. Suhr, *Applications of Nonequilibrium Plasmas to Organic Chemistry*, Hollahan and A. Bell editors, Techniques and Applications of Plasma Chemistry, Wiley & Sons, 1974;

116. World Wide Web, 22.05.2005, 11:00, *Introduction to plasma surface modification of polymers*, http://www.ipfdd.de/people/nitschke/plasma.html#modification;
117. World Wide Web, 17.02.2003, 09:00 Plasma Finish: What is Plasma, http://plasma-finish.com/cgi-bin/anwendung_e.pl?pfad=daten-anwendungen-wasistplasma;
118. M. D. Garcia, F. J. L. Garzon, M. P. Mendoza, *Modifications produced by O_2 plasma treatments on a mesoporous glassy carbon*, Carbon 38(4), 555 – 563, 2000;
119. M. C. Paiva, C. A. Bernardo, M. Nardin, *Mechanical, surface and interfacial characterisation of pitch and PAN-based carbon fibres*, Carbon 38 (9), 1323 – 1337, 2000;
120. J. I. Paredes, A. Martínez-Alonso, J. M. D. Tascón, *Comparative study of the air and oxygen plasma oxidation of highly oriented pyrolytic graphite: a scanning tunneling and atomic force microscopy investigation*, Carbon 38(8), 1183 – 1197, 2000;
121. C. Jones, E. Sammann, *The effect of low power plasmas on carbon fibre surfaces: A comparison between low and high modulus PAN based fibres with pitch based carbon fibres*, Carbon 28(4), 509 – 514, 1990;
122. D. Shi, P. He, *Surface Modifications of Nanoparticles and Nanotubes by Plasma Polymerization*, Rev.Adv.Mater.Sci. 7, 97 – 107, 2004;
123. A. Fukunaga, T. Komami, S. Ueda, M. Nagumo, *Plasma treatment of pitch-based ultra high modulus carbon fibres*, Carbon 37(7), 1087 – 1091, 1999;
124. R. C. Progelhof, J. L. Throne, *Polymer Engineering Principles: Properties, Processes, Tests for Design*, Carl Hanser Verlag, Munich Vienna New Yorg Barcelona, 1993;
125. C. Rauwendaal, *Understanding Extrusion*, Carl Hanser Verlag, Munich, 1998;
126. World Wide Web, 17.10.2005, 09:00, Plastics Technology: Twin Screw Extruder http://www.plasticstechnology.com/articles/200510fa6.html;
127. C. Rauwendaal, *Analysis and experimental evaluation of twin screw extruders*, Polymer Engineering and Science 21(16), 1981;
128. C. Raunwendaal, *Polymer Extrusion*, Carl Hanser Verlag, Munich Vienna New Yorg, 1994;
129. World Wide Web, 11.12.2003, 10:00, Thermoplastic Testing Centre: Twin Screw Extruder, http://www.ttc.bayerpolymers.com/bpo/bpo_ttc.nsf/id/AE776CA424891136C1256D59002CA55F;

130. A. Gaspar-Cunha, J. A. Covas, *RPSGAe – A Multiobjective Genetic Algorithm with Elitism: Application to Polymer Extrusion*, X. Gandibleux, M. Sevaux, K. Sörensen, V. T'kindt, editors Metaheuristics for Multiobjective Optimisation, Springer, Berlin, 2004;
131. J. Avery, *Injection Moulding Alternatives*, Carl Hanser Verlag, Minich, 1998;
132. J. BOWN, J. D. ROBINSON, *Injection and transfer moulding, and plastics mould design*, Business Books, London, 1970;
133. World Wide Web, 11.12.2005, 10:00, Thermoplastic Testing Centre: Injection Moulding: http://www.ttc.bayerpolymers.com/bpo/bpo_ttc.nsf/id/774CD9D7E39AFA00C1256D59002CA5C1;
134. J. Frados, *Plastics Engineering Handbook*, 4th edition, Van Nostrand, New York, 1976;
135. World Wide Web, 05.07.2005, 10:00, Applied Sciences, Inc: Pyrograf III, http://www.apsci.com/ppi-pyro3.html;
136. Grupo Antolin Ingineria S.A., *Ganf Technological Data Sheet*, 2005;
137. J. Goldstein, D. Newbury, D. Joy, C. Lyman, P. Echlim, E. Lifshin, L. Sawyer, J. Michael, *Scanning Electron Microscopy and X-Rays Microanalysis*, 3rd edition, Kulwer Academic / Plenum Publishers, New York, 2003;
138. FEI Company, *Scanning Electron Microscope XL30 ESEM TMP - Technical Manual and Operating Instructions*, 1999;
139. M. H. Loretto , *Electron Beam Analysis of Materials*, Chapman and Hall, London, 1984;
140. World Wide Web, 28.12.2005, 14:00, Adelaide Microscopy: *Transmission Electron Microscope,* http://www.adelaide.edu.au/microscopy/services/instrumentation/tem.html;
141. World Wide Web, 28.12.2005, 14:30, Imaging Technology Group: *Transmission Electron Microscopy: What Information can be Obtained from the Ultrathin Section*, http://www.itg.uiuc.edu/publications/forums/1998-06-02/;
142. World Wide Web, 12.12.2005, 08:30, Wikipedia: The Free Encyclopedia: http://en.wikipedia.org/wiki/X-ray;
143. World Wide Web, 28.12.2005, 13:00, Earth Science Educational Resource Center, http://www.eserc.stonybrook.edu/ProjectJava/Bragg/;
144. J. Marie, J. Mering, Proceeding First Conference of the Society of Chemical Industrial Conference on Carbon and Graphite, London, 1958;
145. World Wide Web, 18.12.2005, 11:00, Department of Chemical Engineering - Technical University of Denmark, http://hekabe.kt.dtu.dk/~vigild/2005_04_melitek/tga.htm;

146. Perkim Elmer, Thermogravimetric Analyser 7 Series / Unix TGA7, Users Manual, 0993 – 8676, Norwalk, Connecticut, USA;
147. World Wide Web, 14.09.2002, 18:00, HyperPhysics Electricity and Magnetism, http://hyperphysics.phy-astr.gsu.edu/hbase/electric/resis.html;
148. Keithley Instruments, *High Resistance Measurements, Application Note Series 312*, 11052KGW, 2005;
149. E.W. Washburn, *Note on a Method of Determining the Distribution of Pore Sizes in a Porous Material*, Proceedings of the National Academy of Science, vol. 7, USA, 1921;
150. D. K. Owens, R. C. Wendt, *Estimation of the surface free energy of polymers*, Journal of Applied Polymer Science 13 (8), 1969;
151. H. P. Boehm, *Functional groups at solid surfaces*, Angewandte Chemie, No. 12, 1966;
152. World Wide Web, 30.06.2005, 14:00, The Science of Spectroscopy: XPS Technique, http://scienceofspectroscopy.info/wiki/index.php?title=Main_Page;
153. World Wide Web, 02.01.2006, 11:00, Surface Area Measurement, Engelhard's FCC Knowledge Base; http://www.refiningonline.com/EngelhardKB/crep/TCR2_10.htm;
154. World Wide Web, 02.01.2006, 12:00, Beckman Coulter, Inc, http://www.beckman.com/products/instrument/partChar/technology/GasAdsorption.asp;
155. K. Katsonis, M. Cornille, G. Maynard, R.E.H. Clark, J. Abdallah Jr., Report on Atomic and Molecular Data for Fusion and Propulsion, www-amdis.iaea.org/DCN/Presentations/2005/Katsonis.doc;
156. Berstorff Hannover, *Operating Instruction*, Hermann Berstorff Maschinenbau GmbH, Hannover, Germany;
157. Brabender Technologie, *Operating Instruction*, Brabender Technologie KG, Duisburg, Germany;
158. International Standard EN ISO 527-1 (-2 and -3):1996, *Plastics – Determination of Tensile Properties*, Beuth Verlag GmbH, Berlin, 1996;
159. International Standard ISO 179:1993, *Determination of Charpy Impact Strength*, 1993;
160. Y. Yang, M. C. Gupta, K. L Dudley, Roland W. Lawrence, *The Fabrication and Electrical Properties of Carbon Nanofibre – Polystyrene Composites*, Nanotechnology 15, 1545 – 1548, 2004.

Publications

1. M. Heintze, V. Brüser, W. Brandl, , G. Marginean, **V. Chirila**, H. Bubert, *Surface activation of carbon nanofibres by plasma treatment*, 12th Conference on Plasma Physics and Applications, Iasi, 1-3 September 2003;
2. W. Brandl, G. Marginean, **V. Chirila**, W. Warschewski (2004), *Production and characterisation of vapour grown carbon fiber/polypropylene composites*, Carbon 42, 5-9, 2004;
3. **V. Chirila**, G. Marginean, W. Brandl, *Effect of the Oxygen Plasma Treatment Parameters on the Carbon Nanotubes Surface Properties*, Surface and Coatings Tehnology, 200(1-4), 548-551, 2005;
4. **V. Chirila**, G. Marginean, T. Iclanzan, W. Brandl, *Plasma Functionalisation of the Vapour Grown Carbon nano-Fibres for Composite Production*, Academic Journal of Manufacturing Engineering 3(1), 20, 2005;
5. **V. Chirila**, G. Marginean, T. Iclanzan, W. Brandl, *Vapour Grown Carbon nano-Fibres Polypropylene Composite and their Properties*, Carbon Nanotubes: From Basic Research to Nanotechnology, Sozopol, Bulgaria, 21-31 May 2005, 2005;
6. **V. Chirila**, G. Marginean, T. Iclanzan, W. Brandl, *Impact Resistance of Carbon nano-Fibres Reinforced Polypropylene Composite*, Carbon Nano Tube (CNT)- Polymer Composites International Conference, September 4-7, 2005, Technical University Hamburg-Harburg, Germany, 2005;
7. **V. Chirila**, G. Marginean, T. Iclanzan, C. Merino, W. Brandl, *Method for Improvement the Adhesion of Nanofibres/Nanoparticles Reinforced Polypropylene*, In Press;
8. **V. Chirila**, G. Marginean, T. Iclanzan, C. Merino, W. Brandl, *Method for Modifying the Mechanical Properties of the Carbon nano-Fibre Polymeric Composites*, In Press.

ANNEXES

Annex 1.

ANOVA: Water contact angle of the VGCNFs – 4 plasma parameters: plasma power, treatment time, chamber pressure and oxygen flow rate.

Plasma treatment parameters	Sum of square	DF	Mean square	F-ratio	P-value
A – plasma	212.592	1	212.592	57.31	0.0016
B – time	207.876	1	207.876	56.04	0.0017
C - O_2 flow rate	1.998	1	1.998	0.54	0.5111
D – pressure	0.014	1	0.014	0.00	0.9539
AB	6.872	1	6.872	1.85	0.2451
AC	3.200	1	3.200	0.86	0.4149
AD	95.914	1	95.914	25.86	0.0071
BC	9.592	1	9.592	2.59	0.1831
BD	87.379	1	87.379	23.56	0.0083
CD	15.905	1	15.905	4.29	0.1071
AA	204.863	1	204.863	55.23	0.0018
BB	208.706	1	208.706	56.28	0.0017
CC	0.732	1	0.732	0.20	0.6843
DD	1.096	1	1.096	0.30	0.6211
Total error	14.878	4	3.701		
Total (corr.)	1725.73	18			
R-squared = 0.991402	R-squared (adj. for d.f.) = 0.961309				

Annex 2.

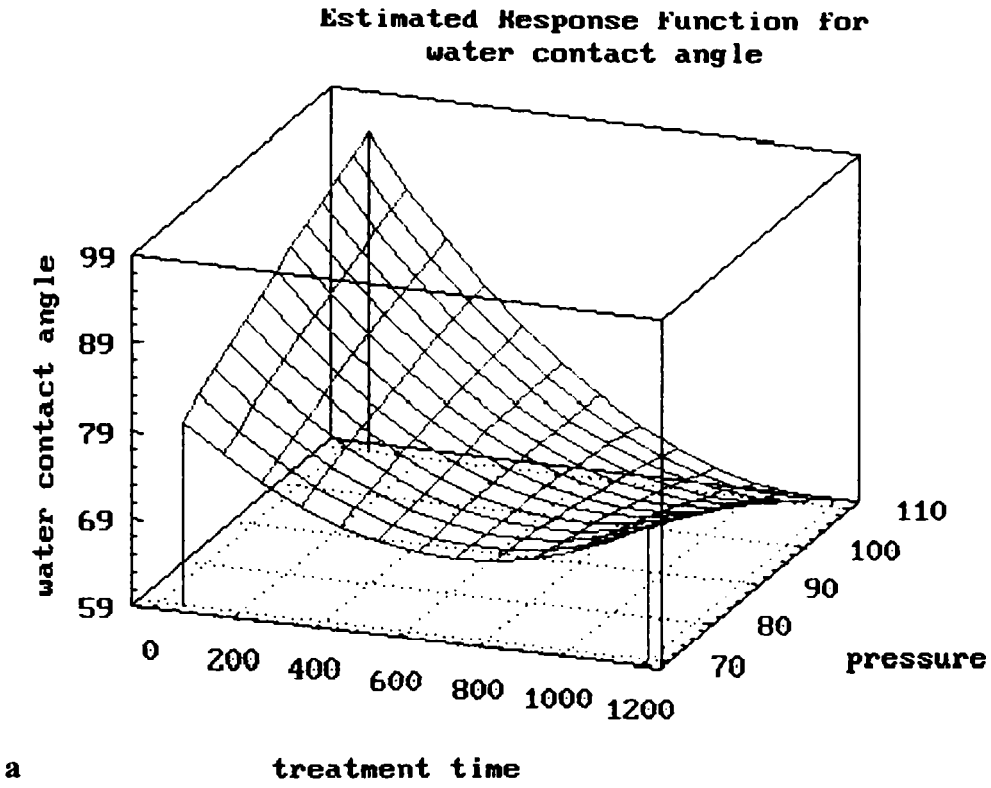

a

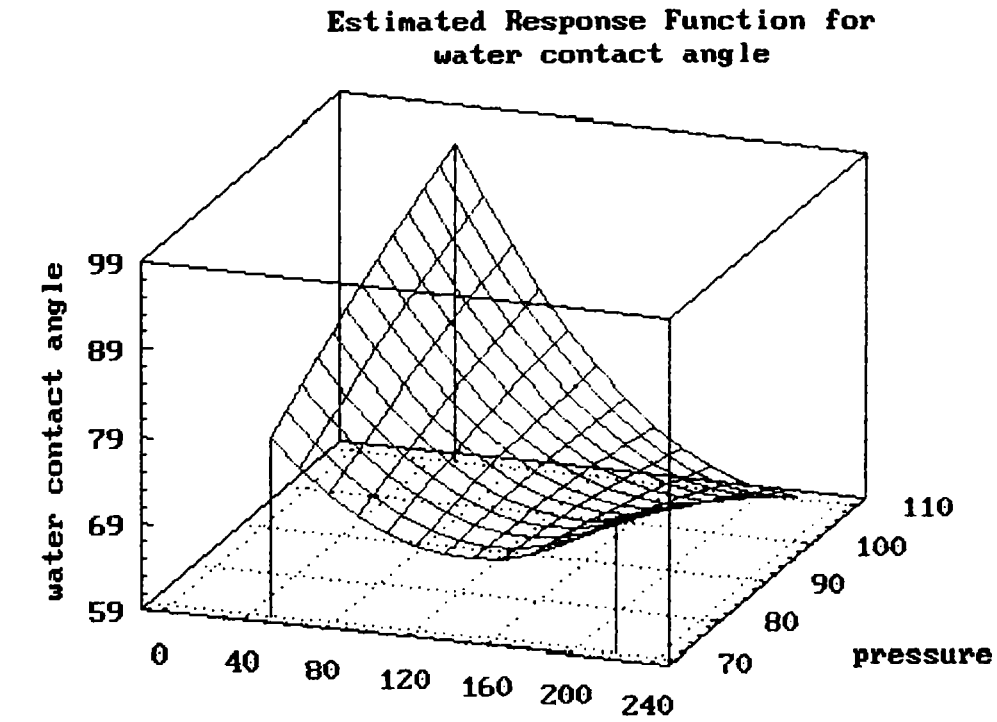

b

Water contact angle of the vapour grown carbon nanofibres depending on the plasma parameters Estimate response: (a) treatment time – chamber pressure, and (b) plasma power – chamber pressure.

Annex 3.

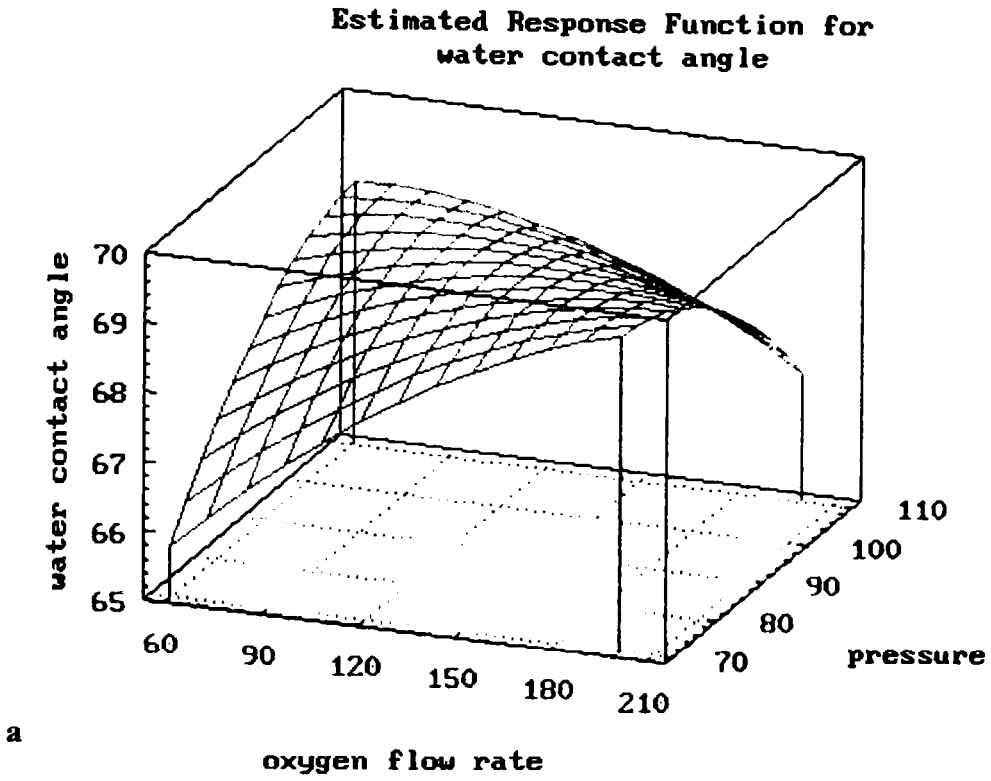

a

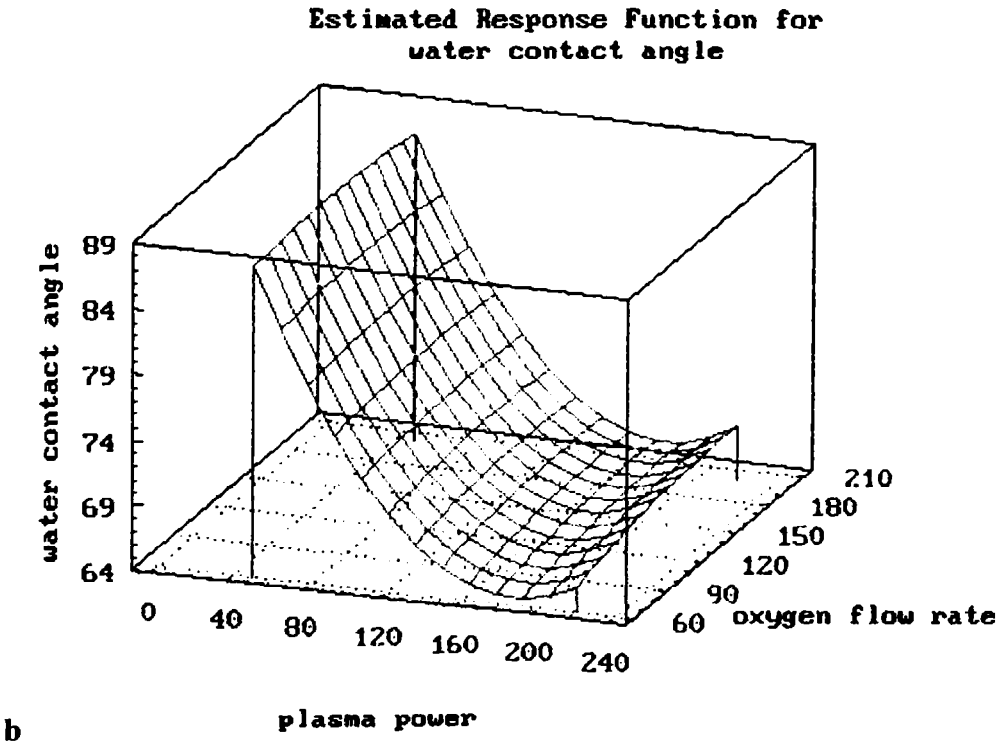

b

Water contact angle of the vapour grown carbon nanofibres depending on the plasma parameters

Estimate response: (a) oxygen flow rate – chamber pressure, and (b) plasma power – oxygen flow rate

Annex 4.

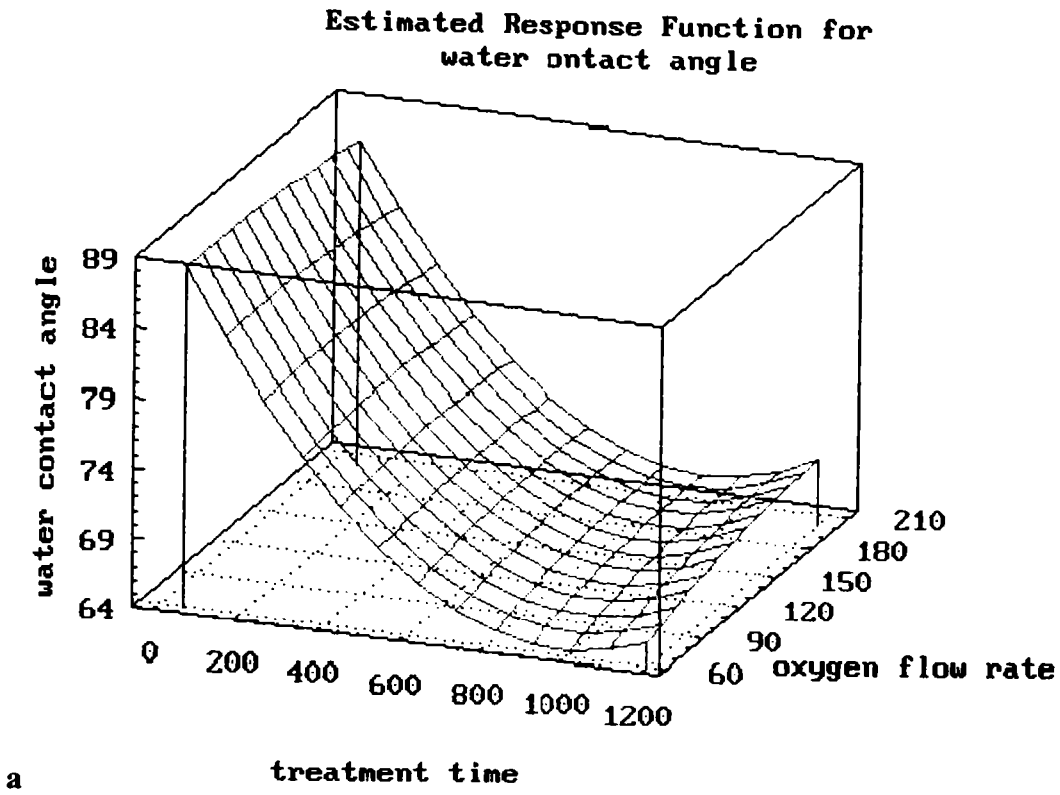

a

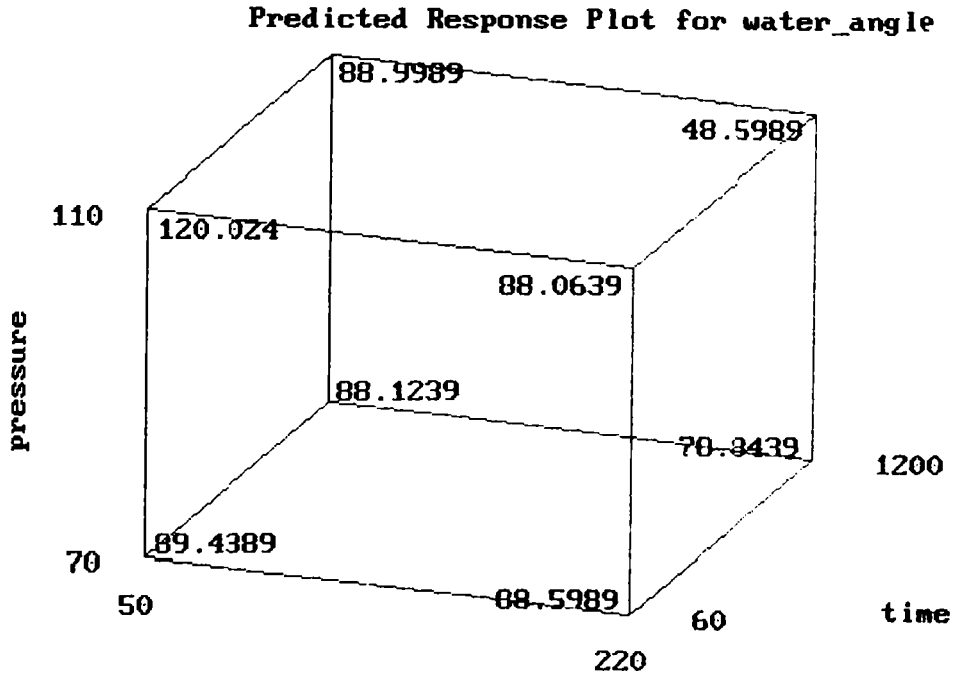

a

Water contact angle of the vapour grown carbon nanofibres depending on the plasma parameters Estimate response: (a) treatment time – oxygen flow rate, and (b) plasma power – treatment time – chamber pressure.

Annex 5.

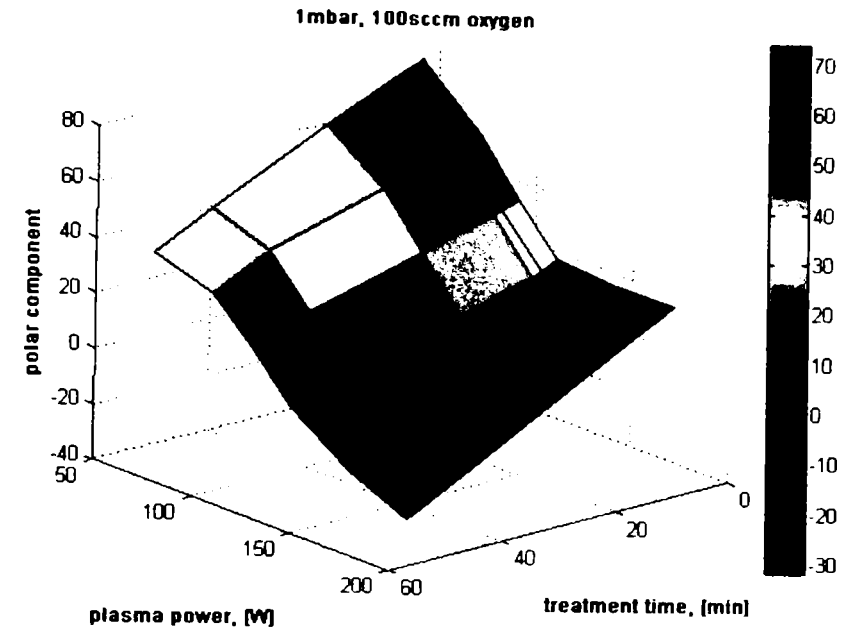

a

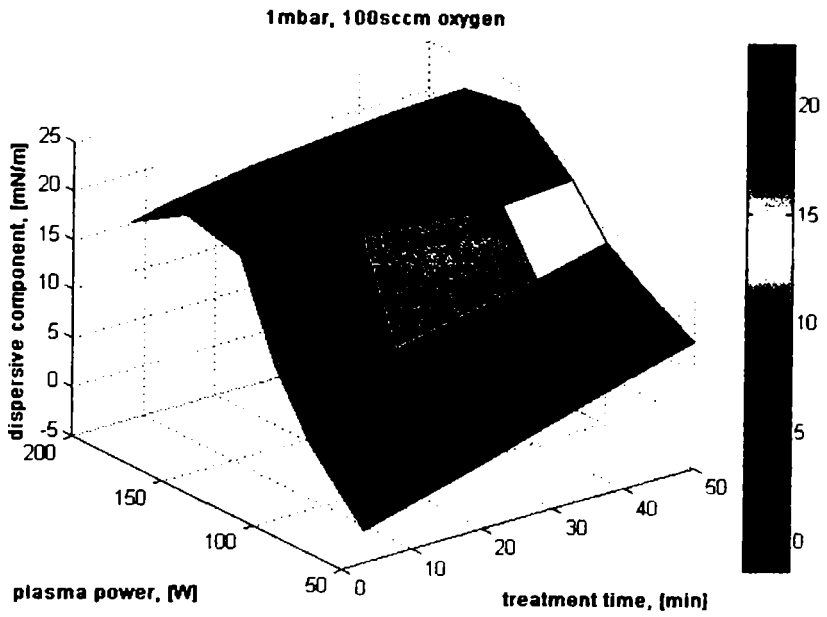

b

Estimation of surface energy (a) and its dispersive component (b) for the oxygen plasma treated Pyrograf fibres.

Annex 6.

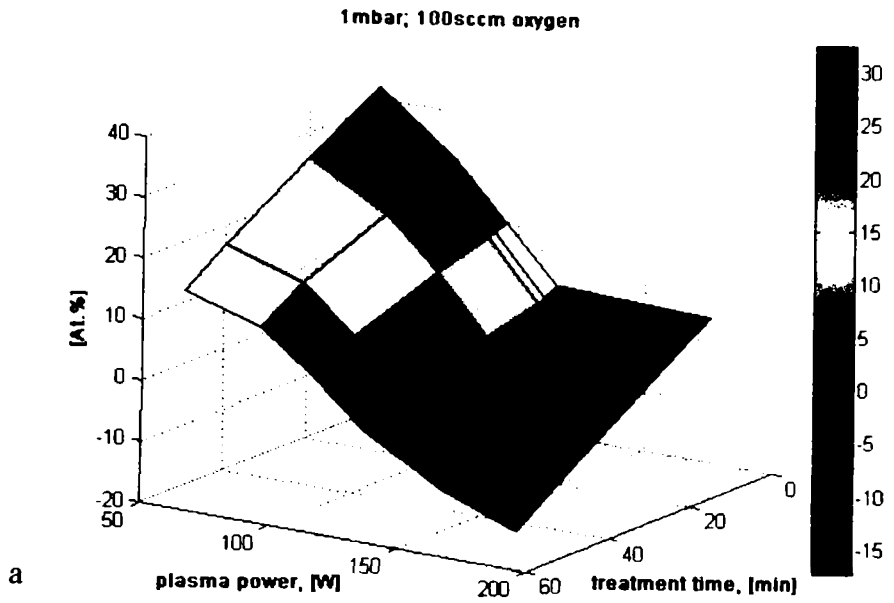

a

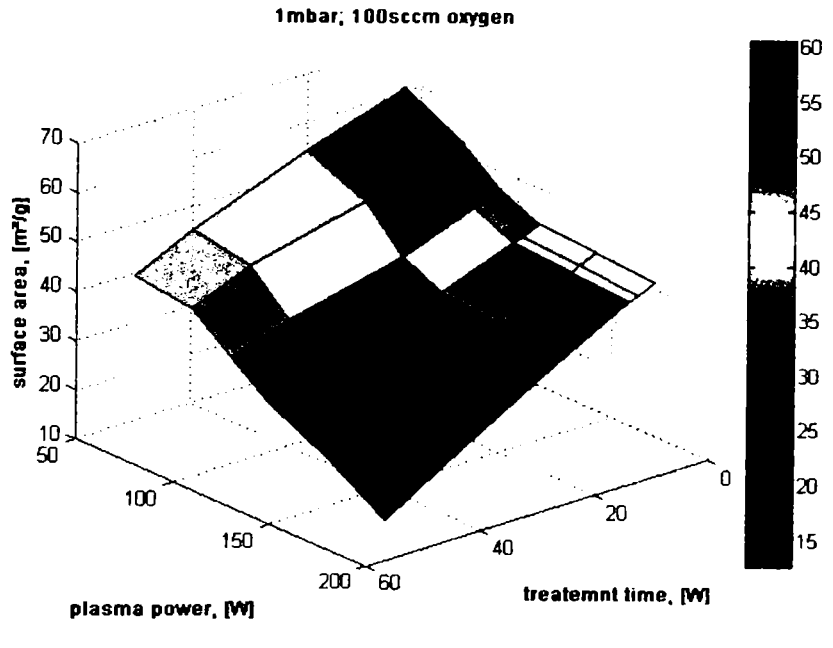

b

Estimation of amount of oxygen groups (a) and surface area (b) for the oxygen plasma treated Pyrograf fibres.

Annex 7.

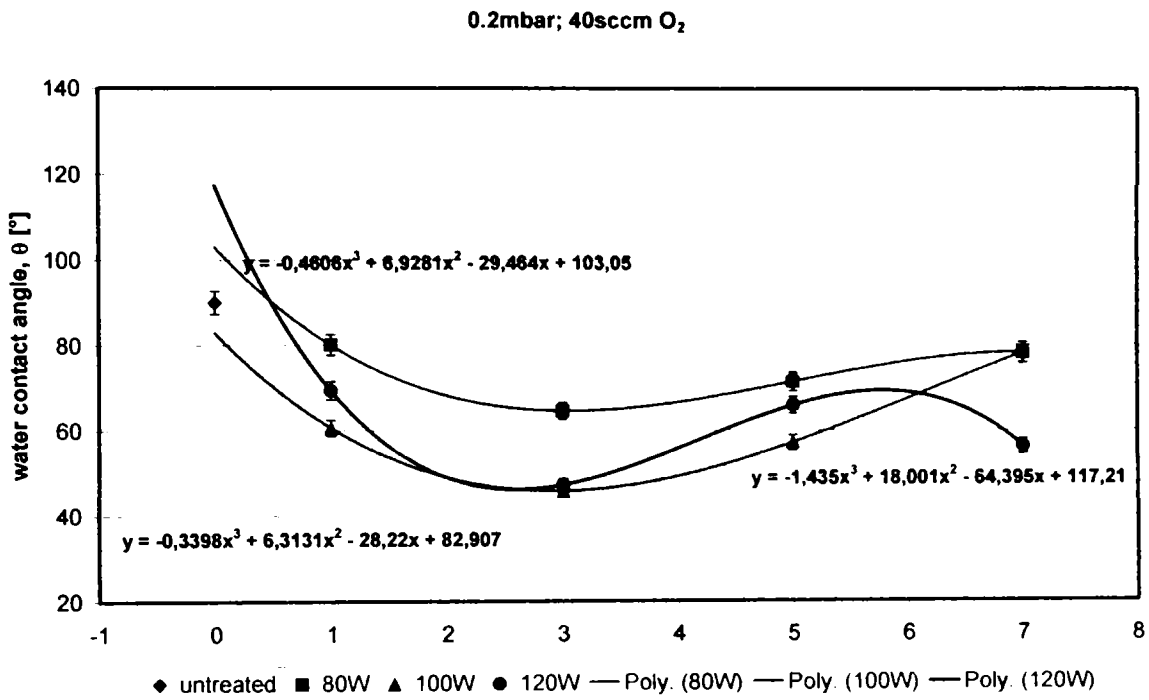

Results of water contact angle measurements of the fibres treated in microwave generated oxygen plasma: plasma power 80 – 120 W; treatment time 1 – 7 min; chamber pressure 0.2 mbar and oxygen flow rate 40 sccm.

Annex 8.

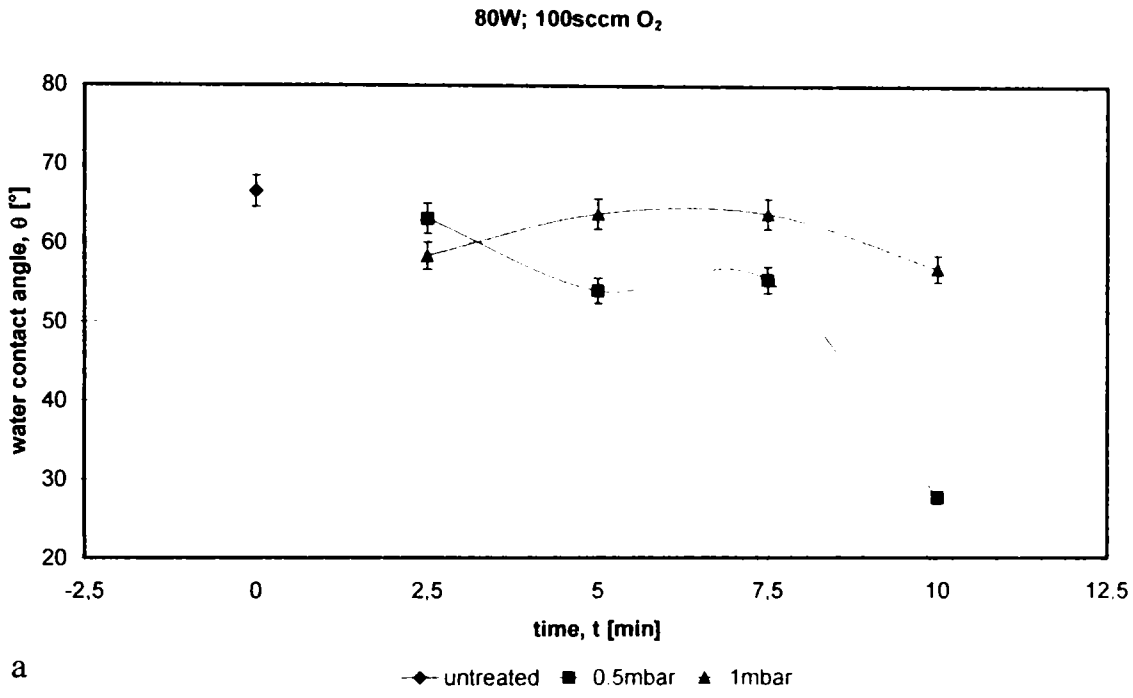

a

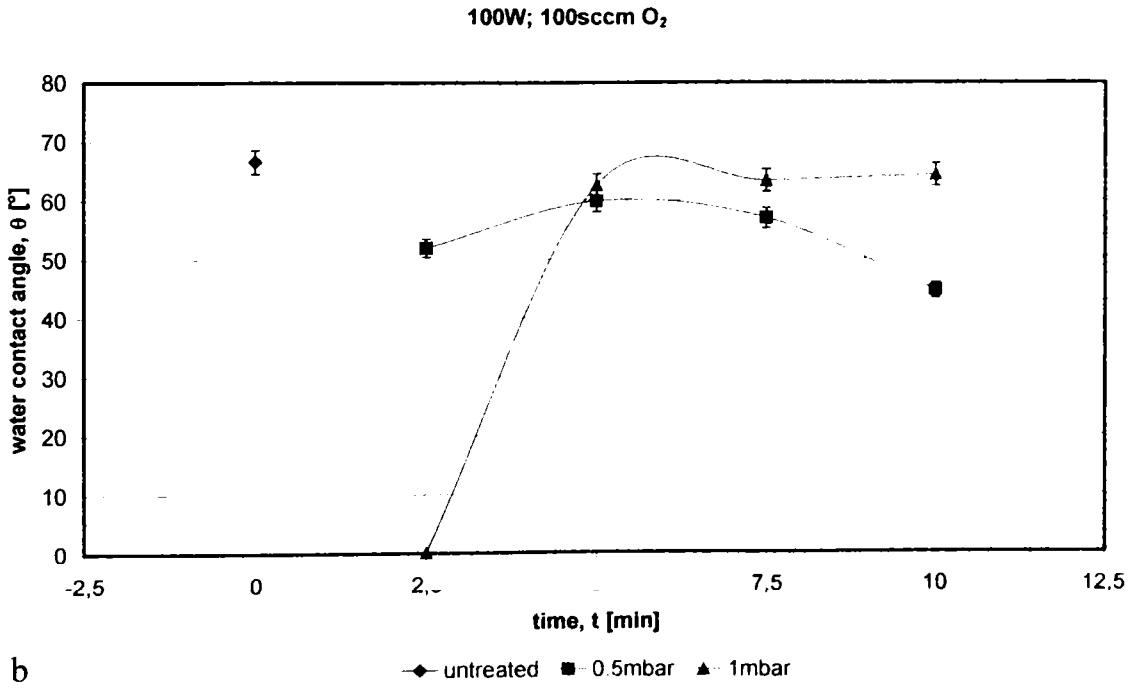

b

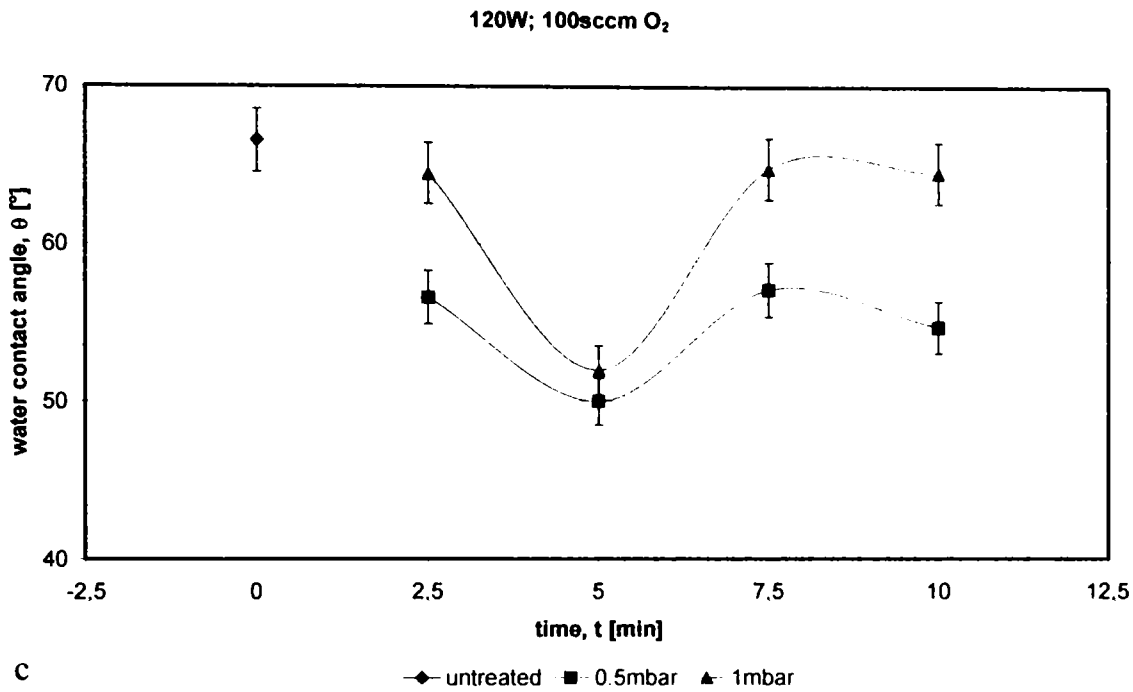

c

The water contact angle results as a function of chamber pressure of the samples treated at:

(a) 80W and 100sccmO_2; (b) 100W and 100sccmO_2 and

(c) 120W and 100sccmO_2.

Annex 9.

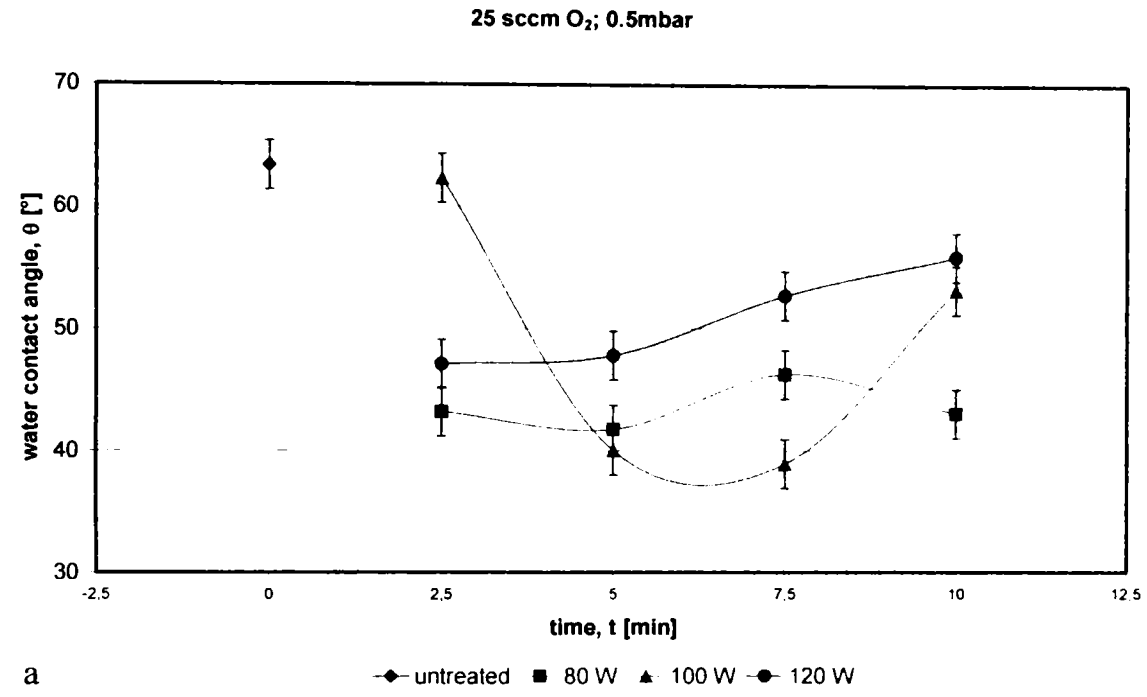

a

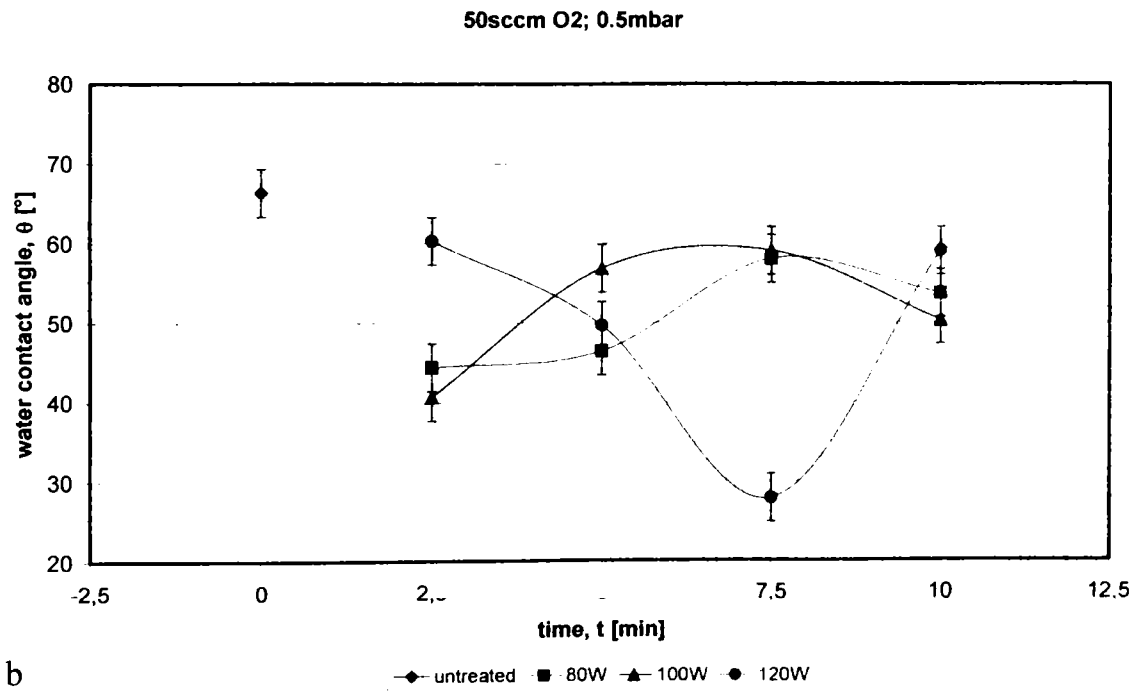

b

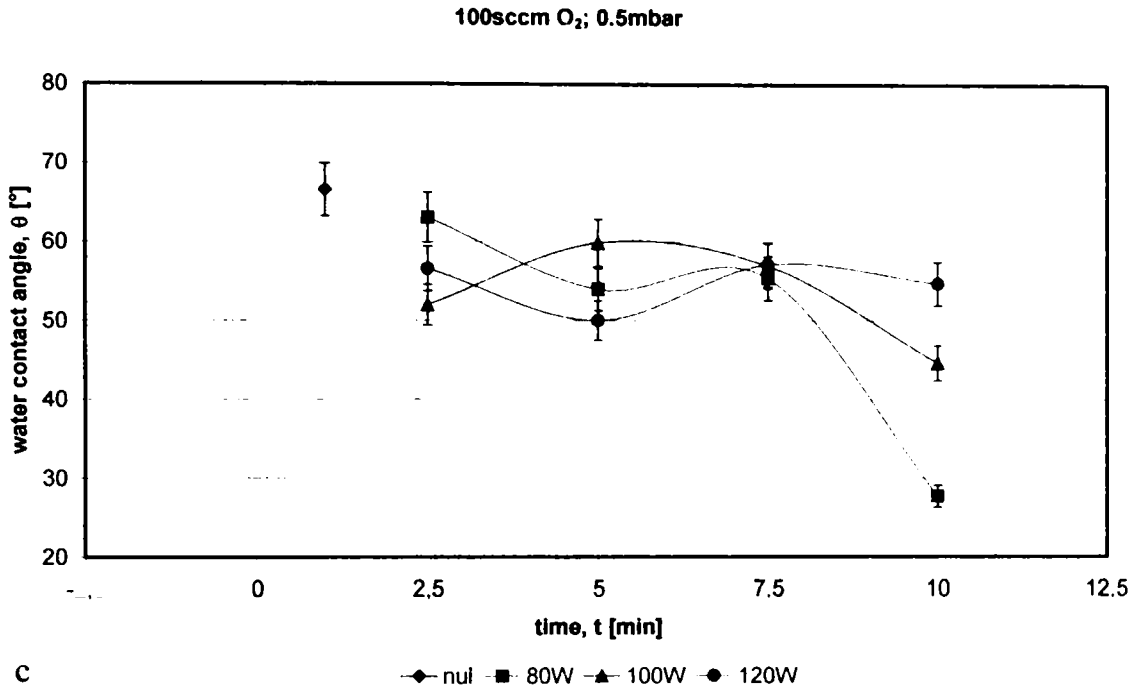

c

The influence of the oxygen flow rate and chamber pressure ratio [(a) – 0.5:1; (b) 1:1; and (c) 2:1] of the samples treated at 80 – 120W; and treatment time 2.5 – 10 minutes.

Annex 10.

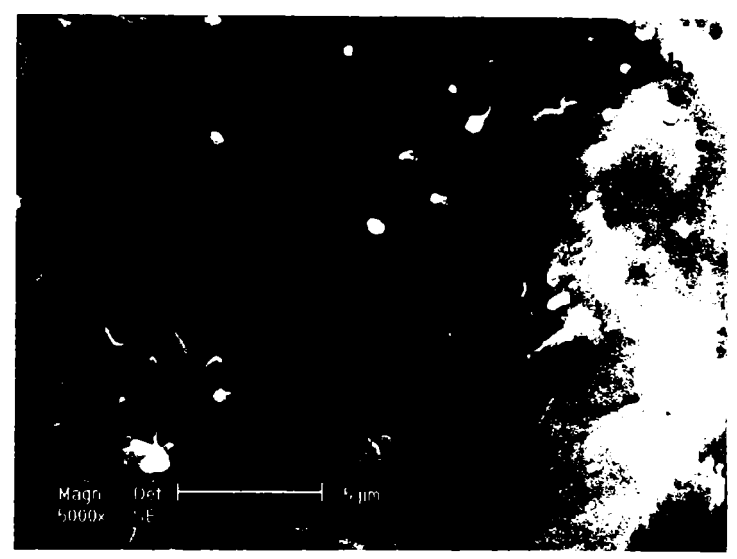

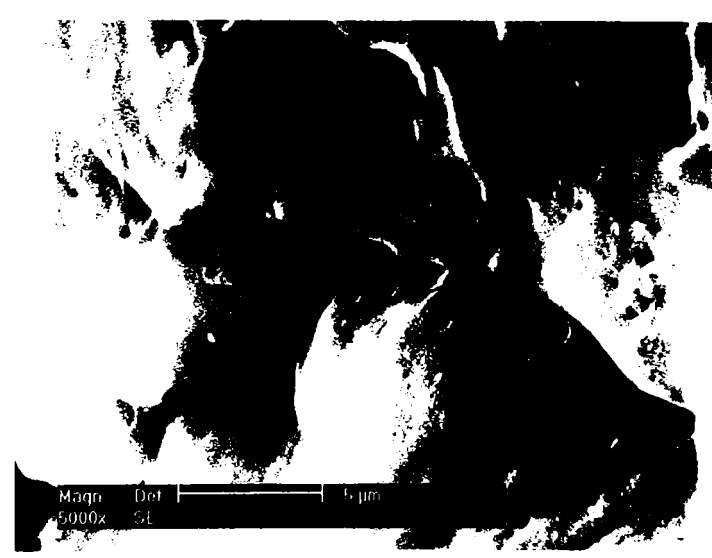

SEM – micrographs of the PP composite containing untreated Semana: a. 5 wt.% fibres; b. 10 wt.% and 5 wt.% plasma treated fibres (c).

Annex 11.

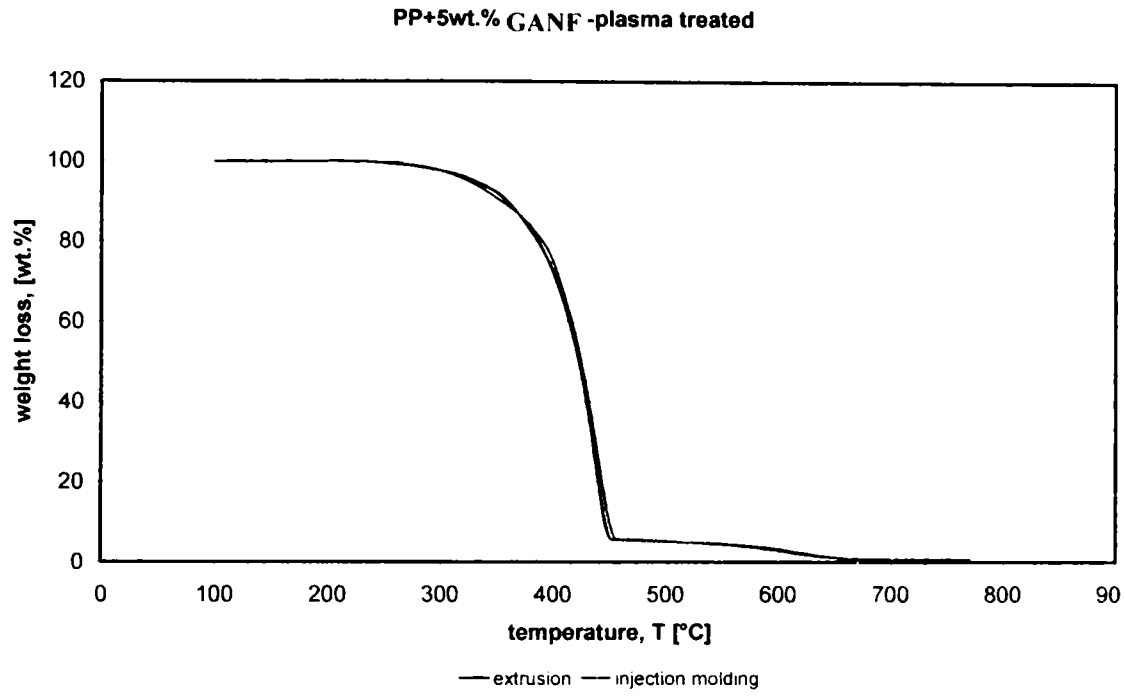

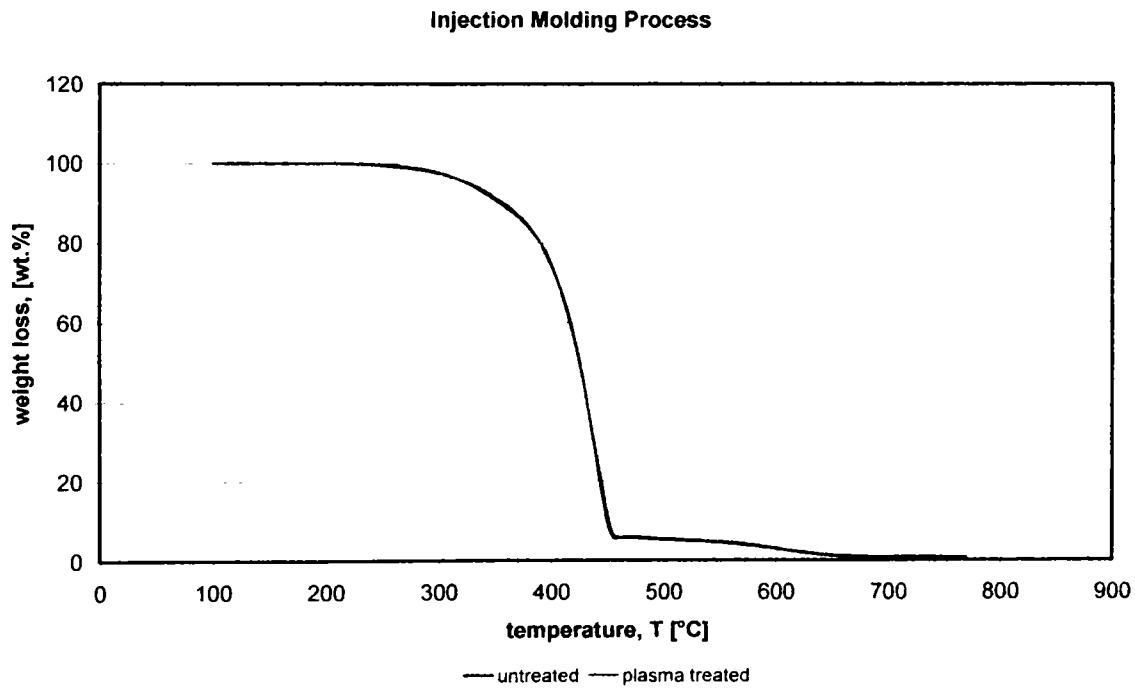

Thermal stability of the PP composite containing5 wt.% GANF fibres: (a) comparison between extrusion and injection moulding process and (b) comparison between injected moulded composites containing 5 wt.% untreated and oxygen plasma treated fibres.